

Improving Sensitivity and Throughput for Bioanalytical Measurements with Mass Spectrometry
using Microfluidics and Online Sample Preparation

by

Shane Wells

A dissertation submitted in partial fulfillment
of the requirements for the degree of
Doctor of Philosophy
(Chemistry)
in the University of Michigan
2021

Doctoral Committee:

Professor Robert T. Kennedy, Chair
Professor Philip Andrews
Professor Kristina Håkansson
Professor Brandon T. Ruotolo

Shane Wells

shanews@umich.edu

ORCID iD: 0000-0003-1939-2510

© Shane Wells 2021

Dedication

I dedicate this work to Holly for her unconditional love and support.

Acknowledgments

There are many people that have helped me reach this point in my education and career who I could not have made it here without. First and foremost, I would like to acknowledge and thank my family. My parents have always encouraged me to do what I love and to pursue my passions in life, both inside and outside of my career. They raised me to become the person and the scientist I am today, and they have offered me unending support throughout my entire education. My brother has been a great support to me always willing to talk and relieve my stress by offering distractions like making me play Fortnite and forcing me to listen to new music. And of course, my wife Holly, who has been my most fundamental support throughout my graduate schooling. Not only has she offered me perpetual emotional and intellectual support, but she moved across the country to share this journey with me and has spent countless hours listening to me and my friends/peers talk about chemistry at supposed social events.

I would also like to acknowledge all of those who helped guide me towards my passion of science. My undergraduate advisor Chris Harrison showed me how interesting analytical chemistry could be and pushed me to explore my options as I moved into the world of science. My current advisor, Robert Kennedy, has been instrumental in shaping the scientist I have become. He has helped guide me and promote my growth and independence throughout my time in graduate school as I have engaged in research I truly enjoy under his advisement. The rest of my doctoral committee has provided substantial support, knowledge, and guidance to me as well. I will even give a little shoutout to my terribly mean AP Chemistry teacher for sparking my interest in chemistry, despite making students cry on a weekly basis.

I have been surrounded by peers and lab mates who have made graduate school more enlightening, collaborative, and enjoyable over the past 5 years. I acknowledge my mentors Paige Malec, Mohamed Dawod, and Daniel Steyer for helping guide my learning and understanding during my first couple of years in graduate school. Others, such as Matt Sorensen, Emory Payne, Alec Valenta, and Cara D'amico, as well as the rest of the lab members, have been great for discussing ideas and for simply creating a fun yet productive working environment. I would like to give a special thanks to Emoru and Alec for working closely with me on a couple of specific projects. Additionally, I acknowledge my collaborators Dr. Alison Narayan and Lara Zetzche who I worked closely with on directed enzyme evolution screening.

Finally, I would like to acknowledge my sources of funding and the companies who have donated materials or instruments to make much of my research possible. Most of my work was funded by NIH 2R01EB003320-21 (RTK). I also acknowledge and thank Agilent Technologies for the loan and assistance with electrophoresis instrumentation on which all CE experiments were performed. I also thank New Objective, for donating all nESI emitters and PicoClear unions that were used in my experiments.

I am excited to being the next chapter of my life, but the time and the people from my five years in the Kennedy lab will always hold a special place in my heart. I wish nothing but the best for all current and future Kennedy lab members.

TABLE OF CONTENTS

| | |
|--|-----------|
| Dedication | ii |
| Acknowledgments | iii |
| List of Figures | vii |
| List of Tables | xiii |
| List of Equations | xiv |
| List of Abbreviations | xv |
| List of Appendices | xvii |
| Abstract | xviii |
| | |
| 1. Chapter 1: Introduction | 1 |
| Electrospray Ionization and Suppression | 3 |
| ESI Sensitivity and Detection | 5 |
| ESI Throughput | 8 |
| Droplet Microfluidics | 12 |
| Droplet-Mass Spectrometry | 15 |
| Dissertation Overview | 18 |
| | |
| 2. Chapter 2: CE-MS with Electrokinetic Supercharging and Application to Determination of Neurotransmitters | 21 |
| Introduction | 21 |
| Materials and Methods | 28 |
| Results and Discussion | 31 |
| Conclusions | 39 |
| | |
| 3. Chapter 3: Droplet-nESI-MS/MS with Microdialysis for Sensitive and High Temporal Resolution Neurochemical Monitoring | 41 |
| Introduction | 41 |

| | |
|--|------------|
| Materials and Methods | 45 |
| Results and Discussion | 51 |
| Conclusions | 58 |
| 4. Chapter 4: High Throughput Liquid-Liquid Extractions with Nanoliter Volumes Using Slug Flow Nanoextraction | 60 |
| Introduction | 60 |
| Materials and Methods | 63 |
| Results and Discussion | 65 |
| Conclusions | 77 |
| 5. Chapter 5: Continuous and Automated Slug Flow Nanoextraction for Rapid Log K_{ow} Determination | 79 |
| Introduction | 79 |
| Materials and Methods | 82 |
| Results and Discussion | 85 |
| Conclusion | 98 |
| 6. Chapter 6: Sensitive and High Throughput Screening for Directed Enzyme Evolution by Droplet-MS | 99 |
| Introduction | 99 |
| Materials and Methods | 101 |
| Results and Discussion | 107 |
| Conclusions | 113 |
| 7. Chapter 7: Conclusions and Future Directions | 115 |
| Sheathless CE-MS Interface with EKS | 116 |
| Real-Time In Vivo Neurochemical Monitoring | 120 |
| SFNE for Rapid Online Sample Clean-up with MS Analysis | 122 |
| APPENDICES | 125 |
| REFERENCES | 144 |

List of Figures

- Figure 1-1: Illustration of the ubiquity of small molecules throughout the central dogma of biology. 1
- Figure 1-2: General mechanism of electrospray ionization and desolvation and the ESI circuit. 4
- Figure 1-3: (A) Simulated image of a water nanodroplet (O red; H white) containing 10 Na⁺ ions (blue). (B) Illustration of the distribution of ions and water dipoles inside of a nanodroplet, showing the effect of competing solvation requirements and dipole distribution on cation positioning within a nanodroplet. 5
- Figure 1-4: Comprehensive overview of high throughput sample introduction methods/instruments using ESI or alternative ionization techniques as of July 2018. 10
- Figure 1-5: Illustration of the common droplet microfluidic operations. 12
- Figure 1-6: Illustration of general droplet microfluidics being paired with ESI-MS. Specific labels provided for the different fluids present and potential droplet volume ranges. 15
- Figure 1-7: (A) Resulting MS data corresponding to droplet-ESI-MS/MS of various concentrations of leucine-enkephalin. (B) Image of the ESI emitter at various times during droplet infusion (1. aqueous sample and 2. carrier phase at tip) and the corresponding MS/MS signals. 17
- Figure 1-8: Droplet-MS data where a single mass transition is monitored for over 2.5 hr using 1.2 nL droplets. 16
- Figure 2-1: Illustration of the general scheme for EKS. Each of the steps are shown, where arrows indicate applied pressure for volume loading and +/- kV indicate applied voltage. 23
- Figure 2-2: (A) Electropherograms of the different buffer systems tested for obtaining sufficient selectivity and resolution for 4 test compounds in a 20 kV 60 cm separation using CE-UV with HDI injections. (B) Comparison of two potential LE candidates using EKI in a 20 kV 60 cm separation. 32
- Figure 2-3: FASI injections performed at varying injection durations and the subsequent resolution changes between NE and EPI (100 nM). 33

Figure 2-4: (A) Comparison of a 15 s 30 kV injection using LE with and without 5 mM taurine as TE. (B) Comparison of varying EKS injection durations without the intentional loading of a TE. 33

Figure 2-5: Extracted ion electropherograms (MS/MS) from a separation of 1 nM standards in water (Ch scaled down by a factor of 250 for scaling). 34

Figure 2-6: Total ion electropherogram of four different injection/preconcentration techniques at concentrations that fit within each methods LDR. 35

Figure 2-7: (A) Concentrations determined in rat brain stem homogenate by EKS with CE-MS/MS (black bars) and validation by LC-MS/MS (grey bars). EKS injections used 100 μ L of sample and LC injections used 5 μ L of sample per injection. Different aliquots of the same of the same supernatant used for each injection (triplicate by each method). (B) Extracted electropherograms for each compound in the rat brain stem homogenate separation (Ch reduced by a factor of 250 for scaling). 36

Figure 2-8: Graph of the determined concentrations from whole *Drosophila* tissue using the developed EKS method and the corresponding standard deviation. 37

Figure 2-9: To test sample stability at room temperature, rat brain homogenate supernatant was analyzed by LC-MS after 0 and 4 hours at room temperature before derivatization. 39

Figure 3-1: (Top Left) MS/MS trace of the calibration curve for ACh with 5 droplets for each of the 6 calibration levels. (All other graphs) Average signal intensity vs. concentration to generate a 6 point calibration curve with error bars for each of the target neurochemicals. 47

Figure 3-2: (A) Low infusion flow rates (50 nL/min) and smaller nESI emitter i.d. (15 μ m) allow for smaller droplets (4.4 nL) and improved analyte response and S/N over a higher infusion flow rates (500 nL/min) and larger i.d. nESI emitter (30 μ m), which required 40 nL droplets. ACh is shown for this comparison. (B) An adjusted matrix with 33% of the standard PO₄ concentration in aCSF along with a final concentration of 1% concentration acetic acid compared to standard aCSF with no acid. DA is shown for this comparison (C) Increased dwell time (100 ms) for the MS/MS scans vs a typical faster dwell time (30 ms). 52

Figure 3-3: . To measure the temporal resolution of the system from sampling to mass analysis, stirred vial experiments were performed in triplicate for test compound ACh. 54

Figure 3-4: In vivo experiments using MD probes sampling the striatum over a 10 min collection period. 500 nL of high potassium aCSF was administer over 30 s beginning at 0 and 5 min, with an approximate 2.5 min dead time. Three biological replicates were obtained over two mice (one mouse with two hemispheres). 55

Figure 3-5: (A) In vivo experiments using MD probes sampling the striatum over a 10 min collection period. 500 nL of high potassium aCSF was administered over 30 s beginning at 0 and 5 min, with an approximate 2.5 min dead time. Three biological replicates were obtained over two mice (one mouse with two hemispheres). Points converted to percent baseline to normalize for concentration differences and all three traces were averaged. SEM shown as a blue-dotted line. Gray squares and connecting lines represent LC fraction method, with fractions collected over 5 min intervals. (B) Basal concentrations determined by droplet-MS and LC-MS in high potassium stimulation experiments and the LODs (blue line) for each by droplet-MS. 56

Figure 3-6: In vivo experiments using MD probes sampling the striatum over 5 min with 500 nL of 100 μ M AMPH administered over 30 s starting at -1 min. Four biological replicates were obtained over three mice (one mouse with two hemispheres). 57

Figure 3-7: Validation of the biological response of 5HT to AMPH presence in one of the AMPH stimulation replicates. 58

Figure 4-1: (A) The two-phase slug generation process is shown, where a length of PFA tubing with applied vacuum is sequentially dipped in PFD, extraction solvent, and aqueous sample. For most experiments, an air plug is also included before each extraction phase. (B) Once a line of tubing is filled with phase pairs, flow is driven towards the outlet allowing the extraction phase to accelerate and contact the sample. The tube can be paired with a variety of detectors, where extractions occur while in-transit to an online detector. (C) Shown are three time points for a single phase pair as the two phases are interfaced. Though initially far apart, the organic plug accelerates towards the leading aqueous plug, forming a partitioning interface and allowing extraction. The photographs show the appearance of the phase pair before and after the extraction occurs, where the second image shows that a majority of Rh6G has transferred from aqueous to organic. (D) Due to the internal mixing within the low volume droplets, contents of the aqueous sample partition rapidly into the extraction phase mode (SRM), where every transition is monitored throughout the infusion 66

Figure 4-2: (A) A train of phase pairs with extraction solvent CHCl_3 was generated and the partitioning of fluorescent dye Rh6G was measured by LIF. Though initially dissolved in water, most of the rhodamine partitioned into CHCl_3 by SFNE. The variation in signal intensity is due to the variations in volumes between phase pairs. (B) Similarly, an offline extraction via microshake-flask extraction was performed with the aqueous rhodamine and extraction solvent CHCl_3 . Three plugs of each layer were generated and analyzed by LIF. (C) The ratios of signal from LLE and SFNE were graphed and show similar extraction efficiency. 68

Figure 4-3: Volume ratios of the two-phases were manipulated for each phase pair in a train. (A) Four pairs of high organic volume, similar volume of each, and high aqueous sample volume were generated and measured by LIF. (B) A plot of concentration in extraction phase at equilibrium vs. volume ratio for each phase pair. 70

Figure 4-4: (A) In a single experiment, acetaminophen K_{ow} was determined by the common shake-flask method and SFNE using UV VIS detection. First, acetaminophen was calibrated from 1.0 – 0.1 mM in water and 2.0 – 0.2 mM in octanol. Second, plugs generated from each layer of the shake flask extraction were measured by UV. The shake flask extraction was performed by placing 100 μ L of pure octanol and 100 μ L of 1 mM acetaminophen (aq) into a PCR tube, vortexing for 1 min, and centrifuging for 5 min. Finally, two-phase slugs initially containing pure octanol and 1 mM acetaminophen (aq) were measured by UV. The K_{ow} was determined from each method by determining concentration of acetaminophen in each layer using the calibrations and taking the quotient of C_{org}/C_{aq} . (B) The calibration of ACP in each phase was plotted and showed good linearity. Error bars are present but hidden by markers. (C) Zooming in on a central phase-pair better displays all of the layers present. Each phase is segregated by PFD and air. 71

Figure 4-5: (A) In a comparison of SFNE-MS and single-phase droplet-MS, a train of phase pairs was generated with sample plug consisting of the drug mixture in plasma (1 μ M) and extraction plug EtOAc. Each train consisted of 10 analyte containing phase pairs alternating with 10 blank phase pairs. For single-phase droplet-MS, a droplet train consisting of the same sample layer was generated, without presence of an extraction phase, alternating 10 analyte containing droplets with 10 blank droplets. Each form of infusion was measured by ESI-MS/MS. The y-axis shows intensity normalized to the highest point between the two EIC traces. (B) Five drug compounds were analyzed by SFNE-MS and single-phase droplet-MS from multiple biological matrices. 72

Figure 4-6: A comparison between droplet-MS and SFNE-MS on synthetic urine droplets containing 1 μ M Dox (using EtOAc extraction phase for SFNE). 74

Figure 4-7: Calibration curves from 0.1 – 10 μ M were obtained for five drug compounds by SFNE-MS using SRMs to monitor each transition simultaneously. 76

Figure 5-1: Automated log K_{ow} determination using slug flow nanoextraction. 85

Figure 5-2: Complete online, automated system for SFNE. 86

Figure 5-3: Online SFNE generation and detection. (A) A mixture of red dyes (aqueous, 3) and extraction phase (octanol, 2) are segmented into 8 nL phase pairs by PFD (fluorous, 1). (B) Continuous online UV Vis detection of the phase pairs in Teflon tubing for an extended period. 87

Figure 5-4: Volume manipulation via flow rate changes. (A) Similar flow rates result in near equal volume in the export tubing. (B) Increasing aqueous relative to organic flow rates reduced VR over two-fold. (C) Flow rate ratio was varied from 1.0 to 0.17 and signal intensity in octanol are reported. 88

Figure 5-5: Theoretical concentrations for acetaminophen (initial concentration in aqueous of 1 mM) as volume ratio is adjusted to achieve preconcentration. 89

Figure 5-6: Images from a video where organic phase is toggle off and on every 10 s. 90

Figure 5-7: Full LC-SFNE-UV workflow. (A) In a single automated run, a calibration in water was performed followed by triplicate injections with SFNE to determine log Kow for acetaminophen. (B) Expansion of a portion of the trace, showing examples of the phase pairs that were used to determine equilibrium concentrations of acetaminophen in water post-extraction. (C) Value comparisons and validations in this study for online SFNE by comparison to previous reports, microshake-flask (aq,oct), and microshake-flask (aq only) log Kow values for ACP. 91

Figure 5-8: (A) Example trace of eserine from full log Kow screen. A five-point aqueous calibration curve in water was injected and generated into aq slugs. Organic (octanol) flow was started at 57 minutes. Unknown determination traces of eserine at pHs 3, 7.4, and 10, at both 1 and 10 mM concentrations. Organic flow was stopped at 65 min in preparation for the next compound screen. (B) Calibration curve generated from the trace ($R^2 > 0.99$). 93

Figure 5-9: Triplicate injections of blank buffer used for extractions standards at each pH during log Kow determination at (A) 214 nm and (B) 254 nm. 94

Figure 5-10: Raw trace of entire 7 compound screen where each compound has Log Kow determined at 3 different biological pH's (3, 7.4, and 10) with a 5 point aqueous calibration curve before extraction for quantification. 94

Figure 5-11: A comparison of the log Kow determined at pH 7.4 for each compound by SFNE and microshake-flask extraction. 96

Figure 5-12: Samples were thawed to room temperature and sampled at 3 different time points during the shaking process (0h, 1h, and 2h) and stored at -80C after sampling. 97

Figure 6-1: Target reaction for work in Chapter 6 of biaryl coupling of C5-methyl coumarin and 2-naphthol. HTS analysis targeted for quantification of limiting reagent SubA and all isomers of cross product AB to determine relative conversion and enzyme activity. 107

Figure 6-2: Comparison of conditions that cause ionization suppression (matrix vs matrix with high concentration reaction substrates present) and two different dilution factors to overcome a degree of suppression. 108

Figure 6-3: . Cross product quantification from a screen with and without the use of internal standard. IS corresponds to 5 μ M ACP which is added to calibration standards and samples. 109

Figure 6-4: (A) Seven-point calibration curve for AB with linearity ($R^2 = 0.998$) from 25 μ M to 25 nM. (B) Raw trace of calibration from droplet-nESI-MS/MS, where five droplets are sprayed from each concentration level, and the middle three of each level are averaged for $n = 3$ in each calibration curve. 110

Figure 6-5: (A) Example of entire plate (96 reactions) run in triplicate within 15 min, where the MS/MS trace for SubA is shown. Zooming in on one of the many sections is an example of the droplet data, where each cluster holds 18 droplets (6 wells in triplicate) and a final “reset” droplet. (B) Fold-improvement over WT reactions shown, where fold-improvement is based on improvement in conversion to AB. Error bars are shown for the triplicate measurements by droplet-MS but were not obtained for LC-MS for time management. (C) Comparison plot of each screening method to demonstrate correlation based on slope and linearity. 112

Figure 6-6: Top 60 reactions from 1,728 reaction screen. Seven statistically significant hits were identified (blue points/error bars), and most reactions analyzed have less than or equal to the relative conversion of the WT reaction. 113

Figure 7-1: Sheathless CE-MS system for use with EKS, where the separation ground is applied by the slightly positive (compared to separation voltage) nESI voltage. 118

Figure 7-2: Image of the separation capillary back-end with a home-pulled, gold-coated, integrated nESI emitter. 119

Figure 7-3: (A) 21.5 kV of separation current was applied while connected to 1.5 kV of nESI voltage, totaling 20 kV across the separation capillary for 16 min, where a stable current was obtained over the period indicating stable ground and interfacing. (B) A solution of 1 μ M neurotransmitters dissolved in water were infused by applying pressure in the CE system to obtain a infusion rate of 100 nL/min, indicating that electrospray can be conducted using the home-pulled separation capillary-nESI system while maintaining stable spray. 119

Figure 7-4: Proposed format for “real-time” high temporal resolution in vivo neurochemical monitoring using droplet-nESI-MS/MS. 121

Figure 7-5: Preliminary results using online phase pair generation devices with aqueous/EtOAc phase pairs. 123

Figure A-1: Set-up for droplet generation using microfluidic cross-junction attached to microdialysis probe outlet. 126

List of Tables

| | |
|--|----|
| Table 2-1: List of all compounds for which the EKS with CE-ESI-MS/MS method was developed. | 27 |
| Table 2-2: EKS compared to other common forms of injection and preconcentration | 35 |
| Table 2-3: Characterization of the calibration curves used for quantification of neurotransmitters in rat brain stem homogenate including LOD, LDR, and linearity. | 35 |
| Table 3-1: List of transitions, dwell times, and collision voltages for MS/MS. | 45 |
| Table 3-2: Important MS, nESI, and sample prep info for in vivo. | 48 |
| Table 4-1: The drugs used for MS experiments were investigated for optimal transitions, fragmentor voltages and collision energies individually. | 64 |
| Table 4-2: Five drug compounds were analyzed by SFNE-MS and droplet-MS from multiple biological matrices. | 73 |
| Table 5-1: Log K_{ow} values determined from screen and microshake-flask validation. | 95 |

List of Equations

| | |
|---|-----|
| Equation 1-1: Electrochemical reaction in ESI | 3 |
| Equation 1-2: Ionization efficiency | 5 |
| Equation 4-1: Volume ratios and partitioning | 69 |
| Equation 5-1: Volume ratio | 88 |
| Equation 5-2: log Kow | 92 |
| Equation 5-3: Estimation of equilibrium concentration | 92 |
| Equation 6-1 Relative conversion of reactions | 104 |

List of Abbreviations

| | |
|-----------------|---|
| 5HT | serotonin |
| ACh | acetylcholine |
| ACP | acetaminophen |
| aCSF | artificial cerebral spinal fluid |
| Ado | adenosine |
| AMPH | amphetamine |
| BGE | background electrolyte |
| CE-MS | capillary electrophoresis – mass spectrometry |
| Ch | choline |
| CZE | capillary zone electrophoresis |
| DA | dopamine |
| DESI | desorption electrospray ionization |
| EKI | electrokinetic injections |
| EKS | electrokinetic supercharging |
| EOF | electroosmotic flow |
| Epi | epinephrine |
| ESI | electrospray ionization |
| EtOAc | ethyl acetate |
| FASI | field amplified sample injection |
| FASS | field amplified sample stacking |
| F _R | flow ratio |
| GABA | γ-aminobutyric acid |
| GC-MS | gas chromatography-mass spectrometry |
| Gln | glutamine |
| Glu | glutamine |
| HDI | hydrodynamic injection |
| HMDB | human metabolome database |
| HPLC | high performance liquid chromatography |
| HTS | high throughput screening |
| IS | internal standard |
| K _{ow} | octanol-water partition coefficient |
| LC-MS | liquid chromatography-mass spectrometry |
| LDR | linear dynamic range |
| LE | leading electrolyte |

| | |
|----------------|---|
| LIF | laser-induced fluorescence |
| LLE | liquid-liquid extraction |
| LOD | limit of detection |
| LPME | liquid-phase microextraction |
| LVSS | large volume sample stacking |
| MALDI | matrix-assisted laser desorption ionization |
| MCE | microchip capillary electrophoresis |
| MD | microdialysis |
| SRM | single reaction monitoring |
| MS | mass spectrometry |
| MWP | microwell plate |
| NE | norepinephrine |
| nESI | nanoelectrospray ionization |
| NMR | nuclear magnetic resonance |
| PFD | perfluorodecalin |
| QQQ | triple quadrupole |
| QTOF | quadrupole time-of-flight |
| Rh6G | rhodamine 6G |
| RPLC | reversed phase liquid chromatography |
| RSD | relative standard deviation |
| S/N | signal-to-noise ratio |
| SD | standard deviation |
| SFME | slug flow microextraction |
| SFNE | slug flow nanoextraction |
| SPE | solid-phase extraction |
| SPME | solid-phase microextraction |
| SU | synthetic urine |
| TE | terminating electrolyte |
| tITP | transient isotachopheresis |
| TOF | time-of-flight |
| UV | ultraviolet |
| V _R | volume ratio |
| WT | wild type |

List of Appendices

| | |
|--|-----|
| Appendix 1: Supporting information for Chapter 3 | 125 |
| Appendix 2: Supporting data for Chapter 3 | 127 |

Abstract

Mass spectrometry (MS) has advantages as an analytical technique including label-free detection, high degrees of specificity and selectivity, capability for simultaneous monitoring/determination of numerous analytes, and rapid ionization/analysis, though throughput and sensitivity improvements are regularly sought. As a result, MS is commonly interfaced with different technologies including separations. Capillary electrophoresis (CE) is often selected over liquid chromatography(LC) for advantages including low volume requirements and faster separations, though online preconcentration is often necessary to improve limits of detection (LODs). In this work, a powerful preconcentration technique is paired with CE-MS to obtain LODs down to 10 pM, addressing the sensitivity limitation. Preconcentration here was shown to improve LODs by 5000-fold compared to a typical hydrodynamic injection for CE-MS. This method was applied for simultaneous determination of seven neurochemicals in biological samples with an excellent linear dynamic range (pM- μ M).

To improve throughputs, microfluidic sample introduction, especially droplet microfluidics, has shown promise for use with electrospray ionization (ESI)-MS, demonstrating sample introduction rates up to 30 Hz and droplet sizes down to 65 pL.^{1,2} In this dissertation, several droplet microfluidic assays are developed and paired with nanoelectrospray ionization (nESI) or ESI (droplet-nESI) for high throughput analyses. In one method, 5 nL droplets are generated at the end of a microdialysis probe to achieve temporal resolution near 10 s, substantially better than a standard LC-MS analysis with 5–20 min temporal resolution with microdialysis, offering much deeper insight into neurochemical dynamics. Using low flow nESI with MS/MS to

overcome ionization suppression, we achieve low nM LODs (down to 2 nM) for simultaneous monitoring of seven neurochemicals, including trace neurotransmitters. This was applied to monitoring neurochemical dynamics in mouse brains in response to multiple drugs.

In another method, droplet-nESI is used for high throughput screening in a directed enzyme evolution workflow. Directed evolution can provide much higher reaction yields, but screening can take weeks. Here, droplets are generated from well-plate reactions and infused into a sensitive nESI-MS/MS method to measure reaction yields with product LODs down to 12 nM. Over 1700 reactions (> 550 in triplicate) are screened in a single day, and over 1700 reactions (in triplicate) are screened in total. Seven enzymes with higher enzymatic activity are identified while achieving 10-fold higher throughput than LC-MS.

Finally, a new mode of liquid-liquid extraction is developed called slug flow nanoextraction (SFNE) that uses only 5 nL of each phase per extraction, and partitioning equilibrium is reached within seconds while flowing in-line with a detector. This was applied for online sample clean-up of pharmaceuticals from biofluids in-line with MS/MS analysis, demonstrating nearly 20-fold-improvements in detection sensitivity with up to 60 extractions performed during a single infusion. Furthermore, an entirely online and automated system is developed for SFNE. This system is applied to screen 21 octanol-water partition coefficients (K_{ow}) within 2 hr. K_{ows} are an important physiochemical characteristic for understanding drug bioavailability, though current measurements are low-throughput. In a comparison, the developed method offers 10-fold higher throughput and 40-fold lower volume requirements than a typical workflow.

The work described in this dissertation, though diverse, pushes forward what can be performed with mass spectrometry and bioanalysis. Each chapter introduces an analytically novel

or innovative approach for the analysis of small molecules that advances important fields of research including physiochemical characterization, high throughput screening with mass spectrometry, and sensitive bioanalysis.

Chapter 1

Introduction

Understanding the role of small molecules in biological systems is crucial for progress in pharmaceutical development, diagnostics, and for a deeper understanding of many diseases and behaviors and their physiological implications (Figure 1-1).³⁻⁵ Due to the broad presence of small molecules, fields of research for a variety of small molecule classes have rapidly grown over the past decades, with special emphasis on metabolomics and lipidomics.^{6,7} These alone accounts for over 100,000 different small molecule compounds according to HMDB.⁸

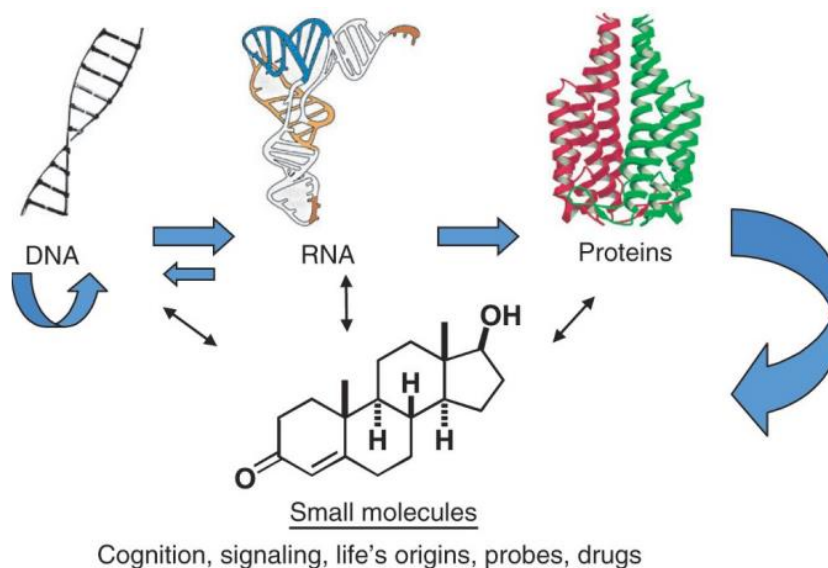


Figure 1-1: Illustration of the ubiquity of small molecules throughout the central dogma of biology. Adapted from Schreiber, 2005.

1).³⁻⁵ Due to the broad presence of small

molecules, fields of research for a variety of small molecule classes have rapidly grown over the past decades, with special emphasis on metabolomics and lipidomics.^{6,7} These alone accounts for over 100,000 different small molecule compounds according to HMDB.⁸

The growth of these fields has led to the development and application of many different instruments to monitor and measure small molecules, including NMR, LC-MS, GC-MS, CE-MS, and various modes of direct MS.⁷⁻¹² Though each method has advantages, LC-MS has become the 'gold standard' for metabolomics and lipidomics due to its quantitative capabilities, variable throughputs, automation, excellent metabolite coverage, and minimal sample preparation.¹³

Utilizing a robust analytical separation technique such as HPLC before MS allows for a separation of small molecules from complex biological mixtures before detection allowing for more potential analytes to be identified, improved selectivity, and a better dynamic range. While separations like LC improves the ability to distinguish two similar analytes (a.k.a. selectivity), MS as a detector allows for a high degree of specificity, often allowing compounds to be unambiguously identified from a complex mixture.

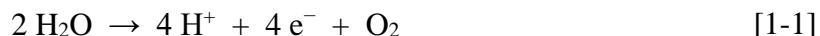
Despite the numerous advantages of LC-MS in small molecule workflows, it has several shortcomings. These shortcomings include relatively large sample volume requirement ($> 5 \mu\text{L}$), relatively low throughputs/long analysis time, and difficulty separating highly polar compounds (for RPLC). CE-MS is another important tool used for small molecule analysis that has many functional similarities to LC-MS, as well as some key advantages. Like LC-MS, CE-MS has become popular in metabolomics due to its automation, minimal sample preparation, variable throughputs, and excellent metabolome coverage, where CE-MS has been used to analyze biofluids and identify hundreds of metabolites per separation.^{12,14,15} CE-MS has many advantages to LC-MS, especially for metabolomics where electrophoresis is more suitable than RPLC for separating small, polar, charged analytes. Other advantages include low sample volume requirements, low buffer/solvent consumption, potential for rapid separations (ms – min), high efficiency/peak capacity, and the availability of various preconcentration techniques. Despite these advantages, CE-MS typically has poor detection sensitivity, and application of preconcentration techniques, though functional, can affect separation speed and/or resolution in the separation.

Though LC-MS and CE-MS have many strong applications and uses, alternative mass spectrometry methods have gained popularity to overcome the shortcomings of LC-MS and CE-MS, or even to use as complementary methods.^{10,16,17} Mass spectrometry is a versatile detector and

analyzer due to its various possible combinations of ionization sources, mass analyzers, and front end separation/automated sample introduction techniques. Specifically, implementing ESI/nESI for ionization can provide much utility and has many advantages.

Electrospray Ionization and Suppression

Electrospray ionization is a robust technique, where an aqueous phase flows through a narrow piece of silica or metal ESI emitter to ensure analytes are charged and transfer analytes to the gas phase. As the flow reaches the narrowed tip of the emitter, a strong electric field from an applied voltage disperses the liquid into a fine mist of strongly charged droplets from the presence of excess small cations (H^+ , Na^+ , etc.) These excess cations are rapidly generated by electrochemical reactions occurring at the emitter tip, such as:



where the ESI source acts as an electrochemical cell.¹⁸ According to the ion evaporation model (IEM) for small molecules, these micrometer diameter droplets from the initial mist shrink due to solvent evaporation/desolvation and coulombic repulsion induced fission events - due to the strong charge within the droplets - until they have reached the size of several nanometers and can successfully eject gas-phase ions due to coulombic repulsion to be mass analyzed (Figure 1-2).¹⁸⁻
²⁰ These ejected gas-phase analytes are often lightly solvated and solvent molecules are generally removed as the ions enter the MS.²¹ Although, solvation of the ejected ion is often minimal or excluded when working with entirely aqueous solutions due to the high surface tension of water.

Being a flow-based ionization technique for liquid-phase samples, ESI has distinct advantages. ESI can be readily paired with liquid-phase separations, such as LC and CE – though CE presents additional challenges – as well as with automated sample introduction such as robotic

instrumentation (i.e. Agilent Rapidfire) or droplet microfluidics.^{22,23} Electrospray ionization is rapid, allowing for samples to be analyzed within seconds, and its ability to continuously ionize sample allows for constant sample introduction, or even to be paired with a continuous sampling

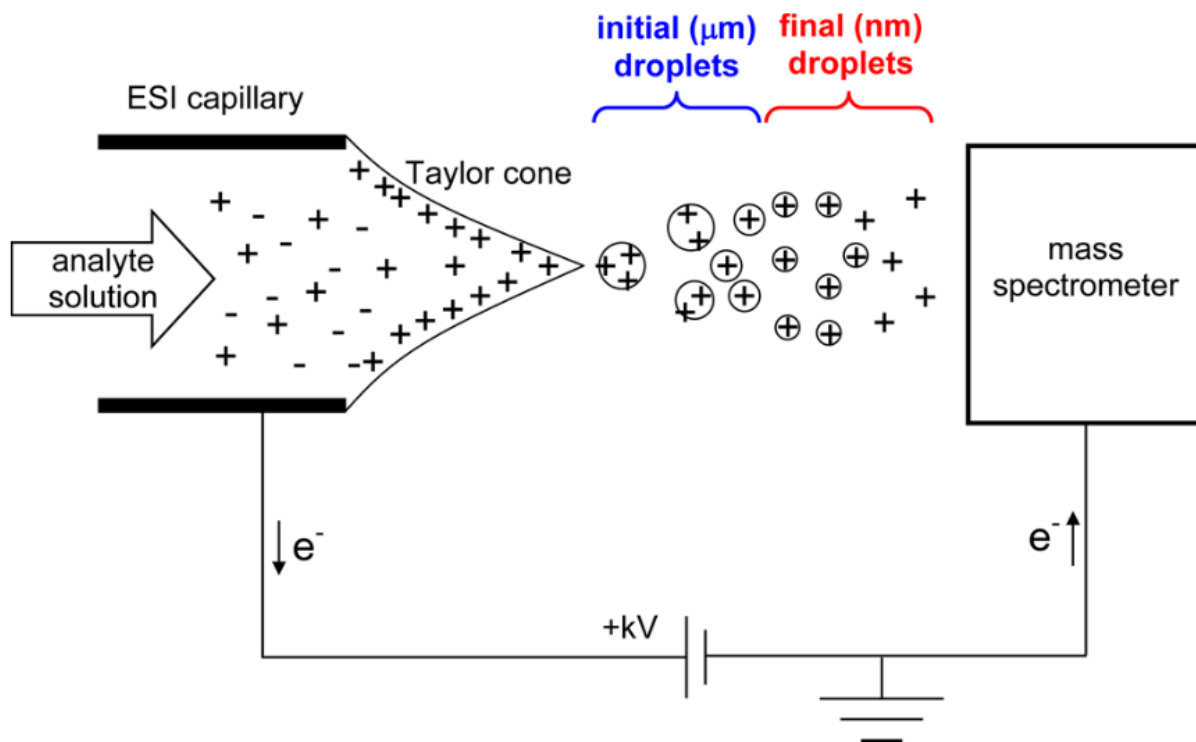


Figure 1-2: General mechanism of electrospray ionization and desolvation and the ESI circuit. *Adapted from Konerman et. al., 2013*

technique such as microdialysis.²⁴

A disadvantage of ESI is ionization suppression. Ionization suppression occurs readily in ESI due to several factors that hinder analytes either from gaining surface activity and charge or from properly desolvating.²⁵ The main matrix effects that cause suppression are attributed to the presence of nonvolatile compounds, high concentration solutes, and competition for charge/surface activity from other present compounds.²⁵⁻²⁷ Low molecular weight species ionize during ESI via IEM, where lightly solvated ions are ejected from a sufficiently evaporated nanodroplet surface due to its high electric field.²⁸ Figure 3 shows a theoretical distribution of compounds and charge within a nanodroplet. Observation of a molecule by a mass spectrometer

is dependent on the molecule gaining surface activity within the nanodroplet and gaining or maintaining charge (via proton or other cation adducts), where it can be ejected into the gas phase and reach the detector. The likelihood of a specific molecule to ionize from a given solution is known as its ionization efficiency (ϵ):

$$\epsilon = \frac{\text{ions/sec}_{\text{detector}}}{\text{molecules/sec}_{\text{emitted}}}$$

where ϵ is equal to the ions detected per second over the total analyte molecules emitted per second.²⁹ The presence of any previously mentioned negative matrix effects, namely those impairing an analyte's opportunity to gain surface activity, charge, and ejection, can drastically reduce an analyte's ionization efficiency and have been shown to reduce signal intensity [1-2] by up to two orders of magnitude.³⁰

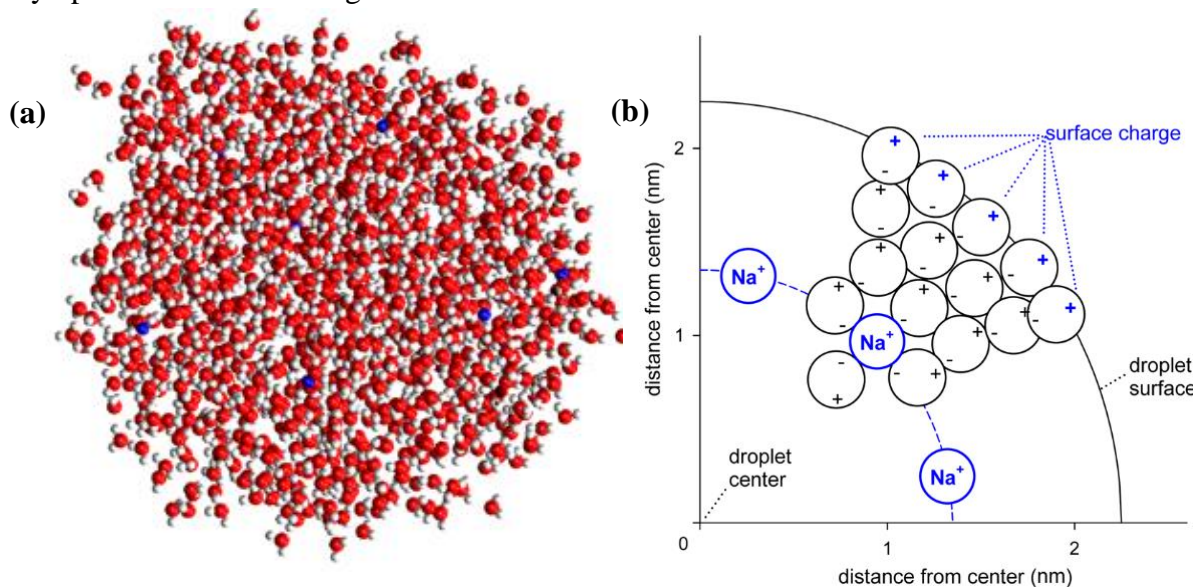


Figure 1-3: (A) Simulated image of a water nanodroplet (O red; H white) containing 10 Na⁺ ions (blue). (B) Illustration of the distribution of ions and water dipoles inside a nanodroplet, showing the effect of competing solvation requirements and dipole distribution on cation positioning within a nanodroplet. Adapted from Konermann, et. al., 2013.

ESI Sensitivity and Detection

Electrospray ionization paired with mass spectrometry has powerful advantages for analysis and detection such as a high degree of specificity and resolution, rapid analysis times, and

label-free capabilities; however, it often has relatively high limits of detection (LOD). High LOD can be especially challenging when working with biological samples and endogenous small molecule analytes. Ionization suppression due to matrix effects is highly present in complex mixtures, such as biofluids, due to the presence of high salt concentrations, proteins, hydrophobic compounds, and a myriad of other compounds present in varying concentrations. These competing matrix effects can make the detection of low concentration analytes difficult or impossible.³¹ Several techniques have been used to overcome ionization suppression and improve upon the relatively low ionization efficiency of standard ESI. These techniques include liquid-phase extractions, solid-phase extractions, front-end separations, and nESI with lowered flow rates. Utilizing different forms of ESI or similar modes of ionization is one way to improve detection limits, the most notable of which is nanoelectrospray ionization (nESI), which can greatly improve ionization efficiency and reduce matrix effects for improved LODs.³²

Using lowered flow rates (nL/min) and smaller diameter emitters ($< 50 \mu\text{m}$) is a variation of electrospray ionization deemed nESI that has been shown to drastically reduce ionization suppression and improve ionization efficiency, among other benefits.^{29,33} These improvements mainly occur due to the generation of smaller initial droplets during electrospray ($< \mu\text{m}$ diameter) resulting from the lower infusion flow rates and smaller tip diameters. Smaller nanodroplets offer a larger surface area-to-volume ratio, increasing the opportunity of a given ion to gain surface activity by providing increased accessible surface area and reduced distance from the droplet interior to the surface. These differences can greatly benefit complex matrices which often have many molecules competing for surface activity. It has been shown that lowering the flow rates substantially alleviates ionization suppression, and suppression is essentially absent once flow rates have reached 20 nL/min.³⁴ Theoretically, the lower the flow rate and spray tip diameter, the

smaller the resulting nanodroplets will be. Using nESI can also drastically improve the base ionization efficiency (ϵ). For example, in a study comparing conventional ESI to nESI, ϵ of 0.0005% was obtained for ESI and ϵ of 0.26% was obtained for nESI, a 512 fold-improvement by nESI.³⁵ The ϵ can be further improved through the use of even lower flow rates, where ϵ of 5% has been achieved when working near 1 nL/min infusion rates, and ϵ up to 12% was reported.²⁹ nESI offers several advantages including increased overall ionization efficiency, higher efficiency for completely aqueous solutions, reduced sample volume requirements, and minimized ionization suppression,^{34,36} and it has grown rapidly in popularity and implementation since its development in 1994³⁷ due to these abundant advantages. Additionally, nESI has facilitated MS interfacing with low flow techniques such as capillary electrophoresis.³⁸

Another common method for improving LODs by ESI-MS is to perform an extraction to cleanup samples before ESI. Sample cleanup is often executed using offline liquid-liquid extractions or solid-phase extractions before analysis.^{39,40} The utility of extractions for MS has led to the development of many extraction techniques for improving MS sensitivity including online SPE/SPME, coated blade spray ionization, packed-ESI tips, parallel artificial liquid membrane extraction, and others.⁴¹⁻⁴⁵ Other than extractions, other pretreatments such as using sample additives, dilutions, or chemical derivatization⁴⁶ can effectively improve LODs by improving ionization efficiency or reducing the strength of matrix effects.

The implementation of LC or CE prior to ESI-MS is another common and effective way to improve LODs, especially when exploiting their ability to perform preconcentration on samples before MS analysis. LC-MS performs preconcentration using its ability to load several column volumes worth of sample onto the front of the packed bed, offering drastically improved LODs over direct ESI-MS or lower volume LC-MS injections.⁴⁷ CE, on the other hand, is notorious for

providing insufficient LODs in many applications, especially with UV-Vis absorbance and MS detection due to small pathlengths and minute injection volumes. While capillary zone electrophoresis (CZE) alone paired with ESI-MS struggles with sensitivity, there is an abundance of applicable CE sample cleanup and preconcentration techniques.^{48,49} Several online sample cleanup techniques have been used with CE-MS. These techniques, such as microelectromembrane extractions and polarity reversing, function by desalting the sample, allowing for reduced ionization suppression.^{32,50}

Additionally, dozens of online CE preconcentration techniques exist, which can provide signal enhancement by up to four orders of magnitude.^{48,49} Many of these techniques have been paired with ESI-MS, and have been shown to offer up to a three order of magnitude improvement in LODs when paired with ESI-MS.⁵¹ CE can also offer benefits due to its inherently low flow rates, making it highly suitable for pairing with nESI. This allows for efficient separation while benefiting from the improved ionization efficiency of nESI.⁵² Furthermore, preconcentration can be combined with CE-nESI-MS for even further enhancements.

All of the techniques described above have been used to improve LODs and sensitivity of ESI-MS. The use of some of these techniques has allowed for LODs down to the pM range by ESI-MS. ESI is continually explored and improved upon due to its many advantages as an ionization technique, as previously mentioned. Another one of its important advantages is the potential for rapid analysis and high throughput sample introduction for mass spectrometry.

ESI Throughput

Electrospray ionization is a rapid ionization technique, able to emit thousands of molecules per second with flow rates in the mL/min range, with the evaporation process requiring only

milliseconds.^{29,53,54} Consequently, ESI has become an important ionization technique for rapid analysis, able to interface with many different instruments and techniques for improved sample introduction rates.⁵³ Being a liquid phase and flow-based ionization source, ESI is often paired with LC. However, despite its core importance across many analytical applications, LC-MS has a couple of prominent limitations. These limitations most importantly include large sample volume requirements ($> 5 \mu\text{L}$) and low throughputs. LC separations can take minutes to hours to perform, making it very low throughput compared to more rapid separations or sample introduction techniques. Some research has been done to improve LC-MS throughputs while maintaining reasonable peak capacity, including implementation of overlapping injections, multiplexing, and employing fast gradients;⁵⁵⁻⁵⁷ however, these techniques are not always applicable and still require tens of seconds to minutes per sample.

Using CE with MS can overcome LC-MS limitations to some extent, using nanoliters of sample per injection and the ability to achieve faster separations.^{15,58} CE-MS also overcomes some of the selectivity limitations of LC-MS, specifically in that CE can efficiently separate the charged, polar compounds that RPLC inherently struggles with. CE-MS also offers the advantage of a variety of preconcentration techniques that can be applied to enhance detection sensitivity. Furthermore, microchip electrophoresis (MCE) has gained popularity due to its ability to achieve millisecond separations, high efficiency, and high throughput sample introduction.^{59,60} More recently, MCE has been paired with MS, presenting unique features including integrated ESI emitters, device arrays, on-chip sample preparation/treatment, high throughput sample introduction, and minimal sample volume requirements for CE-MS.⁶¹

Though advances have been made to improve LC-MS and CE-MS throughputs, direct ESI-MS can achieve much higher throughputs as it does not require a potentially time-consuming

separation prior to sample introduction. The perpetually increasing demand for improved throughputs by ESI-MS has led to the development of many different commercialized and

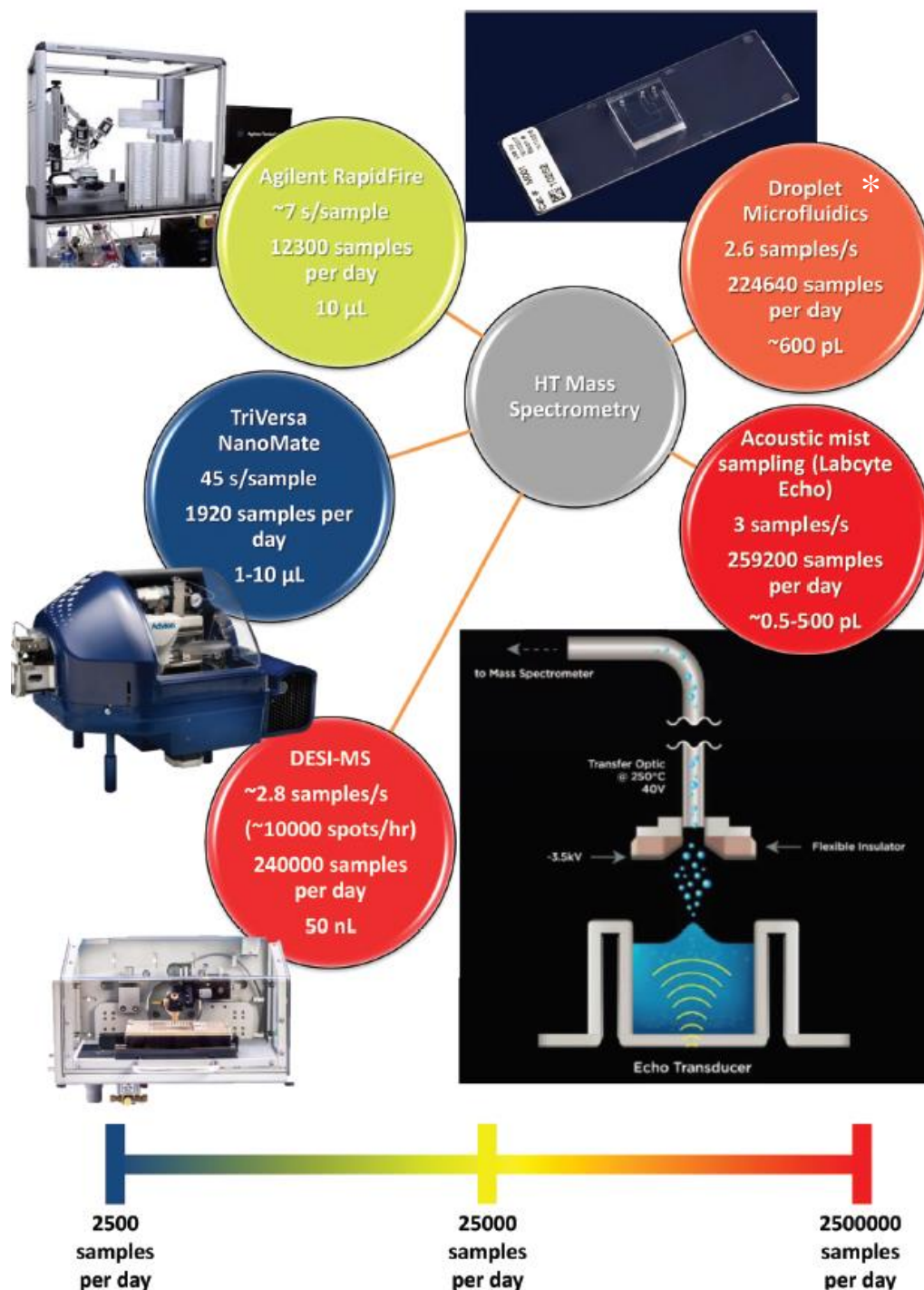


Figure 1-4: Comprehensive overview of high throughput sample introduction methods/instruments using ESI or alternative ionization techniques as of July 2018. Adapted from Kempa. et al., 2019. *Droplet microfluidics for sample introduction has since been reported with substantially higher sampling rates, up to 30 Hz.

homebuilt autosamplers and other sample introduction systems (Figure 1-4). Commercialized systems such as the Agilent RapidFire have become popular as they can introduce samples at a rate of 7 s/sample, which includes the draw, spray, and rinse times while remaining automated. They often even incorporate automated SPE steps during the sample introduction, allowing for improved sensitivity and limits of detection for samples without manual sample preparation.⁶² These systems are robust and easy to operate; however, they are extremely expensive and still on the scale of ~0.1 Hz or lower for sample introduction.

Alternative forms of ionization that function similarly to ESI have been used to improve throughputs for MS. Examples include desorption electrospray ionization (DESI) and acoustic mist ionization (Figure 1-4). DESI functions similarly to ESI, where it emits a stream of charged solvent from an emitter, though this stream is aimed at a sample/surface which then emits subsequent secondary ions for mass analysis. DESI has been applied for high throughput screening and has been shown to achieve up to nearly 3 Hz from a spotted plate.⁶³ Acoustic mist ionization has also been used for HTS.⁶⁴ This technique is performed from a well plate, where acoustic energy is used to emit a fine mist of charged, micrometer-sized droplets from the solution in each well which then enters the mass spectrometer. Sample introduction and analysis can be done rapidly and has been shown to achieve throughputs up to 3 Hz. Though new techniques are constantly being developed, these are the most notable recently developed ionization techniques for use with high throughput screening (HTS) by MS.

Recently, droplet microfluidics paired with ESI-MS has shown promise due to a variety of advantages, including the capability to achieve high throughput analysis. It has been shown that sample introduction rates up to 30 Hz can be achieved, which was achieved using a QTOF with adjusted custom acquisition speeds.² However, extensive engineering was required and the

resulting method had a relatively high standard deviation. Despite several limitations in this report, it indicates the potential of droplet-MS as the fastest method of sample introduction for HTS by ESI-MS.

Droplet Microfluidics

In microfluidics, devices and tubing with micron-width channels are implemented for the miniaturization of a variety of analytical and biological applications. These devices are useful due to their ability to rapidly manipulate small volumes of fluid ($10^{-9} - 10^{-8}$ L), which can be used for studies on a cellular-sized scale, or even smaller.⁶⁵ Microfluidic technology has been used for developments in pharmaceuticals, drug design, diagnostics, chemical synthesis, and high throughput screening, among other applications.⁶⁶

Droplet microfluidics is a subcategory of

microfluidics that uses two immiscible phases flowing together within a microchannel.⁶⁷ Droplet microfluidics can offer higher throughputs and manipulate smaller fluid volumes than traditional microfluidics.

Droplets are generated, representing individual reaction vessels or samples, separated from one another by an immiscible “continuous” phase, such as air or fluorinated oil. Droplets range in

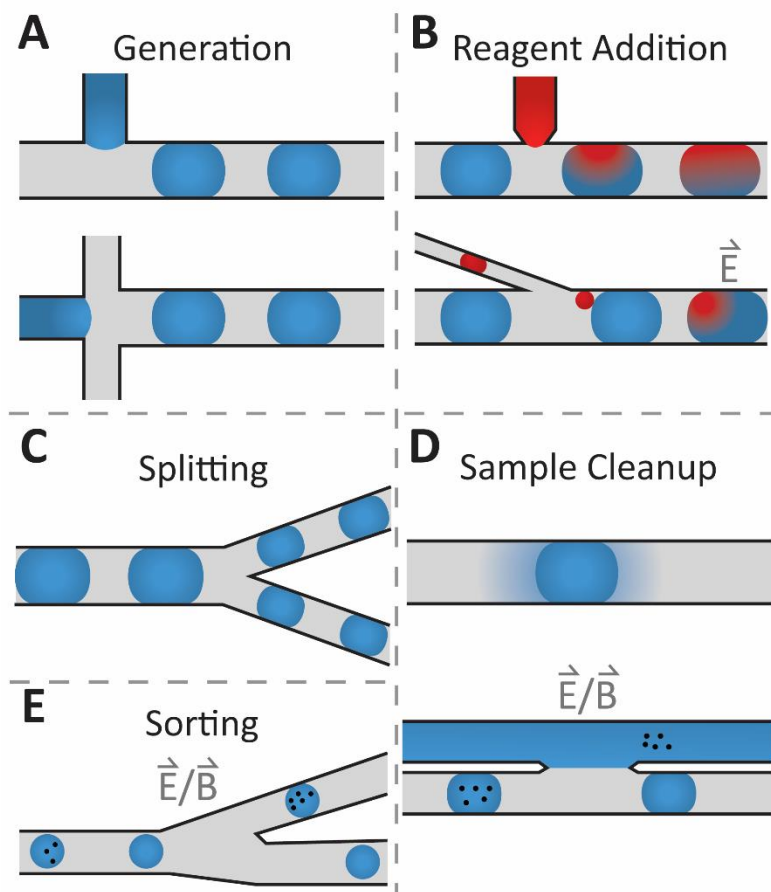


Figure 1-5. Illustration of the common droplet microfluidic operations. Adapted from Emory Payne et. al., 2020.

volume from single femtoliters to tens of nanoliters and offer many advantages including rapid mixing/mass transfer, short diffusion distance, extremely high throughputs/droplet generation rates, discrete samples/reaction vessels, and the ability to manipulate droplets and flow on-chip.⁶⁷ Microfluidic systems can be paired with many different analytical techniques,^{68,69} including various optical detectors, microscopy, and mass spectrometry, for rapid chemical analysis of discrete samples encapsulated in droplets.⁷⁰

Many microfluidic geometries allow for a variety of manipulations and operations to be performed on these droplets at high throughput (Figure 1-5).⁷¹ Droplet generation, a crucial aspect of droplet microfluidics, can be performed off-chip from a well plate or with an on-chip generator. Generating from a well plate has the advantage of easily profiling of a pre-prepared and large sample array. This mode is excellent for screening, as thousands of reactions can be run in parallel within well plates.⁷² The ability for tracking samples (droplets) in this mode drastically simplifies screening workflows compared to on-chip droplet generation, where screening libraries are generated stochastically.⁷¹ However, generation speed and quantity of tandem samples is limited in this mode due to vacuum-driven droplet formation and robotic handling. On the other hand, on-chip generation, as shown in Figure 1-5A, can reach much higher droplet generation frequencies (kHz).⁷³ Generating on-chip also facilitates droplet stabilization and storage for later use, as an abundance of droplets can be continuously generated and surfactant stabilized before being transferred to a storage vessel.⁷⁴

Reagent addition is another important unit operation in droplet microfluidics. The composition of each droplet can be altered by adding a different solution to each droplet. The most common methods for adding reagent are picoinjection/direct injection, to add solution directly from a perpendicular channel, and droplet coalescence, to merge adjacent droplets.⁷⁵⁻⁷⁸ Additions

can be performed at high throughputs (kHz) and offer high delivery volume precision.⁷⁶ Reagent addition can be used to perform dilutions, adjust the solution/solvent composition, or add reaction substrates/components to droplets. Microfluidic systems will often have several reagent addition channels in a device (up to three), allowing for several manipulations to occur in a single workflow.⁷⁹

Other droplet microfluidic manipulations include droplet splitting and droplet sorting. These functions rely on features built into the microfluidic device that can be controlled via applied flow or voltage. Splitting allows for a single droplet to be split, where often one portion is placed in storage and the other is sent to the detector. Volumetric split ratio is controlled by the relative dimensions of the channels that the droplets are split into and their relative flow rate/backpressure.⁸⁰ Droplet sorting allows droplets that meet certain specifications (i.e. presence or absence of a certain compound) to be sorted into a different channel than the others. This is typically done using a colorimetric or fluorescent indicator to select which droplets to sort.⁸¹ The droplets are sorted via electric field or magnetic field, where an activate field will allow droplets to be sorted into a different channel (Figure 1-5E).^{82,83}

The rapid processing, efficient mixing, short diffusion distances, and low volume attributes of droplet microfluidics have made the technique viable for miniaturization and throughput improvements in analytical methods and bioassays.⁷² One example is the use of droplet microfluidics for liquid-liquid and solid-phase extractions. Liquid-liquid extraction techniques have been developed using extraction phase as the carrier fluid to allow for extractions to occur as the droplets flow, facilitated by rapid mass transfer.⁸⁴⁻⁸⁶ These systems have been used to study extraction dynamics and as an analytical tool for low-volume sample cleanup. Droplet microfluidic solid-phase extraction systems have also been developed for sample cleanup. This is often done

utilizing functionalized magnetic solid-phase particles, which can retain different target analytes depending on the type of functionalization.^{83,87,88} Several operations can be easily performed on the magnetic particles before and after retaining analytes, including dispersing, immobilizing, and washing of the particles.⁸⁹ This allows for complete SPE procedures to be integrated into the droplet microfluidic system, with rapid and low-volume extractions.

Droplet microfluidics has been used for the miniaturization of many other bioanalytical tools and bioassays as well. Some of the recent and notable adapted bioassays include RNA sequencing, directed enzyme evolution, cell profiling, and digital PCR.⁹⁰⁻⁹² Droplet microfluidic platforms have been used to offer improvements in bioanalysis as well. This includes applications to biomarker discovery, small molecule detection, macromolecule analysis, single-cell analysis, high throughput screening, and even development of droplet-MS technology.^{72,93-95} Droplet-MS, the coupling of various droplet microfluidic platforms to mass spectrometry, has gained significant momentum over the past decade due to its high information content, label-free capabilities, and capacity for high throughput analysis.

Droplet-Mass Spectrometry

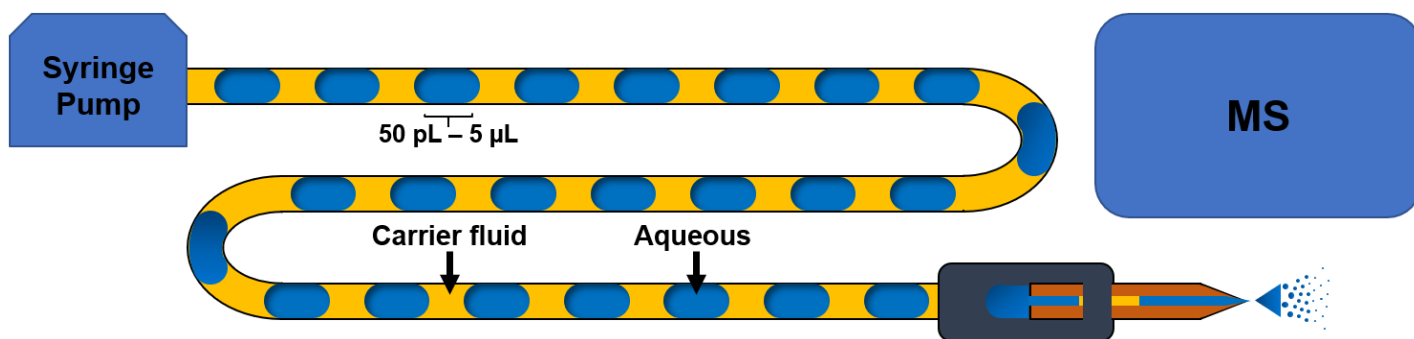


Figure 1-6: Illustration of general droplet microfluidics being paired with ESI-MS. Specific labels provided for the different fluids present and potential droplet volume ranges.

Laser-induced fluorescence is one of the most common detectors for droplet microfluidics due to its low LODs and fast acquisition rates, making it highly compatible with the low volumes

and high frequencies encountered in droplet microfluidics.⁷¹ However, LIF efficacy is dependent on fluorescent analytes, which requires naturally fluorescent compounds or a fluorescent labeling procedure before detection. Coupling MS detection to droplet microfluidics, though less sensitive and having slower acquisition speeds, can provide much more information per droplet than optical detectors and is a widely applicable, label-free detector.⁷⁰ These advantages make droplet-MS much more suitable for analysis of complex mixtures and biological samples than droplet microfluidics paired with optical detection.

As shown in Figure 1-6, droplet microfluidics can be paired with ESI by simply attaching the line of flowing droplets to an ESI or nESI emitter. The applied electric field will spray and ionize the aqueous/sample droplets as they reach the emitter tip, but the electro spray will stop as the non-conductive carrier fluid reaches the tip and temporarily breaks the ESI circuit. This process allows

for rapid introduction of an array of droplet samples or a continuously generated flow of droplet samples by ESI without signal interference from the carrier fluid (Figure 1-7). As a “train” of

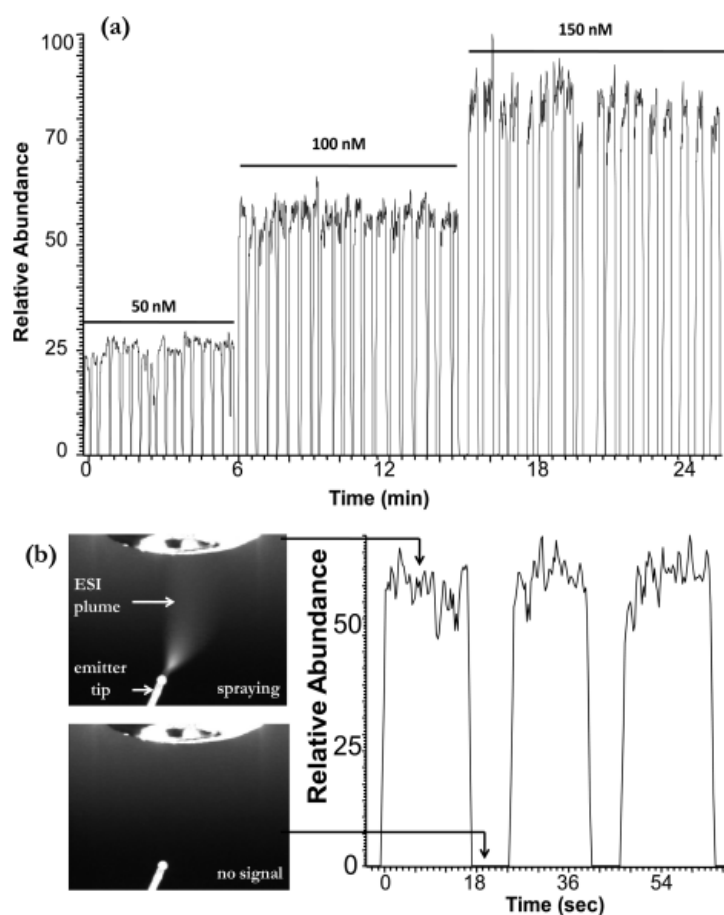


Figure 1-7. (A) Resulting MS data corresponding to droplet-ESI-MS/MS of various concentrations of leucine-enkephalin. (B) Image of the ESI emitter at various times during droplet infusion (1. aqueous sample and 2. carrier phase at tip) and the corresponding MS/MS signals. Adapted from Pei, et. al., 2009.

assorted droplets are sprayed, each will produce an individual and discrete MS signal for the ion(s) being monitored, and there will be no signal as the carrier phase reaches the tip.⁹⁶

Droplet microfluidics paired with MS was initially reported in early 2009, where droplets were generated on-chip and analyzed by MS.⁹⁷ However, this method required removal of the carrier fluid before ESI by extraction of droplets into a continuous aqueous stream, compromising droplet discretization and causing sample dilution. Droplet microfluidics directly interfaced with MS was first reported in late 2009. Using an ion trap mass spectrometer, droplet-MS was able to achieve sample analysis rates of 0.8 Hz using 13 nL droplets (50:50 MeOH:H₂O, v:v) and air as the carrier fluid. Detection limits down to 1 nM were achieved for the target analyte using MS³.⁹⁶ Since this initial report, many improvements have been made to direct droplet-MS. Droplet sizes have been reduced as low as 65 pL for infusion, with rates up to 10 Hz. In a similar experiment reproducible sample signal was obtained for over 2.5 hours (Figure 1-8).¹ Sample analysis rates as high as 30 Hz have been reported.² Employing nESI emitters, droplet-MS has been used to directly analyze complex biological samples obtaining low nM LODs for biological compounds, and many compounds have been monitored simultaneously in experiments.⁹⁸ Droplet-MS has been used for a variety of applications, including high throughput screening, enzyme evolution, mass activated droplet sorting, neurochemical monitoring, and temporal resolution enhancement.^{1,23,24,98,99}

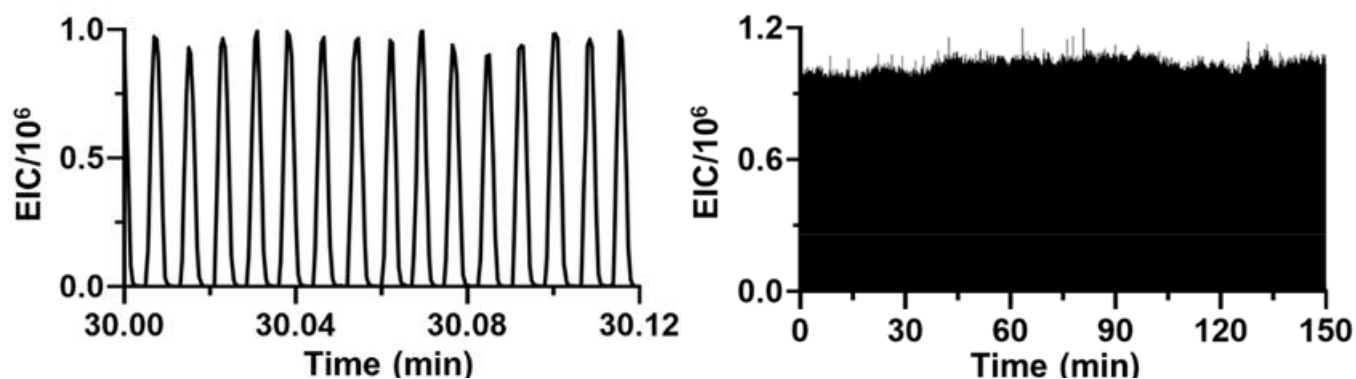


Figure 1-8. Droplet-MS data where a single mass transition is monitored for over 2.5 hr using 1.2 nL droplets. This accounted for over 20,000 individual droplets with RSD of 3.7%. Adapted from Steyer et. al., 2019.

Dissertation Overview

Given the constantly evolving features and applications of electrospray ionization and the techniques that can be interfaced with it, the work in this dissertation aims to develop new systems and manipulate/improve current systems revolving around improving throughputs and LODs with ESI-MS/MS. Chapter 2 focuses on improving the sensitivity and LODs of CE-MS, a technique in constant competition with LC-MS. In this work, we develop a powerful preconcentration technique that has rarely been reported to be interfaced with MS to overcome the significant LOD limitation of CE-MS. The preconcentration technique, electrokinetic supercharging (EKS), is developed with an emphasis on MS compatibility. EKS is compared to other notable preconcentration techniques paired with MS, and some of the fundamental principles of EKS are investigated including injection limitations and formation of a reported but not well-studied system-induced terminating electrolyte. The developed method is then applied to determine several neurotransmitters from biological tissue samples.

Chapter 3 improves upon an existing method that allows for the segmentation of microdialysate into ~5 nL fractions via droplet microfluidics for improvements to temporal resolution during neurochemical monitoring with MS/MS analysis. The initial reports using this method have several limitations, including a limited number of analytes monitored (up to 4) and insufficient LODs for many neurochemicals of interest. The work in Chapter 3 expands the range of the method, allowing for up to 7 neurochemicals (plus 7 internal standards) to be simultaneously monitored and the addition of important low abundance (low nM) neurotransmitter analytes including dopamine, serotonin, and adenosine. The method is applied to monitoring neurochemical

changes in rodent brains in response to drug stimulations, and the temporal information is compared to that obtained by LC-MS/MS.

Chapter 4 describes the development and characterization of a completely new method for rapid and low volume liquid-liquid extractions called slug flow nanoextraction (SFNE). SFNE is a multi-phase system developed utilizing the principles of droplet microfluidics to achieve rapid and in-line extractions while flowing through a capillary, where many extractions can occur simultaneously. SFNE was characterized by comparison to traditional extraction methods and previously reported equations to validate its performance. The developed method is applied to online sample cleanup for mass spectrometry. Here, the signal intensity by ESI-MS/MS with and without the use of SFNE is compared. SFNE was also applied for the determination of K_{ow} values and compared to the shake-flask method for K_{ow} determination.

In Chapter 5, SFNE is re-formatted to allow for continuous, online generation, and automated sample introduction. In this work, a microfluidic device is designed and fabricated that allows for the constant generation of distinct “phase-pairs” as three distinct phases are flowed into the device. The performance of the device is evaluated including the ability to rapidly adjust volume ratios, generation frequency, and the number of phases being used. The automation of sample introduction is investigated and achieved through pairing with an LC autosampler allowing for injections every 78 s. Finally, this method was applied for the screening of K_{ow} values for various compounds under different conditions from a well plate, screening 21 K_{ow} values in under 2 h.

Previously, we have reported studies using droplet microfluidics paired with nESI to screen samples or reactions from well plates. In Chapter 6, this set-up is used to provide a sensitive and high throughput method for the screening portion of a directed enzyme evolution workflow. To

increase the biocatalytic activity of a cytochrome P450 for biaryl coupling, the enzyme is selectively evolved to generate thousands of different mutations. The droplet-MS/MS method being applied in this work is capable of screening hundreds of reactions per day, greatly reducing the time required for this step of the enzyme evolution processes. In this work, the method is optimized for a balance of low LODs (for low initial yield) and high throughput. The method is finally applied to the screening of thousands of reactions (and enzyme variants) within the span of several days.

Chapter 2

CE-MS with Electrokinetic Supercharging and Application to Determination of Neurotransmitters

Reproduced from Wells *et al*, *Electrophoresis* **2019**, *40*, 2946–2953. Copyright 2019 WILEY-VCH Verlag GmbH & Co. KGaA, Weinheim

Introduction

CE and CE-MS have become a popular technique for the analysis of complex biological samples due to its efficiency, small volumes, and separation speeds. However, hyphenation of CE with MS has been difficult to achieve due to complications interfacing via ESI. There have been a variety ESI interfaces developed for CE-MS, both homebuilt and commercial, that have opened CE-MS to application in many fields including proteomics,¹⁰⁰ food science,¹⁰¹ drug analysis,¹⁰² genomics,¹⁰³ and more. CE-MS has more recently gained significant momentum in the fields of neuroscience and both target and untargeted metabolomics, as it can employ high efficiency separations from the limited volume often available for biological samples, and CE can often provide better separation for small, polar metabolites than RPLC.^{12,16}

There are currently two types of common CE-MS interfaces, each with particular advantages.³⁸ Sheathflow interfaces utilize coaxial conduits that introduce both solvent and gas flow along with the electrophoresis eluent to assist with ESI. The other common interface is sheathless, which can generate ESI or nESI directly from the separation capillary without assisted flows. Sheathless interfaces, as they offer zero dilution and can employ nESI, are often the most sensitive CE-MS interface; however, they can be more challenging to achieve and operate. One example is the use of sheathless CE-MS used for the determination of several amino acids and

metabolites with LODs down to 60 nM.¹⁰⁴ Though a low nM LOD may be an achievement for CZE paired with MS, these are relatively high LODs compared to other separation and detection methods. This is due to the small injection volumes encountered in CE, limiting the detectable mass. To overcome this limitation, preconcentration methods are often implemented for improving detection limits and sensitivity by CE-MS.

As previously discussed, a variety of online preconcentration techniques have been developed to improve the often poor detection sensitivity encountered in with CE separations. Some of the more common preconcentration methods include FASS, FASI, tITP, pH-mediated stacking, LVSS, and sweeping, though many other methods exist.^{48,105} Each preconcentration technique functions based on different principles, however the general mechanism is the concentration of disperse analyte molecules into a low volume zone by manipulating an analytes mobility. Many of these techniques have been used with CE-MS including FASI, dynamic pH junction, LVSS, and others.¹⁰⁶⁻¹⁰⁹ Field amplification based preconcentration techniques are the most effective and simple methods for achieving high sensitivity.¹¹⁰ The primary focuses of field amplified stacking techniques are to achieve the minimum possible bandwidth and to inject the maximum amount of analyte. Since most field amplified stacking techniques implement both principles simultaneously, these techniques can drastically improve LODs and maintain or improve separation efficiency.

Of the field amplification stacking techniques, EKS is the most powerful, having achieved over five orders of magnitude improve in detection sensitivity compared to a conventional injection.¹¹¹ EKS can achieve such drastic improvements since it combines both FASI and tITP, allowing injections to overcome limits on FASI, where the separation will rapidly lose efficiency as the amount injected is increased. By utilizing tITP after the FASI injection, the bands can be re-

concentrated during electrophoresis, allowing for a much larger initial injection. Since its 2003 introduction,¹¹² EKS has been combined with UV absorbance detection for several high sensitivity applications, including measurements of rare earth metals,¹¹³ environmental contaminants,¹¹⁴ protein complexes,¹¹⁵ DNA,¹¹⁶ peptides,¹¹⁷ and drugs.¹¹⁸ EKS allows for these analytes to be measured in low abundances.

EKS is achieved using the following steps as shown in Figure 2-1. First, a small plug of high ionic strength leading electrolyte is loaded into the separation capillary followed by a small plug of water which will act as the headspace. Next, a long and/or high electric field injection is performed. During this step, FASI occurs where the high mobility molecules preferentially migrate into the capillary. Once these molecules reach the LE boundary, they experience a significant decrease in mobility due to the lower electric field distributed across this higher ionic strength zone. This stacking principle allows for a long injection to take place before excessive band

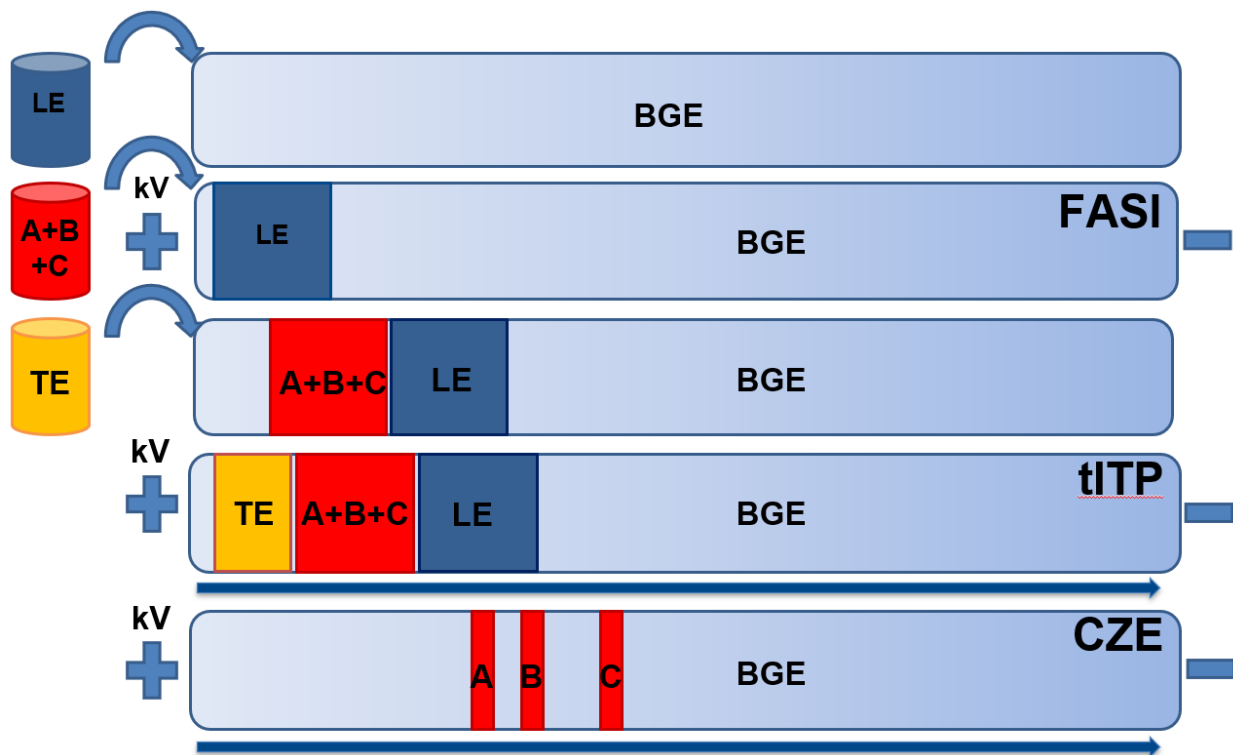


Figure 2-1: Illustration of the general scheme for EKS. Each of the steps are shown, where arrows indicate applied pressure for volume loading and +/- kV indicate applied voltage.

broadening occurs. Finally, a small plug of terminating electrolyte is loaded into the capillary and the separation voltage is applied for the remainder of the separation. Initially during this separation, tITP takes place. Due to the varying ionic strength and mobility of the LE and TE zones, the electric field is distributed as a gradient across the sample zone, allowing the analytes to further concentrate into discrete zones based on their respective electrophoretic mobilities. The presence of tITP allows for a longer FASI injection to occur, as the analytes zones will be further narrowed during this step. Eventually, the LE and TE will dissipate and CZE will occur for the remainder of the separation. To achieve the maximum amount of preconcentration, it is ideal to limit the movement of the LE stacking boundary during the injection step, which is commonly accomplished using counter-flow or environments for reduced EOF.¹¹³⁻¹¹⁶

Despite its powerful preconcentration, EKS has almost no reported work being interfaced with CE-MS. This is due to several challenges specific to EKS with CE-MS, including buffer compatibility, controlling flow, and maintaining robust CE ground at the ESI interface. Many common CE buffers such as phosphates, TRIS, borates, etc., are incompatible with MS. Mass spectrometers with ESI require volatile and non-suppressing buffers, limiting the buffer options when selecting the BGE, LE, and TE. This limited selection can affect the method design when attempting to achieve compatible LE and ionic strength requirements for stacking. Furthermore, suppression of EOF and analyte migration is important for attaining high detection sensitivity and efficiency, though counter-flow cannot be easily implemented with MS detection due to the presence of the ESI interface, as it is often used for EKS with UV detection. This makes flow control and reduce migration largely dependent on the buffer composition. For example, lowering the pH of the buffer can drastically reduce or even remove the EOF of the system, allowing for a much longer injection to be applied while still leaving sufficient capillary length for tITP and CZE.

However, this will come at the cost of overall separation speed and/or efficiency. Finally, maintaining a robust ground to the CE circuit is imperative for the continuous operation of the system. Maintaining ground has proven challenging when interfacing to MS via ESI, especially when using a preconcentration technique like EKS which generates highly concentrated zones that can cause significant fluctuations in conductivity. While using sheathflow, the sheath liquid contacting the migrating CE fluid grounds the separations, however, these concentrated ion zones can interfere with that ground and the stability of the ESI. Proper and robust operation of this interface requires careful selection of the buffer system, sheath liquid composition, and CE and sheath flow rates, as well as reliable assembly of the interface.

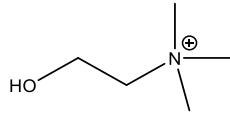
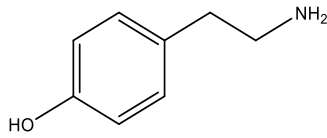
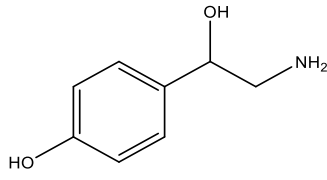
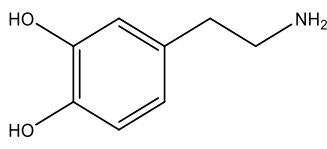
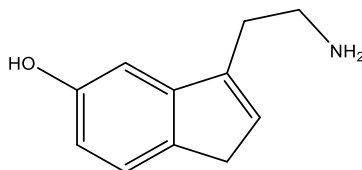
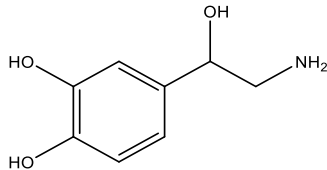
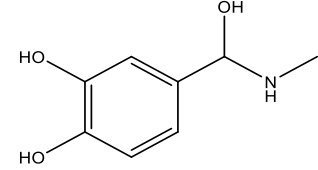
EKS with CE-ESI-MS was first reported in 2009,⁵¹ and has since been only reported once (excluding our study).¹¹⁹ In the original report, the method was able to achieve baseline resolution of five different hypolipidaemic drugs with 1000-fold-improvements in detection sensitivity compared to a “conventional” injection using FASS conditions. This was a novel report that pioneered the implementation of EKS preconcentration with CE-MS, showing that drastic LOD improvements can be obtained while having the unique benefits of MS detection; however, this method had several important limitations. This technique required regular disassembly of the CE-MS interface for capillary treatments with EOF reversal agents as well as an applied pressure during separation to produce and maintain the reversed EOF system to analyze the desired anionic compounds. These steps, along with the selected buffer systems/flows, compromise the robustness, maximum throughput, maximum injection duration, and efficiency that can be achieved using this method. One other method has been reported, where HDI, FASI, and EKI were all applied to for the analysis and preconcentration of three hormone variants by CE-ESI-MS/MS using a sheathless interface.¹¹⁹ This system was able to improve limits of detection for one of the analytes from the

$\mu\text{g/mL}$ to pg/mL range while using EKS, offering significant improvements in limits of detection. This report shows how powerful EKS preconcentration paired with CE-MS can be, especially when using a sheathless interface. However, this method has several limitations due to its use of neutral capillary coatings and applied separation pressure, compromising efficiency, resolution, and throughput, as well as its minimal EKS method development. As a result, when EKS conditions are used, one of the three hormone variants is no longer detected and the two remaining analytes are no longer baseline resolved, resulting in a poor separation.

In this work, we present a new method employing EKS with CE-ESI-MS/MS, as well as an investigation of the merit of a “system-induced” terminating electrolyte. This method provides an online system that uses a buffer system and pH allowing for a normal (cathodic) but highly suppressed EOF to allow for high sensitivity and efficiency without the use of capillary coatings/treatments and no necessary pretreatment of the aqueous samples as reported in previous studies. Omission of any sample preparation and capillary pretreatment steps allow for a more robust system with potential for higher throughputs that is broadly applicable to positively charged compounds. The use of a highly suppressed EOF allows much longer FASI injections and therefore lower LODs. EKS preconcentration here allows for 5000-fold lower LODs compared to a conventional HDI injection by CZE. This method was able to obtain detection limits as low as 10 pM in a 16-minute separation for seven different biogenic amine neurotransmitters.

In this study, the method is applied to the determination of seven different neurotransmitters in multiple types of tissue extracts (Table 2-1). Though EKS for determination of neurotransmitters has been previously reported,^{120,121} these methods have utilized techniques (i.e. counterflow) and buffer systems to achieve sufficient LODs that are incompatible with ESI-MS hyphenation. Due to their use of UV absorbance detection and applied pressure, these

Table 2-1: List of all compounds for which the EKS with CE-ESI-MS/MS method was developed. Molecular weight, pKa, structure and most sensitive mass transition listed for each compound.

| Compound | Abbreviation | M.W. (g / mol) | pKa value | Structure | Mass Transition |
|----------------|--------------|----------------|-----------|--|-----------------|
| Choline | Ch | 104.17 | n/a |  | 104 → 60 |
| Tyramine | TyrA | 137.18 | 9.66 |  | 138 → 121 |
| Octopamine | OA | 153.18 | 8.98 |  | 136 → 119 |
| Dopamine | DA | 153.18 | 9.27 |  | 154 → 137 |
| Serotonin | 5HT | 176.22 | 10.00 |  | 160 → 115 |
| Norepinephrine | NE | 169.18 | 8.85 |  | 152 → 107 |
| Epinephrine | EPI | 183.20 | 8.91 |  | 166 → 107 |

techniques have limited selectivity and specificity, and are limited in the number of neurotransmitters that can be simultaneously determined (three). Studying changes in the composition and distribution of neurochemical in the brain can lead to a better understanding of various behaviors and disease states. Measuring neurochemicals from tissues samples using our method will demonstrate the utility and power of the method to quantify various low concentration compounds from low volume samples.

Materials and Methods

Reagents and Materials. All chemicals and solvents were purchased from Sigma-Aldrich (St. Louis, MO, USA) unless stated otherwise. Formic acid (99%) was from Acros Organics (Geel, Belgium). Stable-isotope labeled internal standards were purchased from CDN Isotopes (Quebec, Canada). Neurotransmitter standards and internal standards were prepared in HPLC-grade water as 100 μ M and 100 nM stocks (respectively), aliquoted, and stored at -80 °C. The standard and internal standard aliquots were thawed daily (single use) and diluted for use. Standard mixes consisted of the seven neurotransmitters of interest and internal standard mixes of deuterated versions of the compounds of interest, excluding tyramine and octopamine. BGE contained 50 mM ammonium formate (pH 2.5) and 40% MeOH (v/v) and LE contained 250 mM ammonium formate (pH 2.5). Buffers were prepared fresh twice weekly, adjusting the pH by formic acid, sonicating for 10 min, and filtering through 0.45 μ m membrane filter. Sheath-flow buffer contained 5 mM ammonium formate and 50% MeOH (v/v).

Instrumentation. Electrophoretic separations were performed on an Agilent 7100 Capillary Electrophoresis System using Agilent Masshunter software for CE-MS and Agilent ChemStation software for CE-UV. Electrophoresis experiments were performed in 80 cm of 50 μ m inner diameter (id) and 360 μ m outer diameter (od) fused silica capillaries coated with

polyimide from Polymicro Technologies (Phoenix, AZ, USA). New capillaries were treated by flushing the capillary with 1 M NaOH for 20 min, HPLC-grade water for 5 min, and BGE for 10 min. ESI was carried out using an Agilent CE ESI-MS Sprayer and an Agilent 1260 Infinity Isocratic Pump to control the sheath-flow. MS detection was performed on an Agilent 6410 Triple Quadrupole, using Agilent Masshunter software.

Injections and Preconcentration. HDI. The capillary was filled with BGE. A short plug of HPLC-grade water was introduced at the inlet at 50 mbar for 1 s. Sample was injected at 50 mbar for 65 s to fill 5% of the capillary volume. A separation of 30 kV was applied. **EKS.** The capillary was filled with BGE, and a plug of LE was injected at 50 mbar for 30 s. A plug of HPLC-Grade water was hydrodynamically introduced at the inlet at 50 mbar for 1 s. Sample was then injected electrokinetically at 30 kV (375 V cm^{-1}) for 150 s. A separation voltage of 30 kV was applied. **FASI.** The capillary was filled with BGE. A short plug of HPLC-Grade water was hydrodynamically introduced at the inlet at 50 mbar for 1 s. Sample was then injected electrokinetically at 30 kV (375 V cm^{-1}) for 30 s, (injections ranged from 5 – 50 s for comparisons). A separation voltage of 30 kV was applied. **FASS.** The capillary was filled with BGE. A short plug of HPLC-Grade water was hydrodynamically introduced at the inlet at 50 mbar for 1 s. Sample was then injected hydrodynamically at 50 mbar for 195 s to fill 15% of the capillary volume (injections filling 5 – 25% capillary volume tested for comparisons). A separation voltage of 30 kV (375 V cm^{-1}) was applied.

ESI-MS. For ESI, sheath liquid flow rate was set to $10 \mu\text{L min}^{-1}$ and nebulizer gas flow at 12 psi. Drying gas was used to assist with desolvation with a flow rate of 8 L min^{-1} at 300 C. The electrospray potential was set to 4 kV. For MS, single reaction monitoring (SRM) mode was used to enhance specificity. Precursor ions were selected in quadrupole one and product ions in

quadrupole three for each compound (Table 1-1) and collision energies were optimized to produce the highest abundance of each product ion with dwell times of 200 ms. The source and drying gas temperature was 250 °C.

Sample Preparation. Rat Brain Stem. Homogenate was prepared from a whole rat brain stored at -80 °C. After thawing, the brain stem was sliced off and homogenized using a pestle homogenizer in a vial with cold ACN (10 $\mu\text{L mg}^{-1}$). The homogenate was centrifuged $13 \times 10^3 \times g$ for 5 min, and the supernatant was collected. The supernatant was dried with nitrogen and resuspended in water (10x original volume). The sample was then aliquoted (100 μL aliquots) into vials which were subsequently frozen and stored at -80 °C until analysis. After thawing, 1% internal standard (v/v) was added prior to analysis. **Whole Fly.** Homogenate was prepared by homogenizing 10 whole *Drosophila* (male) in 150 μL of cold ACN, centrifuging, and removing the supernatant. Aliquots were stored at -80 °C until day of analysis. After thawing, 1% internal standard (v/v) was added and they were dried with nitrogen and resuspended in water (same volume) for immediate analysis.

LC-MS/MS Analysis. Chromatographic separations were conducted using a Waters nanoAcquity UPLC using a 1.0 x 100 mm column with HSS T3 1.8 μm particles interfaced to a mass spectrometer. Mobile phase A and B consisted of 5 mM ammonium formate with 0.15% formic acid and neat ACN, respectively. The gradient ran from 5% to 19% B in 0.01 min, 19% to 26% in 0.67 min, 26% to 75% B in 0.375 min, 75% to 100% B in 0.75 min, and stayed at 100% B for 0.1 min. The flow rate was set at 0.6 mL min^{-1} .

For LC-MS analysis of the brain stem homogenate supernatant (as prepared above, excluding internal standard addition), a benzylation reaction was implemented. Derivatization involved mixing 2 volumes of sample (aqueous supernatant) with 1 volume of 100 mM sodium

carbonate to raise the pH. Then 1 volume of 2% (v/v) benzoyl chloride in ACN was added followed by 1 volume of internal standard in 1% sulfuric acid (v/v) in 20/80 MeOH/water. The resulting mixture was analyzed by LC-MS. The internal standard mixture is comprised of analyte standards derivatized with the same procedure using C¹³ benzoyl chloride as the derivatizing agent.

Results and Discussion

Buffer Selection. Initial experiments for method development were performed using EKS with CE-UV and a smaller subset of our test compounds which included DA, NE, EPI, and 5HT. Experiments for buffer selection revolved around low pH and MS compatible electrophoresis buffers that would both facilitate ionization when paired with ESI and suppress EOF for preconcentration.¹²² EOF suppression is imperative for the EKS method developed to allow for a long electrokinetic injection without excessive migration of the stacking boundary or analytes down the capillary. Excessive migration during injection would lead to limited resolving power and lower separation efficiency for positively charged/higher mobility analytes. Twenty millimolar ammonium formate at a pH of 2.5 was initially selected due to its low pH buffer capacity and volatility for ESI compatibility. This initial selection did not allow for baseline resolution of all four compounds. To further suppress EOF and improve selectivity in the separation, methanol was added to the separation buffer and the ammonium formate concentration of this solution was increased to 50 mM to maintain the initially sought conductivity in the new buffer solution (Figure 2-2A). The final buffer consisted of 50 mM ammonium formate in water/MeOH (60:40, v/v) with pH 2.5 and provides resolution for all four compounds. The chosen buffer offers a highly suppressed EOF to allow for longer electrokinetic injections for preconcentration without diminishing resolution, all without the use of capillary treatments.

Selecting and implementing a LE and TE will provide conditions for EKS to occur, allowing for much longer injections. LE buffer was chosen by testing electrolytes sodium chloride and ammonium formate with 15 s electrokinetic injections (Figure 2-2B). Two hundred and fifty millimolar ammonium formate at pH 2.5 showed the best performance as a LE, with nearly double the peak signal of 100 mM NaCl (similar conductivity). On top of offering stronger signal improvement, ammonium formate is a more

compatible electrolyte for use with MS due to its volatility. To load the LE, 50 mbar is applied for 30 s to fill 2.3% of the capillary volume. This volume allows for a sufficient LE zone while having a negligible effect on overall separation current.

FASI Investigation. To determine the limitations of FASI, this preconcentration method was investigated with varying injection durations. FASI conditions can be met using the previously described buffer with extended electrokinetic injections and no leading electrolyte. Three different injection durations were tested including 10 s, 30 s, and 50 s injections to monitor and understand the changes in peak shape, peak height, and resolution between adjacent peaks as the injection

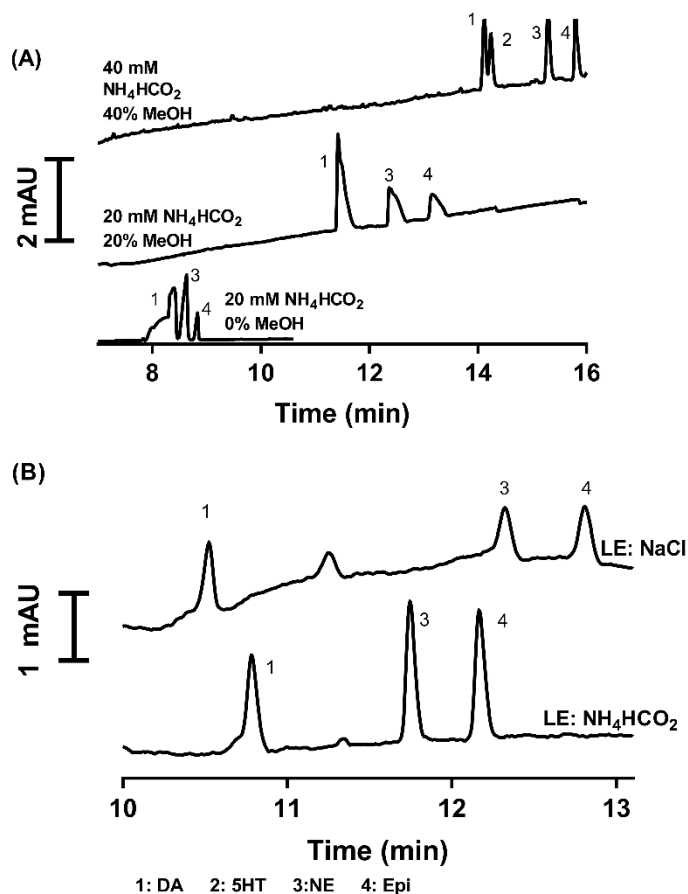


Figure 2-2: (A) Electropherograms of the different buffer systems tested for obtaining sufficient selectivity and resolution for 4 test compounds in a 20 kV 60 cm separation using CE-UV with HDI injections. (B) Comparison of two potential LE candidates using EKI in a 20 kV 60 cm separation.

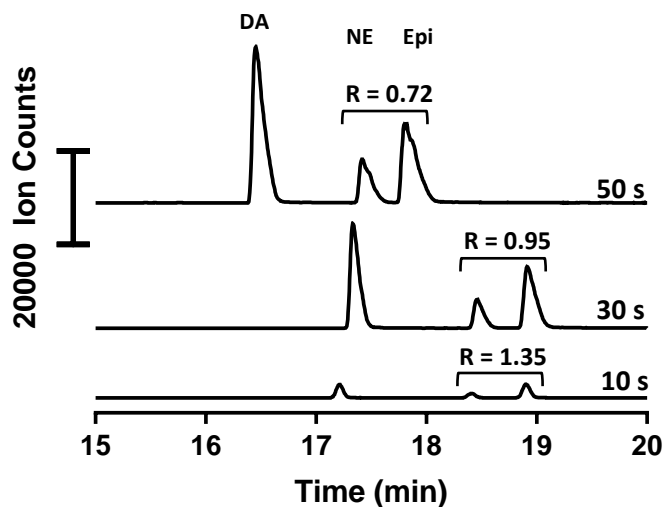


Figure 2-3: FASI injections performed at varying injection durations and the subsequent resolution changes between NE and EPI (100 nM). Injections performed at 30 kV in an 80 cm separation capillary. Resolution calculated using equation $R = (t_2 - t_1) / 0.5(W_{B1} + W_{B2})$

efficiency and without causing peak tailing as seen in Figure 2-3.

Terminating Electrolyte. Initially, 5 mM taurine was tested as the TE for tITP. The solution was loaded by applying 50 mbar for 10 sec after loading the LE and performing a 15 sec 30 kV injection of standards. As predicted, the use of the TE for tITP (and overall EKS) provided improved peak intensity and efficiency compared to the same injection and separation without the TE (Figure 2-4A), showing the activation of tITP and EKS conditions by presenting a TE. In this example, the peak width of DA was reduced from 10.4 s to 5.4 s with 5 mM taurine as the terminator.

conditions are varied. After increasing past 10 s of EKI, both peak tailing and peak broadening become apparent. Under these conditions, FASI is limited to < 30 s before peak broadening and peak tailing become detrimental and affect resolution (Figure 2-3). Utilizing EKS conditions will allow for longer FASI injections to occur without losing

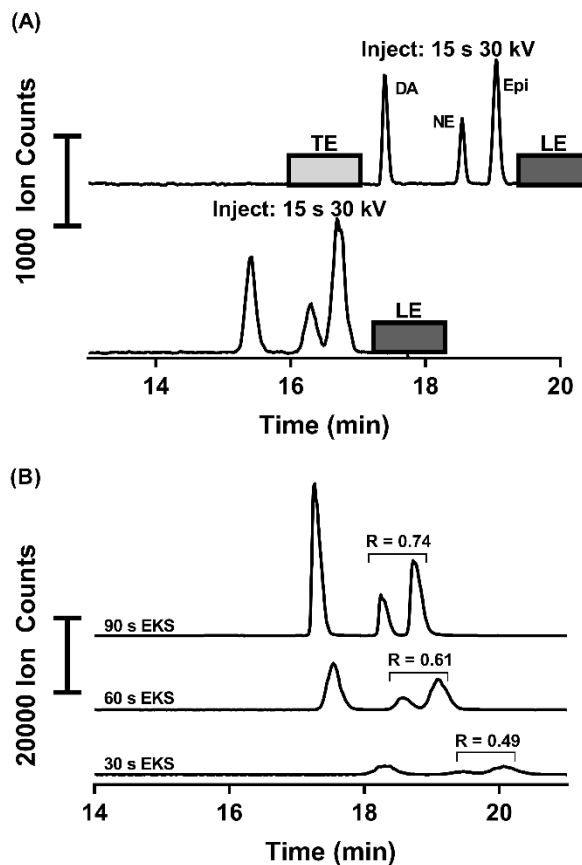


Figure 2-4: (A) Comparison of a 15 s 30 kV injection using LE with and without 5 mM taurine as TE. (B) Comparison of varying EKS injection durations without the intentional loading of a TE. Results suggest presence of a system-induced terminating electrolyte.

Interestingly, it was observed that at longer injections if a TE was omitted, peak width and height were not adversely affected (Figure 2-4B), and intentional loading of the TE offered no improvements. At lower injection durations (15 s, 30 s) under the same conditions, resolution and efficiency were significantly worse without the presence of a loaded TE. However, as injection duration is increased, peaks heighten and narrow. We hypothesize this result is due to the formation of a system-induced terminating electrolyte.¹¹³ System-induced terminator formation is a previously reported phenomenon which results in tITP behavior without the loading of a dedicated terminating electrolyte as seen here.^{123,124} Based on these results, the final injection parameters were set to 30 kV for 150 s, followed by a 30 kV separation voltage in an 80 cm capillary. This method was tested on seven analytes. Applying the selected LE and TE parameters determined above, five of the seven analytes could be baseline resolve within a 16-min separation with LODs down 10 pM (DA) using MS detection (Figure 2-5).

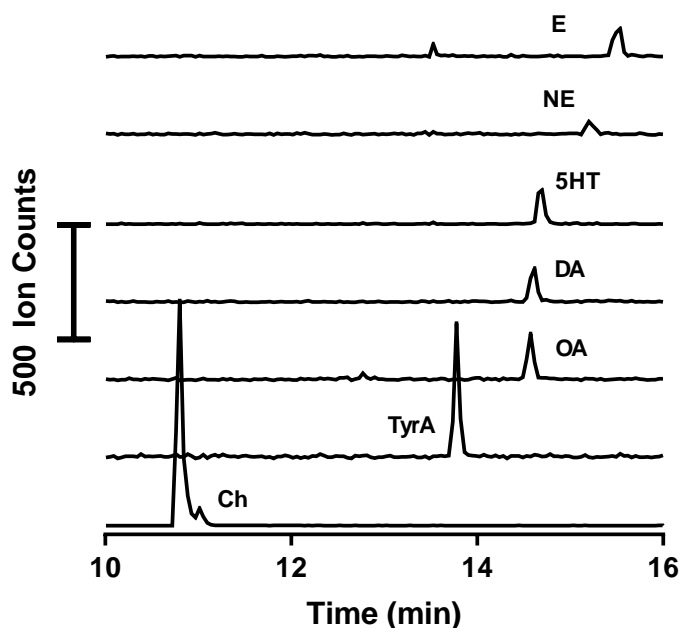


Figure 2-5: Extracted ion electropherograms (MS/MS) from a separation of 1 nM standards in water (Ch scaled down by a factor of 250 for scaling). OA and DA are isobaric compounds but are distinguished by MS/MS.

Preconcentration Method Comparison. To determine the effectiveness and improvement offered by EKS, the developed method was compared to conventional HDI, FASS, and FASI under similar separation conditions (Table 2-2, EKS LOD reported here is improved from the EKS LOD reported in Table 3 due to adjusted MS/MS scan rates. DA LOD is the

exemplary LOD reported for all methods). HDI is the most common form of sample loading used in CZE. It is useful for injecting all compounds in an unbiased fashion, which cannot always be accomplished when using forms of EKI, although it injects a much lower mass of analyte than EKI. With HDI the maximum injection volume is generally limited to 5% of the capillary volume before peak broadening becomes detrimental to separation efficiency.¹²⁵ Comparing EKS with the alternative methods, we see a 5000-fold enhancement using EKS over HDI, and nearly an order of magnitude enhancement over the next strongest mode of preconcentration, FASI. In addition to providing the lowest

Table 2-2: EKS compared to other common forms of injection and preconcentration. LODs, resolution, and peak width are compared for each method, where enhancement factor is a quotient of the methods LOD over the HDI LOD. Resolution calculated using previously listed equation between NE and EPI. FWHM used DA peak width.

| Method | LOD (nM) ^{a)} | Enhancement | FWHM (s) | Res |
|--------------------|------------------------|-------------------|----------|------|
| HDI ^{b)} | 50 | — | 4.7 | 1.09 |
| FASS ^{c)} | 20 | 2.5 | 9.6 | 0.37 |
| FASI (30 s) | 0.07 | 7.1×10^2 | 5.5 | 0.95 |
| EKS (150 s) | 0.01 | 5×10^3 | 4.2 | 1.02 |

a) LODs approximated using $S/N = 3$.

b) HDI loads 5% of capillary volume.

c) FASS fills 15% of capillary volume.

EKS, electrokinetic supercharging; FASI, field-amplified sample injection; FASS, field-amplified sample stacking; HDI, hydrodynamic injection.

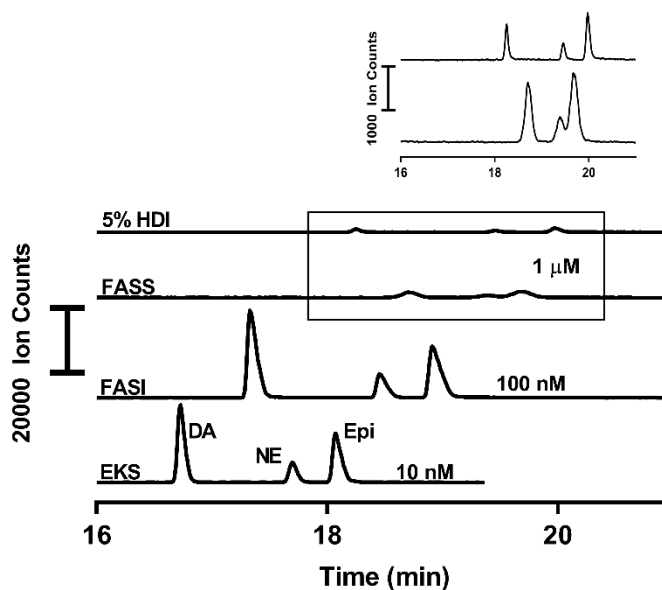


Figure 2-6. Total ion electropherogram of four different injection/preconcentration techniques at concentrations that fit within each methods LDR. A subset of 3 compounds used for this comparison including DA, NE, and EPI. These results are characterized in Table 2-2.

Table 2-3: Characterization of the calibration curves used for quantification of neurotransmitters in rat brain stem homogenate including LOD, LDR, and linearity.

| Compound | Migration Time (min) | LOD (pM) | Linearity (nM) | R ² |
|----------------|----------------------|----------|----------------|----------------|
| Choline | 10.8 | 50 | 20 – 20,000 | 0.9994 |
| Tyramine | 13.7 | 60 | 0.1 - 100 | 0.9926 |
| Octopamine | 14.5 | 90 | 0.1 - 100 | 0.9997 |
| Dopamine | 14.5 | 50 | 0.1 - 100 | 0.9996 |
| Serotonin | 14.6 | 30 | 0.1 - 100 | 0.9977 |
| Norepinephrine | 15.2 | 140 | 0.5 - 100 | 0.9916 |
| Epinephrine | 15.5 | 40 | 0.1 - 100 | 0.9971 |

LOD of all the methods, EKS not only maintains, but decreases the peak width compared to HDI and maintains resolution greater than one, unlike the other preconcentration methods tested here. Additionally, EKS maintains relatively Gaussian peak shape while FASI and FASS display the effects of broadening and peak tailing, which can be detrimental to a separations efficiency and resolution Figure 2-6).

Application to Biological Samples. Calibration curves were obtained for each compound in order to proceed with quantitation of biological samples and determine the quantification capabilities of the developed method, where the results of each calibration curve (used for rat brain stem homogenate) can be seen in Table 2-3. The LODs achieved for each compound make this method

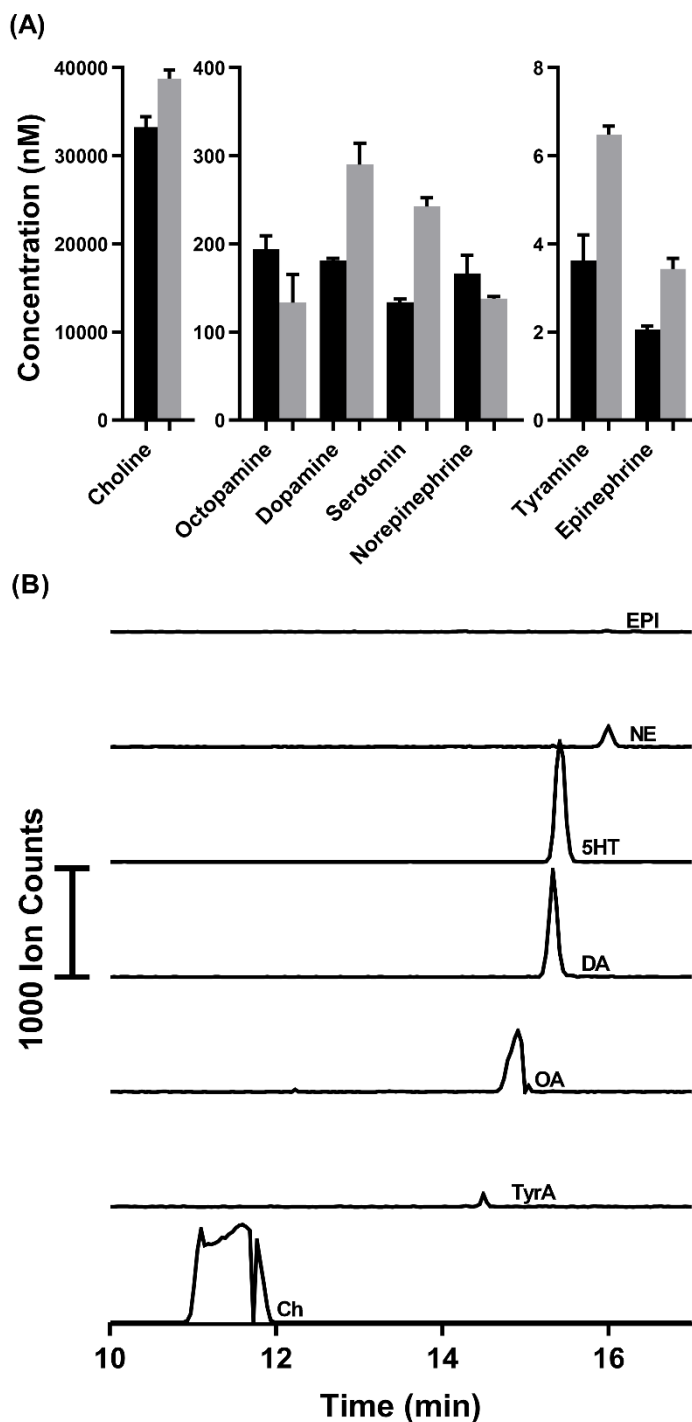


Figure 2-7: (A) Concentrations determined in rat brain stem homogenate by EKS with CE-MS/MS (black bars) and validation by LC-MS/MS (grey bars). EKS injections used 100 μ L of sample and LC injections used 5 μ L of sample per injection. Different aliquots of the same of the same supernatant used for each injection (triplicate by each method). (B) Extracted electropherograms for each compound in the rat brain stem homogenate separation (Ch reduced by a factor of 250 for scaling).

potentially suitable for detecting and quantifying trace neurotransmitters. Calibration curves showed linearity ($R^2 = 0.99$) from 0.1 – 100 nM for most compounds with LODs ranging from 30 – 140 pM during biological sample quantification. To demonstrate the utility of this method to determine these neurochemicals from tissue samples, the method was applied to rat brain tissue and whole *Drosophila* tissue. Supernatant from a rat brain stem homogenate was analyzed and all seven neurochemicals in the method were quantified from triplicate injections (Figure 2-7). To successfully determine these chemicals, a ten-fold dilution of the supernatant in water was necessary to avoid the negative effects of the sample matrix on the stacking. Figure 2-7A shows the concentrations after accounting for the tenfold dilution, reflecting the original concentrations in the tissue extract determined by our method. In Figure 2-7B, each trace shows the detection of one of the seven analytes from the brain tissue. Choline overloads and interacts with capillary surface at high concentrations resulting in poor peak shape; however, this effect did not affect linearity of calibration.

Supernatant of whole *Drosophila* homogenate was also analyzed to measure the neurotransmitters in a sample that contains lower concentrations. Figure 2-8 shows the four neurochemicals and their concentrations in the supernatant. The concentrations correspond to an average of 0.17, 26, 0.010, and 0.046 pmol/fly of DA, Ch, octopamine (OA), and 5HT, respectively. All seven analytes could not be detected as

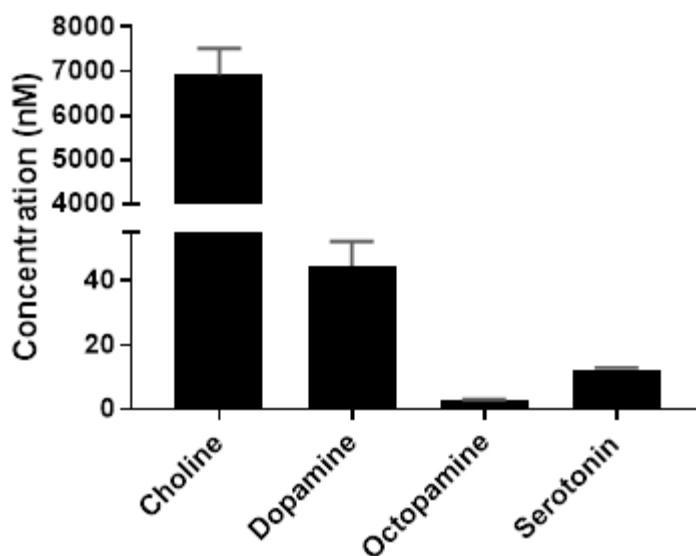


Figure 2-8: Graph of the determined concentrations from whole *Drosophila* tissue using the developed EKS method and the corresponding standard deviation.

epinephrine and NE are not present in flies, and tyramine was below the LOD in this analysis. In this tissue, Ch, DA, 5HT, and OA were able to be quantified with good repeatability, with RSD ranging from 4.8–17.3%. In this analysis, the method demonstrated its ability to simultaneously measure pM (OA) and μ M (Ch) concentrations, as well as the range between.

LC-MS Method Validation. To verify the concentrations quantified by the EKS method, the same rat brain homogenate supernatant was analyzed using a published LC-MS/MS method.¹²⁶ Shown in Figure 2-7A, the concentrations determined by LC-MS/MS were comparable to the values determined by EKS, where concentrations determined differed by 14% – 46% between the two methods. Catecholamines DA, Epi, and NE differed between the two methods by 37%, 40% and -20% respectively. Catecholamine analogues TyrA and OA differed by 44 and -45% respectively and indolamine 5HT by 45%. Ch differed by 14%. Choline, the only compound without oxidizable moieties, had the most similar measured concentration between the methods.

A possible source of the difference in results between CE-MS and LC-MS methods is sample stability.¹²⁷ For CE-MS, samples were kept at room temperature for ~4 h before analysis. In contrast, for LC-MS samples were derivatized immediately before analysis. Derivatization has previously been shown to stabilize many of the oxidation prone neurotransmitters such as catecholamines and indoleamines.^{46,126} All compounds but OA and NE were measured to be higher concentrations by LC-MS, and OA and NE are within error of concentrations determined by each method. To test if sample stability contributes to error between methods, rat brain homogenate supernatant was analyzed by LC-MS after sitting at room temperature for up to 4 h before derivatization (Figure 2-9). DA, NE, Epi, and 5HT saw loss of concentrations by 20%, 11%, 24%, and 3.5%, respectively between 0 hours (n = 5) and 4 hours (n = 4). This loss of concentration for several of the analytes accounts for a substantial portion of error seen in between the methods.

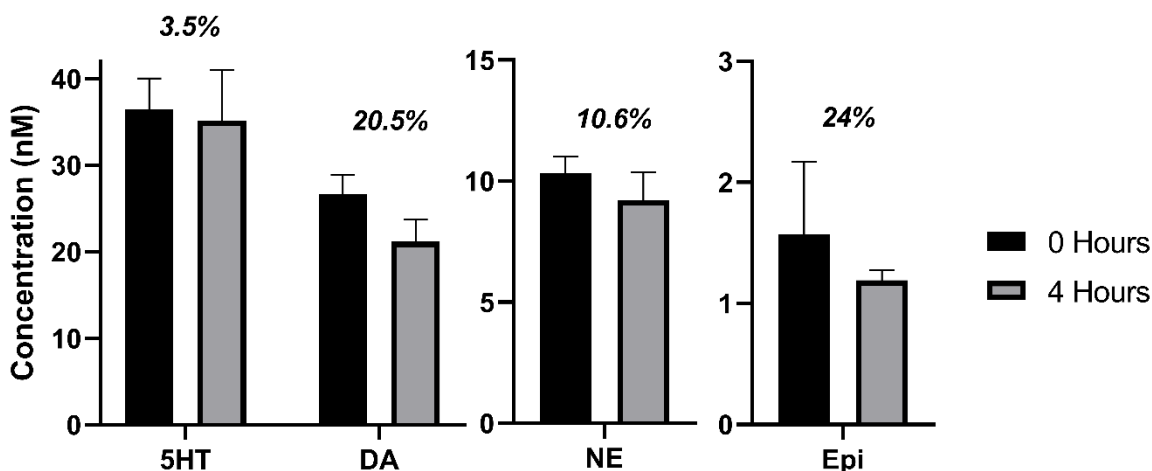


Figure 2-9: To test sample stability at room temperature, rat brain homogenate supernatant was analyzed by LC-MS after 0 and 4 hours at room temperature before derivatization. 6 analytes were measured, including Ch, TyrA, DA, NE, Epi, and 5HT. Ch (as expected) and TyrA showed no significant loss in concentration over the time period. DA, NE, Epi, and 5HT saw loss of concentrations by 20.5%, 10.6%, 24%, and 3.5%, respectively for 0 hours (n = 5) and 4 hours (n = 4).

Other potential sources of error include differences in the sample treatment and separation parameters for each method. These results suggest that more rapid analysis or more care taken in preventing oxidation may be important in increasing the accuracy of the CE-MS method. Though all sources of the differences between these two methods is not completely understood, this comparison proves the utility of the presented method, showing comparable accuracy to existing methods. Being a CE-based method, this can inject from and use less sample volume than LC-based methods, making it advantageous for low sample volume situations. This EKS method can also provide complimentary information that cannot be obtained by LC-MS, due to its orthogonality as a separation method, i.e. resolution of isomers OA and DA (Figure 2-7B).

Conclusions

A sensitive EKS method has been developed that can successfully interface to CE-MS using ESI and tandem mass spectrometry. This method overcomes many challenges and previous limitations of pairing this method of preconcentration to MS through careful selection of buffer systems and positively charged analytes that can be analyzed by the method. The method

development here has allowed for long and sensitive injections to take place for determining low abundance analytes without the use of sample pretreatments or capillary coatings as previously reported. LODs in this system are sufficient to analyze small molecules in many different samples, with detection limits down to 10 pM concentrations from standards, showing 5000-fold enhancements in detection sensitivity over conventional hydrodynamic injections.

Additionally, in this work we performed experiments that provided a validation and deeper understanding of the formation of system-induced terminating electrolytes. Though this phenomenon is still not completely understood, previous studies have simply reported EKS or ITP systems as having formed these terminators without providing data demonstrating their presence and effectiveness as we have here.

This method has been applied to biogenic amine neurotransmitters from tissue samples. In principle the method could be applied to other tissues. Improvements in protection against oxidation would be required for better accuracy. Samples containing high ionic strength matrices such as microdialysate and plasma can also be measured in this method, however they would require a pretreatment to remove or exchange the sample matrix prior to EKS. In theory, the enhancement by preconcentration that has been achieved through this method should make many complex samples analyzable by simply diluting them and maintaining sufficient sensitivity to detect these further diluted compounds. In future work, this method could be combined with MS through a sheathless nESI to offer further improvements to detection sensitivity and be further adapted for lower sample volumes.

Chapter 3

Droplet-nESI-MS/MS with Microdialysis for Sensitive and High Temporal Resolution Neurochemical Monitoring

Introduction

Monitoring neurochemical concentrations and dynamics in the brain is imperative in neuroscience. This process can elucidate how the brain responds physiologically to specific disease states, behaviors, and various drugs.¹²⁶ Recent examples of physiological studies employing neurochemical monitoring include amphetamine (AMPH) maintenance effects on DA and 5HT,¹²⁸ neurochemical changes due to traumatic brain injury,^{129,130} and neurochemical profiles in amyotrophic lateral sclerosis.¹³¹ Monitoring neurochemical dynamics is typically accomplished through the use of microsensors¹³² or sampling techniques such as microdialysis¹³³ (MD) or push-pull probes¹³⁴ paired with an analytical instrument such as mass spectrometry (MS) for analysis.

Microdialysis probes operate by sampling from the extracellular space in brain tissue, where the tip of the probe is comprised of a semipermeable, low molecular weight cutoff membrane. As artificial cerebral spinal fluid (aCSF) is perfused through the probe (0.1 – 3.0 $\mu\text{L}/\text{min}$), salts and small molecules diffuse across the membrane from the extracellular space, and the perfusate can be collected and analyzed.¹³³ MD is largely accepted and respected as a robust technique in neuroscience. It is often preferred over push-pull perfusion for sampling due to its ease of operation, preservation of anatomical and function integrity of the tissue, and generation of a partially cleaned-up sample due to selective diffusion across the membrane.¹³⁵

Microsensors are another common tool used for neurochemical monitoring. Their small size and rapid scan speeds (ms range) allow for unmatched spatial resolution and temporal resolution. Despite these strong advantages, microsensors are typically limited to monitoring one neurochemical at a time, and analyte selectivity and specificity can be difficult to achieve.¹³⁶ Arrays of microsensors can be employed to achieve a broader range of neurochemicals that can be simultaneously monitored, though this can reduce the achievable spatial resolution.¹³² Microdialysis, on the other hand, functions as a sampling tool rather than a mode of monitoring, presenting unique circumstances for MD as a tool for neurochemical monitoring. Though the spatial resolution is directly related to the size of the probe/membrane, temporal resolution and neurochemical range associated with MD are dependent on the perfusion flow rate, fraction size, and instrumentation used to analyze each fraction.

High performance liquid chromatography paired with mass spectrometry (LC-MS) is the most common method for analyzing microdialysate fractions due to its sensitivity, selectivity, specificity, and potential to simultaneously determine many neurochemicals. LC-MS methods in neurochemical monitoring have shown simultaneous measurement of up to 70 different neurochemicals.^{46,137} Though regarded as the gold standard for analyzing microdialysate, LC-MS has some key limitations. Due to the volume requirements of HPLC (1 – 5 μL /injection) and typical perfusion flow rates in MD (1 $\mu\text{L}/\text{min}$), LC-MS is typically restricted to temporal resolution on a minute time scale (5 – 20 min), making LC-MS unsuitable for monitoring rapid concentration fluctuations and short-term neurochemical dynamics. These characteristics make LC-MS most suitable for monitoring long-term pharmacological effect, but make applications such as evaluating neurochemical effects from behavior more difficult.¹³⁸

Many studies have focused on improving the temporal resolution of MD neurochemical monitoring that can be achieved by LC-MS, or through implementation of an alternative separation technique such as capillary electrophoresis (CE).¹³⁴ Recent advances allow for temporal resolution on a second to low-minute time scale. For example, in 2018, Wilson et. al. demonstrated one-minute temporal resolution while monitoring DA from rat brain microdialysate. In this study, DA concentration changes were induced through the administration of either high potassium aCSF or nomifensine and monitored via online LC-MS/MS.¹³⁹ CE is another viable option for neurochemical monitoring due to several advantages such as low volume requirements ($< 1 \mu\text{L}$), high separation efficiency, and the ability to perform online preconcentration of analytes.¹⁴⁰ In one example, Hogerton and Bowser demonstrated 20 s temporal resolution for up to 15 different neurochemicals simultaneously while using MD paired with online, ultrafast CE.¹⁴¹ However, despite various CE methods allowing for significantly improved temporal resolution with MD, CE has a major limitation in detection sensitivity with most detectors such (i.e. UV, MS), limiting potential analytes to high abundance neurochemicals.

A less common approach for overcoming temporal resolution limitations in both MD and push-pull perfusion probes is the implementation of segmented flow. In segmented flow, small volumes (pL – nL) of aqueous sample are segmented by an immiscible, inert carrier fluid, which compartmentalizes the contents of each aqueous droplet and maintains temporal resolution. This approach was first demonstrated in 2008 when Wang et. al. segmented exiting perfusate into 6 – 28 nL droplets in a microfluidic device using an inert carrier fluid and achieved temporal resolution as good as 15 s.¹⁴² Without the implementation of segmented flow, the same system demonstrated a temporal resolution ranging from 25 – 160 s. This was applied for monitoring glucose and its response to high potassium stimulations in rat brains. Since then, similar systems have been

reported in other studies using MD and push-pull perfusion probes. In 2012, MD with segmented flow was implemented to achieve 5 s temporal resolution and 5 nM limits of detection (LOD) for the neurotransmitter ACh using direct ESI-MS/MS for analysis of the droplet fractions.²⁴ Similarly, in a study using microfabricated push-pull sampling probes, perfusate was segmented and analyzed by nESI-MS/MS with temporal resolution of 6 s for four different neurochemicals simultaneously, demonstrating the ability to monitor several compounds simultaneously using direct MS/MS.⁹⁸ Finally, a recent study used a similar approach, where 50 s temporal resolution was achieved for Zn and Cu by segmenting perfusate from a push-push sampling probe, where droplets were analyzed by laser ablation – inductively coupled plasma – mass spectrometry.¹⁴³ Though these methods report drastically improved temporal resolution compared to other modes of microdialysate analysis, they are limited in the number of neurochemicals that are simultaneously monitored from each fraction, an important feature that makes MD sampling appealing.

In this study, we present a method that achieves high temporal resolution neurochemical monitoring with MD that allows for simultaneous monitoring of seven different neurochemicals (ACh, DA, 5HT, GABA, Glu, Ado, Gln), several of which are low abundance neurotransmitters. Here, MD sampling probes are paired with segmented flow via a 50 μm inner diameter (i.d.) microfluidic cross junction to generate dialysis fractions averaging 5.3 nL (0.64 Hz) allowing for temporal resolution of 10.7 seconds. At the cross, internal standards (IS) and diluent are added to the dialysate as it segments. Droplet trains containing over 1,000 dialysate fractions are generated at the probe outlet and subsequently analyzed using a highly sensitive, low flow nESI-MS/MS method. The droplet-nESI-MS/MS method is optimized to achieve LODs for each of the targeted neurochemicals below the predicted basal levels, LODs down to 2 nM (ACh). Factors including

infusion flow rate, spray tip diameter, MS/MS scan speeds, assisting gas flow rates, aCSF composition, diluent composition, and dilution factor were assessed during method development. This method is compared to a conventional LC-MS/MS with temporal resolution of 5 min, and the *in vivo* monitoring dynamics are compared between the two methods. The utility of the droplet fraction method is demonstrated by monitoring dynamics of the seven neurotransmitters in response to brief administration of high potassium/low sodium aCSF. Additionally, to demonstrate the selectivity of the method, we monitored the neurochemicals as AMPH was directly administered to the probe site over a brief period of 30 s, which allows for selective stimulation of DA release and reuptake inhibition.¹⁴⁴

Materials and Methods

Reagents and Materials. All Chemicals and solvents were purchased from Sigma-Aldrich (St. Louis, MO) unless stated otherwise. Perfluorodecalin (PFD) was purchased from Oakwood Chemical (Colombia Hwy, Estill, SC, USA). Isotopically labeled internal standards (d6GABA, Table 3-1: List of transitions, dwell times, and collision voltages for MS/MS

| Compound | Precursor (m/z) | Fragment (m/z) | Dwell (s) | Collision (V) | Calibration High Point (nM) | Calibration Low Point (nM) |
|----------|-----------------|----------------|-----------|---------------|-----------------------------|----------------------------|
| GABA | 104 | 87 | 0.15 | 10 | 200 | 10 |
| d6GABA | 110 | 93 | 0.03 | 12 | | |
| AMPH | 136.1 | 119.1 | 0.03 | 15 | | |
| ACh | 146 | 87 | 0.1 | 17 | 100 | 5 |
| Gln | 147 | 84 | 0.03 | 15 | 100,000 | 5,000 |
| Glu | 148 | 130 | 0.1 | 8 | 600 | 30 |
| d4ACh | 150 | 91.1 | 0.03 | 17 | | |
| d5Gln | 152 | 135 | 0.04 | 10 | | |
| 13C5Glu | 153 | 135 | 0.04 | 10 | | |
| DA | 154 | 137 | 0.15 | 13 | 100 | 5 |
| d4DA | 158 | 141 | 0.05 | 13 | | |
| 5HT | 177 | 160.1 | 0.15 | 12 | 100 | 5 |
| d45HT | 181 | 164 | 0.03 | 15 | | |
| Ado | 268 | 136.1 | 0.05 | 18 | 200 | 10 |
| d1Ado | 269 | 137 | 0.04 | 18 | | |

d4ACh, d5Gln, 13C5Glu, d4DA, d45HT, d1Ado) were purchased from CDN Isotopes (Quebec, Canada). For tuning and optimization, neurochemical standards and internal standards were prepared in HPLC-grade water as 100 μ M stocks, aliquoted, stored at -80 °C, and thawed for use daily as needed (single use). For quantitative calibration curve standards, mixtures of all 7 standards were prepared in HPLC-grade water at 10 times the high point of the calibration curve (Table 3-1), aliquoted, stored at -80 °C, and thawed for use daily as needed (single use). Mixtures of 200 nM internal standards were prepared in HPLC-grade water with 0.2% concentrated acetic acid, aliquoted, stored at -80 °C, and thawed for use daily as needed (single use). aCSF was prepared in 500 mL of water with 145 mM NaCl, 2.68 mM KCl, 1.4 mM CaCl₂ • 2H₂O, 1.01 mM MgSO₄ • 7H₂O, 1.55 mM Na₂HPO₄, and 0.45 mM NaH₂PO₄ • H₂O at pH 7.4. No phosphate (PO₄) aCSF was prepared in 500 mL of water with 145 mM NaCl, 2.68 mM KCl, 1.4 mM CaCl₂ • 2H₂O, and 1.01 mM MgSO₄ • 7H₂O at pH 7.4. To mimic post-perfusion dialysate in standards, conventional aCSF and no PO₄ aCSF were mixed 1:2 (33% PO₄ aCSF). High potassium aCSF (100 mM KCl) was prepared in 250 mL of water with 47.68 mM NaCl, 100 mM KCl, 1.4 mM CaCl₂ • 2H₂O, and 1.01 mM MgSO₄ • 7H₂O at pH 7.4. D-amphetamine hemisulfate was prepared in aCSF to a final concentration of 100 μ M.

Well-Plate Droplet Generation and Transfer. Hamilton (Reno, Nevada, USA) gastight syringes were used (25 μ L, 100 μ L, 1 mL) with Chemyx Inc. Fusion 400 syringe pumps for infusion. For well plate droplet generation, a Harvard Apparatus PHD 2000 programmable syringe pump was used. Droplets were generated using a syringe pump drawing at a rate of 700 nL/min using a 25 μ L syringe with a 20-30 cm length of 150 μ m i.d. by 360 μ m outer diameter (o.d.) PFA tubing from IDEX (Lake Forest, Illinois, USA). Connections were made using low dead volume unions from Valco Instruments Co., Inc. (Houston, TX). Droplet generation was performed using

an XYZ-position manipulator to draw from a 384-microwell plate, where a layer of PFD carrier fluid is deposited on top of aqueous samples, and droplets are generated as the tubing is moved between the two layers while vacuum is applied. For *in vitro* and *in vivo* experiments, droplets are generated as PFD (carrier fluid), diluent (200 nM IS, 0.2% acetic acid), and dialysate are flowed

into a Valco Instruments Co., Inc.(Houston, TX) 50 μm i.d. cross junction at 0.5, 0.25, and 0.25 $\mu\text{L}/\text{min}$, respectively, using syringe pumps to control flow. The dialysate emerging from the MD probe is diluted 1:1 with incoming diluent and the resulting mixture is segmented into 3 – 8 nL droplets at 1 – 3 Hz and exported into a 2 – 5 ft length of 150 μm i.d. x 360 μm o.d. PFA tubing. The resulting

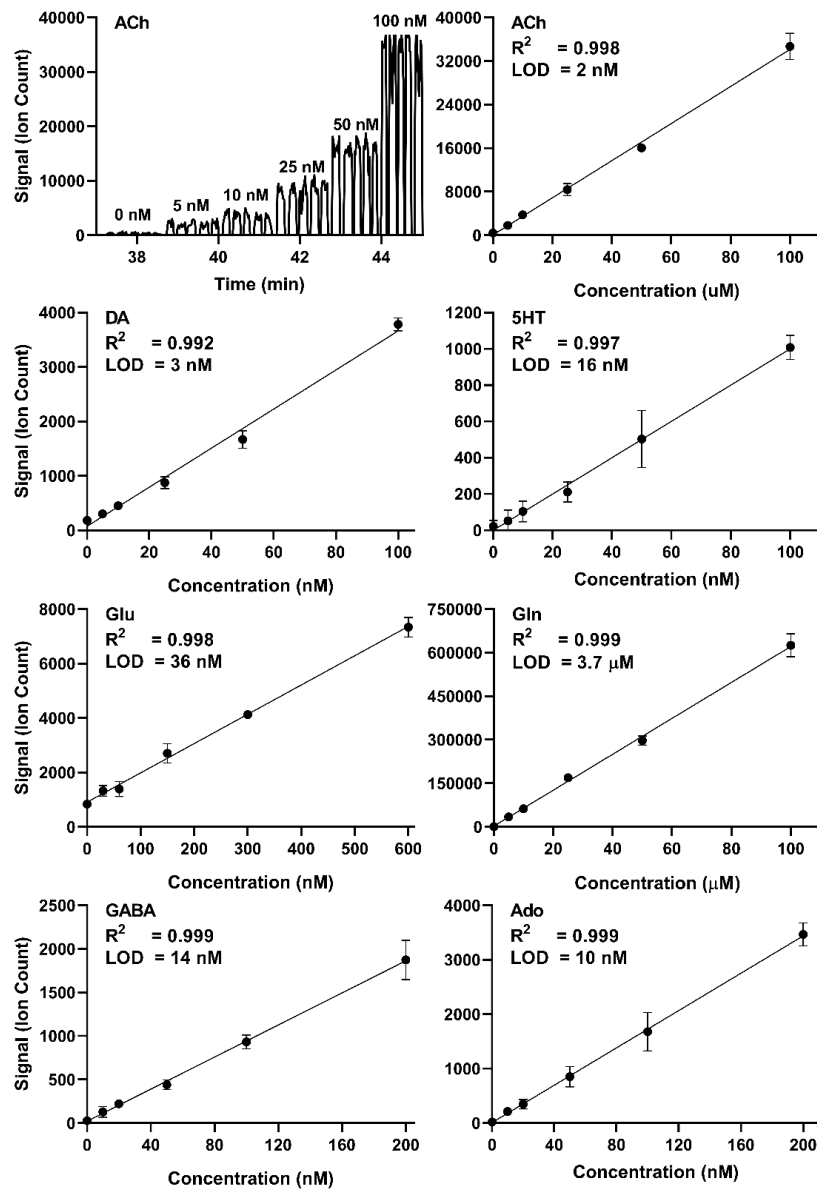


Figure 3-1.(Top Left) MS/MS trace of the calibration curve for ACh with 5 droplets for each of the 6 calibration levels. (All other graphs) Average signal intensity vs. concentration to generate a 6 point calibration curve with error bars for each of the target neurochemicals. These are the curves used for quantitation during one day of *in vivo* experiments (09/21/20). LOD is calculated using the limit of the blank method.²³⁷

droplets were measured under a microscope to calculate average size of droplets in a train before taking to MS for analysis. An illustration of droplet generation can be seen in Appendix 1.

Calibration Curves. Calibration curves were obtained daily prior to collecting *in vivo* samples. Stocks were thawed, diluted 10-fold, and serial diluted (1:2:2:2.5:2) in 33% PO₄ aCSF. For potassium stimulation experiments where abnormally high neurotransmitter concentrations were expected, one additional concentration level was added at five times the standard high point. Five droplets are generated for each concentration level, and the middle three are averaged for a triplicate calibration curve with standard deviation (SD).

nESI-MS/MS. Zero-dead-volume Picoclear unions (New Objective, Woburn, MA) were used to transfer droplets to nESI emitters. Emitters were pulled from 50 μm i.d. x 360 μm o.d. fused silica capillary to an i.d. of 15 μm and coated with conductive platinum (FS360-50-15-CE, New Objective, Woburn, MA). Direct droplet infusion was carried out at 50 nL/min using 1.4 kV capillary voltage. All important final nESI and MS/MS parameters can be found in Table 3-2. Mass spectrometry analysis was performed on a Micromass Quattro Ultima triple-quadrupole mass spectrometry (Waters, Milford, MA). All experiments were performed in MS/MS mode in single reaction monitoring (SRM) mode to scan for multiple mass transitions at the same

Table 3-2: Important MS, nESI, and sample prep info for *in vivo*

| nESI | Flow Rate | Capillary, Cone Voltage | Emitter i.d. | Drying Gas |
|----------|-----------------------------|----------------------------|------------------|-----------------------|
| | 50 nL/min | 1.4 kV, 35 V | 15 μm | 150 L/h |
| Sample | Matrix (cal/tune) | Matrix (Perfusion) | Additive | Dilution |
| | aCSF (33% PO ₄) | aCSF (no PO ₄) | 0.1% Acetic Acid | 1:1, H ₂ O |
| Analyzer | LM Res 1, 2 | HM Res 1, 2 | Ion Energy 1, 2 | Exit, Entrance |
| | 14.7, 14.5 | 14.5, 14.5 | 0.5, 0.4 | 5, -1 V |
| MS/MS | Span | Interscan Delay | Transitions/CE | Dwell Times |
| | 0.3 m/z | 2.5 ms | Table 3-1 | Table 3-1 |

time. Signal from a droplet is defined as the average of the points across a droplet.

Microdialysis Probes. Custom concentric 2 mm microdialysis probes were constructed for *in vitro* temporal resolution and *in vivo* sampling experiments. Inlet and outlet fused silica capillaries (40 μm i.d. x 110 μm o.d.) were glued together offset by 2 mm and inserted into a 4 mm piece of regenerated cellulose dialysis membrane (18 kDa MWCO, Spectrum Life Sciences LLC., Rancho Dominguez, CA). The distal membrane tip was sealed with an epoxy (Loctite, West Lake, OH) 100 μm from the inlet capillary. Dead volume within the membrane was eliminated by sealing the proximal end of the membrane around the inlet/outlet capillaries with epoxy and allowing it to wick into the membrane until it was within 100 – 200 μm of the probe active area. The probe was then secured within a 10 mm (25 G) piece of stainless steel hypodermic sheath tubing (Small Parts Inc., Logansport, In). A fused silica injection shank (75 μm i.d. x 150 μm o.d.) was added adjacent to the center of the membrane for 100 mM K^+ /100 μM d-amphetamine injections. A custom designed 3D printed probe holder (VisiJet M3 Crystal, 3D Systems, Rock Hill, SC) was used to secure the probe. A 150 μm i.d. x 360 μm o.d. fused silica sheath was added to the outlet capillary to enable direct connection to a 50 μm i.d. cross junction for droplet generation.

***In vivo* Microdialysis Sampling.** For *in vitro* recovery and temporal resolution experiments, microdialysis probes were inserted into a stirred vial of 2 mL of aCSF maintained at 37 °C. To estimate system temporal resolution, a rapid physiological concentration change was simulated by spiking 10 μL of a 10 μM (per 50 μM change desired) standard mix into the stirred vial. *In vivo* neurochemical measurements were performed in anesthetized male 25 – 30 g C57BL/6 mice (Envigo, Haslett, MI). Briefly, mice were anesthetized using 2 – 3 % isoflurane and mounted to a stereotaxic instrument (David Kopf Instruments, Tazunga, CA). A 2 mm microdialysis probe

was then implanted into the striatum using the following coordinate with respect to bregma: 0.6 mm anterior, ± 1.75 mm lateral, and 4.2 mm ventral to the surface of the brain. Once lowered into place, probes were flushed continuously with aCSF for 15 min prior to droplet collection. As previously described, droplets were generated directly from the outlet of the MD probe. For neurotransmitter stimulation experiments, either 100 mM K^+ aCSF or 100 μ M AMPH solution were administered locally through the probe injection shank at 1 μ L/min for 30 s, totaling 500 nL. For high potassium stimulation, high potassium aCSF was administered at 0 min and 5 min for a sampling period of 0 – 10 min. For AMPH stimulation, AMPH solution was administered at -1 min for a sampling period of 0 – 5 min.

LC-MS/MS. Chromatographic separations were conducted on an Agilent 1290 HPLC interfaced to an Agilent 6410 triple quadrupole mass spectrometer using a Phenomenex Kinetex C18 chromatography column (100 x 2.1 mm, 1.7 μ m, 100 Å). Mobile phase A and B consisted of water containing 10 mM ammonium formate/0.15% formic acid (v/v) and acetonitrile, respectively. The gradient used was as follows: initial, 5% B; 0.01 min, 19% B; 0.68 min, 26% B, 1.05 min, 75% B; 1.8 min, 100% B; 2.8 min, 100% B; 4 min, 5% B; 5.0 min, 5% B at 600 μ L/min. The autosampler was kept at ambient temperature, and the column was held at 30 °C, with 5 μ L sample injection volumes. MD fraction were collected during *in vivo* experiments to be analyzed LC-MS analysis. For fraction collection, PFD flow was stopped, and the diluent and dialysate flow rates remained at 0.25 μ L/min each into the microfluidic cross. One fraction was collected every 5 min at 0, 5, 10, and 15 min (2.5 μ L each), stored at -80 °C, and thawed for analysis. Upon thawing, the fractions were subject to benzoyl chloride derivatization prior to analysis.⁴⁶ For benzoylation, two parts sample are mixed with one part 100 mM sodium carbonate, one part 2% v/v benzoyl chloride in ACN, and one part internal standard in 1% sulfuric acid v/v in 20:80

MeOH/water (v/v) added, step wise. The mixture was vortexed for 10 s after each addition. The internal standard mixture is comprised of analyte standards derivatized by the same procedure using C13 benzoyl chloride as the derivatizing agent.

Results and Discussion

MS/MS and nESI Conditions. The method developed in this study aims to significantly improve the temporal resolution typically obtained in microdialysis-based neurochemical monitoring while maintaining the advantage of monitoring many neurochemicals simultaneously; however, many neurochemicals, such as many monoamine acid neurotransmitters (i.e. DA, NE, Epi, 5HT, ACh), have low nanomolar basal levels in various brain regions, rendering many modes of analysis difficult or impossible due to insufficient LODs. To achieve sufficient LODs by MS for seven different neurochemicals including trace neurotransmitters DA, 5HT, and ACh, low-flow nESI is combined with the sensitive and selective MS/MS mode of SRM. Many variables are tuned for nESI and MS/MS to improve detection sensitivity, signal reproducibility, and the signal-to-noise ratio (S/N) for LOD optimization (Table 3-2). Though the optimization of many different parameters contributed to LOD improvements, three key conditions had a relatively large impact on LODs including flow regime (nESI vs ESI), sample matrix composition, and MS/MS scan speeds (dwell, Figure 3-2). Though each offered improvements for most/all target analytes, adjusting each condition offered varying degrees of improvement for each analyte. True nESI is achieved at low nL/min flow rates (0 – 50 nL/min) and has been shown to offer drastic improvements to ionization efficiency and reduction of ionization suppression.^{29,34,36} Here, we compared a nESI flow regime (50 nL/min with 15 μ m i.d. emitter) to a flow regime closer to standard ESI (500 nL/min with 30 μ m i.d. emitter, Figure 3-2A). The low-flow method offers 3-fold higher signal intensity and nearly double the S/N for ACh. Though low-flow nESI alleviates

the ionization suppression from aCSF, a degree of suppression remains. Phosphates, a component of standard aCSF, are known to cause ionization suppression in ESI.¹⁴⁵ To further alleviate the suppression, aCSF with 33% of the standard phosphate (PO_4) concentration is used for standards and low concentration acetic acid is added to the matrix, offering a 4-fold increase in signal intensity and nearly $\frac{1}{2}$ the noise for DA, as well as reduced SD in the blank (Figure 3-2B). Finally, decreased interscan delays and longer dwell times can allow for improved signal as a result of longer signal collection periods. Applying a 100 ms dwell time increased from 30 ms allowed for signal and noise to be distinguished for 150 nM Glu, offering nearly a 3-fold-improvement in signal intensity (Figure 3-2C).

In Vitro. Droplet generation and temporal resolution of the system were

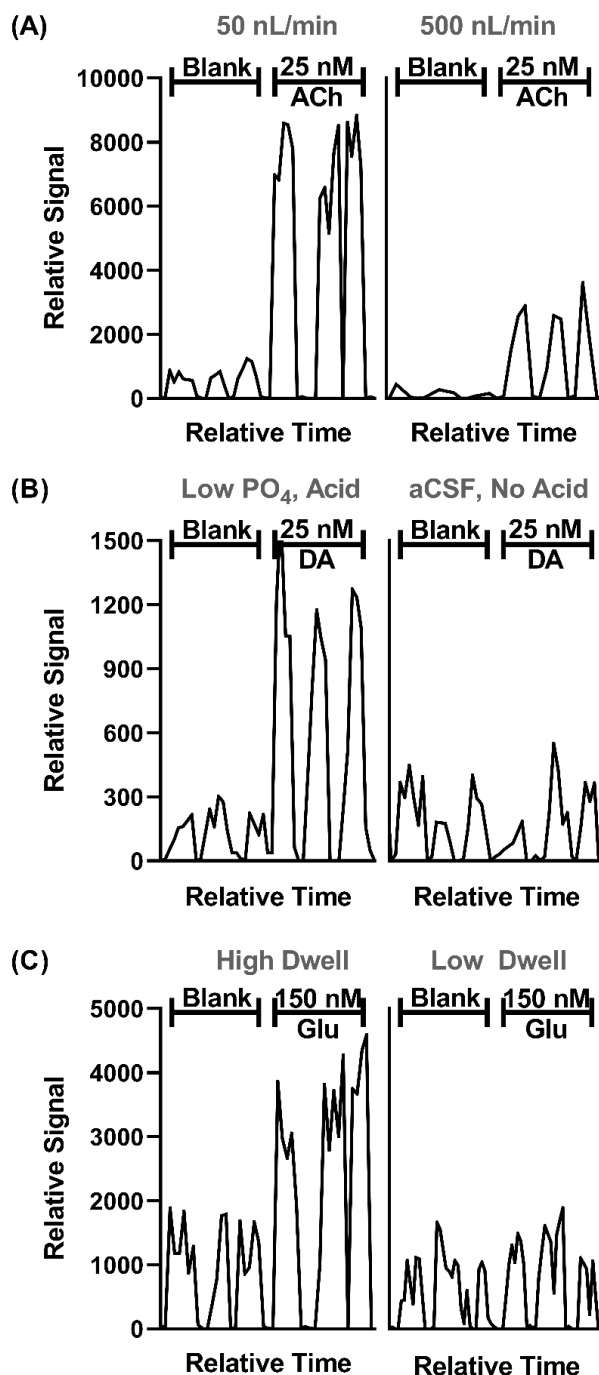


Figure 3-2. (A) Low infusion flow rates (50 nL/min) and smaller nESI emitter i.d. (15 μm) allow for smaller droplets (4.4 nL) and improved analyte response and S/N over a higher infusion flow rates (500 nL/min) and larger i.d. nESI emitter (30 μm), which required 40 nL droplets. ACh is shown for this comparison. (B) An adjusted matrix with 33% of the standard PO_4 concentration in aCSF along with a final concentration of 1% concentration acetic acid compared to standard aCSF with no acid. DA is shown for this comparison. (C) Increased dwell time (100 ms) for the MS/MS scans vs a typical faster dwell time (30 ms). Glu is shown for this comparison.

explored and improved during in vitro experiments via MD sampling from a stirred vial. Parameters including flow rates, probe dimensions, and droplet generation devices were evaluated. In theory, the various flow rates used in this system (carrier phase, diluent, and perfusate) can be manipulated to control droplet generation frequency, droplet size, and the degree of analyte diffusion before segmentation. However, flow rates for PFD, diluent, and perfusate of 0.5, 0.25, and 0.25 $\mu\text{L}/\text{min}$, respectively, are maintained in order to (A) maximize analyte recovery across the dialysis membrane and (B) limit the total dialysate volume that requires MS analysis, since the nESI-MS/MS method requires 20-fold lower flow rates for analysis and reasonable throughput is needed.

While low microdialysis flow rates correspond to high analyte recovery, low flow after the dialysis membrane can negatively impact temporal resolution. At lower flow rates, axial dispersion within the sampling flow path contributes to significant broadening of analyte concentration zones prior to collection,¹⁴⁶ ultimately precluding capture of rapid concentration changes. To preserve dynamic sample information, pre-droplet generation volume was limited by designing a microdialysis probe using low i.d. capillary, filling all non-active area membrane volume with epoxy, and directly mounting the droplet generation cross to the probe outlet. Additionally, three microfluidic crosses were evaluated for droplet formation (50 μm , 100 μm , 150 μm i.d.). Ultimately, the 50 μm i.d. cross was selected for its low dead volume and smaller droplets.

The temporal resolution of the system was measured during in vitro experiments. A stirred vial was sampled using an MD probe while the concentration was adjusted, and the resulting droplets were analyzed by the developed MS method (Figure 3-3A). temporal resolution was measured three times across two different concentration transitions (0 to 50 nM, 100 to 400 nM) to obtain a representative average and to ensure that the degree of change of the concentration

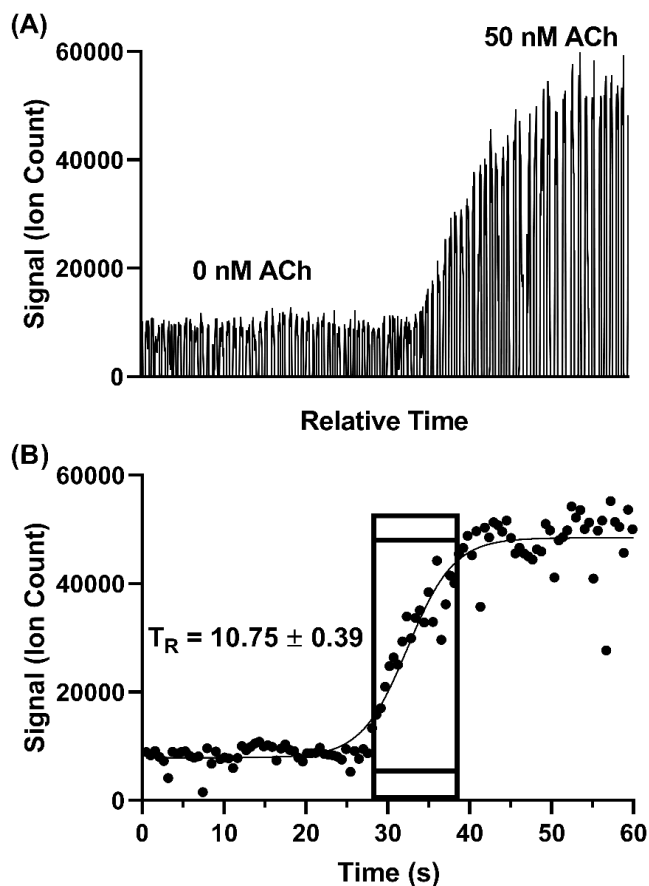


Figure 3-3. To measure the temporal resolution of the system from sampling to mass analysis, stirred vial experiments were performed in triplicate for test compound ACh. temporal resolution measurements were performed by spiking sample into a stirred vial, sampling by MD, segmenting into droplets, and analyzing by MS. The average temporal resolution and error of the three transitions are reported. (A) A raw MS/MS trace of in vitro droplet analysis for ACh. (B) The middle of each droplet is average and correlated to real time based on the droplet volume/generation frequency (4.4 nL / 1.89 Hz).

transition does not impact temporal resolution. The temporal resolution is calculated for each replicate based on the number of droplets during the transition multiplied by the time taken to generate each droplet (determined by average droplet volume in a train divided by aqueous flow rate during generation). The transition is defined as all droplets lying between 10% above the average low concentration signal intensity (i.e. 0 nM ACh) and 10% below the average high concentration signal intensity (i.e. 50 nM ACh, Figure 3-3B). The triplicate temporal resolution measurement

across the two concentration transitions yielded excellent reproducibility (3.6% RSD) with a temporal resolution of 10.75 ± 0.39 . Though a previous method was able to achieve ~5 s temporal resolution for ACh,²⁴ a slightly lower temporal resolution is expected in this system from increased diffusion caused by a lower perfusion flow rate (0.25 $\mu\text{L}/\text{min}$ vs 1.0 $\mu\text{L}/\text{min}$).

In vivo. The developed system was applied to neurochemical monitoring during high potassium and AMPH stimulations. For high potassium administration, the striatum was sampled over 10 min, during which 500 nL of 100 mM KCl (1 $\mu\text{L}/\text{min}$ for 30 s) was administered at two

different time points, starting at 0 min and 5 min during sample collection, respectively, with a dead time of 2.5 min. Three biological replicates were obtained over two mice (two hemispheres in one mouse). Droplet volume for the three replicates ranged from 5 – 5.7 nL, depending on the replicate. The average of all three replicates (% baseline) is plotted with the standard error of the mean (blue-dotted line) for all compounds (Figure 3-4, Figure 3-5A).

To compare the difference in temporal resolution and monitoring dynamics between the droplet-nESI-MS/MS method and a conventional LC-MS/MS method, five-minute fractions were collected from the same mice and analyzed by LC-MS/MS. In Figure 3-4, the averaged traces for 5HT, GABA, DA are plotted from both analysis methods. Though each method was used to analyze MD fractions collected over 10 min, the LC fraction method provides only three time points which offers a temporal resolution of 5 min, while the droplet fraction method provides over 900 points

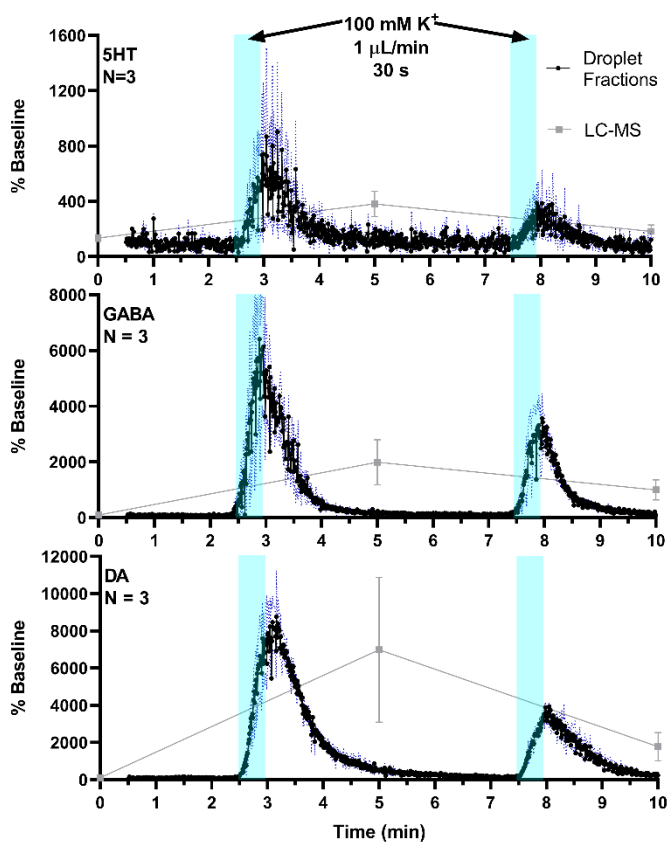


Figure 3-4. *In vivo* experiments using MD probes sampling the striatum over a 10 min collection period. 500 nL of high potassium aCSF was administered over 30 s beginning at 0 and 5 min, with an approximate 2.5 min dead time. Three biological replicates were obtained over two mice (one mouse with two hemispheres). Points converted to percent baseline to normalize for concentration differences and all three traces were averaged. SEM shown as a blue-dotted line. Gray squares and connecting lines represent LC fraction method, with fractions collected over 5 min intervals.

with a temporal resolution of 10.75 s. This difference is clearly reflected in the neurotransmitter dynamics that can be seen in each trace. Though the LC fraction method shows similar percent baseline changes in the neurotransmitter concentrations as the droplet fraction method, important

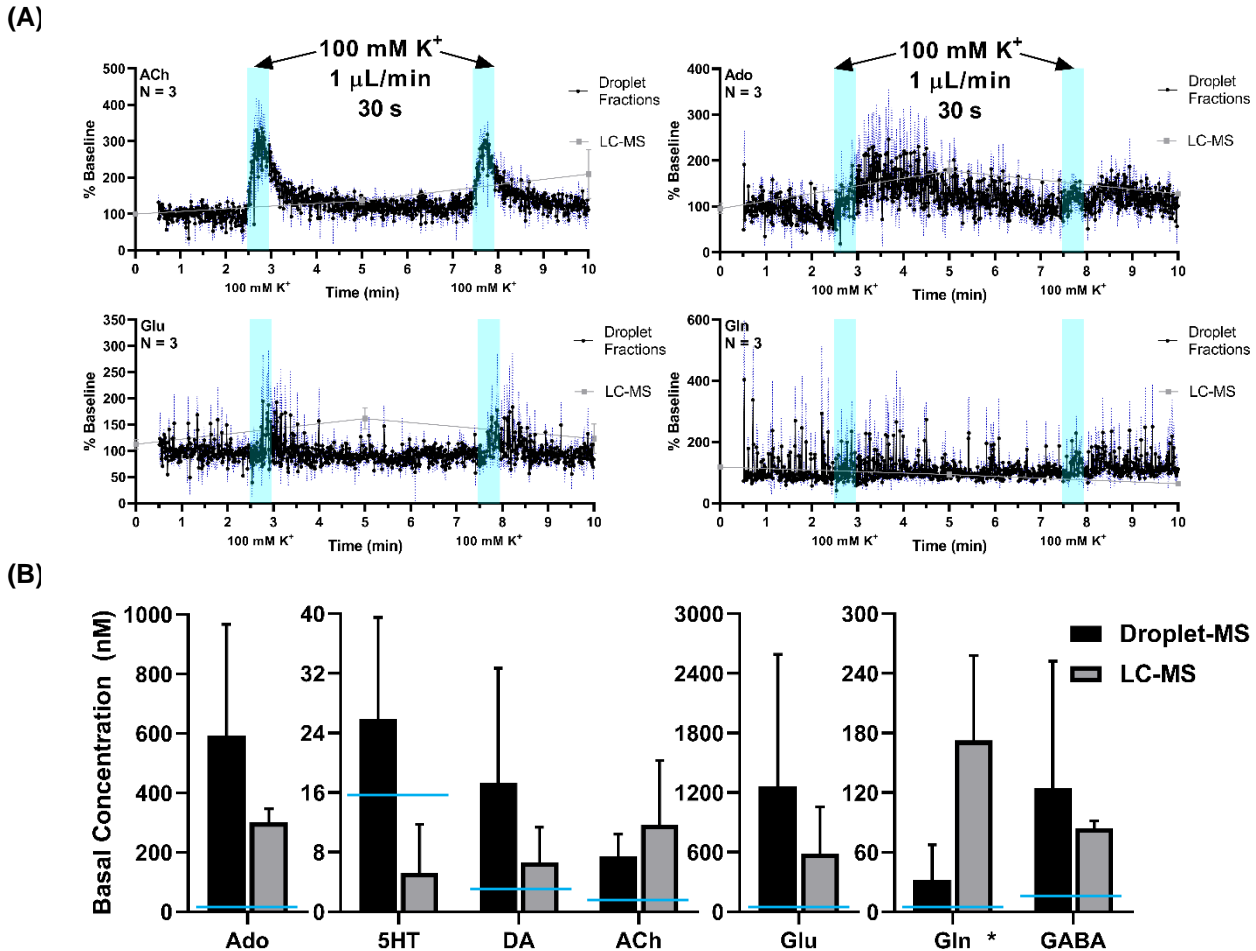


Figure 3-5. (A) *In vivo* experiments using MD probes sampling the striatum over a 10 min collection period. 500 nL of high potassium aCSF was administered over 30 s beginning at 0 and 5 min, with an approximate 2.5 min dead time. Three biological replicates were obtained over two mice (one mouse with two hemispheres). Points converted to percent baseline to normalize for concentration differences and all three traces were averaged. SEM shown as a blue-dotted line. Gray squares and connecting lines represent LC fractionation method, with fractions collected over 5 min intervals. (B) Basal concentrations determined by droplet-MS and LC-MS in high potassium stimulation experiments and the LODs (blue line) for each by droplet-MS.

temporal information is missing such as duration between stimulation and response, duration of elevated neurotransmitter concentrations, and speed of neurotransmitter increase/decrease. On the other hand, each of these details can be seen in the droplet fraction method, showing much more suitability for monitoring short-term dynamics and rapid neurotransmitter changes. Similar neurochemical changes in response to high potassium levels have been reported for DA, ACh, Glu, GABA, and 5HT.^{98,139,147-149} Accuracy and quantitative capabilities of the droplet-MS method are also assessed by comparison of the basal concentrations determined by each method (Figure 3-5B). Though the representative averages obtained by each method show notable error (ranging from 38 – 137%), there was a high degree of variation in the basal concentration measured between

each animal/*in vivo* experiment that may be a result of biological differences or MD probe differences. Based on a paired t-test of the basal concentrations determined for all target compounds by each method and the standard deviation between each biological replicate, the two methods measured statistically similar basal concentrations ($P = 0.26$). The basal levels measured for each neurochemical by droplet-MS were above the LOD for the method, allowing for reliable quantification of baseline concentrations. Additionally, the method generally showed low droplet-to-droplet concentration variation at the basal level, with relative standard deviation among droplets at basal levels averaging 36, 50, 32, 23, 54, 28, and 30% for Ado, 5HT, DA, Glu, Gln, ACh, and GABA, respectively. These variations are slightly higher than those from *in vitro* experiments (10-20% droplet-to-droplet variation for DA, ACh), likely due to the presence of a complex matrix rather than water and lower basal concentrations for *in vivo* experiments than what was used for *in vitro*.

Similarly, the striatum was sampled over a 5 minute period as 500 nL of 100 μ M AMPH was administered locally (1 μ L/min for 30 s). Four biological replicates were obtained over three mice (two hemispheres in one mouse). As expected, AMPH elicits a much more selective response, where quantifiable changes are only present in DA and 5HT (Figure 3-6), and the remaining compounds stayed at basal levels during AMPH stimulation. In addition to the seven

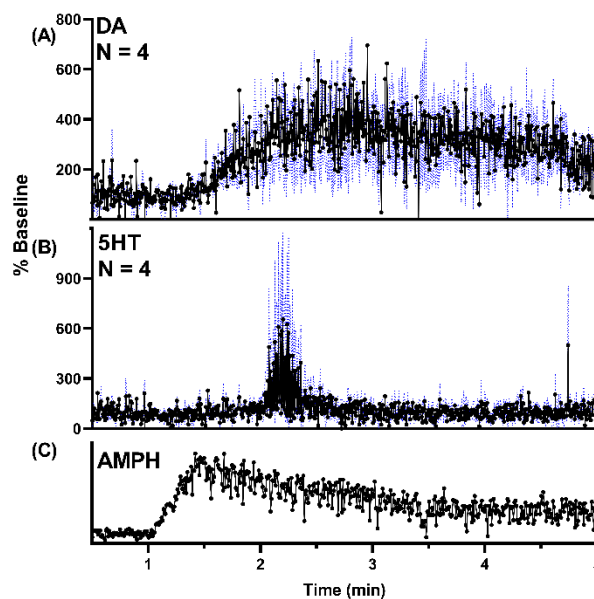


Figure 3-6. *In vivo* experiments using MD probes sampling the striatum over 5 min with 500 nL of 100 μ M AMPH administered over 30 s starting at -1 min. Four biological replicates were obtained over three mice (one mouse with two hemispheres). Points converted to percent baseline to normalize for concentration differences and all three traces were averaged. Black dots and connecting lines represent droplet fraction method with SEM shown as a blue-dotted line. AMPH was monitored for one of the four replicates.

neurochemicals, AMPH in the extracellular space was also monitored for one of the four replicates, allowing for further correlation between drug levels and neurotransmitter response (Figure 3-6C). Though DA was expected to increase in the presence of AMPH, we observed a delayed response, where DA concentrations began to increase approximately 30 s after AMPH appeared (Figure 3-6A). DA increased to 400% of baseline levels within 30 s, and experienced an extended duration of increased baseline, decreasing to 300% baseline after three minutes of increased response. The extended increase in DA levels is most likely caused by the lingering presence of AMPH (Figure 3-6C). AMPH is also known to increase extracellular 5HT.¹⁵⁰⁻¹⁵² Here, we observed 5HT experiences a brief but sharp increase from baseline approximately 60 s after AMPH appeared, also correlating to the time of maximum DA concentration (Figure 3-6B). Though the observed 5HT response has relatively high variability across the biological replicates, it is believed to be a biological response as its response to AMPH is temporally similar to DA and the IS (d45HT) during exhibited no change in signal intensity for the *in vivo* experiment with the largest 5HT baseline change (Figure 3-7). The traces shown are representative averages and SEMs of all biological replicates obtained. All individual traces of each biological replicate for each compound can be seen in Appendix 2.

Conclusions

Utilizing the sensitivity and selectivity of low flow nESI paired with MS/MS in a triple quadrupole mass spectrometer, we have developed a method to monitor several low abundance neurochemicals from dialysate simultaneously with LODs as low as 2 nM (ACh).

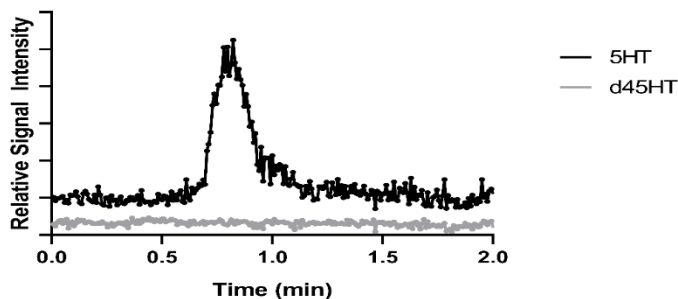


Figure 3-7. Validation of the biological response of 5HT to AMPH presence in one of the AMPH stimulation replicates. The black dots and connecting lines represent 5HT concentrations collected during AMPH stimulation and the gray dots and lines represent the internal standard d45HT used during droplet generation and nESI-MS/MS.

Pairing this analysis with droplet microfluidics yields 10.75 s temporal resolution and can generate down to 3 nL dialysate fractions at up to 3 Hz from an MD probe. In principle, even better LODs and temporal resolution could be obtained if a newer MS were utilized, as it may offer improved ion transmission and faster scan speeds. The monitoring dynamics of the developed system is compared to a conventional LC-MS/MS assay for MD neurochemical monitoring, where the droplet fraction method offers far more temporal information. The system is also applied to monitoring short-term neurotransmitter dynamics in response to selective drug stimulation (AMPH). This method demonstrates excellent suitability for short-term neurotransmitter dynamics and can offer important insights that may not be attained by LC-MS for MD analysis without sacrificing the chemical range offered by MD sampling. Finally, the inclusion of many neurotransmitters in a method with high temporal resolution offers a distinct benefit of potential to correlate the various neurotransmitter changes with one another, a feature that is unavailable in techniques with more limited analyte ranges.

Chapter 4
High Throughput Liquid-Liquid Extractions with Nanoliter Volumes Using Slug Flow
Nanoextraction

Reproduced from Wells *et al*, *Anal. Chem.* **2020**, *92*, 3189-3197. Copyright 2020 American Chemical Society

Introduction

Extractions are widely utilized in chemistry and serve a variety of purposes including compound isolation, partitioning measurements, analyte preconcentration, and sample preparation. The most commonly used extraction techniques are solid phase extraction (SPE) and liquid-liquid extraction (LLE). Though SPEs have several advantages, LLE remain popular because they are cost effective, easy to achieve, and require little method development.^{44,153–155} Much effort has been allotted to reducing the size and scale of LLE. Liquid phase microextractions (LPME)^{44,156} are more rapid, use lower volumes, and better facilitate pairing with analytical techniques compared to their macroscale counterparts.^{157,158}

Liquid phase extractions that can be performed in-line or on-line with analytical techniques or detection methods are attractive for increased automation and throughput. This goal has led to the development of hollow fiber based microextractions,^{159–161} single drop microextractions,^{162,163} liquid-liquid-liquid microextractions,^{164,165} and electromembrane extractions.^{166,167} Besides facilitating coupling to analytical techniques,¹⁵⁸ these methods also allow for reduction of sample and extraction solvent volumes to the hundreds of microliter range rather than the milliliters typical for LLE and can reduce extraction time to minutes. Even further improvements can be obtained

by using microfluidics. Several microfluidic LLE devices have been developed to allow for quicker and lower volume extractions including parallel flow devices,^{168,169} on-chip dispersive liquid-liquid extractions,¹⁷⁰ Y-junction or T-junction devices for extraction,^{86,171} and others. Microfluidic LLE techniques use microliters or less of sample and solvent and have sub-minute equilibration times, though these are still limited to a single sample extraction at a time.

A recently reported variant of low-volume LLE is slug flow microextraction (SFME).¹⁷² In this method, 5 μ L of sample and 5 μ L of organic extraction phase are placed adjacent to one another in a fused-silica capillary nanoelectrospray ionization (nESI) spray tip. Tilting the capillary back and forth resulted in the slugs flowing back and forth in the capillary and interacting at their interface to yield a rapid extraction. The analyte-enriched extraction phase could then be pushed to the end of the tip and quantitatively analyzed by nESI-MS. SFME is a simple, rapid, and low-volume sample preparation method to reduce matrix effects for nESI-MS analysis of samples, and was found to drastically reduce the limits of detection for several analytes. SFME has been utilized in a variety of ways including determination of trace amphetamine-type drugs when coupled to paper spray-MS,¹⁷³ three-phase SFME for polar analyte determination,¹⁶⁵ and for preconcentration of analyte from bulk sample.¹⁷⁴

Here, we report slug-flow nanoextraction (SFNE), a method that combines principles of SFME and droplet microfluidics. In SFNE, sample and extraction solvent plug pairs (“phase pairs”) are juxtaposed in a tube, similar to SFME; however, a multitude of individual pairs are separated by an immiscible oil, like that used in droplet microfluidics,⁷⁹ so that linear arrays of samples, up to 60 in this case, can be entrained in a single capillary or channel. The method uses down to 5 nL of sample, 3 orders of magnitude lower volume than reported by previous SFME experiments. Extraction occurs rapidly as the sample-extraction solvent plug pairs flow through

the tube so that the SFNE format is high-throughput, with 60 extractions completed in under 5 min. Because the method uses continuous flow in one direction, it can be coupled to different detectors to facilitate diverse applications. The method is coupled with on-line UV detection for measurement of octanol-water coefficients (K_{ow} , log D, log P) of drugs and coupled to ESI-MS/MS with improved LODs for determination of drugs in biofluid samples.

The K_{ow} is an important value to know for environmentally and pharmaceutically relevant compounds.¹⁷⁵ The shake-flask and slow stirring methods are traditional means for determining K_{ow} ; however, they have several drawbacks including requiring large volumes (milliliter range) and long times (minutes - hour).¹⁷⁶⁻¹⁷⁸ Chromatography can be used for approximating K_{ow} . This approach can have advantages in reproducibility, insensitivity to impurities, and sometimes speed; but it is limited in the molecules that are amenable.^{175,179} SFNE allows for direct determination of K_{ow} using nanoliters of volume per extraction and rapid extraction times. Since this method uses an octanol-water extraction similar to the shake flask method, it is applicable to a broad range of compounds and makes a direct measurement of K_{ow} rather than approximation as with chromatographic methods.

For ESI in MS, ionization suppression of analytes in complex mixtures can reduce signal making determinations challenging,²⁵ a common problem in biological sample analysis. Because of this, MS analysis often requires sample preparation, such as extraction, prior to analysis.⁴⁴ Selectively isolating a compound / compounds with an extraction prevents or lessens ionization suppression by removing compounds that compete for ionization. Employing SFNE paired with MS, the extraction step is performed in-line, reducing the sample, solvent, and time consumption normally associated with sample preparation. Additionally, the segmented flow format of the system enables arrays of samples to be extracted and analyzed at high-throughput. Here, we show

that SFNE-MS improves S/N for several drugs analyzed from human plasma, artificial cerebral spinal fluid, and synthetic urine.

Materials and Methods

Reagents and Materials. All chemicals and solvents were purchased from Sigma-Aldrich (St. Louis, MI, USA) unless stated otherwise. PFD was purchased from Oakwood Chemical (Columbia Hwy, Estill, SC, USA). Drug standards were prepared in HPLC-grade water at 1 – 10 mM, aliquoted, and stored at -20 °C. Standards were thawed daily for use and diluted to the desired concentration. Rhodamine 6G (Rh6G) stock was prepared at 10 mg/mL and stored at room temperature. Aliquots were taken for daily use. For molecules that required a calibration in the extraction phase, acetaminophen (ACP) and Rh6G were prepared in 1-octanol ($\geq 99\%$) and chloroform ($\geq 99.5\%$), respectively and serial diluted. Surine™ negative urine control was purchased from Cerilliant (Paloma Dr., Round Rock, TX, USA). Pooled human plasma samples were obtained from Michigan Regional Comprehensive Metabolomics Resource Core. aCSF was prepared in 500 mL of water with 145 mM NaCl, 2.68 mM KCl, 1.4 mM CaCl₂ • 2H₂O, 1.01 mM MgSO₄ • 7H₂O, 1.55 mM Na₂HPO₄, and 0.45 mM NaH₂PO₄ • H₂O at pH 7.4. Sheath liquid for ESI consisted of 50:50 MeOH:H₂O (v:v) with 0.1% formic acid (FA).

Droplet Generation and Analysis. Hamilton (Reno, Nevada, USA) gastight syringes were used (25 μ L, 1 mL) with Chemyx Inc. Fusion 400 syringe pumps for infusion. For droplet generation, a Harvard Apparatus PHD 2000 programmable syringe pump was used. Single-phase droplets were generated using a syringe pump drawing at a rate of 300 nL/min using a 25 μ L syringe with a 15-30 cm length of 100 μ m inner diameter (i.d.) 360 μ m outer diameter (o.d.) PFA tubing from IDEX (Lake Forest, Illinois, USA). Connections were made using low dead volume

unions from Valco Instruments Co., Inc. (Houston, TX, USA). Droplet generation was performed using an XYZ-position manipulator to draw from a 384-microwell plate as described before.^{99,180} The positioner was used to alternate the tubing between the fluoruous carrier fluid PFD (0.5 s draw time) and aqueous sample (2 s draw time); 200 single-phase droplets were generated before analysis. The same draw rate and syringe were used for two-phase slugs with the addition of extraction phase and air for segmentation. During two-phase slug generation, an XYZ-positioner would move the tubing to sequentially draw PFD, air, extraction phase, and aqueous phase repeatedly as shown in Figure 1.⁹⁹

A syringe and line of tubing with droplets would be taken to either MS, UV, or laser-induced fluorescence (LIF) for analysis. For LIF, a Coherent (Santa Clara, CA, USA) Sapphire 488-20 CDRH laser was used with a Zeiss (Jena, Germany) D-104 microscope and a PTI (Piscataway, NJ, USA) 814 photomultiplier, with emission collected through a 530 nm bandpass filter. For UV detection, a Linear (Auburn, CA, USA) UVIS 200 variable wavelength absorbance detector with a slot for a capillary flow cell was used for detection of analytes in extraction on-line with the wavelength set to 243 nm. For optical detection modes, the tubing was aligned with the light source and flowed at 500 nL/min. For MS, the tubing was placed through the sheath-flow sprayer so that the tip emerged. The contents then flowed at 500 nL/min and the sheath-flow at 10

Table 4-1. The drugs used for MS experiments were investigated for optimal transitions, fragmentor voltages and collision energies individually. Other MS settings were investigated for signal improvements including drying gas temperature (175 C), drying gas flow (10 L/min), nebulizer gas pressure (7 psi), and capillary voltage (3 kV). The resulting values were used for MS/MS via single reaction monitoring mode (SRM), where every transition is monitored throughout the infusion

| Compound | Precursor Ion | Product Ion | Fragmentor Voltage | Collision Energy |
|-------------------------|----------------------|--------------------|---------------------------|-------------------------|
| Clemastine | 344.1 | 215.1 | 140 | 13 |
| Dextromethorphan | 272.1 | 213.1 | 120 | 28 |
| Doxylamine | 271.1 | 182.1 | 120 | 15 |
| Diphenhydramine | 256.2 | 167.1 | 120 | 17 |
| Methoxyverapamil | 485.2 | 165.1 | 140 | 35 |

$\mu\text{L}/\text{min}$. Droplets or two-phase slugs were analyzed using single reaction monitoring (SRM) mode for MS/MS in all MS experiments, using previously determined and optimized transitions for each analyte of interest (Table 4-1). As previously reported, the PFD does not support ESI because it is inert and non-conductive.^{1,99} We typically observe that PFD forms a bead on the top of the ESI source and flows away. Little contamination of the mass spectrometer has been observed. ESI was carried out using an Agilent CE ESI-MS Sprayer and a syringe pump for sheath-flow with an Agilent 6410B Triple Quadrupole controlled by Agilent Masshunter software.

Results and Discussion

SFNE relies on segmented flow wherein extraction solvent plugs (organic phase), analyte plugs (aqueous phase), and carrier fluid plugs (an immiscible fluid) are arranged in order and pumped through a conduit such as a capillary tube (Figure 4-1). For this work, sample and extraction phase plugs were assembled using a syringe pump to pull fluids into a tube and XYZ-positioner to move the tube inlet from well-to-well on a 384 microwell-plate (Figure 4-1A). The multiphase fluid, consisting of arrays of sample-extraction phase pairs, is pumped toward an online detector for analysis (Figure 4-1B). In this work we used PFD as the carrier fluid because it is immiscible with both water and all tested extraction solvents. Organic phase plugs tend to flow faster through the PFD than aqueous plugs such that an organic phase plug would catch the upstream aqueous phase plug to initiate an extraction (Figure 4-1C). To prevent different sample pairs from interacting with each other, an air bubble was positioned between the phase pairs (Figure 4-1A and 4-1B). Extractions that occur with this method rely on internal mixing resulting from circulation of the contents within a droplet caused by friction from viscous drag as droplets flow throughout the tubing (Figure 4-1D).^{79,181} This mixing constantly refreshes the interface between the extraction phase droplet and the aqueous sample droplet to promote partitioning.

Using rhodamine 6G (Rh6G) to observe partitioning, we observed extractions within seconds (< 5 s) once the interface of the two-phase slug is formed. The rapid extraction can be attributed to both rapid mixing and miniaturization. SFME, which presumably achieves a similar internal recirculation of plugs to establish partitioning equilibrium, required 5 manually induced extraction cycles for 5 μ L samples.¹⁷² Upon scaling the volumes down 3 orders of magnitude for SFNE, the extraction time/flow distance required for partitioning to reach equilibrium is dramatically

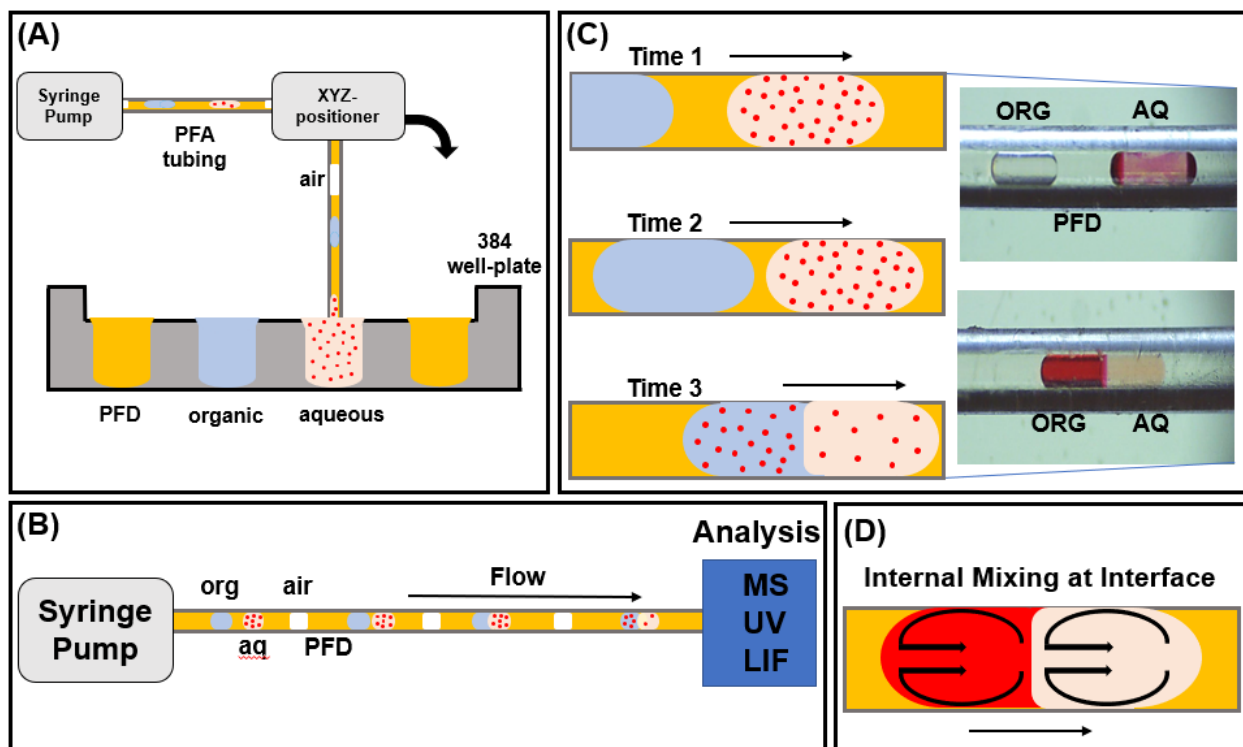


Figure 4-1. (A) The two-phase slug generation process is shown, where a length of PFA tubing with applied vacuum is sequentially dipped in PFD, extraction solvent, and aqueous sample. For most experiments, an air plug is also included before each extraction phase. (B) Once a line of tubing is filled with phase pairs, flow is driven towards the outlet allowing the extraction phase to accelerate and contact the sample. The tube can be paired with a variety of detectors, where extractions occur while in-transit to an online detector. (C) Shown are three time points for a single phase pair as the two phases are interfaced. Though initially far apart, the organic plug accelerates towards the leading aqueous plug, forming a partitioning interface and allowing extraction. The photographs show the appearance of the phase pair before and after the extraction occurs, where the second image shows that a majority of Rh6G has transferred from aqueous to organic. (D) Due to the internal mixing within the low volume droplets, contents of the aqueous sample partition rapidly into the extraction phase mode (SRM), where every transition is monitored throughout the infusion

decreased. This near-immediate extraction and the in-capillary array of extractions makes this technique compatible for hyphenation with other techniques and for many extractions to take place simultaneously. The sample volume and time required for extraction are considerably lower than

other reported LPME techniques such as hollow fiber liquid-phase microextractions,^{182,183} dispersive liquid-liquid microextractions,^{184,185} and SFME. These techniques require between several microliters to milliliters of each phase and take several minutes for extraction.

We sought to compare the results obtained by SFNE to traditional LLE using a flask. To do so, we compared partitioning of 100 μM Rh6G between water and chloroform by the two methods. For SFNE, 60 phase pairs were formed. The resulting plugs were flowed through an LIF detector for on-line detection of the resulting distribution of Rh6G (Figure 4-2A). As shown by the trace, each droplet pair is detected as a fluorescent peak, and each pair has a distinct step from lower to higher signal resulting from detection in each phase. The signal step is not as sharp as might be expected from the images shown in Figure 4-2A. This phenomenon is possibly due to the laser spot not being focused to a sufficiently small spot to detect the change at the interface. It may also reflect aberrations due to a curved interface between the phases. For analysis, we used 10 randomly selected phase-pairs throughout the trace for detection of signal in each phase. For comparison, we also performed extractions of the same concentration of Rh6G using the same sample and extraction phase by a microshake-flask extraction. In this method, 200 μL of each phase were vortexed in a 600 μL vial for 1 min and centrifuged to eliminate any emulsions. Three plugs from each of these phases were generated into a length of tubing and measured by LIF (Figure 4-2B). For each of these modes of extraction, the ratio of the signal in extraction phase over signal in aqueous phase was taken to show the relative partition coefficients obtained by each method of extraction (Figure 4-2C). The results show that partition coefficients between the two methods are the same (based on P-value determined by a t-test). These results confirm the visual observation of rapid equilibration between the phases.

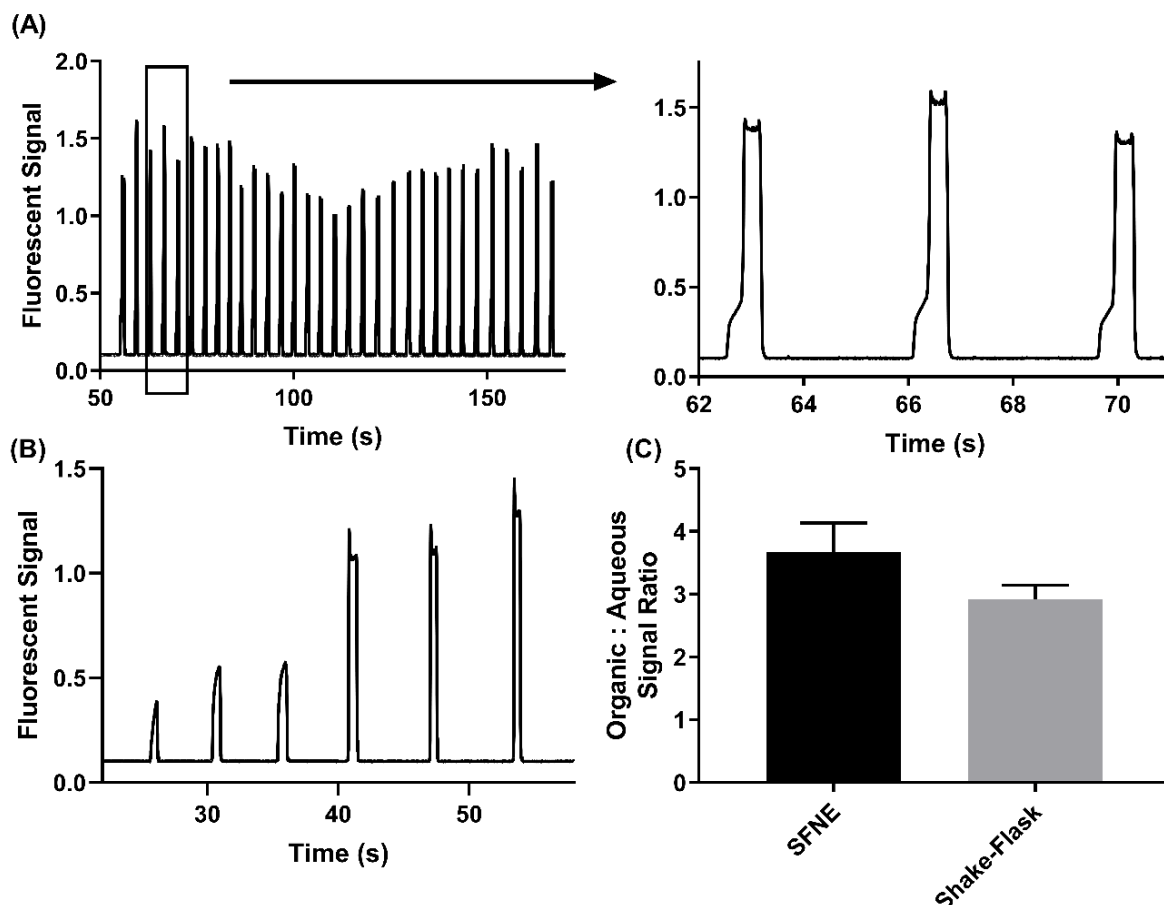


Figure 4-2. (A) A train of phase pairs with extraction solvent CHCl_3 was generated and the partitioning of fluorescent dye Rh6G was measured by LIF. Though initially dissolved in water, most of the rhodamine partitioned into CHCl_3 by SFNE. The variation in signal intensity is due to the variations in volumes between phase pairs. (B) Similarly, an offline extraction via microshake-flask extraction was performed with the aqueous rhodamine and extraction solvent CHCl_3 . Three plugs of each layer were generated and analyzed by LIF. (C) The ratios of signal from LLE and SFNE were graphed and show similar extraction efficiency. The increased ratio by SFNE is due to a slightly higher volume of aqueous sample than organic solvent during extraction.

During creation of phase pairs, it is possible to vary volume ratios of the 2 phases to affect the extraction. Such variations can be useful, for example to concentrate analytes into one phase. The ability to control extractions in this way was tested by generating phase pairs in a train with different volume ratios, using $10 \mu\text{M}$ Rh6G as the analyte in water and chloroform as the extraction phase. The fluorescence signal in each portion of each extraction slug was measured by LIF. Figure 4-3A shows the measurements of fluorescent signal in the phase pairs as the volume ratio (aq/org) increases. With increasing ratio of aqueous volume to extraction phase volume, the signal increases in the organic phase and the aqueous portions of the phase pairs elongate and the organic portions

narrow. These data follow expected trends. As the percent organic volume per phase pair decreases, the concentration in organic phase is expected to increase as shown the following equation,

$$C_{org,eq} = KC_{aq,eq} = \frac{KC_{aq,initial}}{1 + KV_o/V_{aq}} \quad [4-1]$$

where $C_{aq,eq}$ and $C_{aq,initial}$ are the equilibrium and initial concentrations in aqueous, $C_{org,eq}$ is the equilibrium concentration in organic, K is the partition coefficient, and V_o and V_{aq} are the organic and aqueous volumes.¹⁵⁶ This equation reasonably matches a plot of volume ratio (V_o/V_{aq}) against concentration (determined by external calibration) in the organic phase (where $K = 4.8$) as shown in Figure 4-3B. Manipulation of the phase ratio can be useful in different ways. For example, extracting from a large volume sample into a relatively small extraction phase can help concentrate analytes. In Figure 4-3B, C_{org} is over 5 times higher when the phase pair volume ratio is changed from 1.6 to 0.08. This technique can be implemented for preconcentration in SFNE as previously demonstrated in SFME.¹⁷⁴

As illustrated by the results from Figure 4-2, the method allows arrays of samples to be extracted at one time. In this experiment, a throughput of 3.6 s per extraction was achieved during detection by LIF with a total of 32 extractions. However, SFNE is not limited to this throughput or extraction array quantity. The number of extractions that can be achieved in a single run is dependent on the length of capillary tubing used.

Determining K_{ow} . A common use of LLE is to determine K_{ow} . The K_{ow} is used in the pharmaceutical industry to provide information on pharmacokinetics, bioavailability, and permeability through biological membranes.¹⁸⁶ It is also important in environmental analysis as a parameter for assessing the environmental risks of different compounds.¹⁸⁷ We next sought to

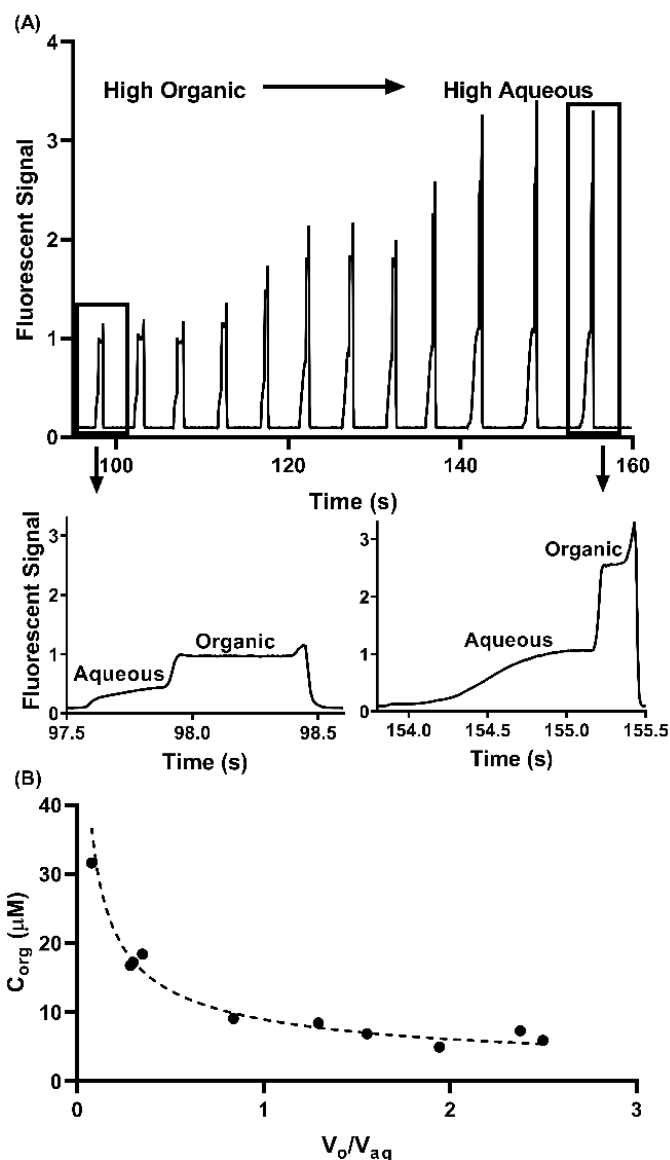


Figure 4-3. Volume ratios of the two-phases were manipulated for each phase pair in a train. (A) Four pairs of high organic volume, similar volume of each, and high aqueous sample volume were generated and measured by LIF. (B) A plot of concentration in extraction phase at equilibrium vs. volume ratio for each phase pair. As the volume is manipulated to increase sample volume and lower extraction phase volume, the final concentration in the extraction phase increases, achieving a preconcentration effect. A trendline (dotted curve) was fitted to theoretical $C_{org,eq}$ values obtained from Equation 4-1 (using $K = 4.82$), which fits the experimentally determined values. Performed with $10 \mu\text{M}$ Rh6G, with flow rates of $0.5 \mu\text{L}/\text{min}$.

determine if SFNE could be used for determining K_{ow} with ACP as the test analyte. For this work, the droplets were passed through an on-line UV absorbance detector to measure the concentration in each phase. Figure 4-4 illustrates a typical data trace from this experiment. The absorbance response trace includes a series of octanol droplets containing ACP from $2.0 - 0.2 \text{ mM}$, followed by a series of water droplets containing ACP from $1.0 - 0.1 \text{ mM}$. These sections of the trace allow calibration within each of the solvents used for the extraction. The next section of droplets contained 5 plugs of each phase collected from a shake-flask extraction so that a comparison to the SFNE could be made. Finally, 12 SFNE two-phase slugs were passed through the

detector. Having both calibrations allows for the concentration of ACP to be determined in each layer after extraction, giving an accurate K_{ow} value. Each calibration curve in the experiment had

good linearity ($R^2 \geq 0.998$). Using calibrations to determine concentration in each layer after extraction in each method, K_{ow} (C_{oct}/C_{aq}) was calculated. The shake-flask yielded K_{ow} of 2.48 ± 0.02 ($\log K = 0.39$) and the SFNE method determined a K_{ow} of 2.49 ± 0.01 ($\log K = 0.40$), showing no statistical differences. Previously reported $\log K_{ow}$ literature values for ACP range from 0.29 - 0.51, further confirming SFNE provides an accurate measurement.^{188–191} SFNE can determine K_{ow} with excellent repeatability, showing an RSD of 0.7%.

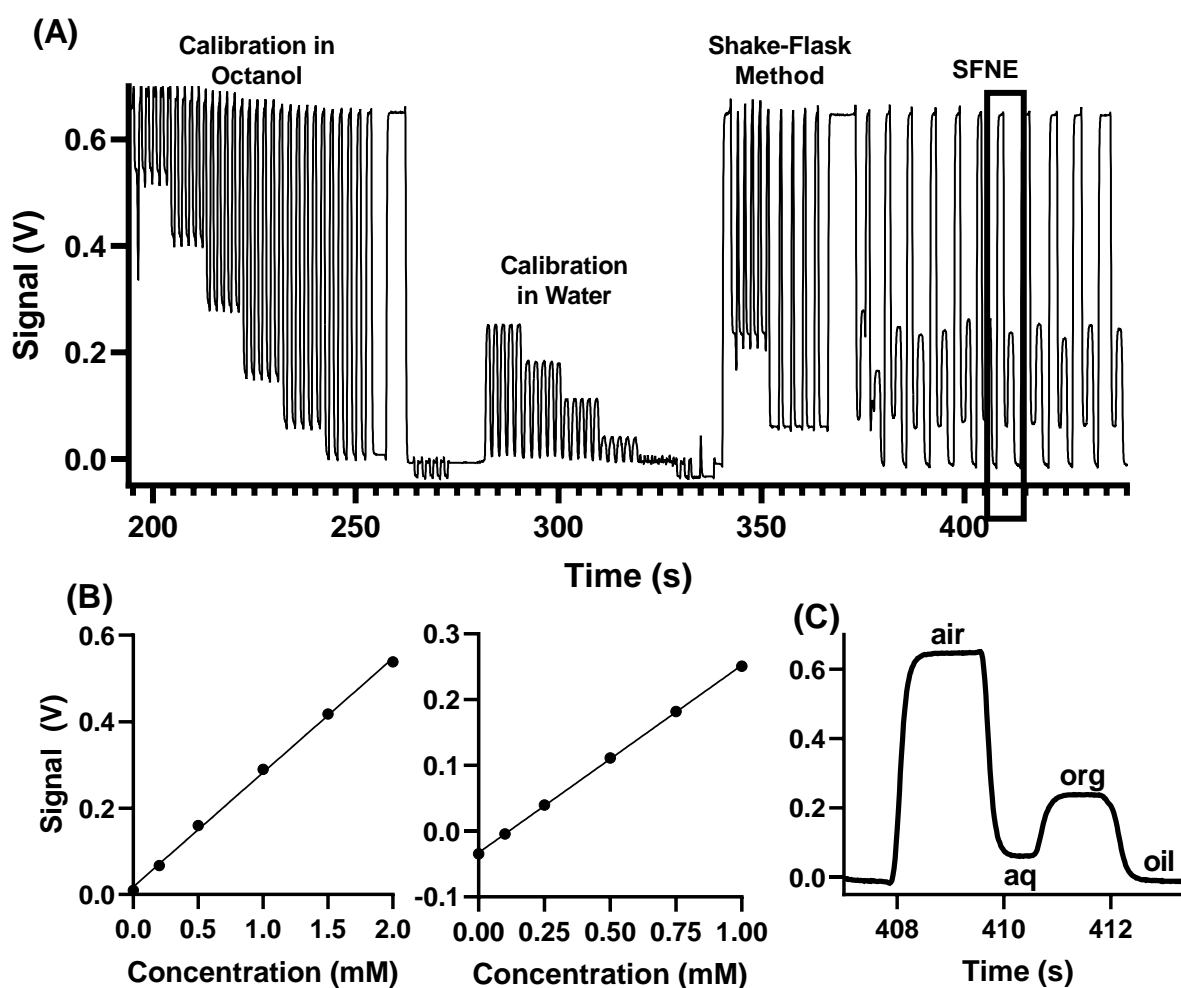


Figure 4-4. (A) In a single experiment, acetaminophen K_{ow} was determined by the common shake-flask method and SFNE using UV VIS detection. First, acetaminophen was calibrated from 1.0 – 0.1 mM in water and 2.0 – 0.2 mM in octanol. Second, plugs generated from each layer of the shake flask extraction were measured by UV. The shake flask extraction was performed by placing 100 μ L of pure octanol and 100 μ L of 1 mM acetaminophen (aq) into a PCR tube, vortexing for 1 min, and centrifuging for 5 min. Finally, two-phase slugs initially containing pure octanol and 1 mM acetaminophen (aq) were measured by UV. The K_{ow} was determined from each method by determining concentration of acetaminophen in each layer using the calibrations and taking the quotient of C_{org}/C_{aq} . (B) The calibration of ACP in each phase was plotted and showed good linearity. Error bars are present but hidden by markers. (C) Zooming in on a central phase-pair better displays all of the layers present. Each phase is segregated by PFD and air.

In this experiment, extractions from the shake-flask method were added to the work-flow to obtain a comparison between SFNE and traditional means of measuring K_{ow} ; but, this addition is not required for determining K_{ow} . Technology for determining partition coefficients has yet to achieve rapid and low volume techniques. With the SFNE method for K_{ow} determination, two-

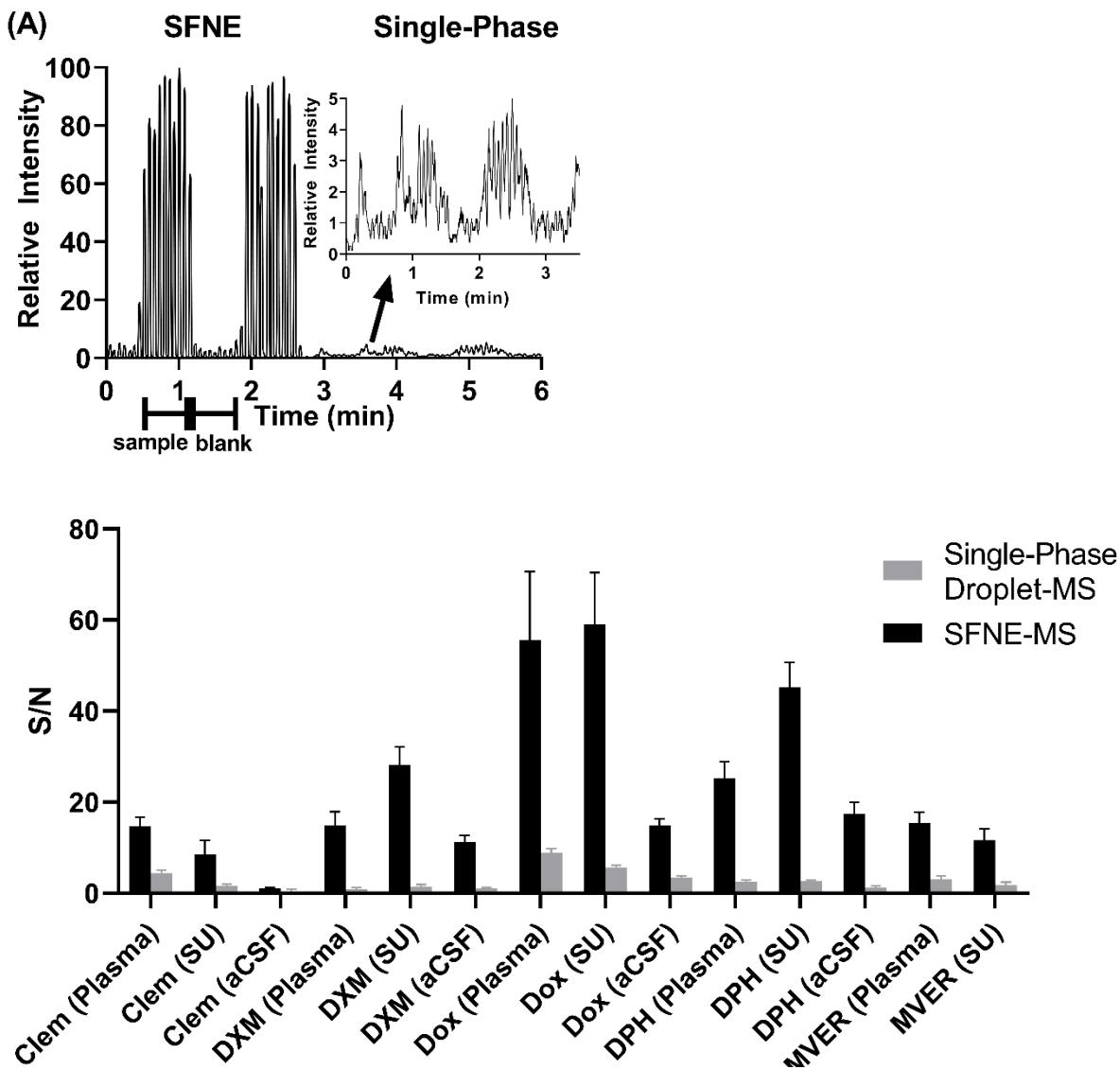


Figure 4-5. (A) In a comparison of SFNE-MS and single-phase droplet-MS, a train of phase pairs was generated with sample plug consisting of the drug mixture in plasma (1 μ M) and extraction plug EtOAc. Each train consisted of 10 analyte containing phase pairs alternating with 10 blank phase pairs. For single-phase droplet-MS, a droplet train consisting of the same sample layer was generated, without presence of an extraction phase, alternating 10 analyte containing droplets with 10 blank droplets. Each form of infusion was measured by ESI-MS/MS. The y-axis shows intensity normalized to the highest point between the two EIC traces. (B) Five drug compounds were analyzed by SFNE-MS and single-phase droplet-MS from multiple biological matrices. Measurements made from each method used the same sample solutions on the same day, forming them into a train of two-phase/one-phase droplets for measurements. Average S/N calculated by subtracting average noise from each signal and dividing by the root mean square of the noise peaks. The average and standard deviation of these values are reported here.

phase slug generation and analysis by UV detection are automated. This format, along with near-immediate extractions and potential for an array of compounds per experiment, allow for high-throughput K_{ow} measurements by SFNE. The low organic phase volume and amount of compound required for each measurement allow for greener chemistry, especially compared with other high-throughput measurements which use high microliter to milliliter volumes of octanol per extraction.^{179,192} The benefits provided by SFNE are potentially significant given the widespread use of K_{ow} .

SFNE-MS. Most biological sample analysis by ESI-MS requires a sample separation or extraction step to reduce matrix effects such as ionization suppression. Previous extractions used for ESI-MS are on microliter scale and are limited to a single sample per infusion.^{50,160,164,172} We tested the utility of SFNE paired directly with ESI-MS/MS for the determination of several drugs simultaneously in complex biological samples. Several extraction phases were investigated including $CHCl_3$, dichloromethane (DCM), and ethyl acetate (EtOAc). EtOAc was the only extraction phase tested that showed significant signal response with MS and was selected for all SFNE-MS experiments in this work. Similarly, previously reported SFME-ESI studies found

Table 4-2. Five drug compounds were analyzed by SFNE-MS and droplet-MS from multiple biological matrices. Measurements made from each method used the same sample solutions on the same day, forming them into a train of phase pairs/droplets for analysis. Also shown, LODs and linearity were determined from calibrations of each compound in plasma for SFNE-MS. The R^2 value denotes linearity from 10 μM to 0.1 μM .

| | S/N (1 μM Standards) | | | | | | SFNE Calibration | | | |
|-------------------------|------------------------------|---------|------|---------|------|---------|------------------|----------------|-------------|-------|
| | Plasma | | SU | | aCSF | | Plasma | | | |
| | SFNE | Droplet | SFNE | Droplet | SFNE | Droplet | LOD (nM) | LOD (ng/mL) | LOD (fg) | R^2 |
| Clemastine | 14.6 | 4.4 | 8.5 | 1.6 | 1.0 | 0.4 | 40 | 14 | 70 | 0.98 |
| Dextromethorphan | 14.9 | 3.0 | 28.2 | 1.5 | 11.2 | 1.0 | 60 | 16 | 80 | 0.99 |
| Doxylamine | 55.6 | 8.8 | 59.1 | 5.7 | 14.8 | 3.4 | 7 | 1.9 | 9 | 0.99 |
| Diphenhydramine | 25.2 | 2.5 | 45.2 | 2.6 | 17.5 | 1.3 | 50 | 13 | 60 | 0.98 |
| Methoxyverapamil | 15.5 | 3.1 | 11.7 | 1.8 | n/a | n/a | 30 | 15 | 70 | 0.98 |

EtOAc to be the most effective solvent for extraction and ionization.^{165,172–174} Fortunately, since EtOAc has a weak polarity, it is an effective solvent for extracting a broad range of compounds.

To test the effectiveness of SFNE for reducing the effects of ionization suppression on analytes, SFNE-MS was compared to direct infusion of single-phase droplet samples under the same conditions for ionization and MS/MS analysis. Five drugs were tested including clemastine (Clem), dextromethorphan (DXM), doxylamine (Dox), diphenhydramine (DPH), and methoxyverapamil (MVER), all spiked to

near therapeutic concentrations into human plasma. A summary of figures of merit from these experiments are given in Table 4-2. We found that SFNE prior to ionization resulted in higher signal intensity over direct infusion of single-phase spiked plasma droplets (Figure 4-5). In Figure 4-5A, in an infusion of DPH droplets in plasma, 20-fold higher maximum signal from an extracted ion count (EIC) was obtained by SFNE-MS/MS over single-phase droplet-MS/MS. Not only is signal intensity improved by SFNE, but also S/N. We see S/N from plasma for Clem, DXM, Dox, DPH, and MVER improve by 230, 1760,

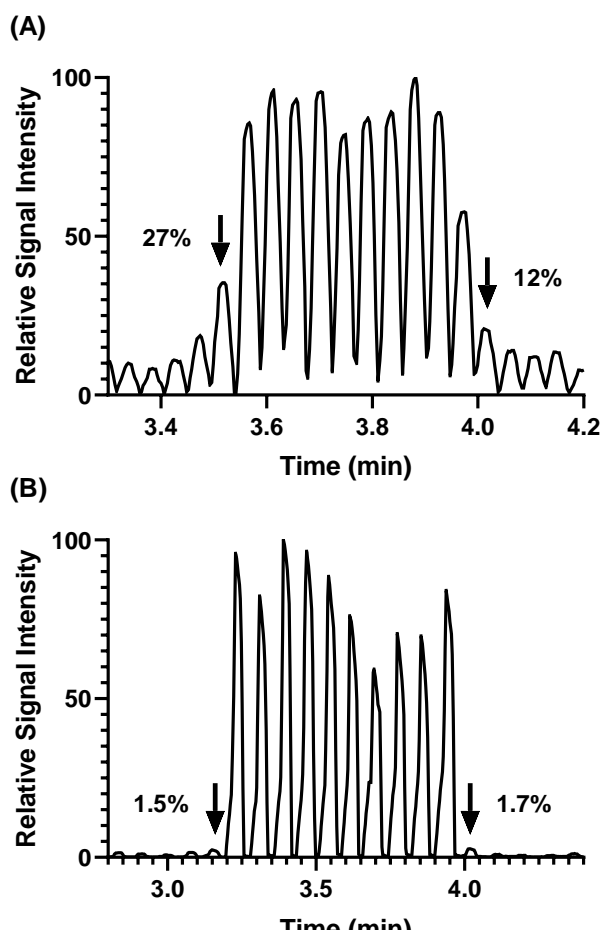


Figure 4-6. A comparison between droplet-MS and SFNE-MS on synthetic urine droplets containing 1 μ M Dox (using EtOAc extraction phase for SFNE). Figure 4-6A shows the trace of droplet-MS. There is a substantial amount of carry over that can be seen here, with 27% analyte carry over into the adjacent droplet prior to samples and 12% carry over into the adjacent droplet post samples. This carry over effect is greatly reduced in SFNE as seen in Figure 4-6B, with 1.5% carry over before samples and 1.7% carry over after. The other tested compounds also show reductions in carry over using SFNE-MS over droplet-MS.

530, 900, and 400%, respectively (Figure 4-5B). The S/N improvements by SFNE shown in Figure 4-5B are due to the extraction of the analytes by SFNE which reduces ionization suppression caused by components present in plasma such as salts, which will not extract into the ethyl acetate.

Additionally, we observe that SFNE reduces the carry-over of analyte between phase-pairs compared to direct infusion by single-phase droplet-MS for many of the compounds. Though this effect is observed in plasma, it is even more apparent when using the SU sample matrix. An example of this effect is seen in Figure 4-6, where 1 μM Dox was spiked into SU and measured by single-phase droplet-MS and SFNE-MS. In single-phase droplet-MS, a carry-over of 27% and 12% is observed in the droplet immediately before and after the samples, respectively; however, in SFNE-MS the carry-over is reduced to 1.5% and 1.7% before and after the phase pairs. The reduction in carry-over is most likely due to a combination of air plugs assisting segmentation and preferential partitioning into an extraction phase, helping to reduce uncontrolled cross-talk.

In addition to analysis from plasma, SFNE-MS was tested on the drug mixture spiked into SU and aCSF (Figure 4-5B). All five drug compounds (MVER not included in aCSF) showed improved S/N by SFNE-MS over single-phase droplet-MS in all 3 matrices, with improvements ranging from 3 to 19-fold. Not only does SFNE-MS provide benefits over single-phase droplet-MS, but it has many advantages over typical extractions before MS/MS analysis such as allowing for automated extractions and sample introduction since the partitioning occurs within the tubing. SFNE also allows for high-throughput analysis since an array of samples can be extracted in-line and directly infused every experiment, with sample introduction rates at approximately 6 s per phase pair (Figure 4-5), compared to the several minutes for a typical LPME per extraction followed by manual introduction. The typical SFNE-MS experiment in this study used 60

extractions per infusion. Additionally, SFNE has nanoliter volume requirements which allows for negligible consumption of finite samples.

To evaluate SFNE-MS/MS as a quantitative tool, calibration curves for the drug mixture in plasma were obtained (Figure 4-7A). Calibration curves for these 5 drugs were obtained over a range of biologically relevant therapeutic concentrations¹⁹³ (10 – 0.1 μM) and showed acceptable linearity ($R^2 \geq 0.98$) (Figure 4-7B). Limits of detection in plasma were 7, 40, 60, 30, and 50 nM for Dox, Clem, DXM, MVER, and DPH respectively, which were obtained using approximately 2 volumes of aqueous sample per volume of extraction phase. Further adjusting the volume ratios, utilizing a newer mass spectrometer with enhanced ion transmission, and implementing nESI rather than ESI could possibly yield even better LODs. Table 4-2 shows calibration curve linearity and limits of detection for each individual compound, where reproducibility at the low concentration point ranged from 1.8 – 15.3%. Compared to another relevant method (SFME), SFNE is able to detect significantly lower absolute mass at 9 fg compared to the lowest reported LOD for

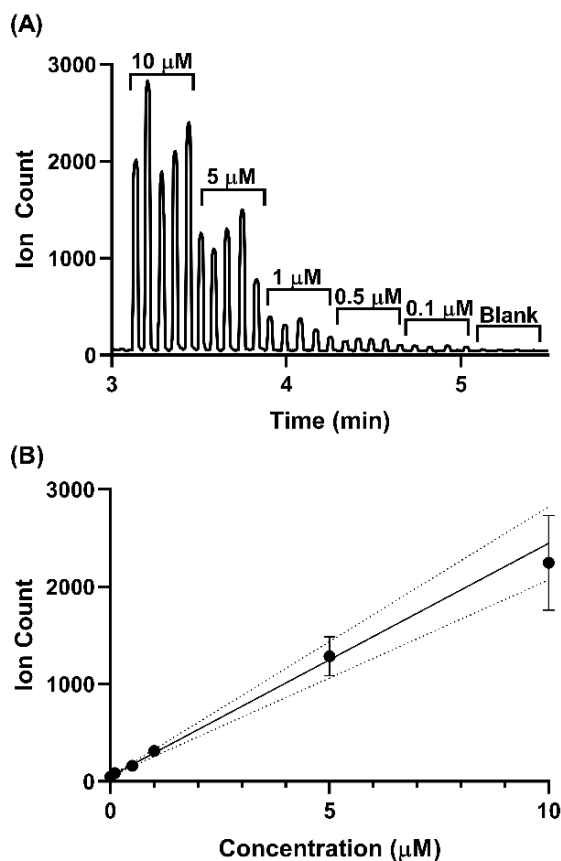


Figure 4-7. Calibration curves from 0.1 – 10 μM were obtained for five drug compounds by SFNE-MS using SRMs to monitor each transition simultaneously. (A) Shown is the extracted SRM trace of the DXM transition that was used for calibration. A train of two-phase slugs was generated with five replicates of each concentration level to form the calibration. The outside slugs for each concentration were treated as a spacer or wash slug, and the inside three replicates had peak height averaged to obtain average signal response. (B) Dextromethorphan shows linearity across the calibration curve ($R^2 = 0.99$). All compounds have an R^2 value of at least 0.98 in their calibration curves. Omitting the high point in the curve yields an R^2 value of 0.99 for all compounds. Reproducibility at the low concentration point for DXM was 5.9%. RSD for the low point of all compound calibration curves ranged from 1.8 – 15.3%.

SFME of 150 fg. However, SFME was able to detect at a lower concentration (0.2 nM) than SFNE (7 nM). A number of differences in experimental conditions by contribute to the better LOD by SFME including use of: nESI, 10-fold dilution of blood (decreased matrix effects), and different instrumentation in SFME experiments.

Conclusions

In this study, we have demonstrated SFNE as a novel LLE technique that allows for low nanoliter extraction volumes, extraction in seconds, and compatibility with on-line detectors. SFNE was demonstrated to be compatible with different extraction solvents (EtOAc, chloroform, octanol), three different detectors (UV, LIF, MS), and several different aqueous matrices with varying analyte concentrations. Due to these positive qualities, this technique can be used for a variety of applications. SFNE has shown utility for rapidly and accurately determining K_{ow} using low volumes, consuming small amounts of analytes and allowing for greener chemistry due to lower organic solvent consumption. The small samples may also enable extraction for applications where nanoliter samples are generated such as single cells, laser capture microdissection, microdialysis samples from the brain, and droplet microfluidics reaction screening. SFNE has also shown utility for sample clean-up for ESI-MS, offering significant improvements in signal. However, SFNE has some limitations, including MS experiments being limited to EtOAc as the extraction solvent and the number of two-phase slugs that can be generated per experiment; though, lengthening the capillary and generating more two-phase slugs could allow for more extractions to occur in a single experiment. Future work for this will focus on development of an online slug flow generator. This device will allow for further applications including pairing with online sampling or other microfluidic devices. SFNE may also be implemented in a large scale K_{ow} studies. In principle the system could be used to obtain K_{ow} at

high-throughputs and across a wide range of conditions including varying temperatures and concentrations.

Chapter 5

Continuous and Automated Slug Flow Nanoextraction for Rapid Log K_{ow} Determination

Introduction

Liquid-liquid extractions (LLEs) are a fundamental tool useful for sample clean-up in complex matrices, determination of partition coefficients, and isolation of target compounds. One such application of LLE is for octanol-water partition coefficient ($\log K_{ow}$) determination. $\log K_{ow}$ (often reported as K_{ow} , $\log K$, or $\log P$) is routinely used in both drug development to estimate bioavailability of pharmaceuticals,^{194–196} and in environmental studies to better understand aqueous remediation techniques.¹⁹⁷ The most accurate and reliable method for determination of $\log K_{ow}$ is the shake-flask method.¹⁹⁸ Similar to many other commonly used LLE techniques, the shake-flask method has large volume requirements (mL), long procedures (hours), and remains difficult to automate.^{178,199} In this work, we describe a microfluidic chip interfaced with an autosampler and UV-absorbance detector for rapid and automated LLE and apply it to $\log K_{ow}$ determinations using microliters of sample.

Microfluidic tools have been applied to miniaturizing LLEs for numerous applications. Parallel flow is a continuous microfluidic LLE technique in which two immiscible streams are co-flowed forming an extraction interface.²⁰⁰ Several variations have been reported, demonstrating extractions from biological,^{201,202} environmental,²⁰³ and other complex matrices,^{204,205} however, parallel flow and similar continuous flow approaches are limited in extraction speed and range of

extractable analytes.^{201,206} Additionally, longitudinal sample diffusion in these methods limit sequential analysis of different samples and must be accounted for when determining extraction coefficients.²⁰²

The use of slug flow (also known as segmented flow) or droplet microfluidics has enabled many high throughput applications and has been shown as a viable alternative to conventional continuous flow microfluidics by limiting diffusion and increasing sample introduction rates.⁷¹ Individual samples may be encapsulated in fL - nL aqueous plugs or droplets and processed discretely.²⁰⁷ Sample plugs or droplets experience internal mixing due to shear forces with the channel or tubing walls, which can be beneficial when applied to microfluidic LLEs.²⁰⁸ Segmented flow LLEs, in which aqueous plugs are segmented by an extraction phase, have been shown for a variety of applications including the study of mass transfer,^{171,208,209} preconcentration,²¹⁰ sample preparation,^{86,211} and continuous synthesis.²¹² However, the demonstrated segmented flow techniques are not easily applied to high-throughput screening (HTS) applications. Automation and rapid sample introduction remain difficult to integrate into LLE microfluidic devices,⁷¹ and “cross-talk” due to phase interactions inhibit screening discrete samples once introduced to the microfluidic device.⁸⁶

Recently, our group demonstrated slug flow nanoextraction (SFNE) in which 5 nL plugs of extraction phase and aqueous sample are juxtaposed in a line of microfluidic tubing to form extraction “phase pairs.”²¹³ The extractions occur in-line due to rapid mixing from internal recirculation within each droplet as the phase pairs flow towards a detector (UV, fluorescence, mass spectrometry). In droplet microfluidics, the use of a fluorinated oil continuous phase allows for chemical containment and low cross-talk between samples.²¹⁴ Phase pairs were generated by “sipping” from 384-well plates with wells containing aqueous sample, organic extraction phase,

and fluororous carrier fluid. The use of a fluorinated liquid spacer between phase pairs reduces cross-talk that inhibits SFNE and other plug-based approaches. Internal recirculation of the individual aqueous and organic plugs expedites extraction due to the constant refreshing of the extraction interface, demonstrating improvements to extraction speed over parallel flow approaches.²⁰⁶ SFNE was shown for in-line sample cleanup of biofluids for analysis by mass spectrometry (MS) and for log K_{ow} determination.²¹³

A miniaturized, automated method for rapid determination of log K_{ow} values could be useful in a pharmaceutical environment, where large compound libraries are generated, and determination of physiochemical characteristics are important at early stages where material is limited. Chromatographic methods have been used to automate log K_{ow} screening; however, these methods often approximate log K_{ow} based on calibration curves using compounds with known log K_{ow} .^{175,177} Additionally, chromatographic methods are limited in analyte scope and are relatively low throughput. Though the SFNE method previously described achieved miniaturized log K_{ow} determination, its overall throughput is limited by the initial sipper step and the need to move tubing of sample from droplet formation to detector flow systems.²¹³

Here, we address previous limitations with a fully automated, online system for the rapid determination of pharmaceutical log K_{ow} values using SFNE. A microfluidic device was designed for the generation of SFNE phase pairs in the first three-liquid-phase microfluidic system. Liquid/liquid/gas systems are commonly reported, but the gas results in high interference signals during detection and inconsistent flow due to compression. The microfluidic device is coupled to a liquid chromatography autosampler for the rapid introduction of low volume samples (< 20 μ L) from a well plate, allowing for a user-friendly system for the rapid determination of log K_{ow} values from an array of compounds. One injection per 78 s into the device is achieved, though this may

be further improved with newer or faster autosamplers. The device can rapidly switch between aqueous/perfluorodecalin (PFD) slug (aq droplets) generation and aqueous/octanol/PFD phase pair generation, allowing for rapid, online calibration curve generation (aq droplets) and unknown determination (phase pairs). The developed system is applied to screening a library of seven compounds at three pH values, resulting in 21 log K_{ow} measurements in 2 hours, using only 5 μ L of extraction standard and 2.9 μ L of octanol per extraction standard measured. A subset of these results was validated by the microshake-flask method.^{191,215} The automated SFNE method reduces preparation and analysis time by 10-fold and sample/extraction phase volume requirements by 40-fold compared to microshake-flask method adapted for this study.

Materials and Methods

Reagents and Materials. All chemicals and solvents were purchased from Sigma-Aldrich (St. Louis, MO) unless stated otherwise. PFD was purchased from Oakwood Chemical (Colombia Hwy, Estill, SC). Drug compounds were prepared in HPLC-grade water and 1-octanol at 1-10 mM (for compounds requiring calibrations), aliquoted, and stored at -80 °C. Standards were thawed daily for use and diluted to the desired concentration. For droplet visualization, dyes were diluted to an arbitrary concentration with strong visibility and used for experimentation. The red dye mixture used in some experiments consisted of equal parts rhodamine B, methyl orange, erythrosine B, phenol red, and neutral red.

Device Design and Fabrication. Microfluidic devices were designed using Autodesk Inc. AutoCAD software (San Rafael, CA) and printed onto a Fineline Imaging transparency (Colorado Springs, CO). Microfluidic master molds were generated with 150 μ m feature height using standard photolithography procedures; SU8 2075 negative epoxy photoresist was spun onto silicon wafers from University Wafer (South Boston, MA), patterned with ultraviolet irradiation through

the transparent mask, and developed to leave polymerized features. Curbell Plastics Polydimethylsiloxane (PDMS) (Livonia, MI) was prepared 1:10 activator to monomer ratio, degassed, and poured over the SU8 master. Fluidic ports were produced in the PDMS stamps. PDMS stamps fabricated with fluidic channels were bound to either glass slides (PDMS/glass devices) or to PDMS slabs (PDMS/PDMS devices) using oxygen plasma activation generated by a Harrick Plasma Inc. PDC-32G (Ithaca, NY). Microfluidic devices were flushed with 2% tridecafluoro-1,1,2,2-tetrahydrooctyl trichlorosilane in PFD for surface treatment.

Device Operation and Phase Pair Generation. All flow was applied using Hamilton (Reno, NV) gastight syringes (250 μ L, 500 μ L, 1 mL) with Chemyx Inc. Fusion 400 syringe pumps. Syringes filled with octanol, PFD, and water (or aqueous sample) were connected to their respective fluidic ports of the phase pair generator via 150 inner diameter (i.d.) by 360 outer diameter (o.d.) fused silica capillary coated with polyimide from Polymicro Technologies (Phoenix, AZ). Connections were made using low dead volume unions from Valco Instruments Co., Inc. (Houston, TX). For two-phase slug generation, 2.0 and 1.5 μ L/min flow rates were applied for aqueous and PFD, respectively, unless stated otherwise. For three-phase slug generation (phase pairs), 2.0, 2.0, and 1.5 μ L/min flow rates were applied for aqueous, octanol, and PFD, respectively, unless stated otherwise. Phase pairs (or droplets for two-phase) are segmented from one another as they reach the continuous PFD flow in the device, discretizing individual samples or extractions. These are exported from the device using 100 μ m i.d. x 360 o.d. PFA tubing from IDEX (Lake Forest, IL) or fused silica capillary, which is also positioned within an online UV detector. UV detection used a Linear (Auburn, CA) UVIS 200 variable wavelength absorbance detector or a Linear UVIS 205 variable wavelength absorbance detector slotted for capillary flow cells. The wavelength was adjusted to the various analytes being screened or

assessed. National Instruments (Austin, TX) LabView UV data acquisition software was used for UV absorbance data acquisition and analysis. The UV system had a maximum and minimum signal response at 1.1 and -1.1 V, respectively, corresponding in a cut-off signal in some traces.

For automation, the device is interfaced to a Thermo Fisher Scientific (Waltham, MA) UltiMate 3000 Autosampler using a Thermo Fisher Scientific 1 μ L nanoViper sample loop. A syringe pump was interfaced to the six-port valve for aqueous flow. This flow acted as the water/aqueous flow during device operation. Injection and wash parameters optimized to provide frequent injections for HTS, where final settings are described in results and discussion. In initial experiments, standards were injected from 100 μ L of solution in polypropylene autosampler vials. For HTS, standards were injected from 20 μ L of solution in a 96-microwell plate.

For validation of the HTS via microshake-flask method, offline extractions were performed, and each phase was injected using the LC autosampler through the UV detector. The microshake-flask method was performed by placing 500 μ L of aqueous extraction standard and 500 μ L of octanol in vial, shaking for 60 min, and centrifuging for 10 min. Both phases were pipetted into an autosampler vial and injected for UV analysis with calibration curves in the aqueous phase.

A camera and microscope were often used to capture video of slug formation and export during experiments. For this, an AmScope (Irvine, CA) MU500 camera was positioned onto an AmScope microscope to capture video of slugs forming or being exported before going to the online UV detector. Video was captured using AmScope 3.7 digital camera software and edited using NIH (Bethesda, MD) ImageJ software. High resolution images and videos were taken using a Phantom Miro C110 (Wayne, NJ) on a Nikon (Tokyo, Japan) TS100 inverted microscope and Phantom Camera Control (PCC) software.

Results and Discussion

Device Characteristic and Features. Phase pair generation is achieved by flowing the three phases into a PDMS device designed similar to a standard two-reagent droplet generation by flow focusing, where aqueous flow enters from the LC autosampler (Figure 5-1).⁷¹ In the device, equal volumes of aqueous and organic (sample and extraction phases, respectively) are segmented into phase pairs by the fluoruous phase. Extractions occur at the interface between the organic and aqueous phases as they flow through capillary to the detector.

Though the online SFNE generation device allows for rapid extraction times and minute volumes, rapid introduction of different samples remains challenging. To overcome this challenge, the phase pair generator was interfaced with an autosampler at the inlet which allows for various samples to be injected into a

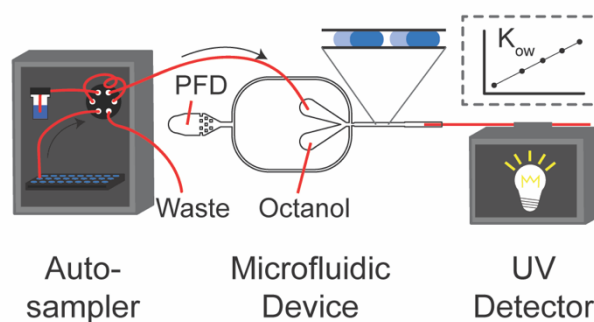


Figure 5-1. Automated log K_{ow} determination using slug flow nanoextraction. Compounds are aliquoted into a well-plate and injected by an auto-sampler. A microfluidic device generates phase-pairs by segmenting sample and octanol with PFD. Aqueous and octanol phases are briefly co-flowed before segmentation by PFD. Phase pairs are exported parallel with the channel into tubing or capillary. An in-line UV detector is used for the analysis of analytes in both aqueous and octanol phases.

continuous aqueous stream from a sample array without stopping flow (Figure 5-2). In this format, throughput is only limited to how frequently samples can be injected using the autosampler and the preparation time of calibration/extraction standards. To maximize injection frequency, several key autosampler parameters were adjusted including sample loading parameters (draw speed, dispense speed, inter-step delays, injection volume), wash settings (wash speed, wash volume, inter-step delays), and injection loop settings (overflow factor, flush volume, loop volume). By maximizing most draw rates and dispense rates during sample loading and washing and minimizing most delays, an injection cycle of 78 s was achieved. Suitable flow rates were selected

to allow for baseline resolution of each injection and were set to a total flow rate through the device of $3.5 \mu\text{L}/\text{min}$ for aqueous droplet generation and $5.5 \mu\text{L}/\text{min}$ for phase pair generation. The injection frequency is the limiting factor to throughput using this autosampler,²¹⁶ faster/newer technology would enable higher throughputs for $\log K_{ow}$ determination.^{217–219}

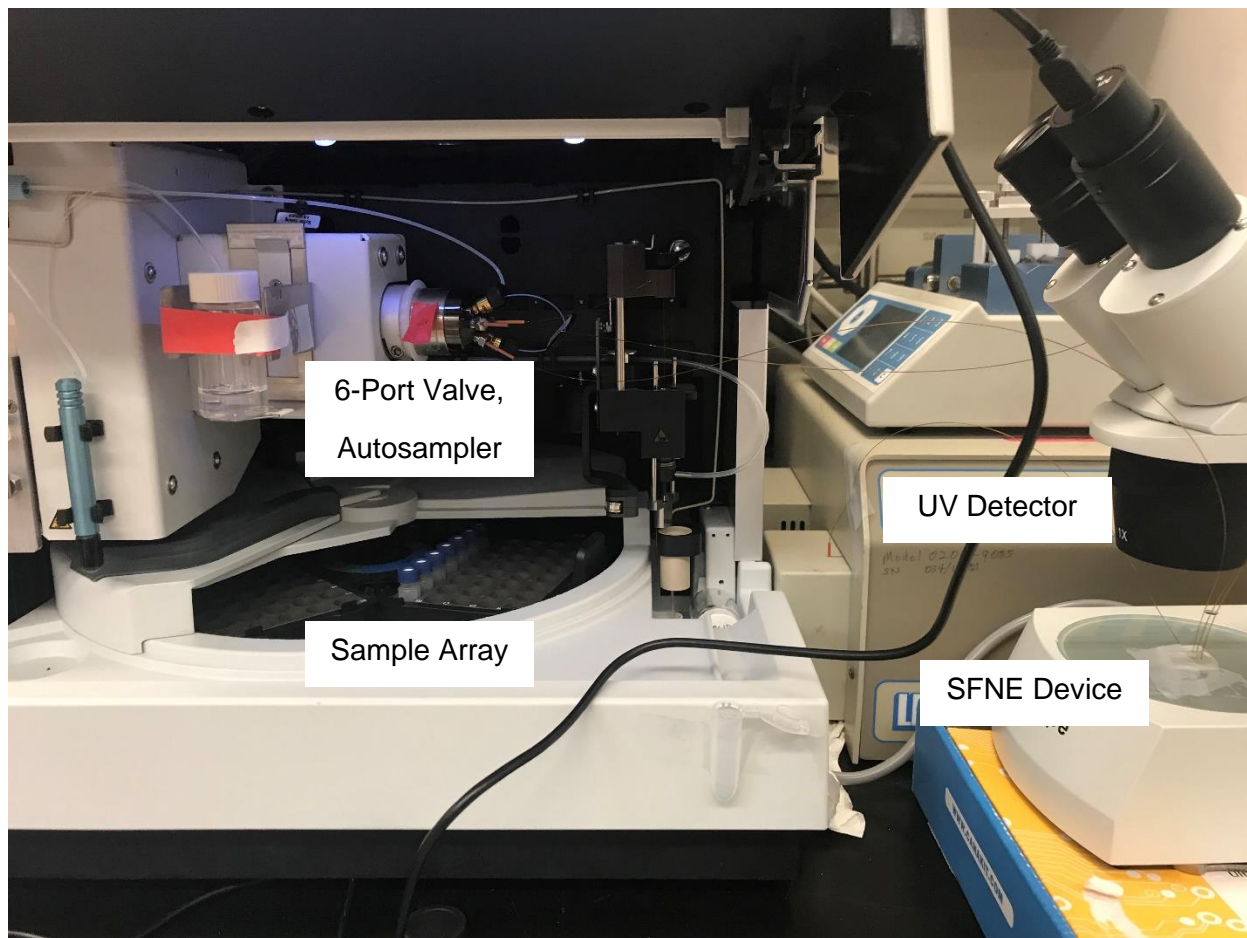


Figure 5-2. Complete online, automated system for SFNE. The autosampler can be loaded with a vial holder or a microwell plate from which calibration and extraction standards can be injected (through the 6-port valve). This allows for the device to be connected to the 6-port valve with continually flowing aqueous phase and various samples/standards to be introduced into the continuous aqueous phase. The device is then connected to the UV detector, where calibration standards and unknown extraction equilibrium concentrations can be quantitated.

In an example of the online SFNE method, phase pairs were continuously generated, exported into capillary, (Figure 5-3A) and analyzed using in-line UV detection of red dye in each phase (Figure 5-3B). In a six-minute window of continuous generation and online UV analysis, 194 replicate extractions were performed (0.5 Hz) reproducibly with a relative standard deviation of signal intensity from the aqueous layer (RSD_{AQ}) of 6.8%. Distinct signals of each phase were

observed corresponding to PFD at baseline and different concentrations of dye in each phase at equilibrium (Figure 5-3B). The ability to continuously and reproducibly generate phase pairs, extractions, and analysis in this online system is crucial to successfully implementing the system for automated, serial extractions of different samples.

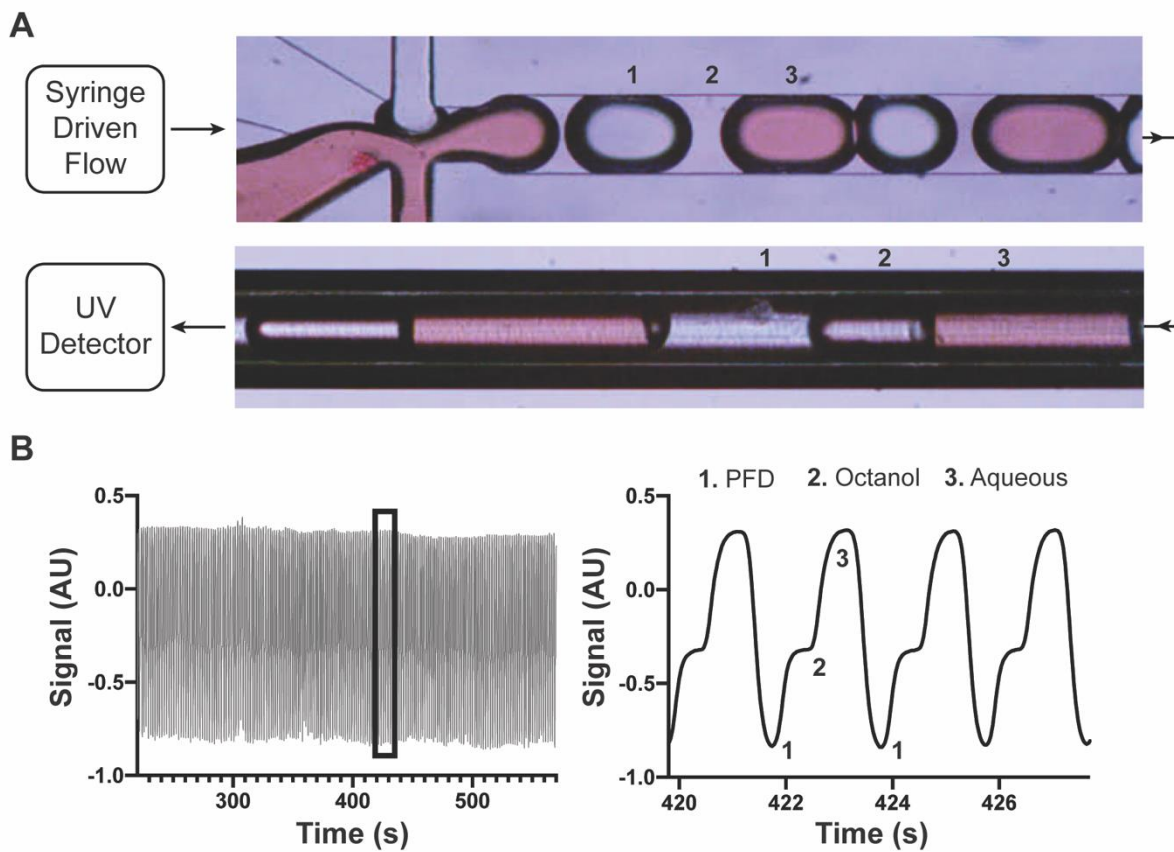


Figure 5-3. Online SFNE generation and detection. (A) A mixture of red dyes (aqueous, 3) and extraction phase (octanol, 2) are segmented into 8 nL phase pairs by PFD (fluorous, 1). (B) Continuous online UV Vis detection of the phase pairs in Teflon tubing for an extended period. Expansion of the trace is shown of distinct signals for each phase. Phase pairs are generated and analyzed at 0.5 Hz.

Phase pair generation is dependent on the flow of three different phases. Relative flow rates into the generation device are responsible for the phase pair volume, aqueous to organic volume ratio, overall flow rate, and potential throughput in this system. Controlling the flow rates of each phase modulates both throughput and volume ratios of phase pairs and enables rapid switches between aqueous droplet generation and phase pair generation. As reported in the original SFNE method,²¹³ manipulation of the volume ratio in phase pairs allows for preconcentration or dilution during extraction. Using the online generation device, the volume ratio (V_R),

$$V_R = V_{\text{org}}/V_{\text{aq}} \quad [5-1]$$

of the phase pairs can be adjusted by changing relative flow rates (Figure 5-4). For example, when using flow rates of 1.5, 1.0, and 0.8 $\mu\text{L}/\text{min}$ for PFD, octanol, and aqueous, respectively, a V_R of ~ 0.75 was observed (Figure 5-4A). By adjusting the PFD, octanol, and aqueous flow rates to 0.6, 0.5, and 1.0 $\mu\text{L}/\text{min}$, respectively, the V_R was reduced by a factor of 2.2 to ~ 0.34 (Figure 5-4B).

Though V_R is not directly proportional to flow ratio ($\text{Flow}_{\text{org}}/\text{Flow}_{\text{aq}}$, F_R), as demonstrated above (i.e. $V_R = 0.75$ when $F_R = 1.25$, $V_R = 0.34$ when $F_R = 0.5$), preconcentration effects can be achieved through modulation of the F_R . The online SFNE device was used to perform an extraction of 1 mM ACP with several different flow ratios to demonstrate preconcentration in this system through F_R modulation (Figure

3C). Reduction of the F_R resulted in the increase of the final signal intensity in octanol, showing a 2.6-fold increase in signal intensity when the ratio was reduced from 1.0 to 0.167 (Figure 5-4C).

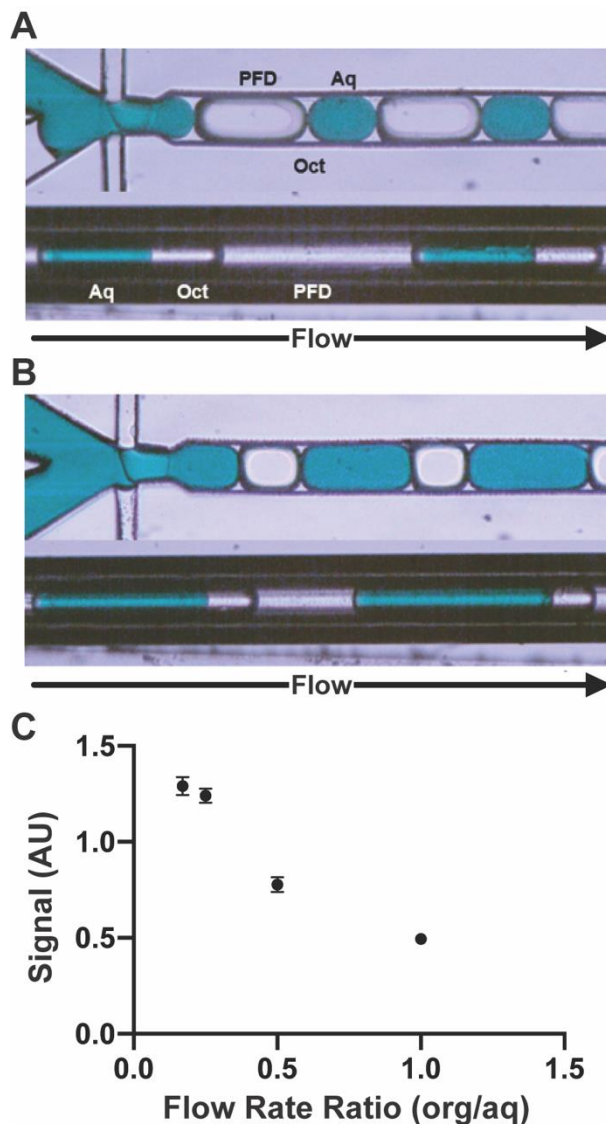


Figure 5-4. Volume manipulation via flow rate changes. (A) Similar flow rates result in near equal volume in the export tubing. (B) Increasing aqueous relative to organic flow rates reduced V_R over two-fold. (C) Flow rate ratio was varied from 1.0 to 0.17 and signal intensity in octanol are reported. Signal increases as the flow ratio decreases, showing the effective preconcentration. At least 400 replicates (equilibrium octanol plugs) were measured for each flow ratio.

Based on a theoretical concentration curve as volume ratio is adjusted, ACP equilibrium concentration in octanol should increase by 150, 200, and 220% as V_R is decreased from 1 to 0.5, 0.25, and 0.17, respectively (Figure 5-5).

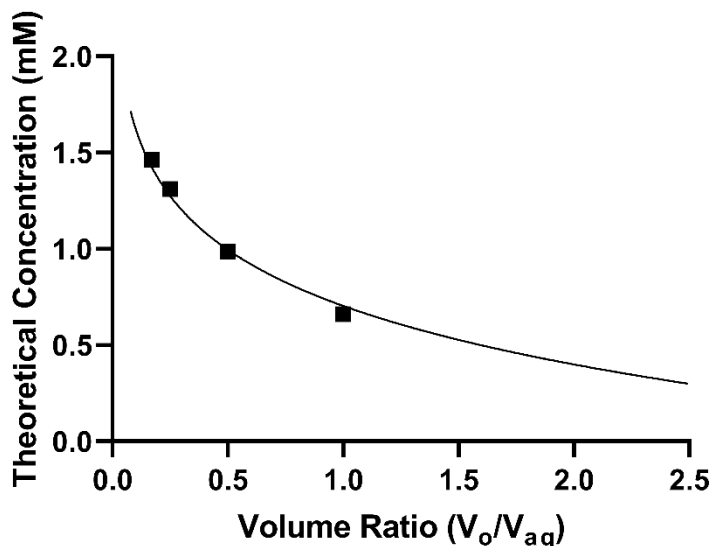


Figure 5-5: Theoretical concentrations for acetaminophen (initial concentration in aqueous of 1 mM) as volume ratio is adjusted to achieve preconcentration. Values were obtained through calculation using Equation 4-1. The theoretical curve is represented by the solid line. The squares are the mirrors volume ratios for the flow ratios demonstrated in Figure 5-4

The signal intensity increased by 160, 250, and 260% as F_R was decreased from 1 to 0.5, 0.25, and 0.17, respectively, reflecting a

trend similar to that of the theoretical concentration curve. Theoretical concentrations in the extraction phase at equilibrium ($C_{org,eq}$) were determined by the following equation,

$$C_{org,eq} = KC_{aq,eq} = \frac{KC_{aq,initial}}{1+KV_o/V_{aq}} \quad [4-1]$$

where the octanol-water partition coefficient, K , is equal to 1.95 and the initial concentration in water ($C_{aq,initial}$) is equal to 1 mM. The theoretical curve is represented by the solid line. The squares represent the volume ratios for the flow ratios demonstrated in Figure 5-4.

Phase Toggle and Calibration. Quantitative log K_{ow} determination requires determining concentration in each phase. UV absorbance is a generalizable detector for measuring concentrations, but calibration is required for quantitative results. To overcome this challenge, the phase pair generation device was designed to allow for the organic flow to be readily toggled on and off. When organic flow is off, a segmented flow of aqueous solution and PFD is formed. When

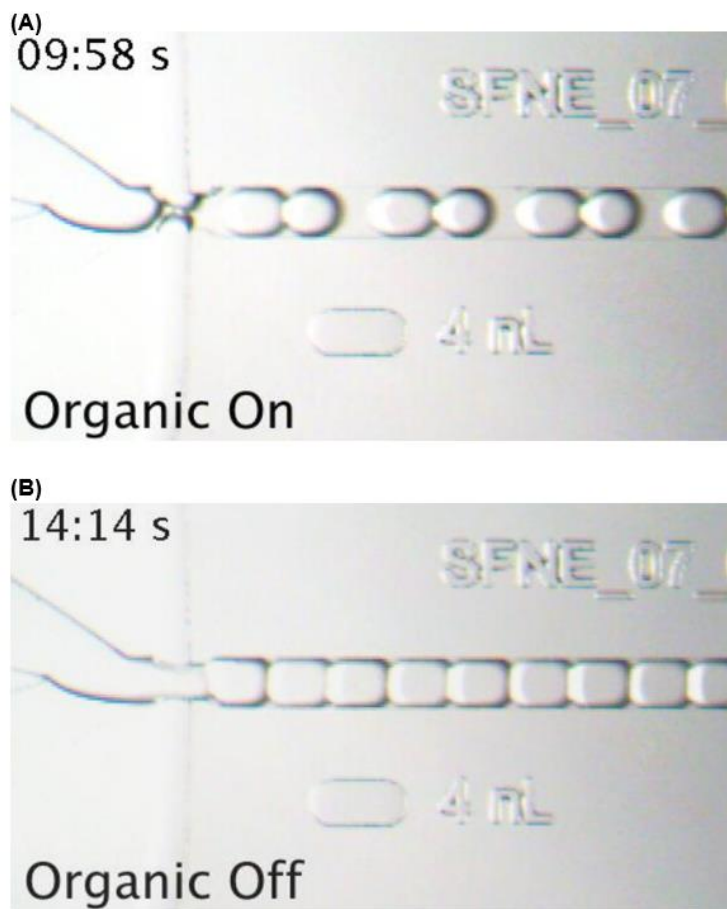


Figure 5-6. Images from a video where organic phase is toggle off and on every 10 s. Phase toggling rapidly and reliably equilibrates in the microfluidic device between generating three phase “phase pairs” and two phase droplets when the organic phase is toggled on or off. (A) Snapshot of the device just before the organic (octanol) flow is toggled on. Phase pairs are being reliably generated here. (B) Snapshot of the device ~four seconds after the organic has been toggled off, with reliable two-phase droplet generation.

organic flow is on, phase pair generation occurs where extractions can occur during transit. This feature allows for single phase calibrations in water and multi-phase extractions to occur, enabling quantitative determination of unknown equilibrium concentrations without disassembly of the system components or an additional microfluidic device. The system adapts from aqueous droplet generation to phase pair generation in under five seconds after toggling the organic phase, providing rapid switching between calibration and

unknown determination modes in an entirely online system (Figure 5-6) Calibrations were performed by sequential injection of five or six different concentration levels while in aqueous droplet generation mode. Unknown determination was performed by injecting a known concentration (1 mM, 10 mM) while in phase pair generation mode and measuring the resulting equilibrium concentration in water.

Automated Log K_{ow} Measurements. The autosampler interface and the organic flow toggle feature allow for automated injection of aqueous calibration standards followed by

injections of extraction standards and in-line extractions to occur in one system. This method was used in a demonstration to determine the $\log K_{ow}$ of a test compound (acetaminophen, ACP) with an online and automated method (Figure 5-7A). Six aqueous calibration standards ranging from 0.1 – 1.0 mM in water as well as a blank were injected, followed by triplicate injection of the extraction standard (1 mM ACP in water). The detector was zeroed using PFD. Differences in refractive indices resulted in a negative value for absorbance of ACP in water and octanol at some concentrations. During the injection of all calibration standards, the organic (octanol) pump was

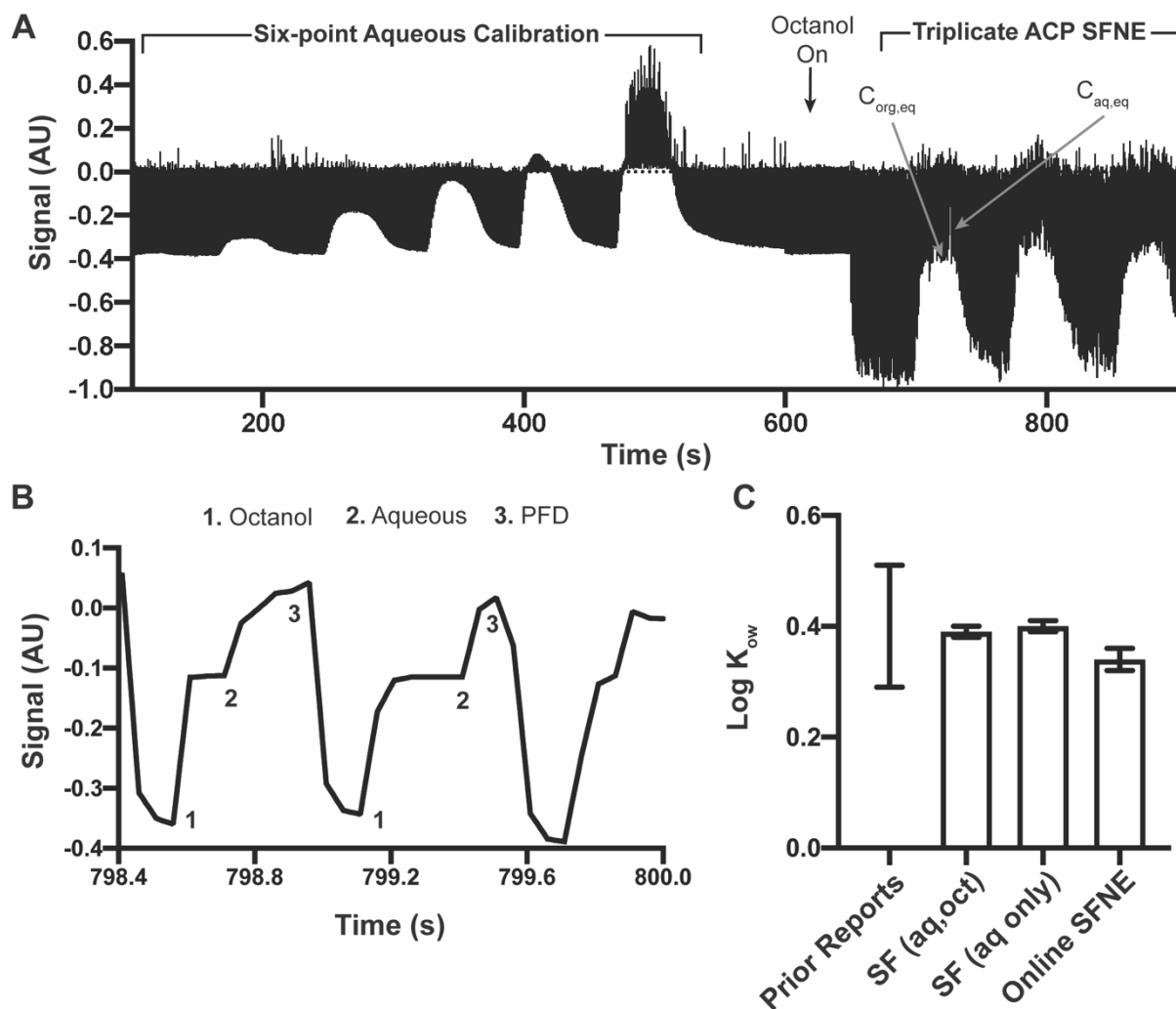


Figure 5-7. Full LC-SFNE-UV workflow. (A) In a single automated run, a calibration in water was performed followed by triplicate injections with SFNE to determine $\log K_{ow}$ for acetaminophen. (B) Expansion of a portion of the trace, showing examples of the phase pairs that were used to determine equilibrium concentrations of acetaminophen in water post-extraction. (C) Value comparisons and validations in this study for online SFNE by comparison to previous reports, microshake-flask (aq,oct), and microshake-flask (aq only) $\log K_{ow}$ values for ACP. Microshake-flask is denoted as SF.

programmed to switch off and aqueous droplets were generated for the calibration standards. For the injection of the extraction standard, the organic pump was programmed to switch on and phase pairs were generated for extractions between octanol and water. The aqueous portion of the phase pairs were selected from the leveled top of each injection and used for quantification (Figure 5-7B).

Using the six-point calibration to determine the equilibrium concentration of ACP in the aqueous layer of the phase pairs, the $\log K_{ow}$ could be determined using equation 2:

$$\log K_{ow} = \log (C_{oct,eq}/C_{aq,eq}) \quad [5-2]$$

Since the extraction uses equal volumes of octanol and aqueous sample for each phase pair, along with known extraction standard concentrations, $C_{oct,eq}$ can be calculated once $C_{aq,eq}$ is known, where

$$C_{oct,eq} = C_{initial} - C_{aq,eq} \quad [5-3]$$

The $\log K_{ow}$ determined by SFNE (0.28 ± 0.01) is comparable to previously reported values and the values^{190,191,194,220} determined by the microshake-flask method. $\log K_{ow}$ was determined by the microshake-flask method twice, once using calibrations in both octanol and water with direct measurements of each extraction layer to determine $C_{oct,eq}$ and $C_{aq,eq}$ ($\log K_{ow} = 0.28 \pm 0.01$) and once using only an aqueous calibration and measurement of the aqueous extraction layer, using Equation 3 to calculate $C_{oct,eq}$ ($\log K_{ow} = 0.31 \pm 0.005$). The error between these two modes of determining $\log K_{ow}$ using the microshake-flask method is minimal (6%), indicating that SFNE determinations can use aqueous-only measurements to accurately determine $\log K_{ow}$, doubling the throughput. The $\log K_{ow}$ determined by online SFNE demonstrates suitable accuracy, as it fits within the range of previously reported $\log K_{ow}$ values for ACP and reasonably matches the

microshake-flask determined $\log K_{ow}$. The good linearity of the calibration suggested that fewer points could be used to increase throughput. Therefore, further $\log K_{ow}$ determination applications of this method only use five concentration levels (one of which is a blank) and single extraction standard injections, as each extraction standard injection generates several quantifiable phase pairs since multiple phase pairs are compartmentalized during injecting (Figure 5-7B).

Rapid Log K_{ow} Determination. The developed system was applied to a determining $\log K_{ow}$ for an array of compounds and conditions. Injections were performed from 20 μL of each standard in 96-microwell plate that contained a total of seven pharmaceutical compounds at three pHs (pH 3, 7.4, and 10) and their corresponding five-point calibration standards. The compounds were injected at both 1 mM and 10 mM for each condition to increase the range of measurable $\log K_{ow}$, as 1 mM standards are more likely below the calibration range at partition equilibrium if $\log K_{ow} > 1.5$. The octanol syringe pump was programmed to automatically switch between calibration

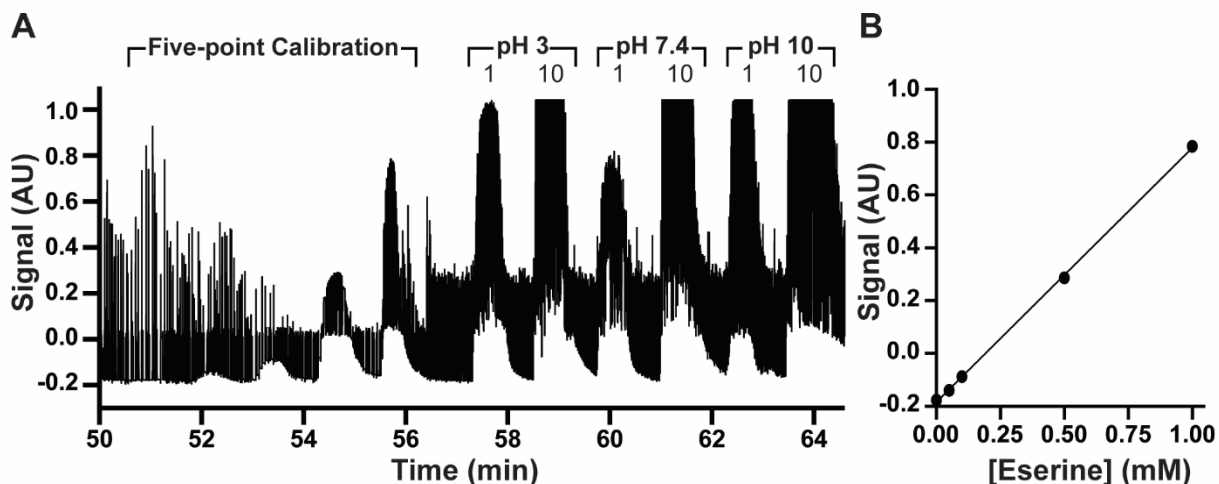


Figure 5-8. (A) Example trace of eserine from full $\log K_{ow}$ screen. A five-point aqueous calibration curve in water was injected and generated into aq slugs. Organic (octanol) flow was started at 57 minutes. Unknown determination traces of eserine at pHs 3, 7.4, and 10, at both 1 and 10 mM concentrations. Organic flow was stopped at 65 min in preparation for the next compound screen. (B) Calibration curve generated from the trace ($R^2 > 0.99$).

and $\log K_{ow}$ determination modes. An exemplary trace of a compound in the screen, eserine, is shown in Figure 5-8. Octanol flow was automatically turned on at approximately 57 min, following the final calibration standard. The standard curve demonstrates excellent linearity (Figure 5-8B).

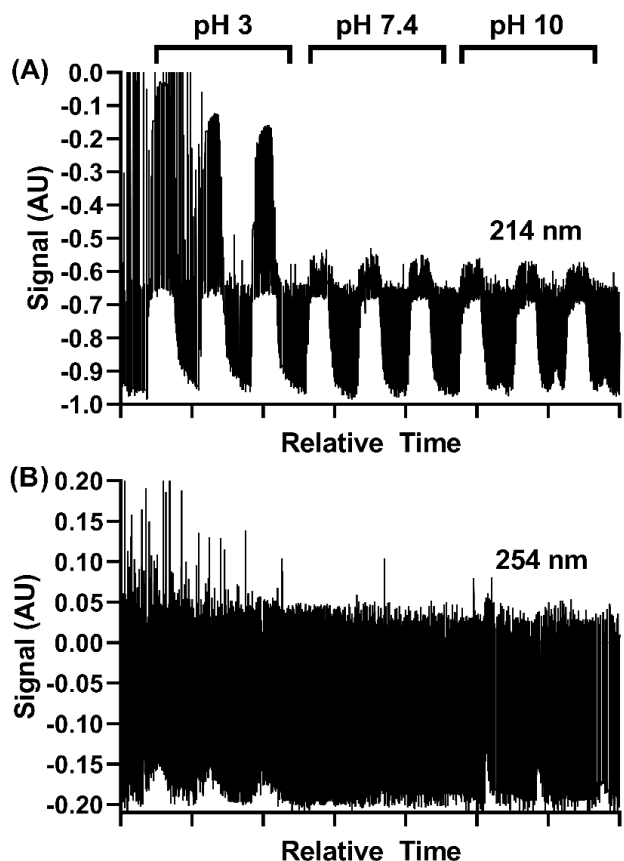


Figure 5-9. Triplicate injections of blank buffer used for extractions standards at each pH during log K_{ow} determination at (A) 214 nm and (B) 254 nm. The average of the signal intensity for each pH was subtracted from the corresponding extraction standards when measuring $C_{aq,eq}$.

After injection of the compounds at each of the pH levels, octanol flow automatically stopped (approximately 65 minutes) to allow for the standards of the next compound to be analyzed. Blank buffer injections were performed separately for baseline subtractions (Figure 5-9).

The entire well plate was screened using the automated system in under 2 h, consuming 5 μ L of extraction standard and 2.9 μ L of octanol per extraction standard analyzed (Figure 5-10), with all extractions reaching equilibration in-transit after injection. From the seven compounds

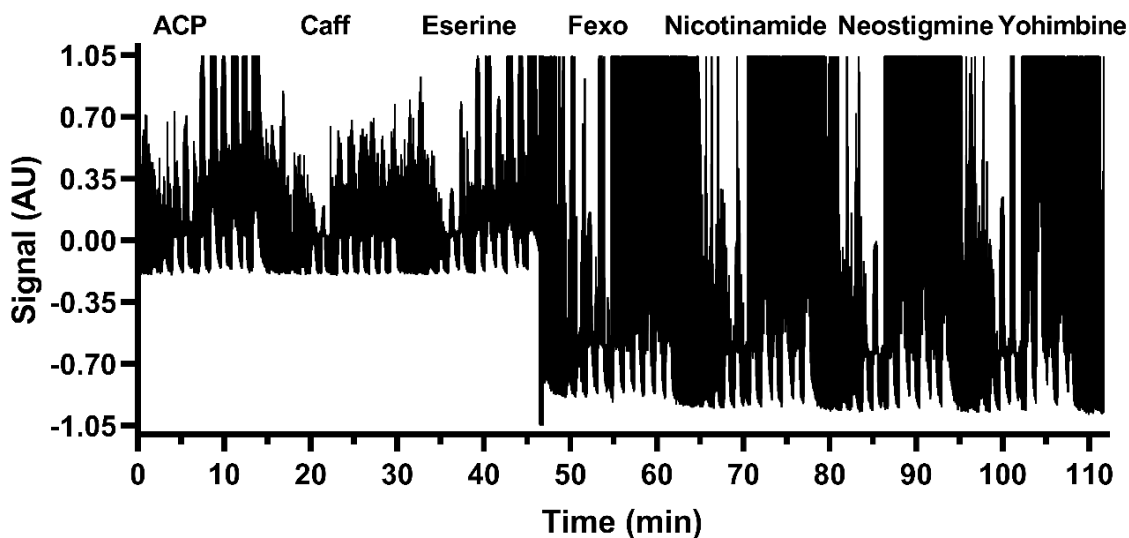


Figure 5-10. Raw trace of entire 7 compound screen where each compound has Log K_{ow} determined at 3 different biological pH's (3, 7.4, and 10) with a 5 point aqueous calibration curve before extraction for quantification. All 21 K_{ow} s were measured in under 2 h of analysis using automated sample introduction and pumps (including the toggle of octanol phase).

screened at the three pH conditions, 18 log K_{ow} values were successfully determined (Table 5-1).

The three log K_{ow} values that are unable to be measured in the screen (yohimbine pH 3,

| Table 5-1. Log K_{ow} values determined from screen and microshake-flask validation. | | | | | |
|--|----------------------------|------------------------|--------------------------|-------------------------|--|
| Compound | pKa Values ^a | log K_{ow} (pH 3) | log K_{ow} (pH 7.4) | log K_{ow} (pH 10) | log K_{ow} (Shake Flask, pH 7.4) |
| Acetaminophen | -4.40, 9.46 | 0.29 ± 0.11 | 0.29 ± 0.07 | 0.28 ± 0.07 | 0.29 ± 0.02 |
| Fexofenadine | 4.04, 9.01 | 2.03 ± 0.24 | 0.42 ± 0.01 | 0.48 ± 0.03 | 0.30 ± 0.03 |
| Caffeine | -0.92 | 0.03 ± 0.05 | -0.02 ± 0.08 | 0.05 ± 0.06 | -0.30 ± 0.01 |
| Nicotinamide | 3.63 | 0.11 ± 0.04 | -0.58 ± 0.04 | -0.31 ± 0.08 | -0.44 ± 0.02 |
| Eserine | 6.59 | 0.07 ± 0.08 | -0.29 ± 0.05 | 0.52 ± 0.04 | 0.16 ± 0.02 |
| Neostigmine | n/a | -0.59 ± 0.04 | < -1 | < -1 | < -1 |
| Yohimbine | 7.65, 14.68 | < -1 | 0.16 ± 0.06 | 0.4 ± 0.02 | 0.40 ± 0.02 |

^a Values obtained from human metabolome database (hmdb)

neostigmine pH 7.4 and 10) were due to insufficient sensitivity to measure the minimal amount of analyte (if any) that partitioned out of aqueous.

To validate the accuracy of the screen, each log K_{ow} at pH 7.4 was determined using the microshake-flask method (Figure 5-11). The method used for validation required substantially higher volumes (500 μ L of extraction standard and octanol per extraction) and much longer equilibration times (1 h of shaking, 10 min of centrifugation).¹⁹⁸ Additionally, for triplicate analysis of each microshake-flask extraction, three injections of each extraction standard were required; for SFNE, the segmentation of each injection into compartmentalized phase-pairs allows for triplicate (or more) analysis per injection of extraction standard. Some deviation between SFNE

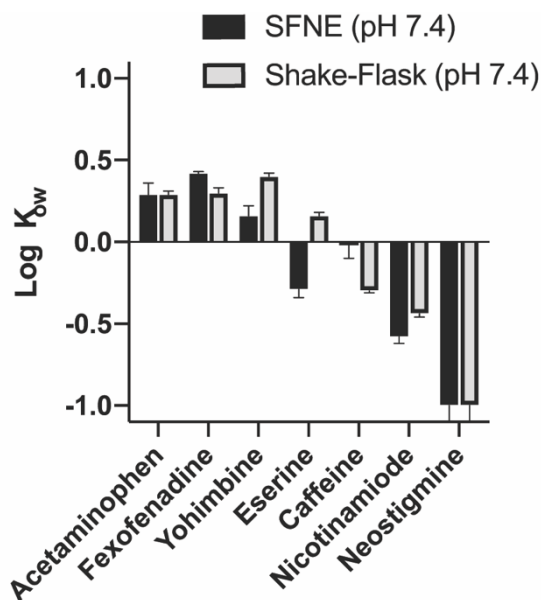


Figure 5-11. A comparison of the log K_{ow} determined at pH 7.4 for each compound by SFNE and microshake-flask extraction.

and shake flask values were observed with percent difference of 1.6%, 24%, 48%, 28%, 64%, and 41% for ACP, Fexofenadine, caffeine, nicotinamide, eserine, and yohimbine, respectively. These changes are most likely attributed to the commonly reported deviations of analyte degradation in the shake flask method due to long shake times at room temperature in ambient light,²²¹ and preparation of calibrations in buffer (shake flask method) versus baseline subtraction

(SFNE method). Degradation during shake-flask procedures is likely the major source of error. This was validated experimentally, where all target compounds were shaken (following microshake-flask procedures) for zero, one, and two hours and the corresponding changes in signal intensity were measured by direct UV detection (Figure 5-12). In this experiment, significant changes in signal intensity were observed in response to increased shake times for several compounds, suggesting impactful degradation. For example, eserine, which displays the largest error between shake-flask and SFNE (64%), saw a 59% change in signal after shaking for 1 hour, and 120% after 2 hours. The limited sample preparation and rapid analysis times associated with online SFNE has potential to determine more accurate log K_{ow} values by avoiding degradation of target compounds.

One notable test compound was yohimbine, which demonstrates significantly different partitioning across the pH ranges tested (Table 5-1). Yohimbine has multiple ionizable groups including both basic and acidic moieties. The pK_as are 7.6 and 14.7, indicating that at the lowest

pH the compound is cationic, limiting its extraction into octanol. Upon raising the pH, the compound is neutral, allowing for octanol extraction. Additionally, fexofenadine appears to be more lipophilic in acidic environments, possibly due to its cationic charge shielded by large steric effects, but more hydrophilic when on the surface acid group is charged (pH 7.4 and 10). These variations in the log K_{ow} may be of interest for understanding the bioavailability in both basic and acidic regions of the body such as absorption through the acidic stomach versus the more alkaline colon or small intestine.^{222,223}

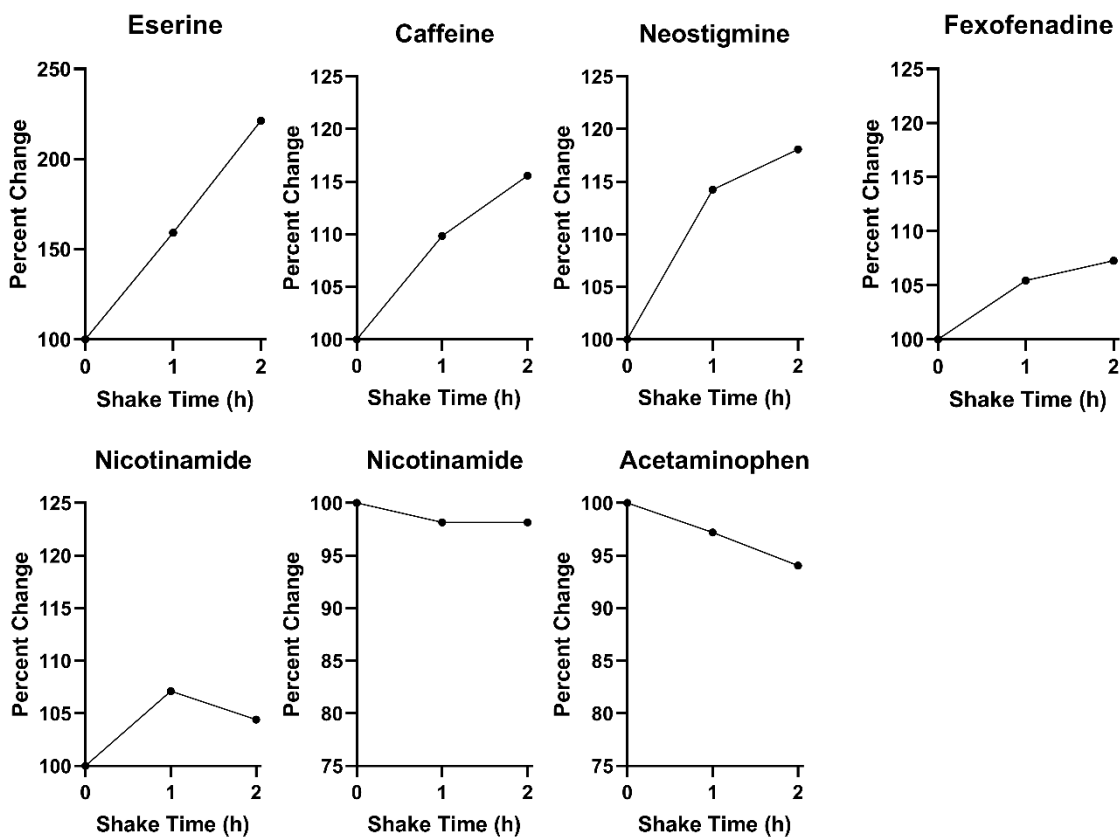


Figure 5-12. Samples were thawed to room temperature and sampled at 3 different time points during the shaking process (0h, 1h, and 2h) and stored at -80C after sampling. These samples were then sequentially injected for online UV detection, where signal change was measured as a function of shake time. Though concentration change is not directly proportional to signal change since degradation products are not distinguished from initial analyte, change in signal intensity indicates degradation for most of these compounds during long shake times. Most notably eserine, which had a 64% difference in K_{ow} determined by SFNE vs shakeflask, shows that signal intensity changes by 59% after 1 h of shaking. Degradation of analyte can increase or decrease the final K_{ow} measured by direct UV detection based on molar absorptivity and lipophilicity of the degradation products.

Conclusion

A system has been developed using microfluidics and applied for rapid screening of octanol-water partition coefficients. In most existing online microfluidic extractions, aqueous sample continuously flows into the device allowing for frequent sampling; however, changing the incoming sample stream often requires stopping flow and/or manually swapping the sample, limiting many automated applications. To overcome this, an autosampler was interfaced with an extraction phase pair generation device and in-line UV absorbance detection for automated screening. The set-up allowed for seven compounds to be screened for log K_{ow} values at three pHs each in under one hour including calibration curves for each compound, allowing for direct and accurate quantitation of partition coefficients using 5 μL of extraction standard and 2.9 μL of octanol per extraction standard analyzed. This system has several limitations, primarily associated with the UV detection. Though exceptional for in-line use and small volume analysis, capillary UV detection has poor sensitivity and linear range, ultimately limiting the method to use with high concentration chromophores. Possible solutions include use of alternative detectors such as mass spectrometry for label-free detection. Additionally, throughput could be further increased with newer/faster autosamplers, with injection cycles down to 22 s.²¹⁷ In the future, this method may be used for other extractions, such as rapid sample clean-up.

Chapter 6

Sensitive and High Throughput Screening for Directed Enzyme Evolution by Droplet-MS

Introduction

Directed enzyme evolution is a rapidly growing field for the development of biocatalysts for synthetic reactions due to desirable enzymatic stereo- and regio-selectivity and potential for drastic improvements to yield and reaction rate.^{224,225} The workflow begins with diversification of a target gene and expression of that library to obtain a multitude of enzyme variants. Selection or screening is imposed to identify variants that offer improvements to the desired property (i.e. stereoselectivity, regioselectivity, reaction rate), and the corresponding genes are subjected to further rounds of mutation until a suitable biocatalyst is achieved.²²⁶

Though this process has potential to develop biocatalysts with unparalleled efficiency and selectivity for specific reactions, the directed evolution generates thousands of enzyme variants and subsequent reactions that need to be assessed. Screening these massive reaction libraries is typically regarded as the rate-limiting step in the directed enzyme evolution workflow.²²⁷ Much effort has been allotted to the development of innovative high throughput screening (HTS) techniques to expedite the analysis steps. Common HTS techniques applied for enzyme screening include fluorescence-activated cell sorting²²⁸ and microtiter plate activity-based assays.^{229–231} Though having excellent high-throughput capabilities, these techniques are fluorometric or colorimetric assays and are subsequently limited in the variety of substrates and products that can be screened. A recent effort has been made to develop HTS methods with broader application,

including techniques such as analytical separations paired with UV detection²³² and direct mass spectrometry (MS) approaches, where MS in particular has become an attractive tool for screening reaction libraries due to its wide variety of ionization techniques, label-free capabilities, and ability to interface with various sample loading/sample introduction assays.²³³ Direct MS has been paired with various sampling and ionization techniques for enzyme reaction screening including robotic sample loading with Agilent RapidFire,²³⁴ MALDI-MS from arrays of spotted enzyme reactions,²³⁵ droplet microfluidics with electrospray ionization (ESI),²³⁶ and acoustic-mist ionization directly from well plates.²³⁷

As mentioned above, droplet microfluidics, more specifically segmented flow, has been reported with ESI-MS for rapid screening of enzyme reactions from a well plate, allowing for label-free detection and rapid introduction of a sample array.²³⁶ In this previous study, enzyme variants are created and enzymatic reactions are carried out in multi-well plates. Using syringe pumps and Teflon tubing, droplets segmented from one another by an immiscible carrier fluid are generated directly from the wells in the well plates and infused into ESI-MS for HTS with sample introduction rates up to 3 Hz. Though this method shows excellent utility for label-free directed evolution HTS, the high flow rates used and the utilization of a diluting sheath-flow sprayer for ESI make this method unsuitable for low concentration measurements, especially from complex biological matrices.

In this work, we develop a droplet-nESI-MS/MS method to achieve a sensitive, high throughput method with application for HTS as a cytochrome P450 is evolved for increased biocatalytic activity for a biaryl coupling reaction. Biaryl scaffolds are present in many different natural products that are known to offer efficacy as therapeutics in both modern drug development and historically in naturopathy.^{238,239} Unfortunately, biaryl molecules have not been fully explored,

as significant quantities remain challenging to obtain synthetically.²⁴⁰ To develop a synthetic route for the biaryl coupling of C5-methyl coumarin and 2-naphthol with substantial yields, a cytochrome P450, a class of enzymes which has been previously identified as a catalyst in biosynthetic biaryl coupling,^{241,242} is evolved for increased activity. The HTS method developed in this work utilizes several features to obtain sufficient product LODs for the low initial activity in this reaction.

Using nESI and high dilution factors, limits of detection (LOD) for the reaction product down to 12 nM and a linear dynamic range from 0.025 to 25 μ M. High levels of ionization suppression are expected by ESI. Several steps are taken during method development to combat suppression, including implementation of nESI, dilution, organic modifier addition, and use of an internal standard (IS). The developed method is compared to a standard LC-MS method (3 min analysis time) for screening a single reaction plate (96 enzyme reactions). The method is finally applied for HTS of an entire library comprised of 1,728 reactions, where 1,512 of the reactions are different enzyme variants and 216 are either positive wild type (WT) or no enzyme (-) controls. During screening, sample introduction rates up to 2.4 s per sample are achieved, where each 96-multiwell plate is screened – in triplicate – within 16 min, whereas triplicate screening of one plate by LC-MS takes over 14 h. Statistically significant “hits” are selected that show higher enzymatic activity than WT controls. Seven hits are identified.

Materials and Methods

Reagents and Materials. All chemicals and solvents were purchased from Sigma-Aldrich (St. Louis, MO) unless stated otherwise. Perfluorodecalin (PFD) was purchased from Oakwood Chemical (Colombia Hwy, Estill, SC). Calibration standard mixtures were prepared by dissolving standards directly in blank reaction matrix at 250 μ M, which were aliquoted and stored at -20 °C. Blank reaction matrix generated by performing reactions (as described below) without the addition

of substrates. Aliquots of calibration standards brought to room temperature daily before use and spiked with 50 μM acetaminophen (ACP) dissolved in HPLC-grade water to a final concentration of 5 μM as the internal standard (IS).

Droplet Generation. Hamilton (Reno, NV) gastight syringes were used (25 μL) with a Harvard Apparatus PHD 2000 programmable syringe pump for droplet generation. Enzyme reaction mixtures were received in 96-well plates and were transferred to 384-well plates for droplet generation using micropipettes (35 μL aliquots from each reaction). 384-well plates were divided into four sections via epoxy walls: three 96-well sections (6 x 16 wells) and a calibration standard section (7 x 1 wells). Walls were formed by depositing several layers of epoxy along the outside of each section. Once the reaction mixtures were transferred to the 384-well plate, inert fluorinated carrier fluid, PFD, was gently pipetted over the filled wells up to the height of the epoxy walls. Droplets were generated using a syringe pump drawing rate of 700 nL/min with a 25 μL syringe attached to 40 cm of 150 μm inner diameter (i.d.) by 360 outer diameter (o.d.) PFA tubing from IDEX (Lake Forest, IL). Connections were made using low dead volume unions from Valco Instruments Co., Inc. (Houston, TX). Droplet generation was performed using an XYZ-position manipulator to draw from the 384-well plate, as previously described. The positioner was used to alternate the tubing between PFD (0.2 s draw) and sample (0.8 s draw) until the line was filled with three droplets from each reaction mixture, totaling 288 droplets per generation cycle (96 reactions per analysis, 5 – 10 nL droplets). For calibrations, five droplets for each of the seven concentration levels were generated, where calibration levels can be seen in Figure 6-4.

Droplet-nESI-MS/MS. Syringes and attached droplet trains were used with Chemyx Inc. Fusion 400 syringe pumps for direct droplet infusion. Seven point calibrations were infused at the beginning of each day to obtain a calibration curve with $R^2 \geq 0.990$ prior to quantitative analysis.

For calibrations and reaction screening, droplets are infused at 0.5 $\mu\text{L}/\text{min}$ using platinum-coated 30 μM i.d. spray tips from New Objective (Littleton, MA) at 2 kV, with a drying gas set to 150 L/h. All mass spectrometry was performed on a Micromass Quattro Ultima triple-quadrupole mass spectrometer (Waters, Milford, MA). Tandem mass spectrometry (MS/MS) was used for all experiments in single reaction monitoring mode (SRM) to monitor all mass transitions simultaneously. The mass transitions (parent ion \rightarrow daughter ion m/z), collision energy, and dwell times used for each compounds are as follows: C5-methyl coumarin (Sub A, 177 \rightarrow 77.1, 30 V, 30 ms), cross product AB (319.1 \rightarrow 115, 30 V, 50 ms), and ACP (156 \rightarrow 110.1, 15 V, 30 ms). LC-MS comparison/validation was performed on an Agilent 1290 Infinity Series II LC UHPLC system using a Waters Acquity UPLC HSS TS 1.8 μm C18 2.1 x 50 mm column interfaced to an Agilent 6230 TOF MS with a Dual AJS ESI source.

Data Analysis. Data collected by MS is comprised of droplet MS/MS traces for SubA, AB, and IS, where several points of signal are obtained for a droplet before signal returns to baseline as non-conductive PFD reaches the spray tip. Microsoft Excel is used for most data analysis, where the raw points for each trace (time, ion count) are used. Droplets are identified in a trace using “IF” functions to identify when droplet signals start and end, where any points higher than the PFD noise threshold are selected and extracted into a different column. Each set of extracted points are averaged across the middle (shoulder points excluded), and the subsequent values are used as the signal intensity of a given droplet, where 288 droplets are expected per plate screened. However, since reaction mixtures contain 50% MeOH, droplet splitting is a common phenomenon from lack of surface tension, which results in higher than expected droplet quantities in the subsequent readout. Several steps were taken to overcome this including “COUNT” functions and implementation of “RESET” droplets. COUNT functions were used as an automated

step (as was droplet selection, extraction, and averaging) to eliminate small pieces of droplets that break off from the main droplet. COUNT functions in tandem with “IF, AND” functions allow points across a droplet to be averaged only if they meet a quantity threshold (e.g. point clusters less than 4 points would not be counted as a droplet). Though COUNT elimination often resolved splitting issues in data analysis, occasionally they would eliminate entire droplets from a trace, and the readout would report fewer droplets than what was infused. To speed up the location and identification of these splitting issues, evenly spaced RESET droplets were added to infusion experiments. A RESET droplet is a long droplet (~20-30 nL) that occurs after every row of reactions (six reactions, in triplicate, 18 droplets). During droplet selection in Excel, a COUNT function is added to identify RESET droplets based on droplets that exceed a quantity threshold (e.g. more than 20 points are identified as RESETs). In the final list of droplets from 96-well plate screen, droplets can be easily assigned to their corresponding wells based on which number RESET droplet they come after/before, and droplet quantities not equal to 18 between two RESET droplets can be quickly identified and corrected.

Internal standardization is implemented to improve accuracy and reproducibility of results by mirroring nESI changes caused by matrix effects or electrospray fluctuations. This is especially useful, as the presence of high concentration 2-naphthol drastically affects ionization (See Results and Discussion). During data analysis, signal response is reported as a ratio of analyte signal intensity divided by IS signal intensity (S/IS). The results for each reaction screened are reported as relative conversion to AB (percent of Sub A converted to cross product AB). Relative conversion is defined using the following equation:

$$Conversion = \frac{[AB]}{(0.5[A] + [AB])} \quad [6-1]$$

Where [A] and [AB] are the concentrations of SubA and AB after the reaction, respectively. To standardize the results obtained across each of the eighteen 96-well plates screened in this study, each plate is normalized so that relative conversion of the average WT reaction is equal to 1. This normalization allows for the data shown to also represent fold-improvement (y-axis) over the conversion from the WT reactions for each well (x-axis). Hit identification carried out using standard T-Test in GraphPad Prism to define P values, where P values less than 0.05 are defined as statistically significant hits

KtnC Variant Library Generation. Using a homology model generated of KtnC (generated using Phyre 2.0 software and modeled after PDB 4LXJ), 96 residues within 12 Å of the predicted substrate binding region were selected. Blunt-end degenerate codon (NNK) primers were designed for the incorporation of a random mutation at each of the selected positions and ordered from Integrated DNA Technologies (Coralville, IA). Site saturated mutagenesis (SSM) polymerous chain reactions (PCRs) were performed in 96-well plates with 25 µL reaction volumes containing 1X HF Phusion buffer, 4% DMSO, 0.4 mM dNTPs, 0.8 µM of each the forward degenerate and reverse primers, 10 units of Phusion DNA polymerase, and 2.5 ng pESC-HIS::KtnC template plasmid. The reaction conditions were programmed as follows: 98 °C denaturation for 2 min; 25 cycles of 98 °C for 20 sec, 56 °C for 20 sec, 72 °C for 4.5 min; and a final 72 °C extension for 10 min. PCR products resulting from each of the 96 different primer pairs were pooled and concentrated by ethanol precipitation. The combined and concentrated PCR products were extracted from a 0.8% agarose gel. Wild-type template DNA was digestion in a reaction containing 1X Cutsmart buffer from New England Biolabs (NEB, Ipswich, MA)and 60 units of DpnI that was incubated at 37 °C overnight. DNA was cleaned using a Qiagen (Hilden, Germany) spin column before phosphorylation of the blunt end DNA with 20 units polynucleotide

kinase (PNK) in 1X T4 DNA ligase buffer (NEB). After 30-min incubation of the phosphorylation reaction at 37 °C, 400 units of T4 DNA ligase were added directly to the reaction. The ligation reaction was incubated at 16 °C overnight before the DNA was cleaned using a Qiagen spin column. DH5 α competent *E. coli* cells (NEB) were transformed with the ligated DNA using standard electroporation protocols before the cells were plated on luria broth (LB) agar plates. *E. coli* colonies were cultured and minipreped to provide the mutated DNA library. *S. cerevisiae* cells could then be transformed with this DNA library using a standard protocol for lithium acetate transformations. Transformed cells were plated on histidine dropout plates containing 2% glucose and incubated at 25 °C for 3 days.

KtnC Library Reactions. The KtnC variant library was reacted in high-throughput biotransformations in *S. cerevisiae* cells. Histidine dropout minimal media (800 μ L, 2% glucose) was added to each well of a 96-well culture plate (2-mL capacity, VWR International, Radnor, PA). To inoculate the cultures, 84 wells were each inoculated with a single colony from an agar plate containing the colonies each harboring a single mutated *ktnC* gene, ten wells were inoculated with control cells harboring the wild-type *KtnC* gene (WT), and two wells were left blank as negative controls. The cells were grown at 30 °C, 315 rpm for two days until all wells had reached saturation. The plate was centrifuged at 1,000 x g for 10 min to pellet the uninduced cells and the growth media was decanted. To induce expression and initiate the biotransformation, the cells were resuspended in 250 μ L histidine dropout minimal media containing 6% galactose and the target substrates (250 μ M 2-naphthol and 750 μ M 7-hydroxy-5-methyl-2*H*-chromen-2-one). The biotransformations were incubated at 30 °C, 315 rpm for 3 days. To quench the reactions, 10 μ L CellLytic™ Y Cell Lysis Reagent was added to each of the wells and incubated at 30 °C, 315 rpm for 30 min before adding 2 equiv. of MeOH, 2 equiv. of H₂O, 2 equiv. of MeOH, and 2 equiv. of

H₂O in that order. Samples were centrifuged and the supernatant was analyzed for product formation by MS or LC-MS.

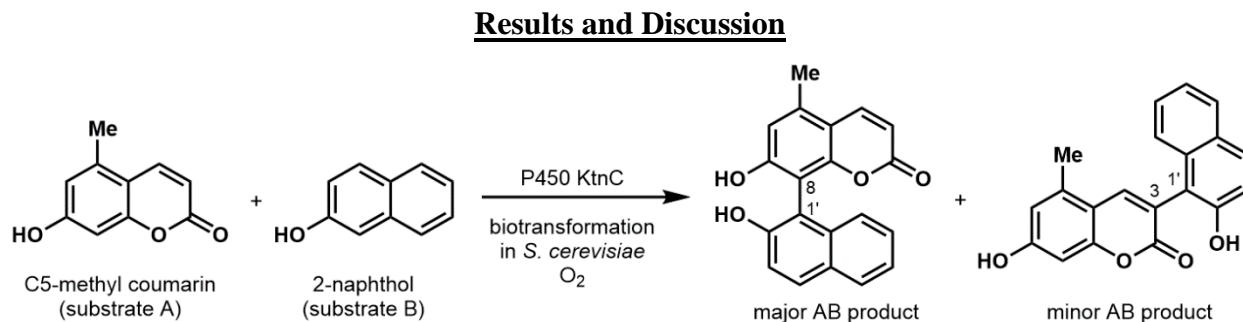


Figure 6-1. Target reaction for work in Chapter 6 of biaryl coupling of C5-methyl coumarin and 2-naphthol. HTS analysis targeted for quantification of limiting reagent SubA and all isomers of cross product AB to determine relative conversion and enzyme activity.

Method Development. Reactions received for screening in this work are comprised of cell lysis supernatant with high micromolar Substrate A (SubA) and millimolar Substrate B (SubB), both of which are relatively hydrophobic (Figure 6-1) and are expected to express high surface activity within electrospray droplets. Additionally, WT reactions are expected to achieve relatively low reaction yields with final concentrations of the cross product (AB) in the low nanomolar range. These conditions are predicted to cause substantial ionization suppression, so several steps are taken during method development to overcome suppression and improve LODs, including implementation of nESI, dilutions of the reaction mixture, addition of organic solvent (MeOH), and use of an IS. Implementation of nESI over ESI, as discussed in Chapter 1, can allow for improvements to ionization efficiency and reduction of ionization suppression, where small spray tip geometries and infusion rates of 1 nL/min can improve ionization efficiency over three orders of magnitude (Chapter 1). However, since this method is being implemented for HTS, compromises must be made between throughput and sensitivity, therefore a flow rate of 500 nL/min with a 30 μm i.d. nESI emitter was initially selected. Higher flow rates would be beneficial for improving throughput, although even minor increases begin to affect the attainable LOD for

AB, with an increase from 500 to 600 nL/min increasing the LOD by 67% based on calibration curves obtained for each flow rate on a given day. Therefore, 500 nL/min was maintained moving forward. Additionally, the final reaction mixture was composed of 50% MeOH (v/v) which most likely positively contributed to the AB LOD, as organic additives are known to assist with electrospray and can greatly improve LODs;²⁴³ however, further adjustments were not investigated, since droplets experience excess splitting at higher organic content from lack of surface tension.

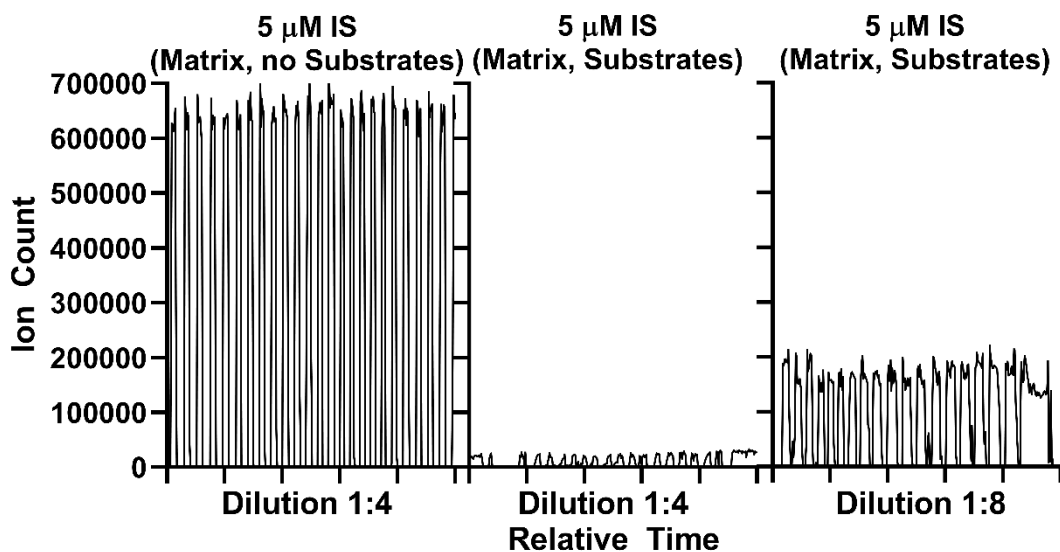


Figure 6-2. Comparison of conditions that cause ionization suppression (matrix vs matrix with high concentration reaction substrates present) and two different dilution factors to overcome a degree of suppression. (Left) A demonstration of IS spraying from final reaction matrix diluted 1:4 in diluent (50:50 MeOH:water, v/v) without substrates present. (Middle) IS spraying from final reaction matrix diluted 1:4 in diluent with substrates present. (Right) IS spraying from final reaction matrix diluted 1:8 in diluent with substrates present.

Another important condition we explore is the dilution factor (Figure 6-2). For the final step of the reaction, a 2-fold dilution of the reaction mixture with MeOH is required (1 part reaction mixture, 2 parts MeOH). For droplet generation stability and to avoid droplet splitting, higher water content is desired. Therefore, 2 parts water is added, bringing the final mixture to 50:50 MeOH:water (v/v), having diluted the original reaction mixture 4-fold (1:4). More dilution was investigated for potential to further minimize ionization suppression from the biological matrix

and high substrate concentrations, where an additional 2 parts MeOH and 2 parts water were added, ending at an 8-fold dilution of the original reaction mixture (1:8). During this investigation, it was discovered that the matrix has a minor contribution to overall suppression compared to the high reactant concentration. In Figure 6-2, IS (5 μM ACP) was added to a blank final reaction matrix (no substrates present) and to a real final reaction matrix (substrates present). In this comparison, IS signal was 19-fold lower when substrates were present vs in the matrix alone without substrates present (1:4 dilution). Further dilution (1:8) allowed for significantly less ionization suppression, where IS signal was only 3-fold lower with substrate present than without. Despite reducing the final concentration of AB by 50% with the additional dilution, suppression was reduced 6.3-fold with the 1:8 dilution, allowing for significantly higher signal response. Additionally, ACP at 5 μM was selected as the IS because of its structural similarities to the analytes. Since the calibration standards experience substantially less ionization suppression than reaction plates, presence of ACP in each allows for more accurate measurements of AB and SubA as suppression differences are reflected in the IS. For example, for one of the plates screened in the study, AB concentrations were measured with and without the use of the IS for quantification (Figure 6-3). The concentrations of AB determined in each well was on average 4.7-fold lower without IS, as

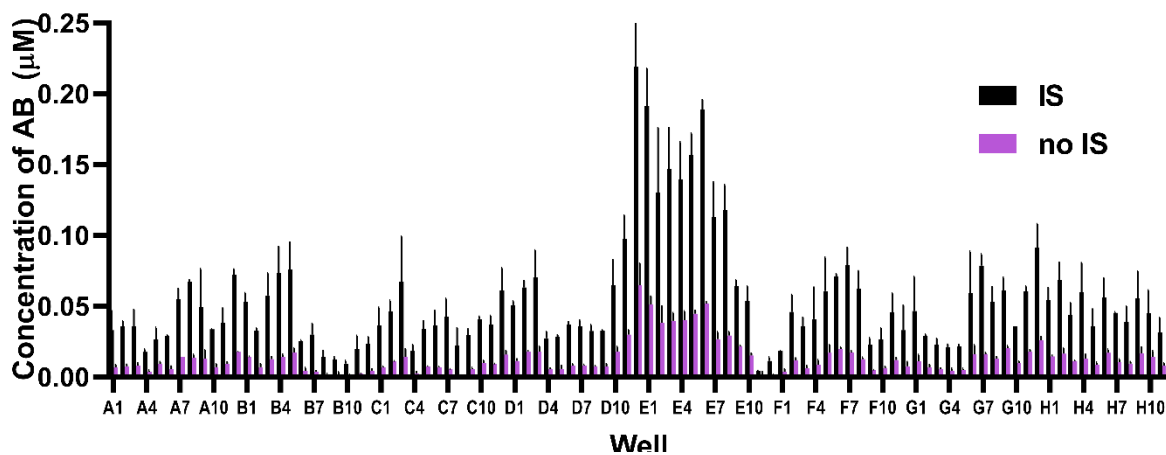


Figure 6-3. Cross product quantification from a screen with and without the use of internal standard. IS corresponds to 5 μM ACP which is added to calibration standards and samples.

suppression differences between the calibration and reaction screening are not accounted for, causing concentrations in the samples to appear lower when suppression is greater.

Using the previously described reaction mixture and nESI conditions with a sensitive MS/MS mode of analysis, LODs down to 12 nM for AB were obtained using the limit of blank method to calculate LOD from a seven-point calibration curve (Figure 6-4A).²⁴⁴ To account for a potentially broad range of reaction yields, a calibration from 0.025 to 25.0 μM was used demonstrating linearity ($R^2 = 0.998$) over a three-order of magnitude concentration range for SubA and AB. During calibrations, five droplets were infused at each concentration and the three middle droplets for each were used to generate a triplicate calibration curve in an infusion span of 1.5 min (Figure 6-4B). During calibration, standard droplets were introduced to nESI at a rate of 2.4 s per sample.

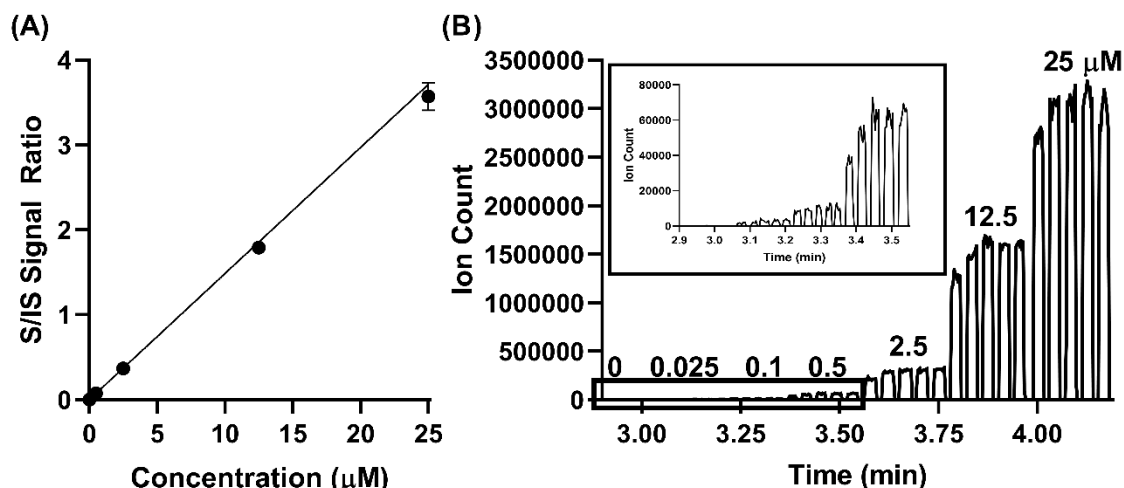


Figure 6-4. (A) Seven-point calibration curve for AB with linearity ($R^2 = 0.998$) from 25 μM to 25 nM. (B) Raw trace of calibration from droplet-nESI-MS/MS, where five droplets are sprayed from each concentration level, and the middle three of each level are averaged for $n = 3$ in each calibration curve.

LC-MS Comparison. Without special precautions, LC-MS methods for screening have throughputs of minutes (3 – 5 min) per sample.²³⁶ While LC-MS methods are robust and useful when front-end sample clean-up is necessary, 96 samples (a typical microwell plate reaction panel) will take approximately 14 h to screen. As a comparison, the developed droplet-nESI-MS/MS was

applied to the screen a single MWP (96 wells) of enzyme reactions in triplicate within 15 min of infusion, over 50-fold faster than the same screen run by LC-MS (Figure 6-5A). Triplicate analysis is performed by generating three droplets from each well in the MWP to be analyzed during infusion, where sample infusion occurs at 2.4 s per sample. The results obtained by the droplet-MS screen were compared to the same reactions screened in singlet by LC-MS for validation, with the improvement over the WT reaction reported for each well for both methods (Figure 6-5B). To determine fold-improvement over WT, the relative conversion (% SubA conversion to AB) was determined for each reaction, and all conversions were multiplied by a normalization factor to bring the average relative conversion in the WT reactions equal to one. Most conversions determined by method were within reasonable error of one another, the average error between the two methods was 23% for all reactions with fold-improvements over 0.25. The most likely source of high error at the lower conversion is due to insufficient LODs from the LC-MS, as the LC-MS method is not specifically tuned for low LODs or extensive quantification. The LC-MS method used peak areas for quantification rather than calibration curves and concentrations, making the method only semi-quantitative. Eleven of the reactions screened in this comparison were even below the LOD for AB in the droplet-MS method (< 12 nM), also contributing to error at lower conversions. Nonetheless, if relative conversion determined by each method are placed in a comparison plot, good linearity ($R^2 = 0.83$) and a slope near 1 is obtained, demonstrating the overall correlation between the two screening methods (Figure 6-5C).

Full Library Droplet-MS HTS. Eighteen 96-well plates were screened in triplicate corresponding to 1,728 enzyme reactions or 5,184 individual samples. Though samples could be infused at a rate of 2.4 s/sample (under 20 min per triplicate 96-well plate), several factors limit how many plates could be screened in a day including time to load well plates with samples and

PFD, time to generate droplets (~ 20 min), preparation and execution of calibrations, and potential trouble shooting (i.e. excessive droplet splitting or leaks in the well plates). After accounting for all time constraints, up to six plates were screened in triplicate in a single day (10 h/day), corresponding to 576 enzyme reactions or 1,728 individual samples and 33% of the entire library in a single day. This number of samples corresponds to nine days (10 h/day) of LC-MS screening, without accounting for any time constraining factors with LC-MS. The top 60 enzyme reactions with the highest relative conversion are plotted, where all plates are normalized so that WT = 1, so the y-axis effectively corresponds to fold-improvement over the WT enzyme, as well as adjusted relative conversion (Figure 6-6). Of the 1,728 enzyme variants screened, 21 variants showed

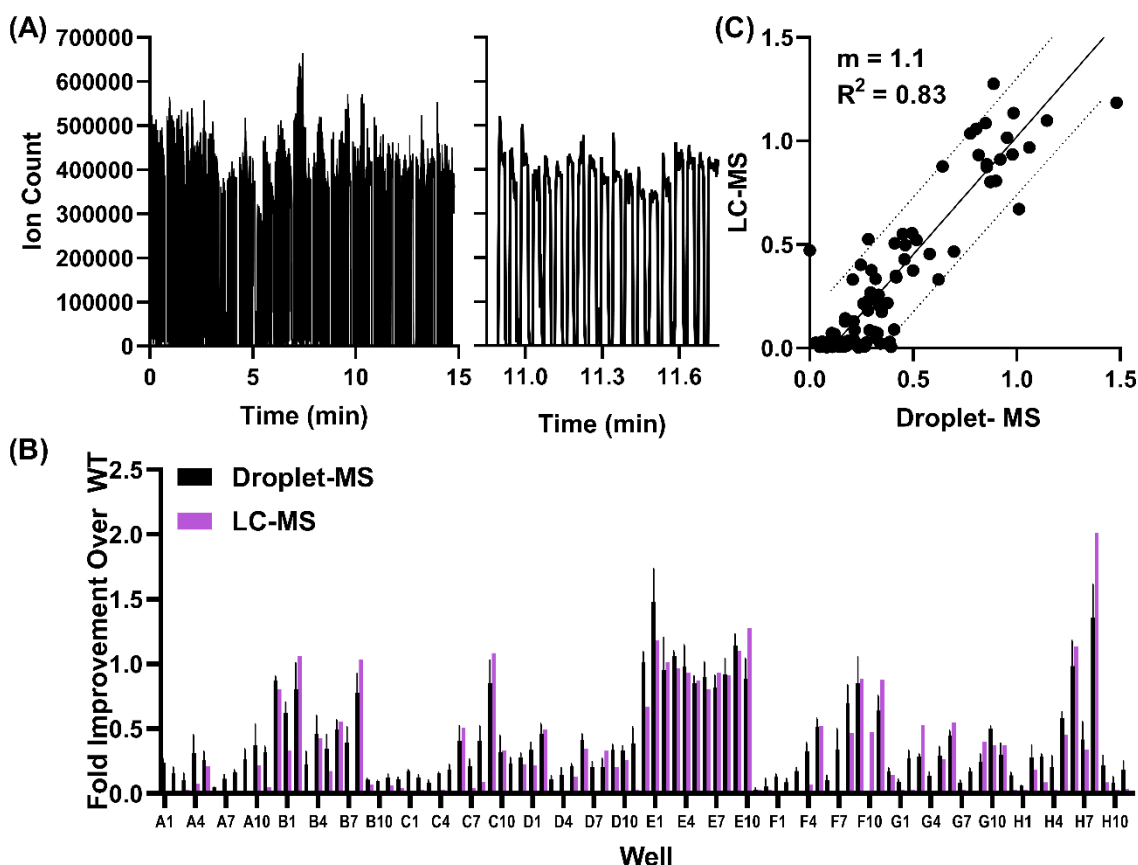


Figure 6-5. (A) Example of entire plate (96 reactions) run in triplicate within 15 min, where the MS/MS trace for SubA is shown. Zooming in on one of the many sections is an example of the droplet data, where each cluster holds 18 droplets (6 wells in triplicate) and a final “reset” droplet. (B) Fold-improvement over WT reactions shown, where fold-improvement is based on improvement in conversion to AB. Error bars are shown for the triplicate measurements by droplet-MS but were not obtained for LC-MS for time management. (C) Comparison plot of each screening method to demonstrate correlation based on slope and linearity.

higher conversion than average WT with up to 3.5-fold-improvement. Hits were selected using a t-test that accounts for various conditions including degree of improvement over WT, SD of WT reactions (averaged across all plates), and SD of the potential hit. Using this method, seven statistically significant hits were identified. These hits and other nearly hits were validated by LC-MS, and the variant with the highest improvement over WT identified by LC-MS was selected for further evolution.

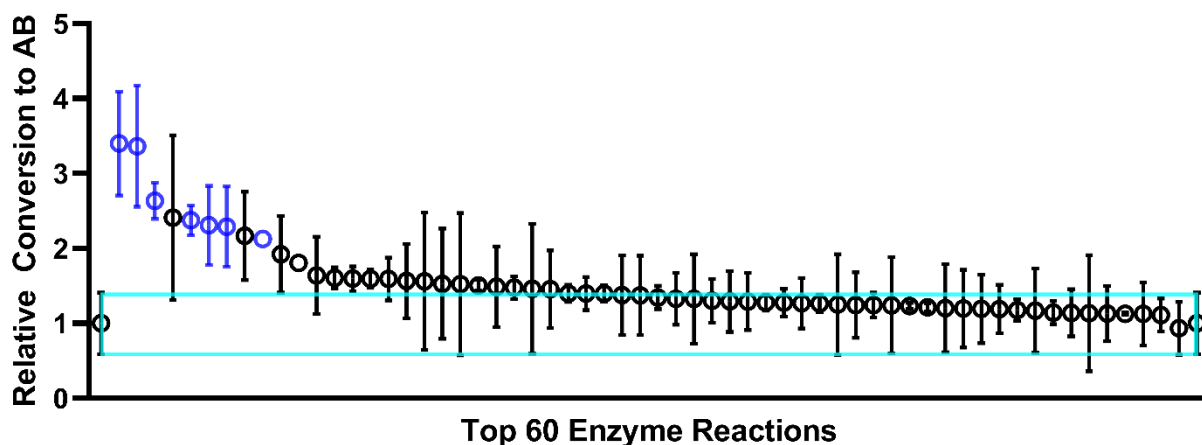


Figure 6-6. Top 60 reactions from 1,728 reaction screen. Seven statistically significant hits were identified (blue points/error bars), and most reactions analyzed have less than or equal to the relative conversion of the WT reaction. The WT reaction and its SD is shown by the light blue box and the points at the beginning and end of the box (average = 1).

Conclusions

MS is an excellent tool for screening enzyme catalyzed reactions in a directed evolution workflow as it is label-free, sensitive (compared to UV, colorimetric), structure elucidating, and can interface with various techniques/instruments. However, most MS screening approaches rely on LC-MS which is limited in its throughput. In this study, droplet microfluidics (segmented flow) has been paired with direct nESI-MS/MS for the first time to achieve a highly sensitive method (LOD = 12 nM) with sample introduction rates of 2.4 s per sample. This method was applied to screening a full enzyme variant library of 1,728 different reactions in triplicate, with up to 576 reactions (1,728 samples) analyzed in a single day, where seven statistically significant hits were identified with up to 3.5-fold-improvement over WT reactions. Though this method sacrifices

faster sample introduction rates for improved sensitivity, this caveat has little impact on overall throughput. The major limitation on throughput in this screening procedure comes from the relatively long sample preparation/droplet generation times and restriction to finite volumes that can fit in the microfluidic tubing. Generally, a length of tubing can only fit enough droplets for a single 96-well plate (in triplicate), requiring regular manual swapping of tubing pieces between droplet infusion and generation. This limits the screening to ~576 reactions (in triplicate) in a 10 hr workday, though this is still nearly 10-fold higher throughput than screening by a typical 3 min LC-MS gradient which would be limited to ~60 reactions (in triplicate) in a 10 hr workday.

Chapter 7

Conclusions and Future Directions

In the previous chapters, various methods and systems have been developed to address common analytical limitations in throughput and sensitivity, generally in mass spectrometry-based systems. These include the development of a novel method and application using powerful EKS online preconcentration with CE-MS, high temporal resolution monitoring of seven neurochemicals using droplet microfluidics with direct MS, the first report of droplet-nESI for HTS in a directed enzyme evolution workflow, and development of a new form of online liquid-liquid extraction. Though the work in this dissertation is diverse with projects including analytical separations, droplet microfluidics, or mass spectrometry (and often combinations of these), each project introduces a novel method for sample preparation or sample introduction to an analytical platform that pairs various analytical technologies in innovative ways. Droplet microfluidics (or segmented flow) is frequently utilized in these workflows in novel, advantageous, and innovative ways, and the under-represented field of droplet microfluidics paired with mass spectrometry is advanced in this work. Novel methods pairing these technologies has allowed for high throughput and sensitive sample introduction, achievements with high temporal resolution for many analytes simultaneously, and rapid microfluidic extractions for in-line sample clean-up.

The methods developed in previous chapters generally aim to improve throughputs and/or detection sensitivity for various technologies and applications. Though each of the platforms and methods developed in this dissertation demonstrate novelty and utility, each has potential to be

adjusted for further improvements or alternative applications. Many of the platforms developed were tuned for either throughput or sensitivity, and optimization of one of these parameters is often sacrificed for the other. Examples include capillary CE-EKS-MS/MS, where extended injection/preconcentration times were applied to drastically improve limits of detection; or in droplet-nESI-MS/MS for neurochemical monitoring, where sufficient LODs were obtained for seven neurochemicals simultaneously through reduction of direct-MS infusion flow rates, though this substantially increased analysis times. In this chapter are several alternatives or improvements to the previously discussed methods that could be developed to further advance the work presented in this thesis, including a proposed sheathless electrospray platform for EKS with CE-nESI-MS/MS, “real-time” *in vivo* neurochemical monitoring, and online and continuous sample clean-up using automated SFNE with MS.

Future Directions

Sheathless CE-MS Interface with EKS

The CE-EKS-MS/MS method in Chapter 2 interfaced CE with MS via a robust co-axial sheathflow sprayer. The sprayer establishes a ground to the migrating solution and assists the electrospray process by diluting CE eluent with an ESI friendly solution at a constant and relatively high flow rate as well as providing an assisting gas flow. This interface is one of few CE-MS interfaces that is commercially available and is well regarded for providing robust, grounded separations and interfacing.²⁴⁵ Though robust for CE-MS, sheathflow interfaces in general can significantly hinder detection sensitivity, as migrating compounds are diluted up to three orders of magnitude at the interface due to the highly contrasting flow rates of the electroosmotic flow and sheathflow. This effect can be detrimental to CE-MS since LODs are often already insufficient

without additional dilution as a result of the minute injection volumes (pL - nL) associated with CE.¹¹⁰

Sheathless CE-MS interfaces are often used to gain additional detection sensitivity in CE-MS methods, and studies have found that simply employing this type of interface can improve LODs over 5-fold compared to a sheathflow interface.^{52,104} Employing a sheathless interface with the CE-EKS-MS/MS platform could provide several improvements or alternative approaches to the method. If the majority of the original conditions used in the method were maintained while a sheathless interface were employed, nearly a 1000-fold dilution factor would be avoided which could drastically improve detection sensitivity with potential fM LODs (based on the original low pM LODs for various neurotransmitters). This improvement could allow for several changes to the existing method including trace analysis of neurotransmitters in different sample types (i.e. dialysate, plasma, etc.), addition of new target analytes (i.e. low concentration neuropeptides),²⁴⁶ and could lead to reduction in volume requirements for EKS-based injections. Another route that could be taken while employing a sheathless interface with EKS is reduction of the injection duration/voltage and separation capillary length to offer faster separations. With the original method, long and powerful injections (150 s, 375 V/cm) are implemented, limiting the ultimate length of separation capillary remaining after injection to electrophoretically resolve target analytes. Theoretically, a shorter injection would increase the remaining separation capillary available after injection for CZE to occur and could result in (a) higher resolution/peak capacity or (b) allowance for a shorter separation capillary while maintaining the original resolution/peak capacity, and subsequently higher throughputs with similar LODs due to improvements by the sheathless interface.

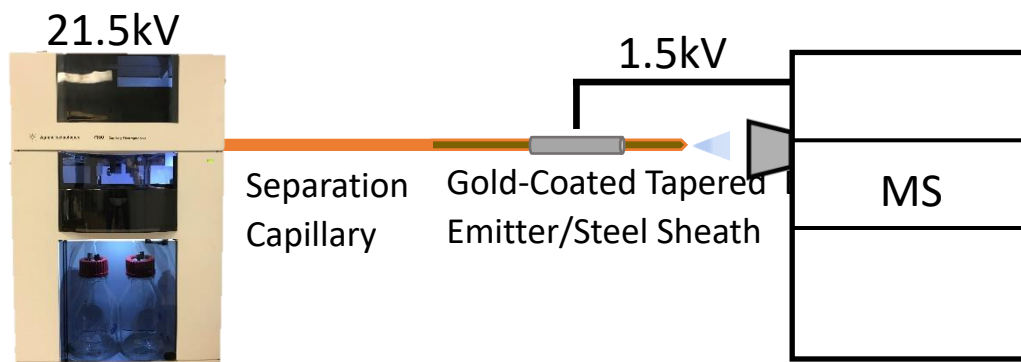


Figure 7-1. Sheathless CE-MS system for use with EKS, where the separation ground is applied by the slightly positive (compared to separation voltage) nESI voltage.

The proposed system consists of a separation capillary with a narrow $\sim 10 \mu\text{m}$ i.d.) conductively coated (gold) nESI emitter directly integrated onto one end of the separation capillary, where the ground/electrospray voltage is applied to a stainless steel tubing that sheathes the emitter (Figure 7-1). In this set-up, the same capillary electrophoresis system used in Chapter 2 can still be used, where the autosampler/power source are connected to the front-end of the separation capillary, the majority of the separation capillary is stored in the air-cooled holder, and the eluting end of the separation capillary is sheathed in the stainless steel tube and fixed to the nESI source. Using the Agilent 7100 CE System, pressure can be applied to achieve a constant flow rate in conjunction with the EOF. This may be an important feature for functionality of the proposed system, as the minimal bulk flow associated with the EOF in this high pH buffer system ($\sim 6 \text{ nL/min}$) may make it difficult to achieve robust spray and grounding with EOF alone.

Preliminary results were obtained to ensure the validity of the proposed platform. To prepare the spray tips, a Sutter Instrument Co. P-2000 capillary puller was used to evenly pull apart 120 cm of $50 \mu\text{m}$ i.d. by $360 \mu\text{m}$ o.d. capillary, forming two 60 cm separation capillaries with approximately $10 \mu\text{m}$ i.d. tips, which were subsequently coated in gold using a Quorum Technologies SC7620 Mini Sputter Coater to obtain a conductive finish on the integrated nESI emitter (Figure 7-2). The resulting separation capillary with the integrated nESI emitter was

placed, as demonstrated by Figure 7-1, with the front-end of the capillary positioned within the CE system and the nESI end affixed onto a stainless steel nESI platform on a Micromass Quattro Ultima triple quadrupole mass spectrometer.

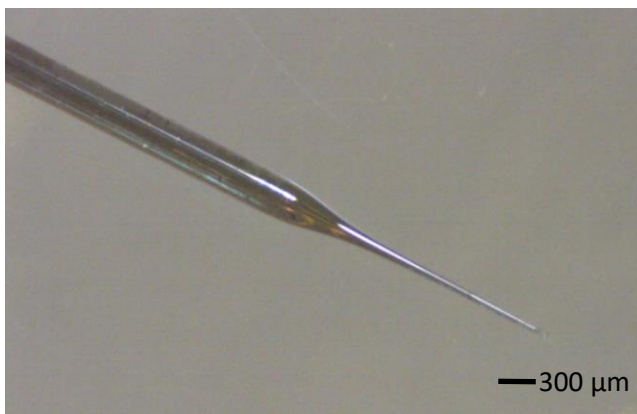


Figure 7-2. Image of the separation capillary back-end with a home-pulled, gold-coated, integrated nESI emitter. The inner diameter of the spray tip was measured to be approximately 10 μm .

Extensive method development was not performed for preliminary experiments, and therefore the separation, nESI, and MS/MS parameters were not optimized for complete analysis. However, important observations were made on this

assembly. A stable ground and separation current could be obtained for a reasonable duration of time corresponding to a relatively long electrophoretic separation (Figure 7-3A). Additionally, nESI was successfully performed on a set of test compounds including DA, NE, E, and Ch (Figure 7-3B).

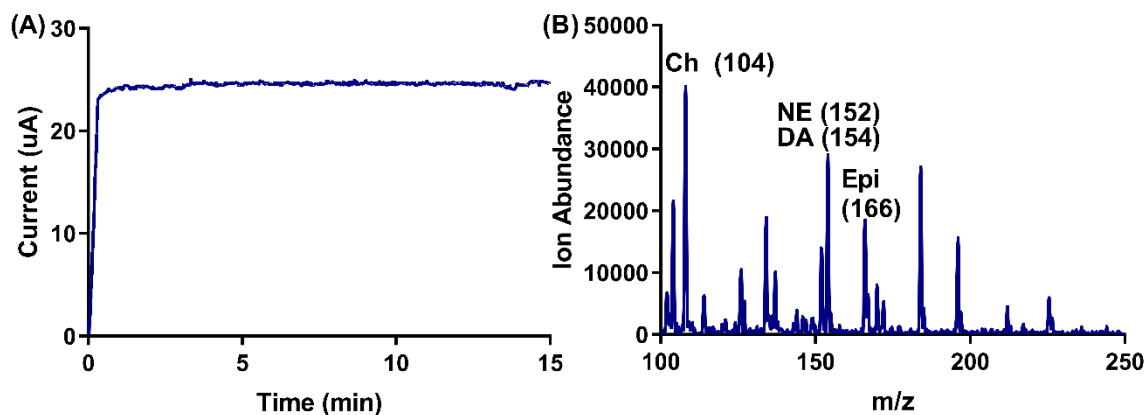


Figure 7-3. (A) 21.5 kV of separation current was applied while connected to 1.5 kV of nESI voltage, totaling 20 kV across the separation capillary for 16 min, where a stable current was obtained over the period indicating stable ground and interfacing. (B) A solution of 1 μM neurotransmitters dissolved in water were infused by applying pressure in the CE system to obtain a infusion rate of 100 nL/min, indicating that electrospray can be conducted using the home-pulled separation capillary-nESI system while maintaining stable spray.

Real-Time In Vivo Neurochemical Monitoring

While previous reports have shown low-second temporal resolution while monitoring one – four neurochemicals from microdialysate,^{24,98,142} LC-MS is required when more compounds are being monitored, typically raising the temporal resolution to 5 – 20 min. The method developed in Chapter 3 for high temporal resolution in vivo monitoring of neurochemicals improves temporal resolution compared to what could previously be obtained while monitoring many (seven here) neurochemicals simultaneously. Although robust, sensitive, and high throughput given the number of samples generated in a single in vivo collection (>1000 fractions per in vivo experiment) the method has one major limitation. Since the flow rate of direct-MS infusion is substantially lower than the flow rates during in vivo fraction collection/droplet generation (0.05 $\mu\text{L}/\text{min}$ vs 1.0 $\mu\text{L}/\text{min}$), analysis takes 20-times longer than collection, meaning 10 min of neurochemical monitoring takes 3 h to analyze by droplet-nESI-MS/MS. This limits the use of this method to fewer in vivo experiments in a day and/or to shorter time-spans of neurochemical monitoring.

To overcome this challenge, I propose a system for “real-time” monitoring where the in vivo sampling is flowed directly to the nESI-MS/MS for online analysis. To achieve this while maintaining low nM LODs and at most 10 s TR, the in vivo fraction collection/droplet generation platform used in Chapter 3 is largely left unchanged, where the MD probe perfusate and internal standard/diluent mixture merge in a microfluidic cross and are segmented into droplets by an inert fluoruous carrier fluid (perfluorodecalin, PFD), but larger droplet fractions are generated. These droplets and corresponding flow rates are then split into two channels in a microfluidic device at a 1:20 ratio, one which takes a bulk of the flow and droplet volume (0.95 $\mu\text{L}/\text{min}$) to collection, and the other that takes a nESI compatible flow rate (0.05 $\mu\text{L}/\text{min}$) to nESI-MS/MS for analysis (Figure 7-4). In this format, the flow rate for infusion will remain identical to the original method,

allowing for similar LODs to be obtained while assessing fractions in near-real-time as they are generated. The dialysate collected could then be used to validate any interesting results. This will also make the method suitable for long-term analysis. A possible limitation to this proposed system incurs from the larger droplet fractions generated, which will diminish the sampling rate closer to 5 – 10 s per fraction as opposed to 0.35 – 0.7 s per fraction. However, while reduction of the sampling rate has potential to worsen temporal resolution, it will most likely remain unaffected or minimally affected, as axial diffusion before droplet generation is the major source of temporal resolution limitation (10 - 11 s) in Chapter 3, not the sampling rate.

Finally, this method could offer more information on neurotransmitter dynamics and their implications if even

more compounds could be monitored simultaneously.

Though the developed method includes a total of seven neurochemicals of interest, several compounds were omitted to improve temporal resolution by reducing droplet

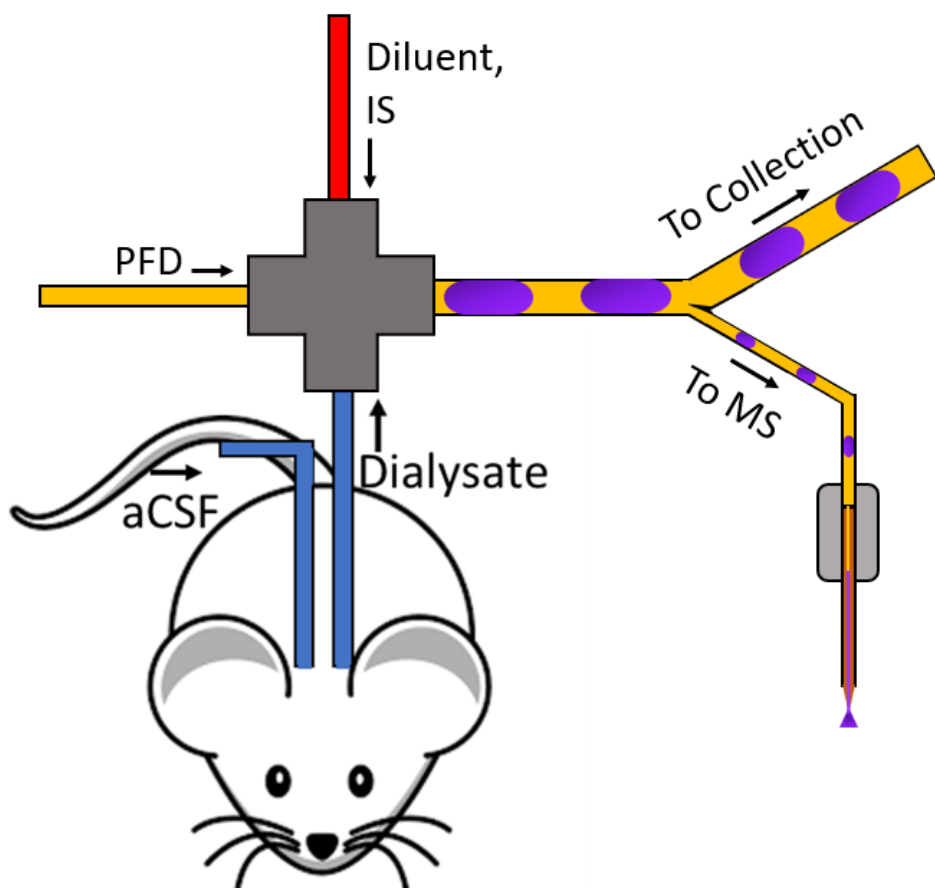


Figure 7-4. Proposed format for “real-time” high temporal resolution in vivo neurochemical monitoring using droplet-nESI-MS/MS. A 1:20 split on large dialysis droplets, where the 1 is sent to MS and 20 is sent to collection.

size and because of difficulties achieving sufficient LODs. Including additional neurotransmitters of interest (i.e. histamine, histidine, norepinephrine, epinephrine) could provide further insight if this method were applied for biological studies. Several steps need to be taken to achieve these additions, including increased droplet size and enhanced LODs for the targeted additions, which may potentially be obtained through further investigation of buffer additives and diluents

SFNE for Rapid Online Sample Clean-up with MS Analysis

While the online and continuous SFNE system developed in Chapter 5 proved successful for rapidly determining $\log K_{ow}$ values for pharmaceutical compounds, SFNE initially demonstrated strong applicability for rapid in-line sample clean-up for direct MS analysis, where LLEs would occur while in-transit to the ESI source (Chapter 4). While technology for robotic sample introduction already exists (i.e. Agilent RapidFire) that can perform in-line SPME and achieve sample injection cycles under 10 s, there has been no technology capable of performing rapid automated sample introduction in tandem with LLE for MS. As discussed in Chapter 5, various online microfluidic LLE techniques exist, but few have been able to achieve rapid sample introduction from an array and none of these have been interfaced with MS. Pairing this system with MS could offer several uses including MS detection for $\log K_{ow}$ determination, where MS could provide enhanced sensitivity, specificity, and label-free measurements compared to direct UV Vis detection. It could also be used to achieve rapid biological sample screening in applications such as drug screening from biofluids or biomarker monitoring in disease states, where biofluids can be directly injected into the system for analysis without any additional sample preparation, and detection sensitivity is increased since matrix effects are avoided.

Using the system in its current state, samples could be injected with 78 s injection cycles, though faster injection cycles could be achieved with different autosamplers as previously discussed. There is one key challenge associated with interfacing the LC-SFNE system with MS. Ethyl acetate (EtOAc) was identified as the best extraction solvent to be used with ESI, where good signal could be obtained when spraying analytes from EtOAc (after extraction) in conjunction with 50:50 MeOH/H₂O (v/v) from a sheathflow sprayer. However, the devices used for SFNE phase pair generation are largely composed of PDMS, which is incompatible with EtOAc. In initial tests, EtOAc would rapidly permeate the PDMS, affecting the flow rate, phase pair volume ratios, and cause PDMS to swell which would also affect flow rates, or even block flow. To overcome this, an entirely glass device mimicking the layout of the original PDMS device must be fabricated using hydrofluoric acid etching to create the channels. The glass device may then be paired with the autosampler and PFD, EtOAc, and aqueous pumps for phase pair generation, extraction, and finally flowed to ESI-MS/MS for analysis.

Preliminary experiments were performed to verify the potential capability of this proposed system. Glass devices, similar to the original PDMS devices, were fabricated for use with EtOAc. During preliminary experiments, an LC autosampler was not used for sample introduction, rather an aqueous solution

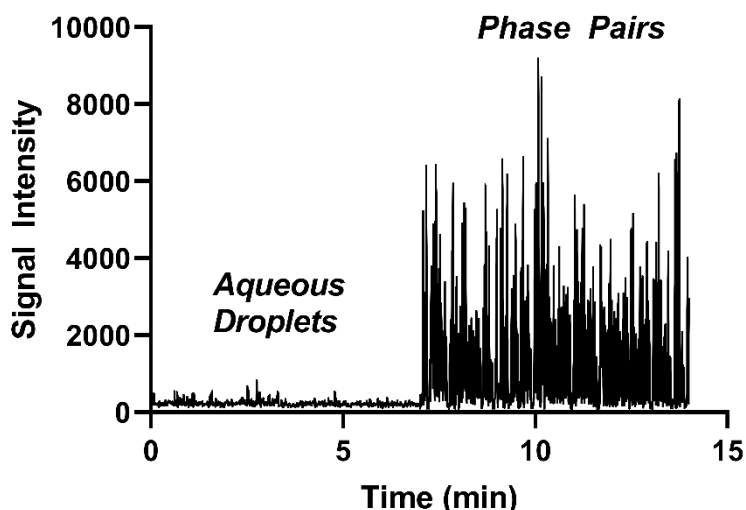


Figure 7-5. Preliminary results using online phase pair generation devices with aqueous/EtOAc phase pairs. Extraction phase flow begins at 7 min. 1 μ M Doxylamine is the test analyte in this example.

comprised of analytes dissolved in water was assessed with and without extractions (Figure 7-5). Six drug compounds at 1 μ M in pooled human plasma were assessed. Initially, extraction phase was not flowing, and aqueous droplets were being formed and sprayed. At 7 min, flow of the extraction phase was initiated, upon which phase pairs could form and extractions occur. Signal intensity drastically increased when performing ESI on the analytes after extraction into EtOAc, where analyte could not be distinguished from baseline noise without extractions. Online phase pair formation shows utility for online biofluid clean up and extraction of select compounds for MS/MS measurements. Implementing this method for clean-up and identification/quantification of drugs from biofluids could offer solutions for rapid drug screening, where several replicates could be obtained from a single injection thanks to compartmentalization of many droplets from a single injection of sample.

Appendix 1

Supporting data for *in vivo* experiments in Chapter 3

Below is the scheme for droplet generation directly from a microdialysis probe. As dialysate and diluent merge in a 50 μm i.d. microfluidic cross at 0.25 $\mu\text{L}/\text{min}$ (1:1), they are segmented by PFD at 0.5 $\mu\text{L}/\text{min}$ to generate reproducible droplet volumes (~ 5 nL) at 1-3 Hz. The cross is a 50 μm i.d. microfluidic cross junction from Valco Instruments Co., Inc with 360 μm o.d. finger-tight connections. Tightness of these connections on the capillaries/export tubing noticeably affects droplet generation in terms of droplet size and reproducibility. Anecdotally, incoming flows, which are through 50 μm i.d. x 360 μm o.d. fused silica capillary, should have extremely tight connections (by finger-tightening), and the tightness on the export tubing, which is 150 μm i.d. x 360 μm o.d. PFA tubing, may be adjusted until ideal droplet generation is achieved. When connecting the cross to the probe outlet (360 μm o.d. fused silica capillary), extra caution must be taken as the probes are fragile. Making this connection has proven less difficult when the probe is already secured in a holder.

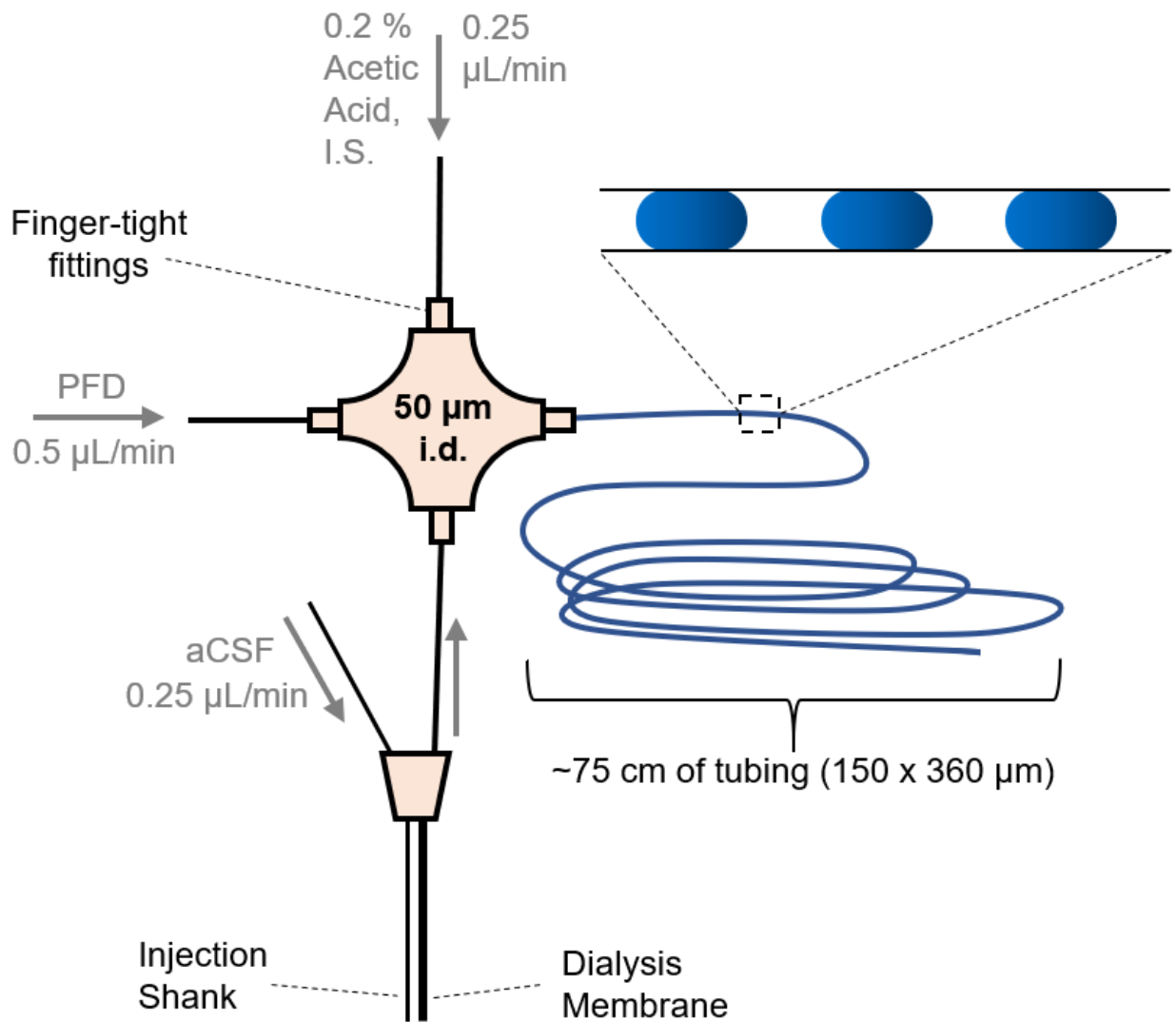


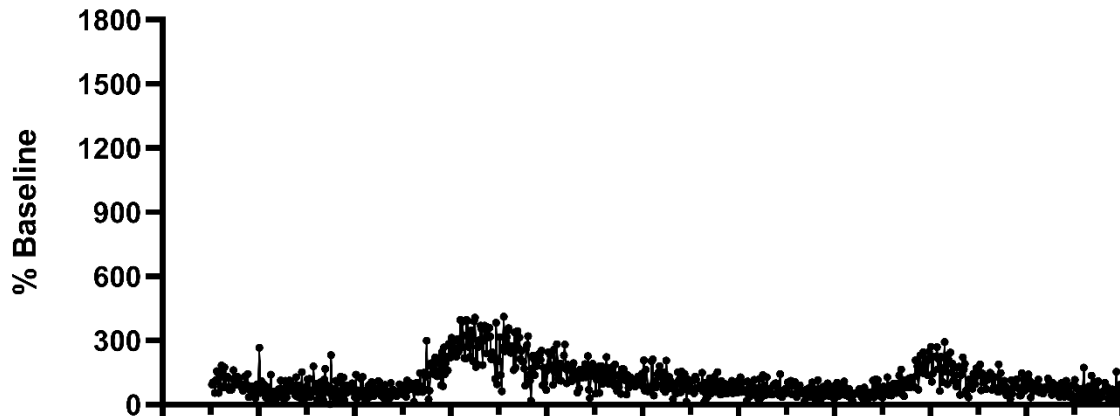
Figure A-1: Set-up for droplet generation using microfluidic cross-junction attached to microdialysis probe outlet. As diluent and dialysate merge (1:1), they are segmented by PFDE to form roughly 5 nL droplets with 5 nL PFDE spacing into a long line of tubing.

Appendix 2

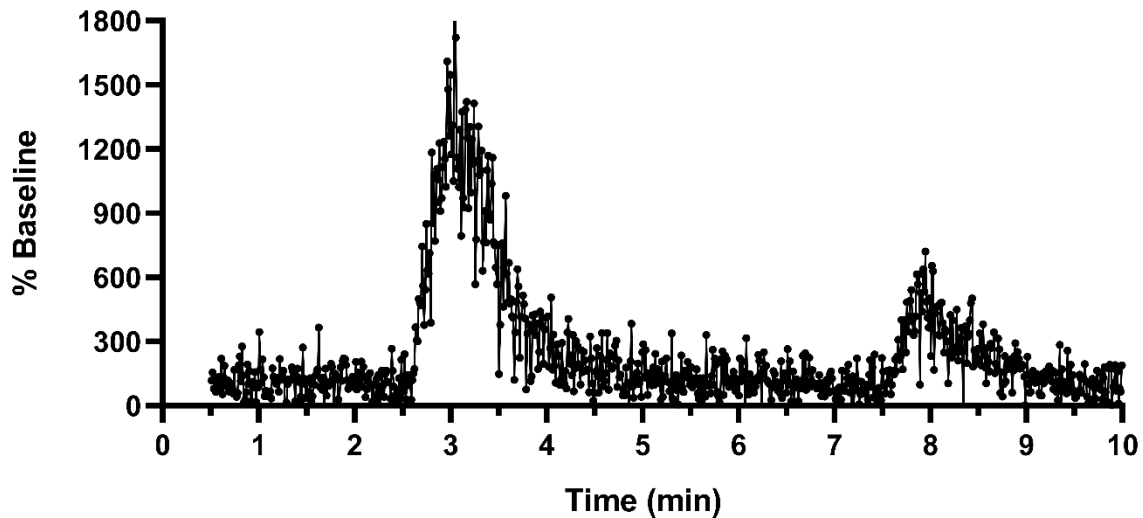
Supporting data for *in vivo* experiments in Chapter 3

Below are the individual traces for each biological replicate from *in vivo* experiments that used droplet fractions. The compound, biological replicate (001, 002, 003, 004), and type of stimulation (high potassium: K⁺, amphetamine: AMPH) are denoted above each graph.

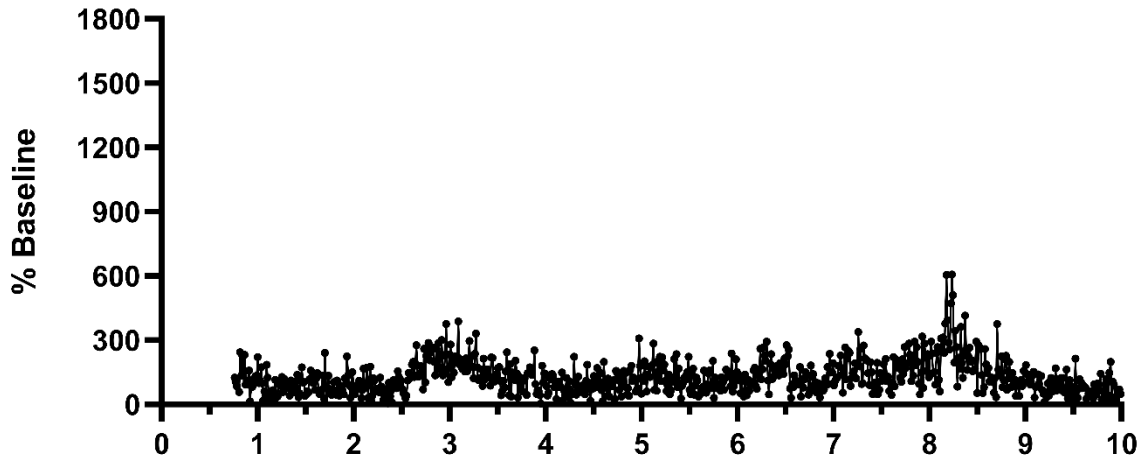
5HT 001 K⁺



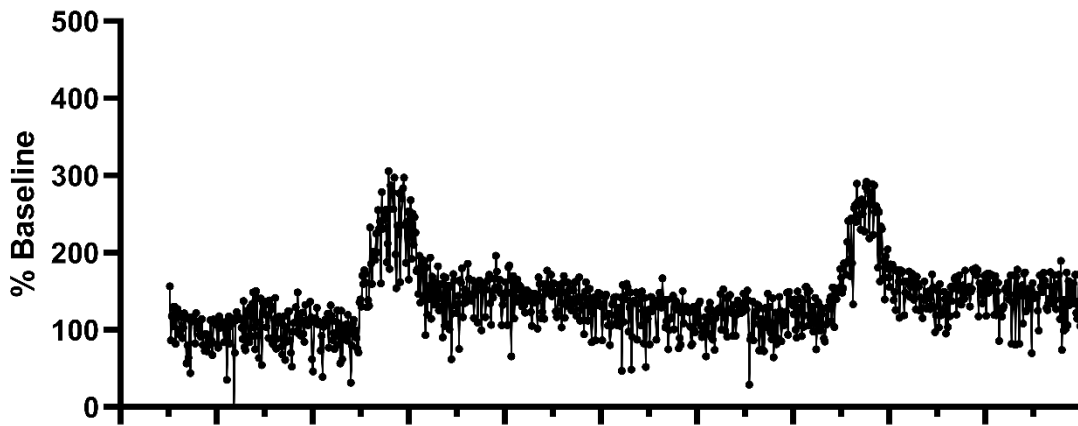
5HT 002 K⁺



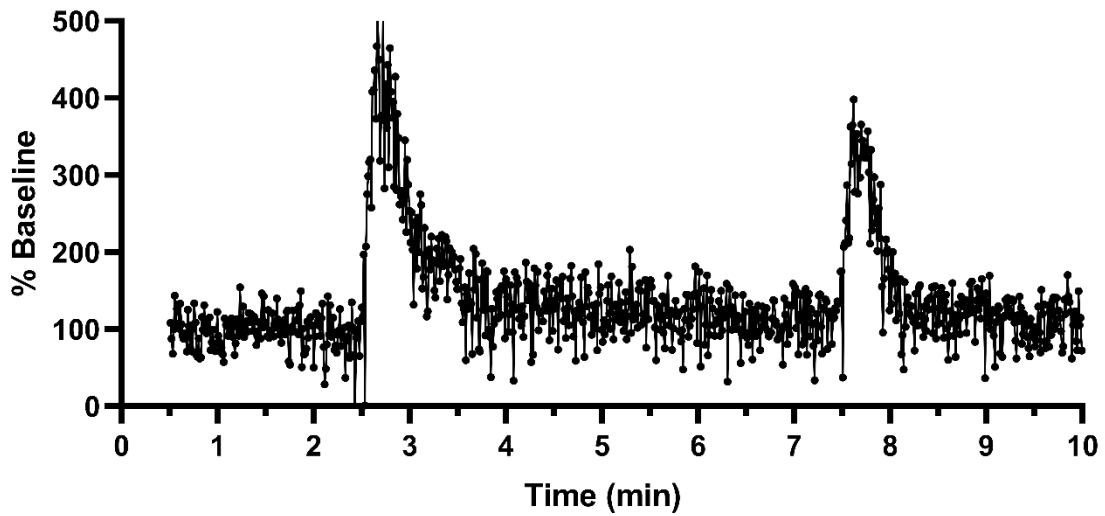
5HT 003 K+



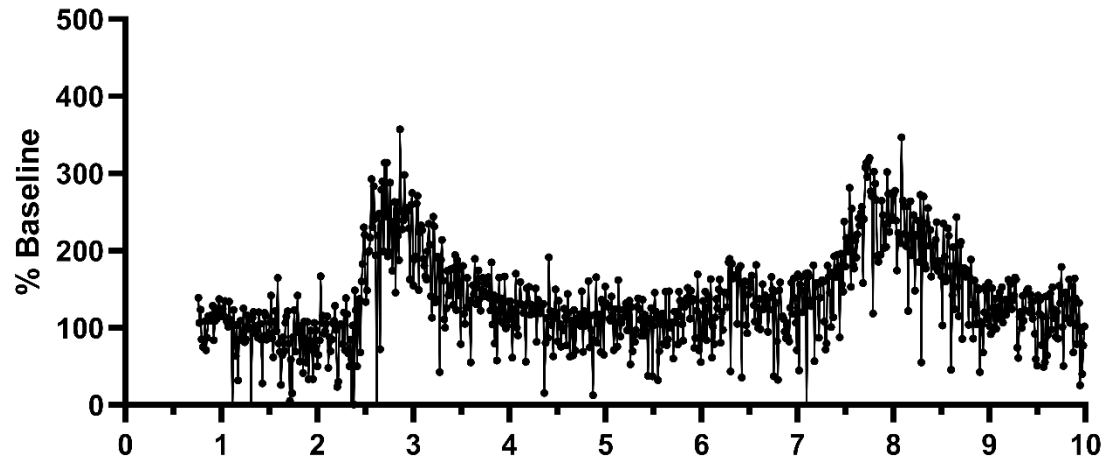
ACh 001 K+



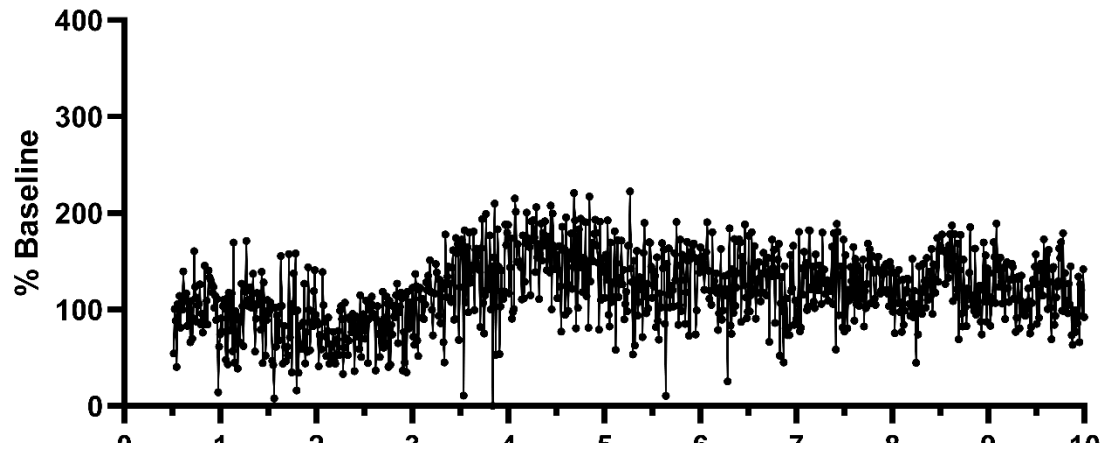
ACh 002 K+



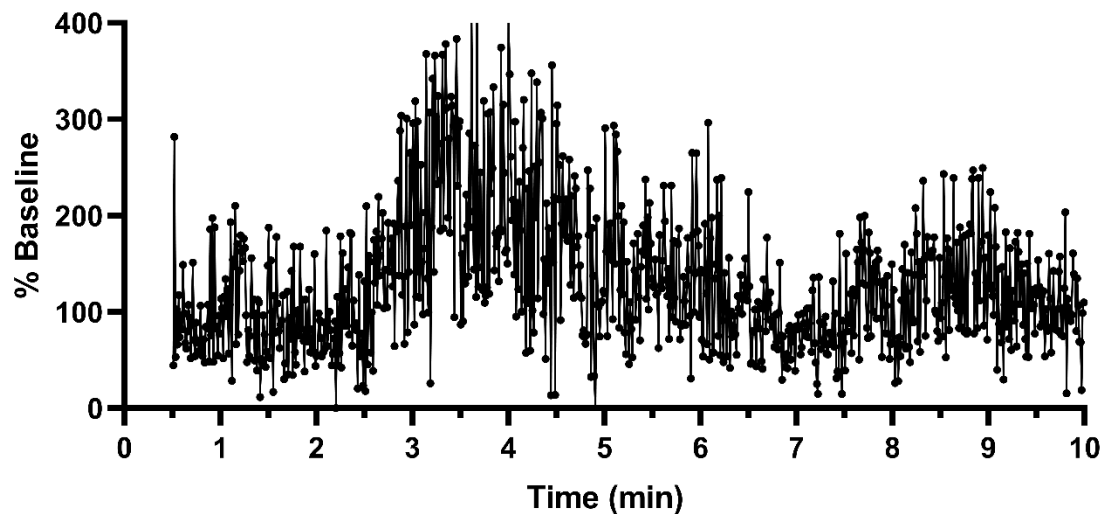
ACh 003 K+



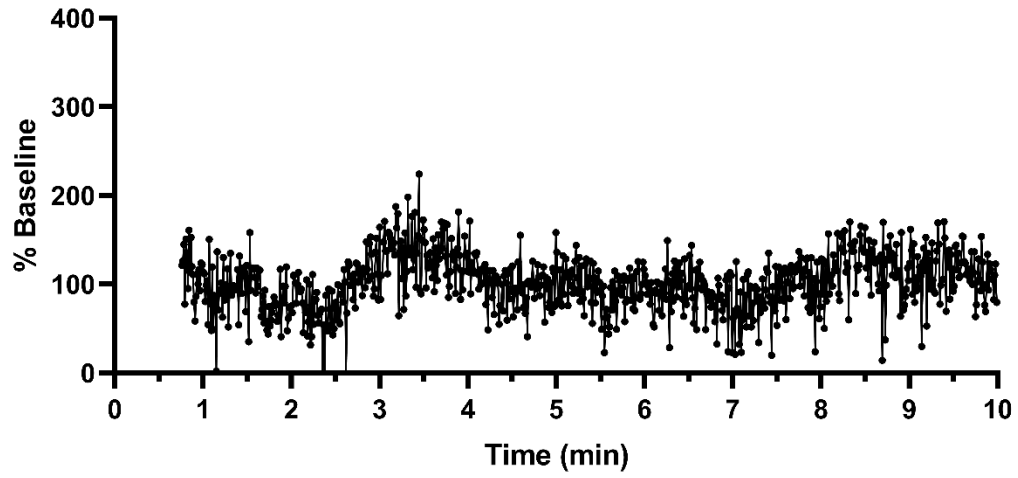
Ado 001 K+



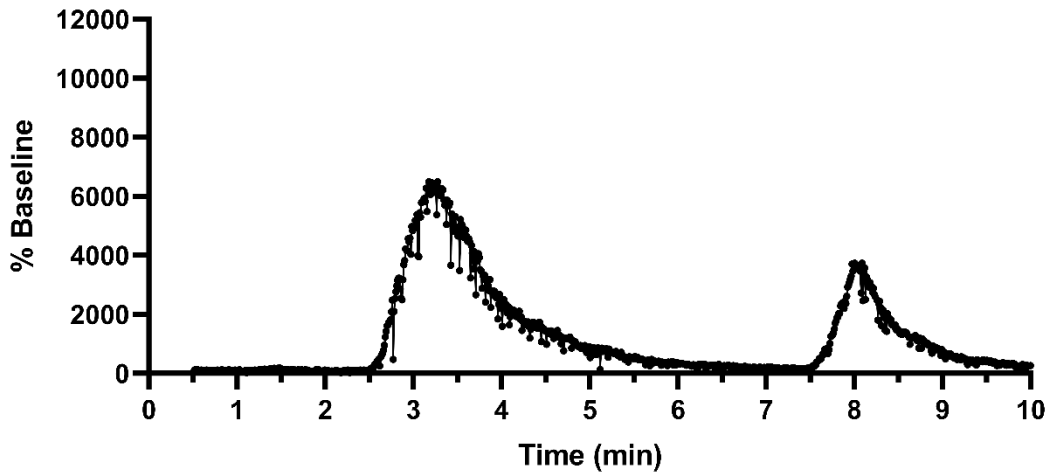
Ado 002 K+



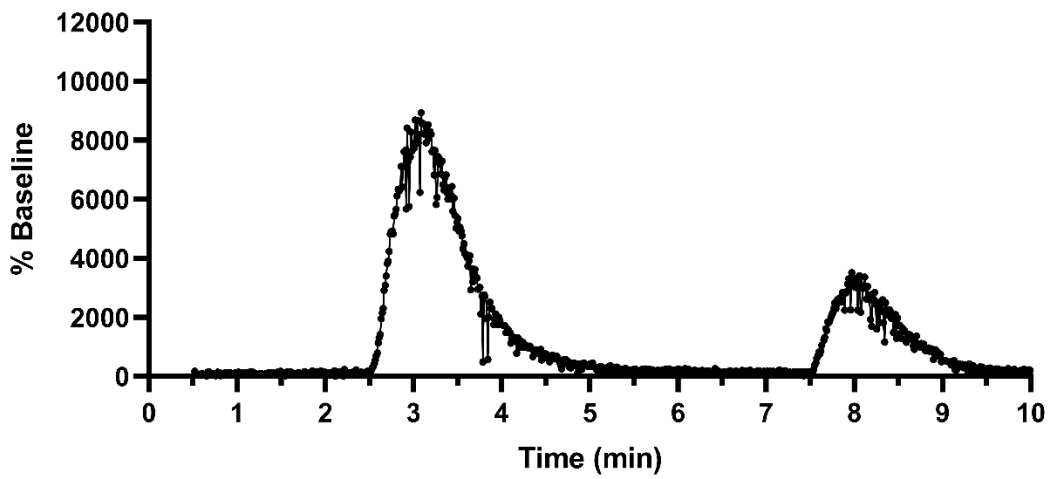
Ado 003 K+



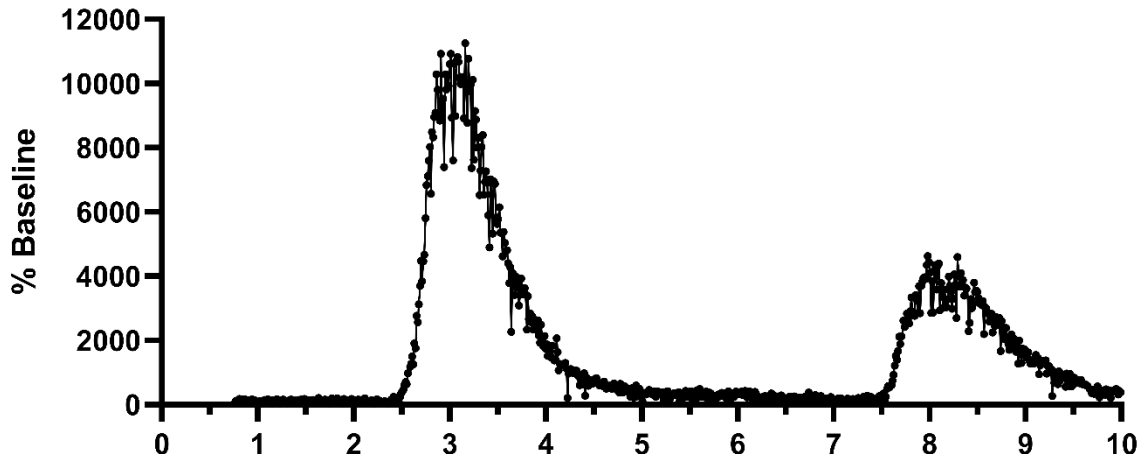
DA 001 K+



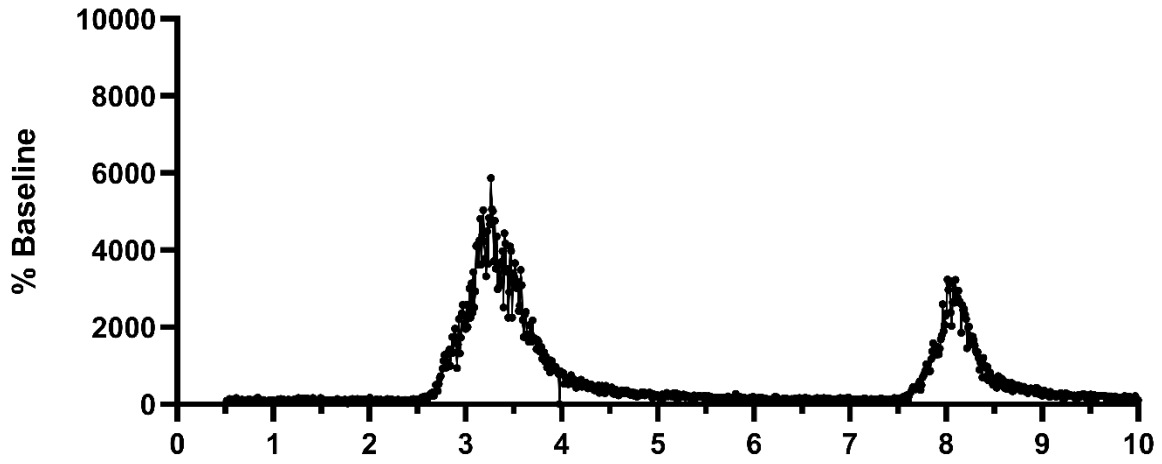
DA 002 K+



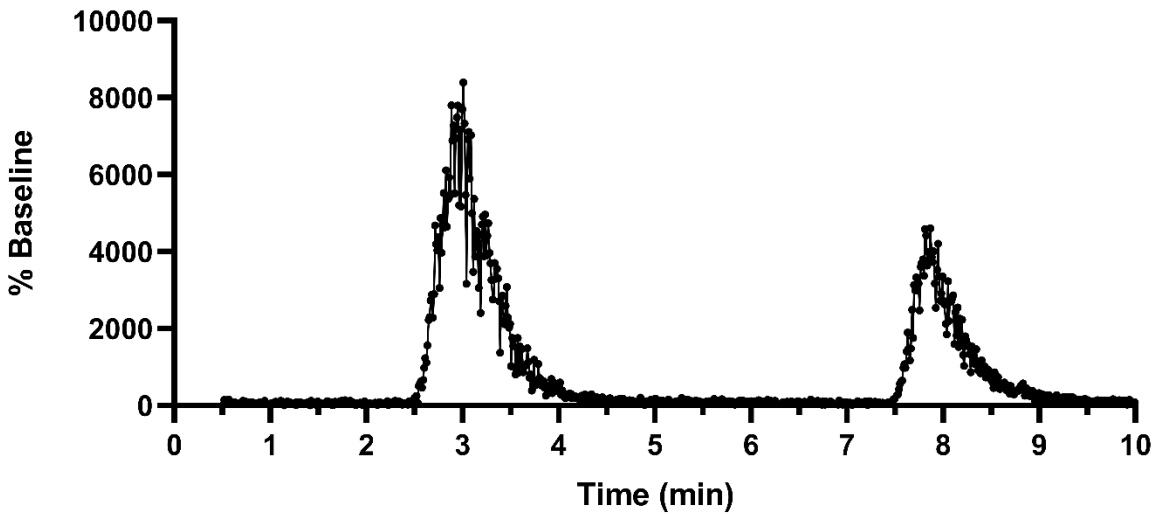
DA 003 K+



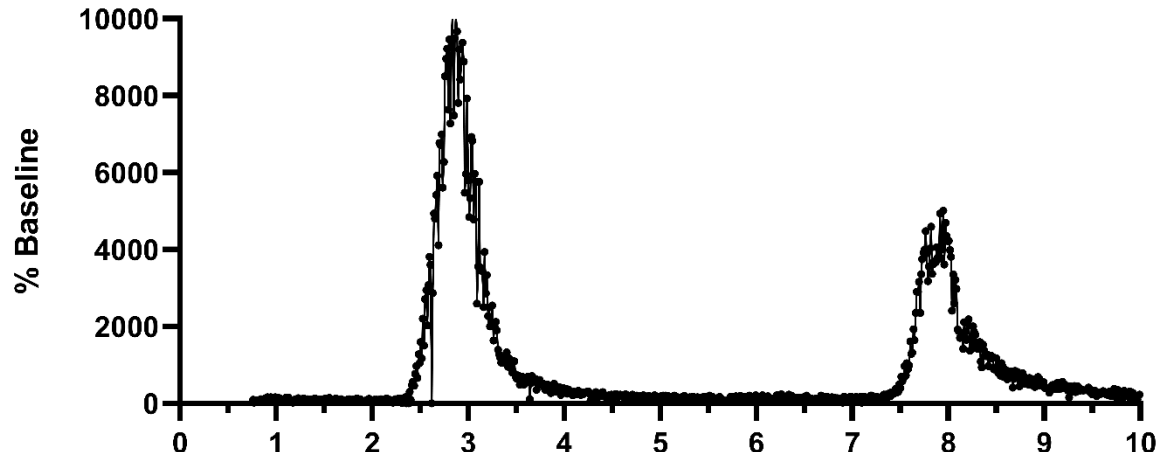
GABA 001 K+



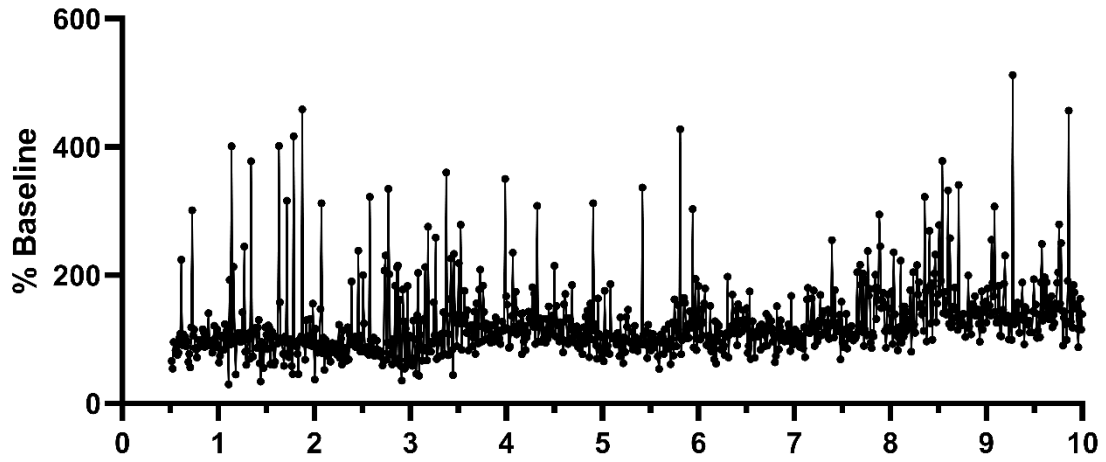
GABA 002 K+



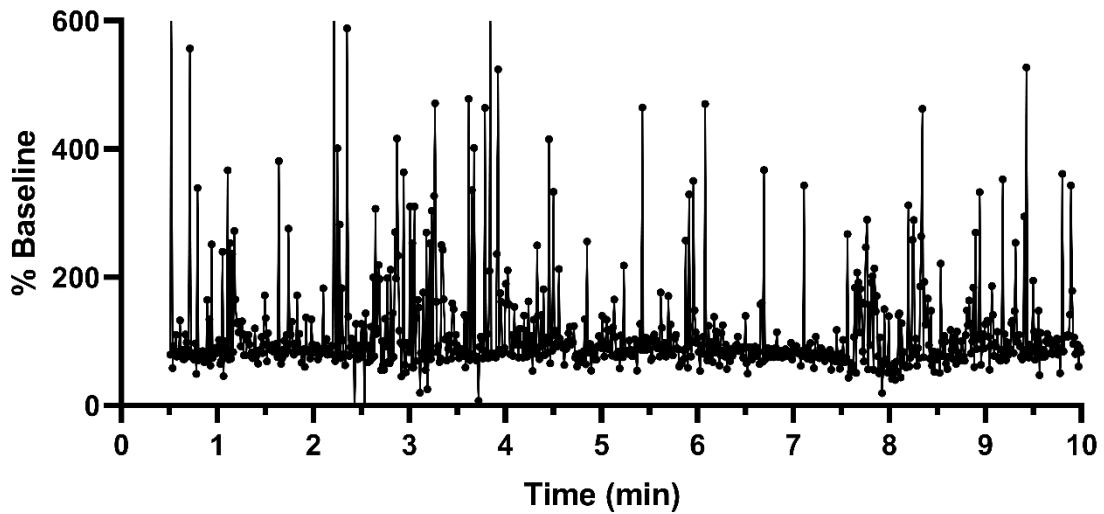
GABA 003 K+



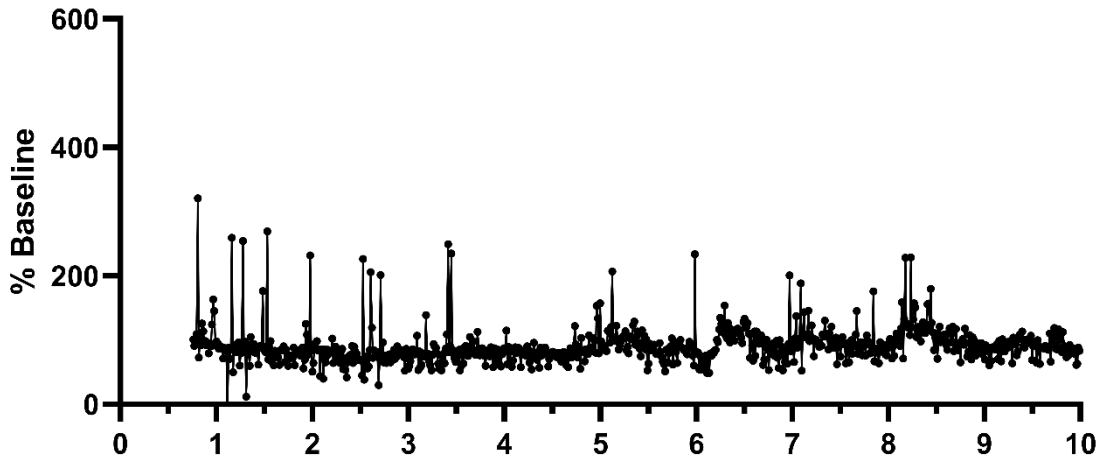
Gln 001 K+



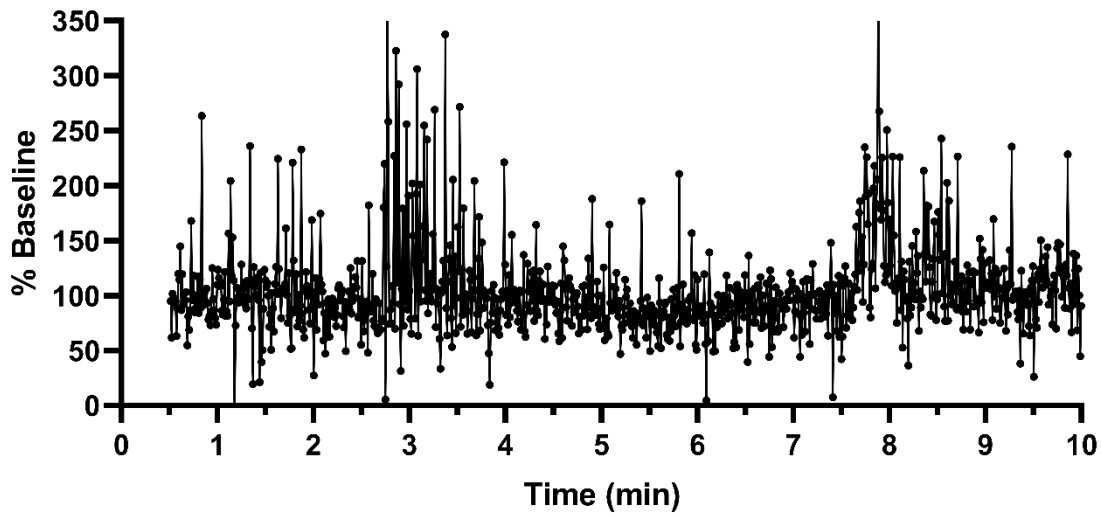
Gln 002 K+



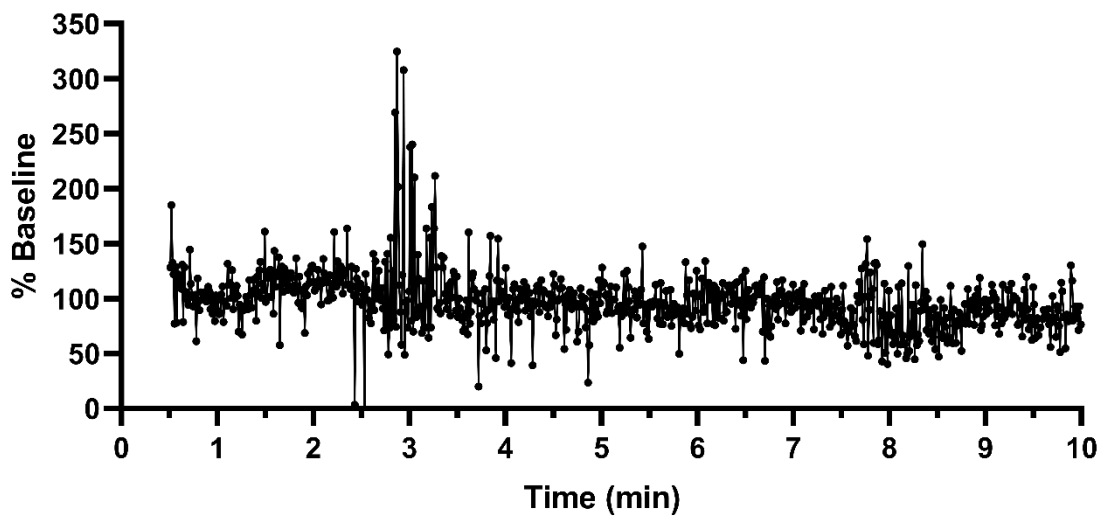
Gln 003 K+



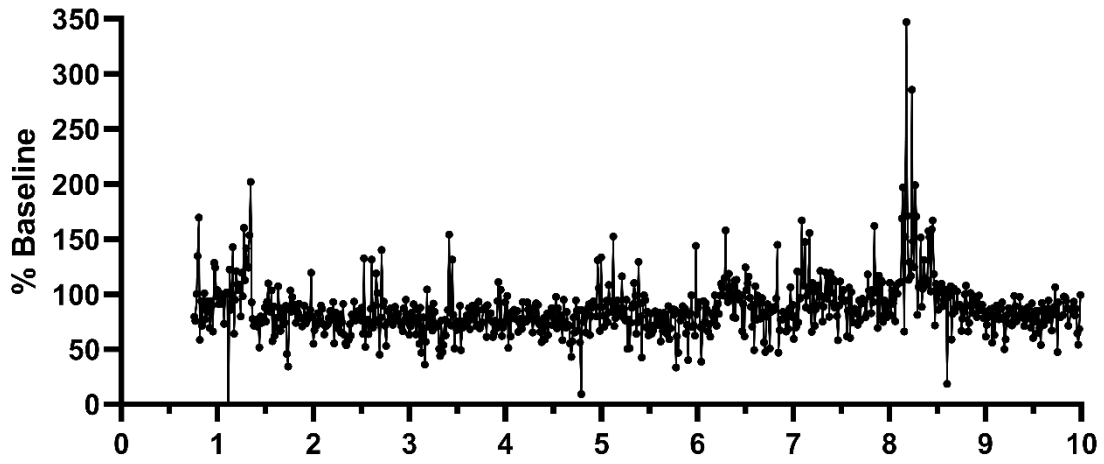
Glu 001 K+



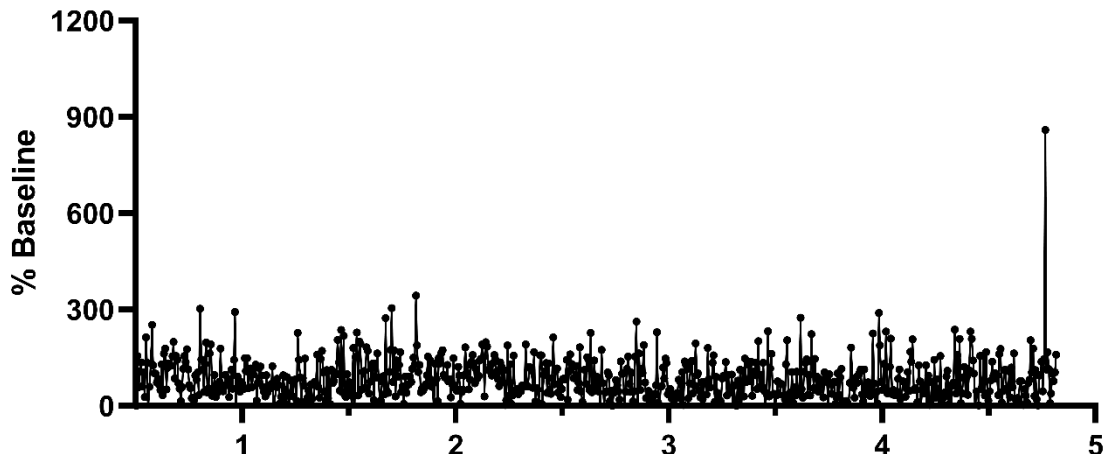
Glu 002 K+



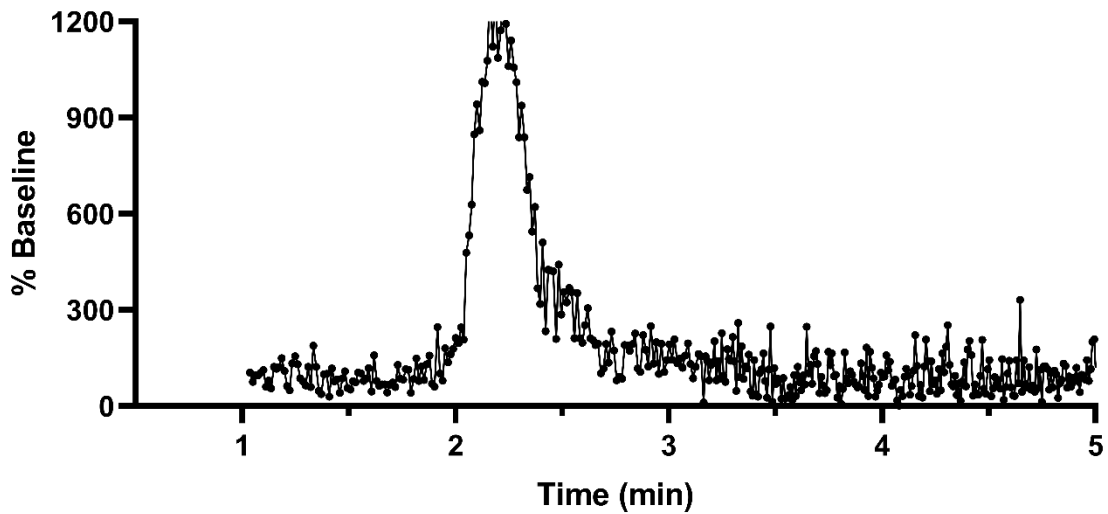
Glu 003 K+



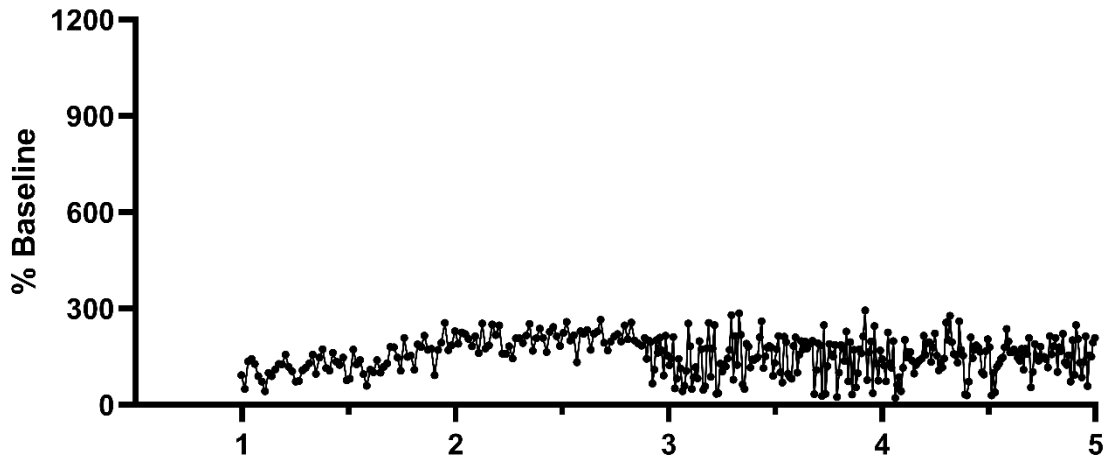
5HT 001 AMPH



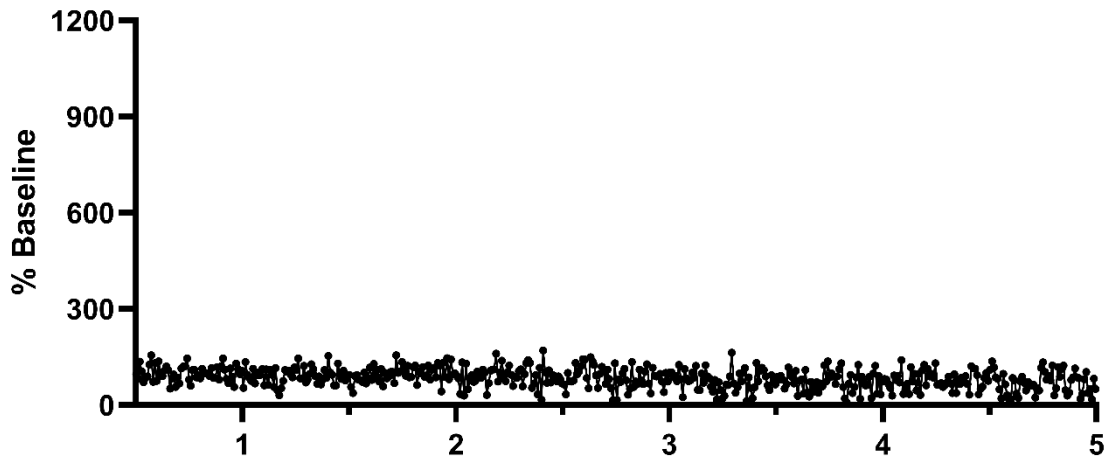
5HT 002 AMPH



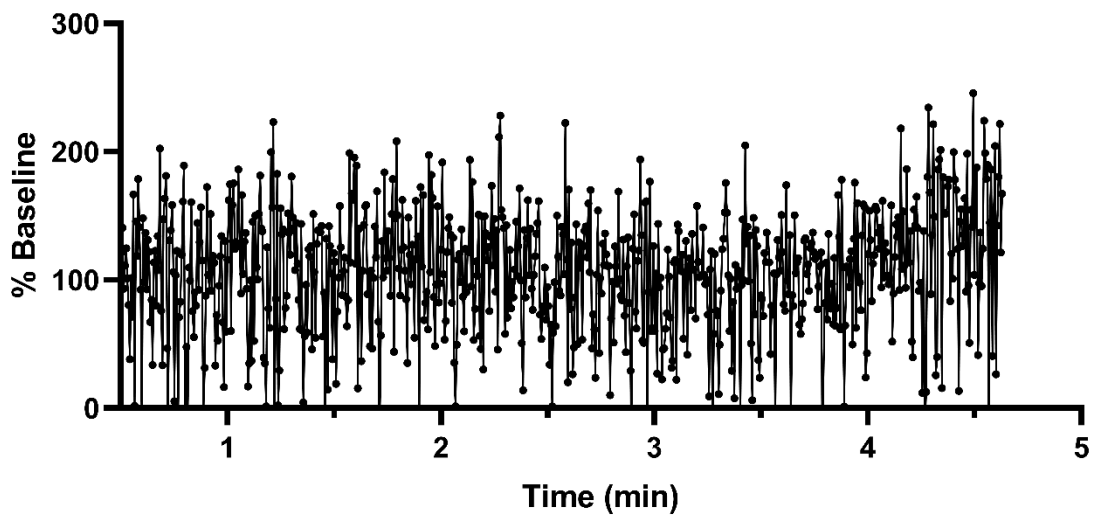
5HT 003 AMPH



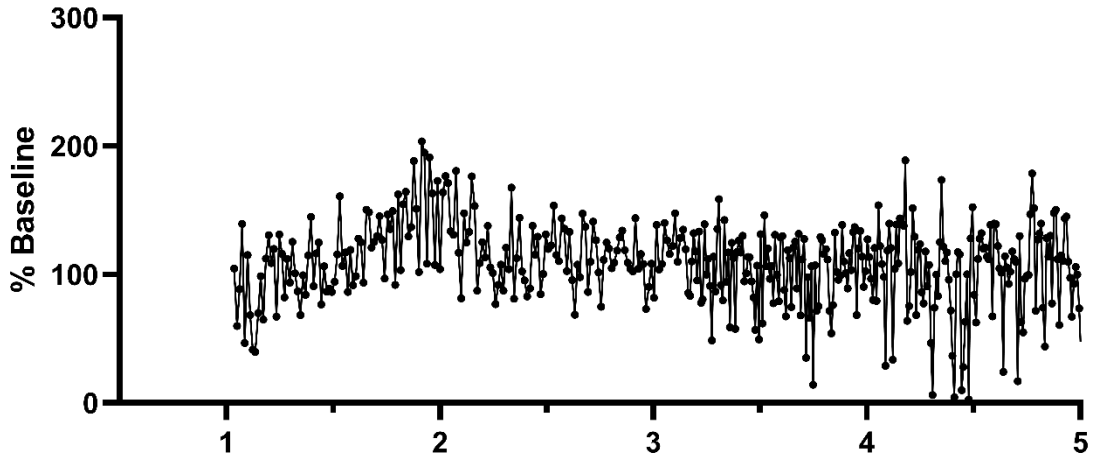
5HT 004 AMPH



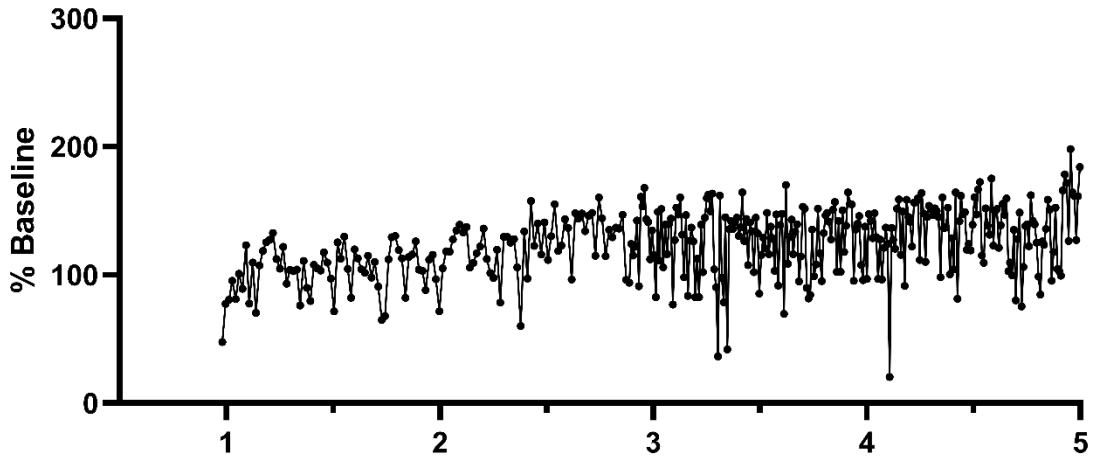
ACh 001 AMPH



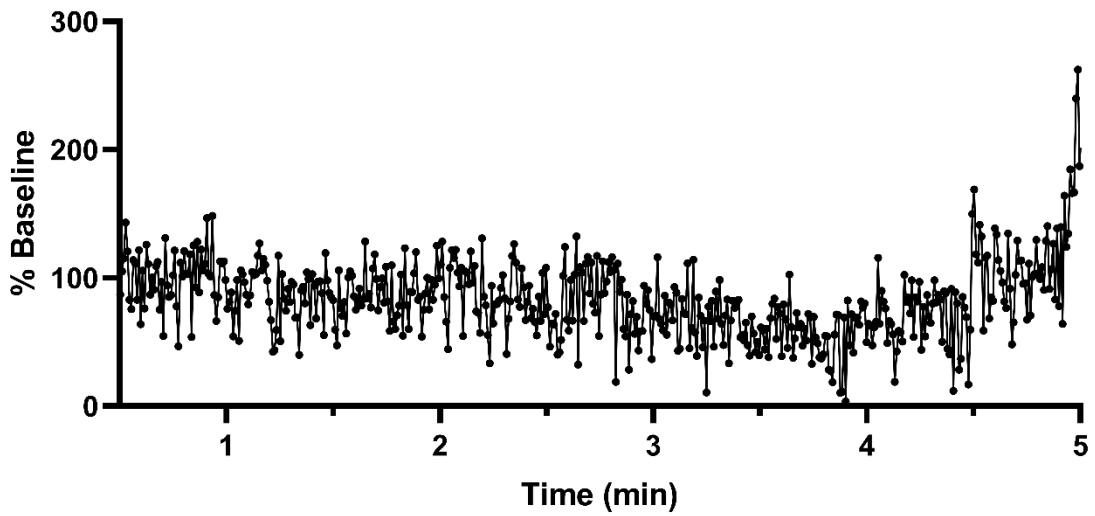
ACh 002 AMPH



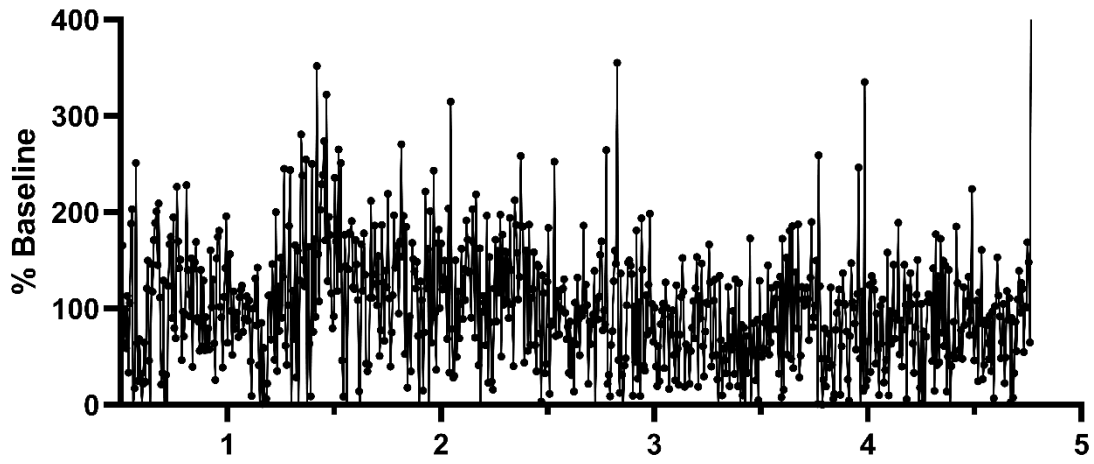
ACh 003 AMPH



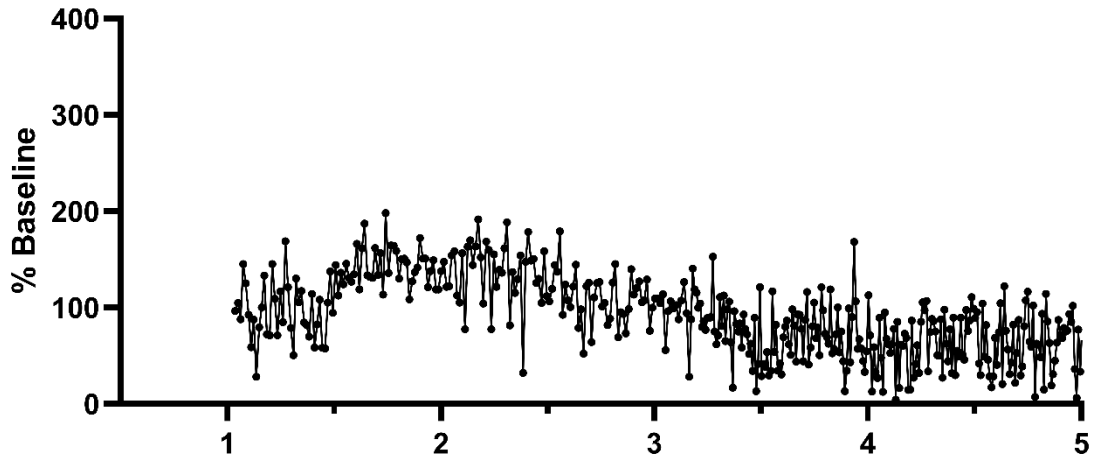
ACh 004 AMPH



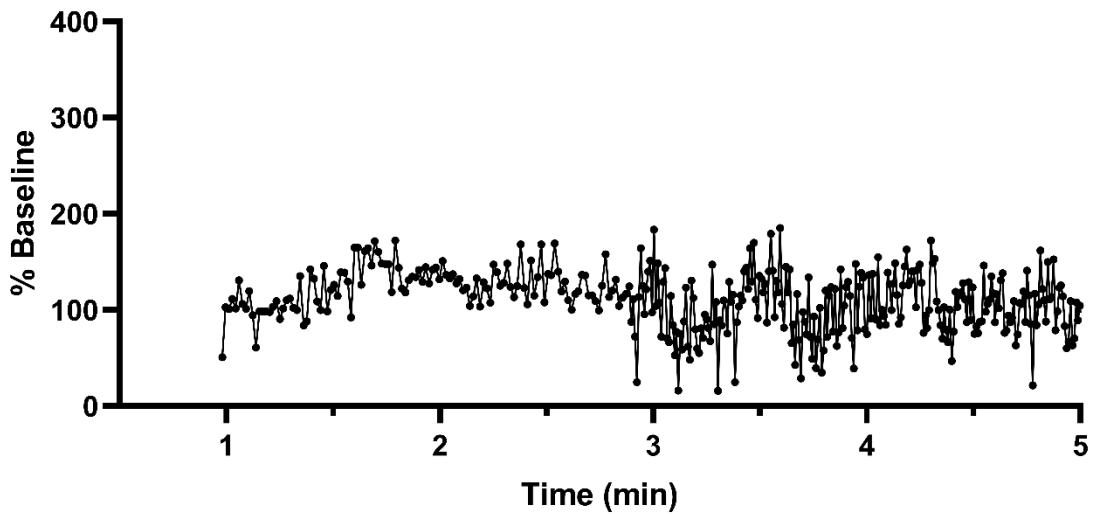
Ado 001 AMPH



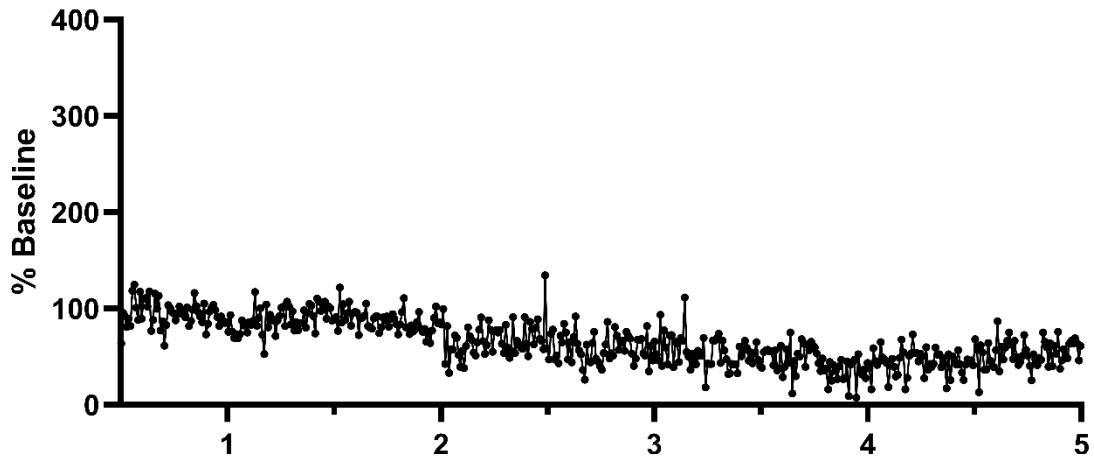
Ado 002 AMPH



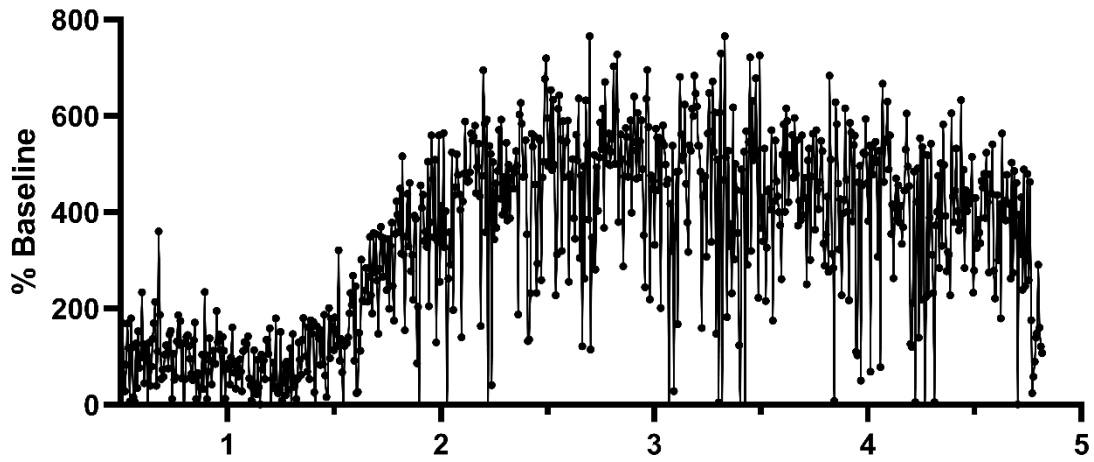
Ado 003 AMPH



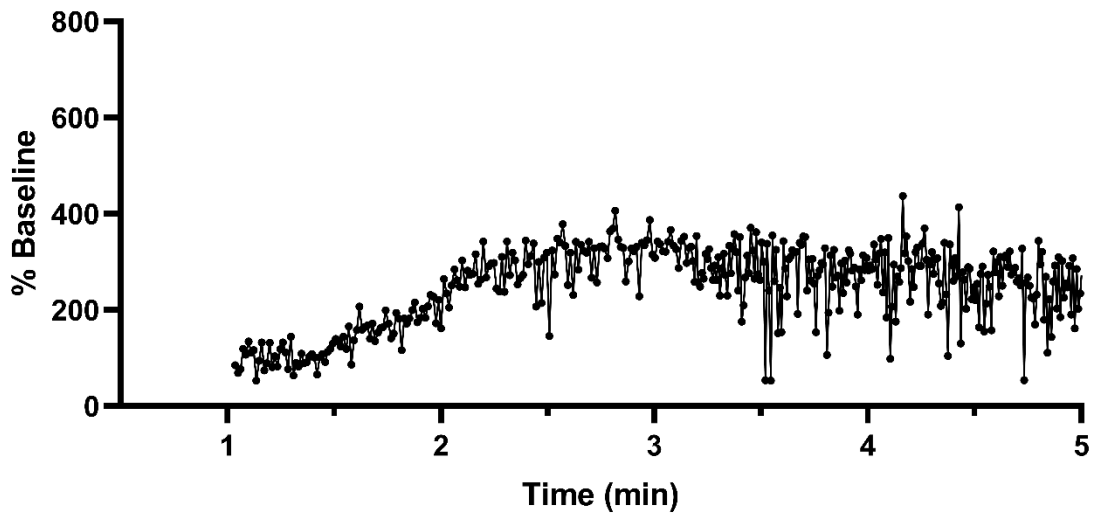
Ado 004 AMPH



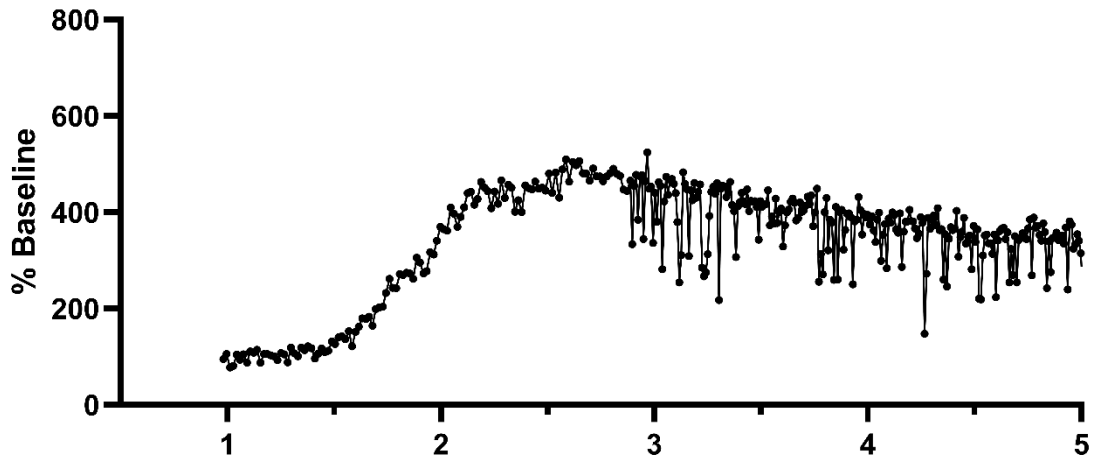
DA 001 AMPH



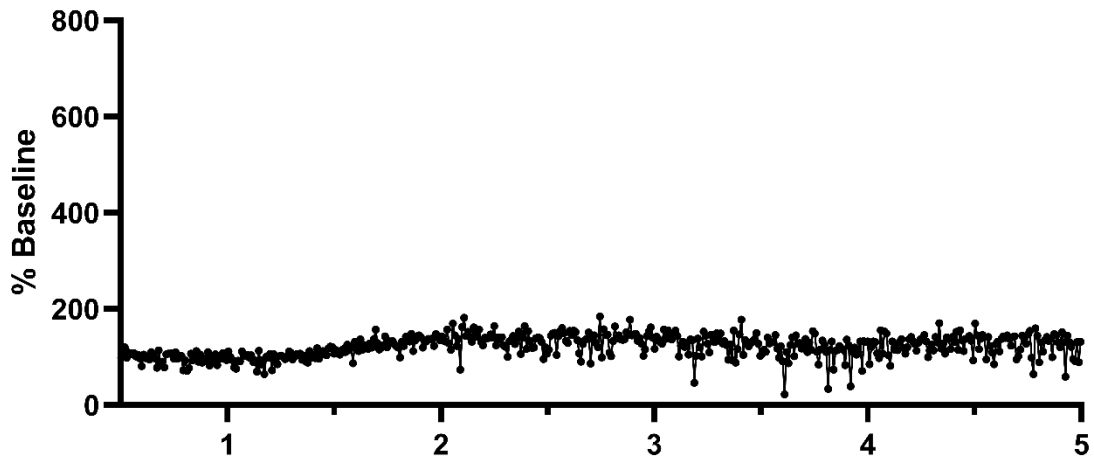
DA 002 AMPH



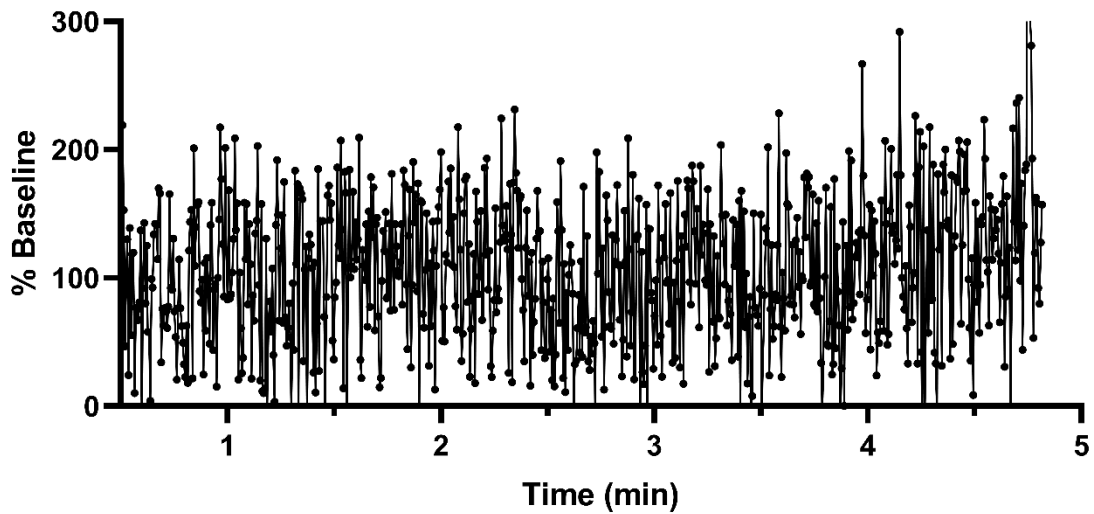
DA 003 AMPH



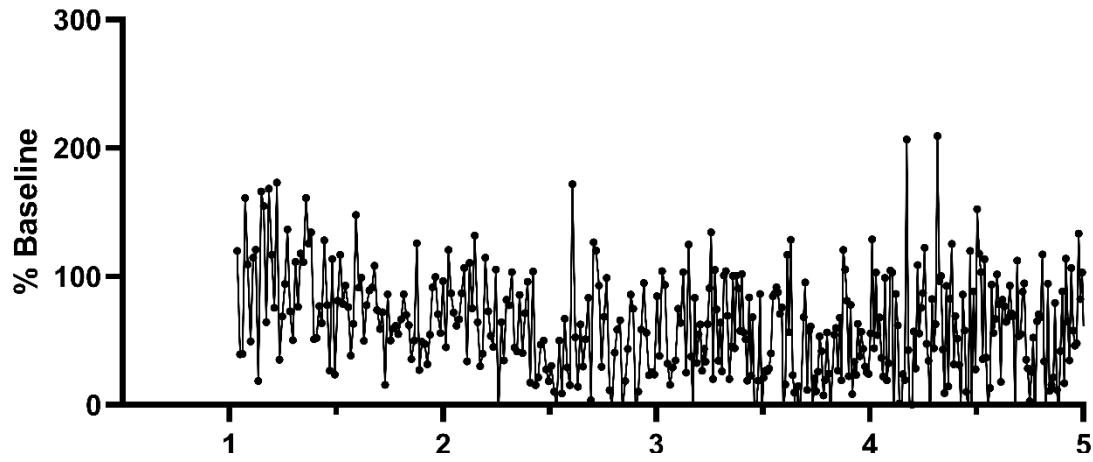
DA 004 AMPH



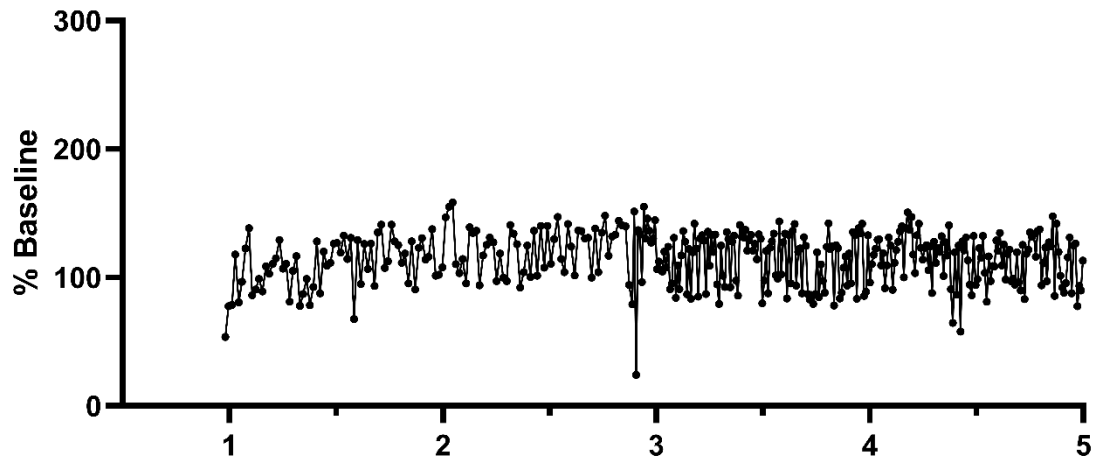
GABA 001 AMPH



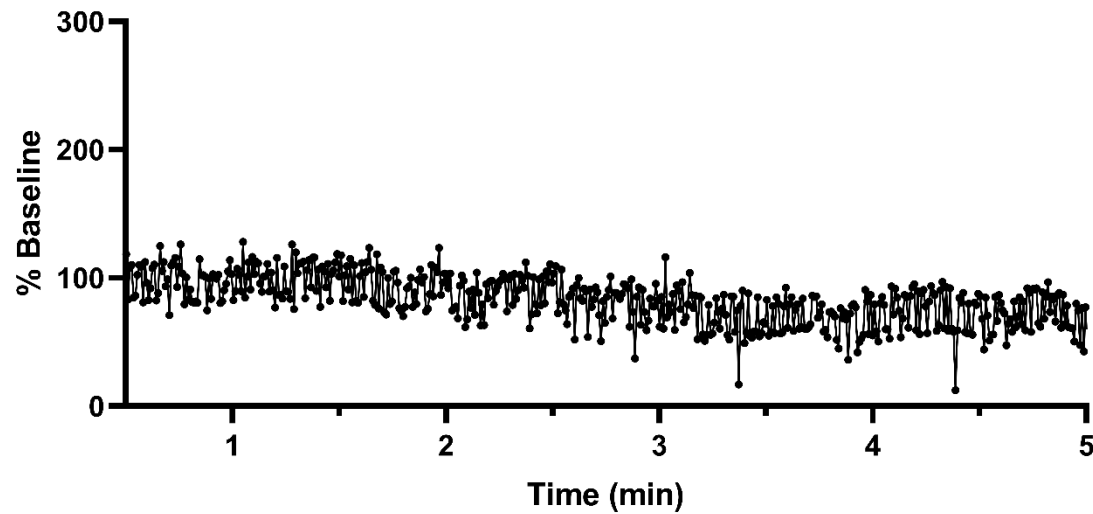
GABA 002 AMPH



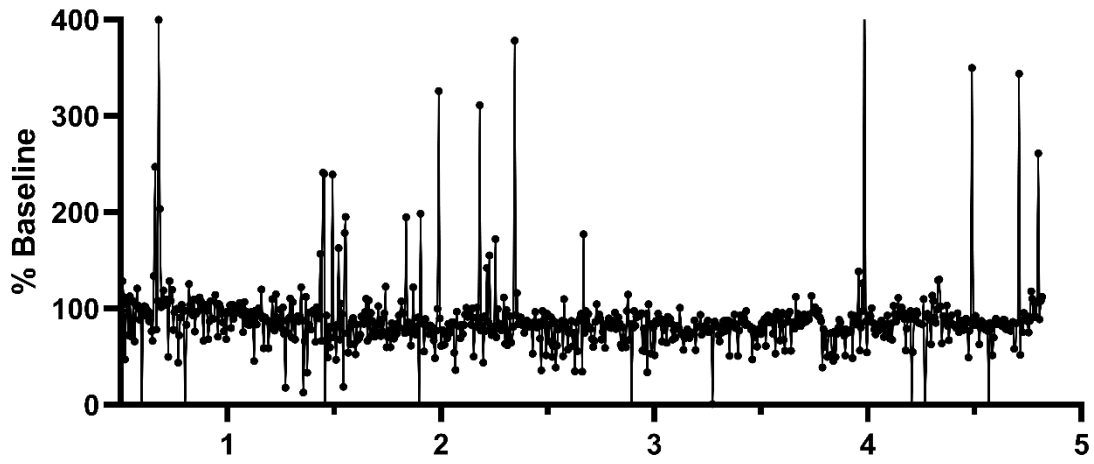
GABA 003 AMPH



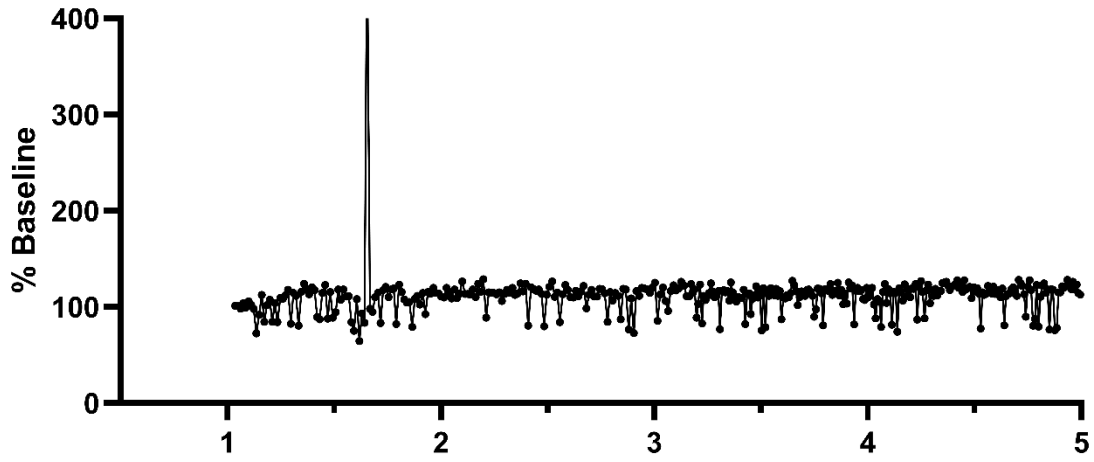
GABA 004 AMPH



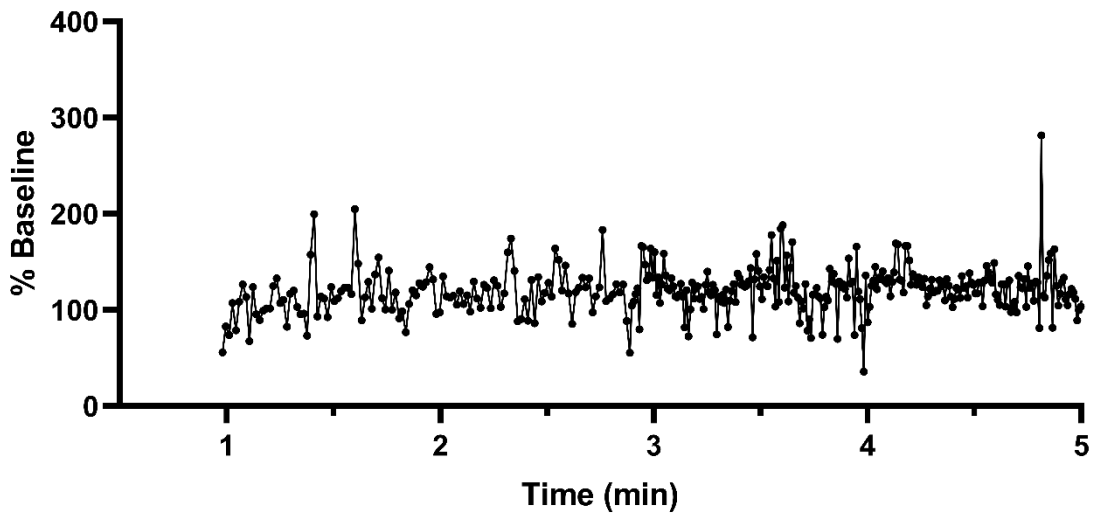
Gln 001 AMPH



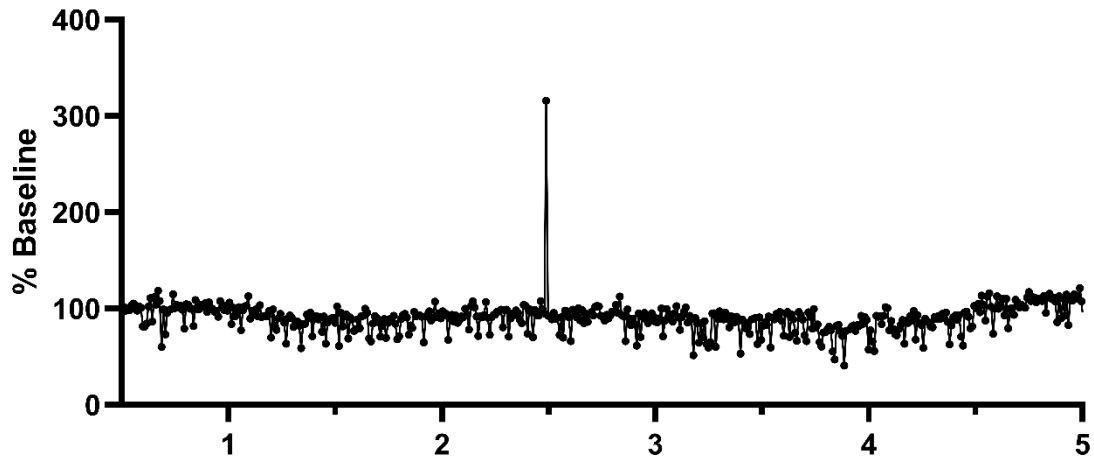
Gln 002 AMPH



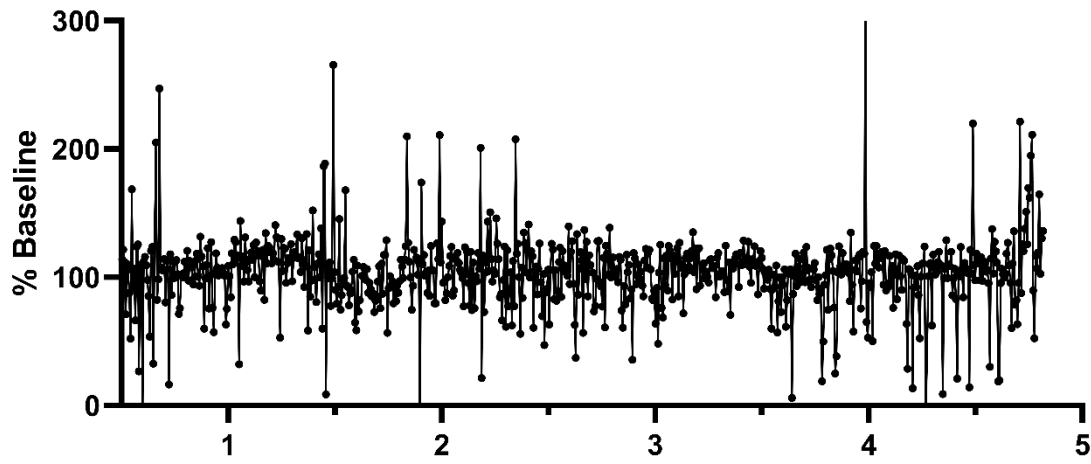
Gln 003 AMPH



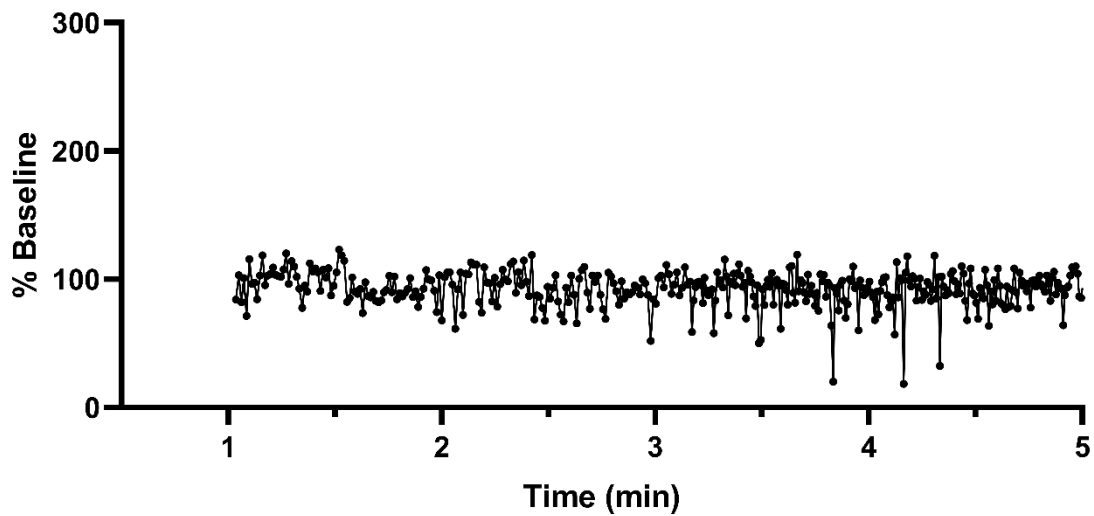
Gln 004 AMPH



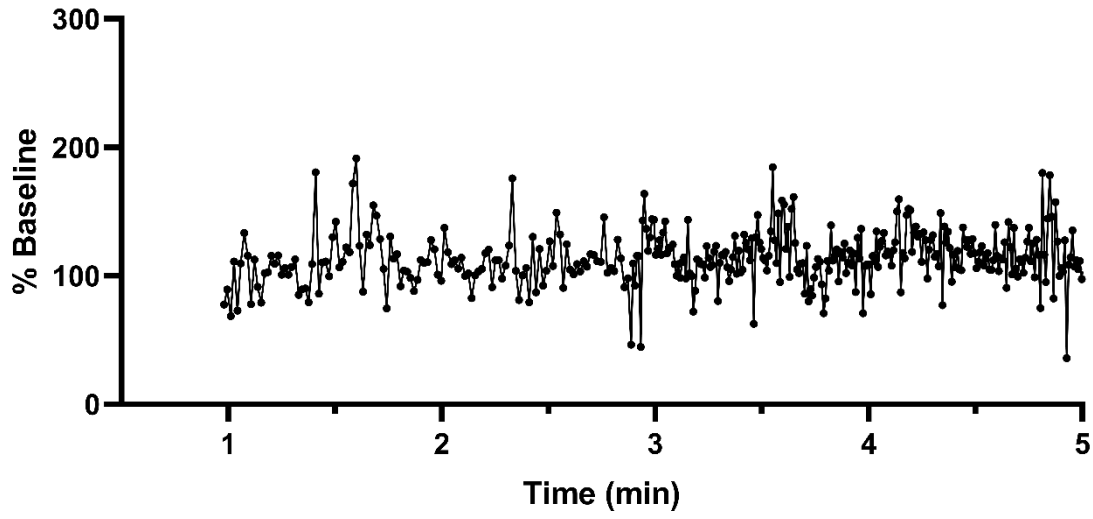
Glu 001 AMPH



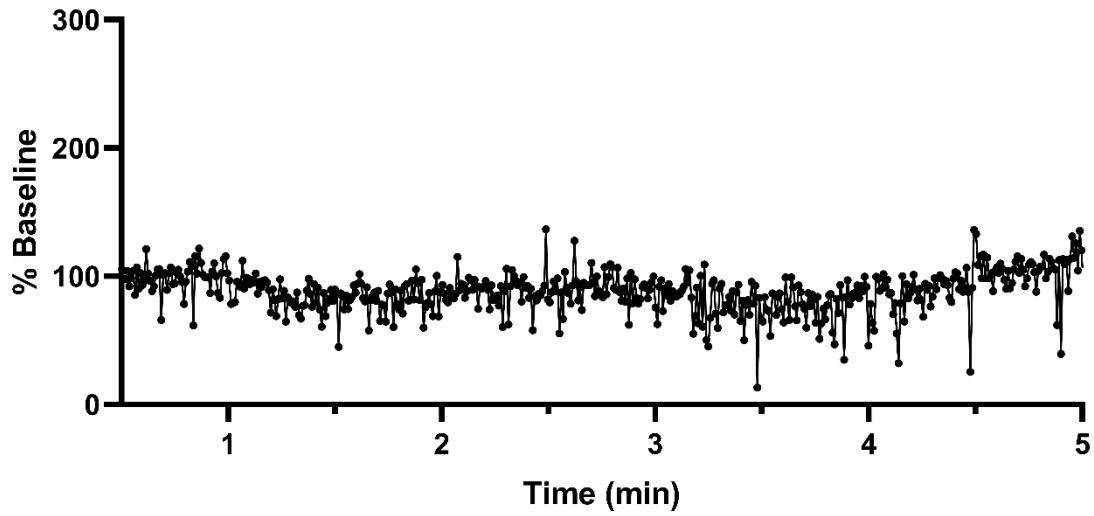
Glu 002 AMPH



Glu 003 AMPH



Glu 004 AMPH



References

- (1) Steyer, D. J.; Kennedy, R. T. High-Throughput Nanoelectrospray Ionization-Mass Spectrometry Analysis of Microfluidic Droplet Samples. *Anal. Chem.* **2019**, *91*, 6645–6651.
- (2) Kempa, E.; Smith, C.; Li, X.; Richardson, K.; Pringle, S.; Barran, P.; Kempa, C.; Kempa, E. E.; Smith, C. A.; Li, X.; et al. Coupling Droplet Microfluidics with Mass Spectrometry for Ultrahigh-Throughput Analysis up to and Above 30Hz. *Chem Rxiv* **2020**.
- (3) Schreiber, S. L. Small Molecules : The Missing Link in the Central Dogma. *Nat. Chem. Biol.* **2005**, *1* (2), 64–66.
- (4) Stockwell, B. R. Exploring Biology with Small Organic Molecules. *Nature* **2004**, *432* (December), 846–854.
- (5) Kouskoumvekaki, I.; Panagiotou, G. Navigating the Human Metabolome for Biomarker Identification and Design of Pharmaceutical Molecules. *J. Biomed. Biotechnol.* **2011**, *2011*, 1–19.
- (6) Zheng, X.; Kang, A.; Dai, C.; Liang, Y.; Xie, T.; Xie, L.; Peng, Y.; Wang, G.; Hao, H. Quantitative Analysis of Neurochemical Panel in Rat Brain and Plasma by Liquid Chromatography – Tandem Mass Spectrometry. *Anal. Chem.* **2012**, *84*, 10044–10051.
- (7) Wenk, M. R. THE EMERGING FIELD OF LIPIDOMICS. *Nature* **2005**, *4*, 594–610.
- (8) Wishart, D. S.; Feunang, Y. D.; Marcu, A.; Guo, A. C.; Liang, K.; Rosa, V.; Sajed, T.; Johnson, D.; Li, C.; Karu, N.; et al. HMDB 4 . 0 : The Human Metabolome Database for 2018. *Nucleic Acids Res.* **2018**, *46*, 608–617.
- (9) Wishart, D. S. Quantitative Metabolomics Using NMR. *Trends Anal. Chem.* **2008**, *27* (3), 228–237.
- (10) Dettmer, K.; Aronov, P. A.; Hammock, B. D. Mass Spectrometry-Based Metabolomics. *Mass Spectrom. Rev.* **2007**, *26*, 51–78.
- (11) Wenk, M. R. Primer Lipidomics : New Tools and Applications. *Cell* **2010**, *143* (6), 888–895.
- (12) Soga, T.; Ohashi, Y.; Ueno, Y.; Naraoka, H.; Tomita, M.; Nishioka, T. Quantitative Metabolome Analysis Using Capillary Electrophoresis Mass Spectrometry. *J. Proteome Res.* **2003**, *2* (5), 488–494.
- (13) Theodoridis, G.; Gika, H. G.; Wilson, I. D. LC-MS-Based Methodology for Global Metabolite Profiling in Metabonomics / Metabolomics. *Trends Anal. Chem.* **2008**, *27* (3), 251–260.

- (14) Monton, M. R. N.; Soga, T. Metabolome Analysis by Capillary Electrophoresis-Mass Spectrometry. *Journal of Chromatography A*. 2007, pp 237–246.
- (15) Jong, G. J. De. CE-MS in Metabolomics. *Electrophoresis* **2009**, *30*, 276–291.
- (16) Ramautar, R.; Shyti, R.; Schoenmaker, B.; De Groote, L.; Derks, R. J. E.; Ferrari, M. D.; Van Den Maagdenberg, A. M. J. M.; Deelder, A. M.; Mayboroda, O. A. Metabolic Profiling of Mouse Cerebrospinal Fluid by Sheathless CE-MS. *Anal. Bioanal. Chem.* **2012**, *404* (10), 2895–2900.
- (17) Blanksby, S. J.; Mitchell, T. W. Advances in Mass Spectrometry for Lipidomics. *Annu. Rev. Anal. Chem.* **2010**, *3*, 433–465.
- (18) Konermann, L.; Ahadi, E.; Rodriguez, A. D.; Vahidi, S. Unraveling the Mechanism of Electrospray Ionization. *Anal. Chem.* **2013**, *85*, 2–9.
- (19) Kebarle, P.; Verkerk, U. H. Electrospray: From Ions in Solution to Ions in the Gas Phase, What We Know Now. *Mass Spectrom. Rev.* **2009**, *28*, 898–917.
- (20) Society, A. C. Using the Electrochemistry Electrospray Ion Source. *Anal. Chem.* **2007**, 5510–5520.
- (21) Daub, C. D.; Cann, N. M. How Are Completely Desolvated Ions Produced in Electrospray Ionization : Insights from Molecular Dynamics Simulations. *Anal. Chem.* **2011**, *83*, 8372–8376.
- (22) Kempa, E. E.; Barran, P. E.; Hollywood, K. A.; Smith, C. A. High Throughput Screening of Complex Biological Samples with Mass Spectrometry – from Bulk Measurements to Single Cell Analysis. *Analyst* **2019**, *144*, 872–891.
- (23) Holland-moritz, D. A.; Wismer, M. K.; Mann, B. F.; Farasat, I.; Devine, P.; Guetschow, E. D.; Mangion, I.; Welch, C. J.; Moore, J. C.; Sun, S.; et al. Mass Activated Droplet Sorting (MADS) Enables High-Throughput Screening of Enzymatic Reactions at Nanoliter Scale Research Articles. *Angew. Chemie* **2019**, *46202*, 4470–4477.
- (24) Song, P.; Hershey, N. D.; Mabrouk, O. S.; Slaney, T. R.; Kennedy, R. T. Mass Spectrometry “Sensor” for in Vivo Acetylcholine Monitoring. *Anal. Chem.* **2012**, *84* (11), 4659–4664.
- (25) King, R.; Bonfiglio, R.; Fernandez-Metzler, C.; Miller-Stein, C.; Olah, T. Mechanistic Investigation of Ionization Suppression in Electrospray Ionization. *J. Am. Soc. Mass Spectrometry* **2000**, *11*, 942–950.
- (26) Tang, K.; Page, J. S.; Smith, R. D. Charge Competition and the Linear Dynamic Range of Detection in Electrospray Ionization Mass Spectrometry. *J. Am. Soc. Mass Spectrometry* **2004**, *15*, 1416–1423.
- (27) Beaudry, F.; Vachon, P. Electrospray Ionization Suppression , a Physical or a Chemical Phenomenon ? *Biomed. Chromatogr.* **2006**, *20*, 200–205.
- (28) Iribarne, J. V.; Thomson, B. A. On the Evaporation of Small Ions from Charged Droplets. *J. Chem. Phys.* **1976**, *64*, 2287–2294.

- (29) El-Faramawy, A.; Siu, K. W. M.; Thomson, B. A. Efficiency of Nano-Electrospray Ionization. *J. Am. Soc. Mass Spectrom.* **2005**, *16* (10), 1702–1707.
- (30) Johnson, J. S.; Rainville, P. D.; Murphy, J. P.; Waters Corporation. *Taking Advantage of Significant Reductions in Ion Suppression Using Ionkey/MS Compared to Standard-Flow LC/MS*; 2014.
- (31) Chen, D.; Han, W.; Su, X.; Li, L.; Li, L. Overcoming Sample Matrix Effect in Quantitative Blood Metabolomics Using Chemical Isotope Labeling Liquid Chromatography Mass Spectrometry. *Anal. Chem.* **2017**, *89* (17), 9424–9431.
- (32) Gong, X.; Xiong, X.; Zhao, Y.; Ye, S.; Fang, X. Boosting the Signal Intensity of Nanoelectrospray Ionization by Using a Polarity-Reversing High-Voltage Strategy. *Anal. Chem.* **2017**, *89* (13), 7009–7016.
- (33) Gibson, G. T. T.; Mugo, S. M.; Oleschuk, R. D. Nanoelectrospray Emitters: Trends and Perspective. *Mass Spectrom. Rev.* **2009**, *28*, 918–936.
- (34) Schmidt, A.; Karas, M.; Du, T. Effect of Different Solution Flow Rates on Analyte Ion Signals in Nano-ESI MS , or: When Does ESI Turn into Nano-ESI? *J. Am. Soc. Mass Spectrometry* **2003**, *14*, 492–500.
- (35) Wilm, M.; Mann, M. Analytical Properties of the Nanoelectrospray Ion Source. *Anal. Chem.* **1996**, *68*, 1–8.
- (36) Juraschek, R.; Dulcks, T.; Karas, M. Nanoelectrospray — More Than Just a Minimized-Flow Electrospray Ion Source. *J. Am. Soc. Mass Spectrometry* **1999**, *10*, 300–308.
- (37) Wilm, M. S.; Mann, M. Electrospray and Taylor-Cone Theory , Dole’s Beam of Macromolecules at Last? *Int. J. Mass Spectrom. Ion Process.* **1994**, *136*, 167–180.
- (38) Lindenburg, P. W.; Haselberg, R.; Rozing, G.; Ramautar, R. Developments in Interfacing Designs for CE–MS: Towards Enabling Tools for Proteomics and Metabolomics. *Chromatographia* **2014**, *78*, 367–377.
- (39) Vas, G.; Vekey, K. Solid-Phase Microextraction : A Powerful Sample Preparation Tool Prior to Mass Spectrometric Analysis. *J. Mass Spectrom.* **2004**, *39*, 233–254.
- (40) Online, V. A.; Bylda, C.; Thiele, R.; Kobold, U.; Volmer, D. A. Recent Advances in Sample Preparation Techniques to Overcome Difficulties Encountered during Quantitative Analysis of Small Molecules from Bio Fluids Using LC-MS / MS. *Analyst* **2014**, *139*, 2265–2276.
- (41) Ding, J.; Neue, U. D. A New Approach to the Effective Preparation of Plasma Samples for Rapid Drug Quantitation Using On-Line Solid Phase Extraction Mass Spectrometry. *Rapid Commun. Mass Spectrom.* **1999**, *13*, 2151–2159.
- (42) Gómez-ríos, G. A.; Pawliszyn, J. Development of Coated Blade Spray Ionization Mass Spectrometry for the Quantitation of Target Analytes Present in Complex Matrices. *Angew. Chemie* **2014**, *53*, 14503–14507.
- (43) Fu, X.; Qin, Y.; Xia, B.; Wang, Y.; Shi, P.; Zhou, Y. High-Sensitivity Detection of

Therapeutic Drugs in Complex Biofluids Using a Packed Ballpoint-Electrospray Ionization Technique. *Anal. Bioanal. Chem.* **2020**.

- (44) Reddy, G. N.; Zagade, A. D.; Sengupta, P. Current Direction and Advances in Analytical Sample Extraction Techniques for Drugs with Special Emphasis on Bioanalysis. *Bioanalysis* **2019**, *11* (04), 313–332.
- (45) Gjelstad, A.; Rasmussen, K. E.; Parmer, M. P.; Pedersen-, S. Parallel Artificial Liquid Membrane Extraction : Micro-Scale Liquid – Liquid – Liquid Extraction in the 96-Well Format. No. 1, 1377–1385.
- (46) Wong, J. M. T.; Malec, P. A.; Mabrouk, O. S.; Ro, J.; Dus, M.; Kennedy, R. T. Benzoyl Chloride Derivatization with Liquid Chromatography-Mass Spectrometry for Targeted Metabolomics of Neurochemicals in Biological Samples. *J. Chromatogr. A* **2016**, *1446*, 78–90.
- (47) Zhou, Y.; Mabrouk, O. S.; Kennedy, R. T. Rapid Preconcentration for LC-MS Assay of Trace Level Neuropeptides. *J. Am. Soc. Mass Spectrometry* **2013**, *24* (11), 1700–1709.
- (48) Breadmore, M. C.; Grochocki, W.; Kalsoom, U.; Phung, S. C.; Rokh, M. T.; Cabot, J. M.; Ghiasvand, A.; Li, F.; Shalan, A. I.; Keyon, A. S. A.; et al. Recent Advances in Enhancing the Sensitivity of Electrophoresis and Electrochromatography in Capillaries and Microchips (2016 – 2018). **2019**, 17–39.
- (49) Breadmore, M. C.; Tubaon, R. M.; Shalan, A. I.; Phung, S. C.; Abdul Keyon, A. S.; Gstoettenmayr, D.; Prapatpong, P.; Alhusban, A. A.; Ranjbar, L.; See, H. H.; et al. Recent Advances in Enhancing the Sensitivity of Electrophoresis and Electrochromatography in Capillaries and Microchips (2012-2014). *Electrophoresis* **2015**, *36* (1), 36–61.
- (50) Kuban, P. Salt Removal from Microliter Sample Volumes by Multiple Phase Microelectromembrane Extractions Across Free Liquid Membranes. *Anal. Chem.* **2017**, *89* (16), 8476–8483.
- (51) Dawod, M.; Breadmore, M. C.; Guijt, R. M.; Haddad, P. R. Electrokinetic Supercharging-Electrospray Ionisation-Mass Spectrometry for Separation and on-Line Preconcentration of Hypolipidaemic Drugs in Water Samples. *Electrophoresis* **2010**, *31* (7), 1184–1193.
- (52) Hirayama, A.; Tomita, M.; Soga, T. Sheathless Capillary Electrophoresis-Mass Spectrometry with a High-Sensitivity Porous Sprayer for Cationic Metabolome Analysis. *Analyst* **2012**, *137* (21), 5026–5033.
- (53) Garcia, J. F.; D. Barceló. An Overview of LGMS Interfacing Systems with Selected Applications. *J. High Resolut. Chromatogr.* **1993**, *16*, 633–641.
- (54) Bruins, A. P. Mechanistic Aspects of Electrospray Ionization. *J. Chromatogr. A* **1998**, *794*, 345–357.
- (55) Tiller, P. R.; Romanyshyn, L. A.; Neue, U. D. Fast LC/MS in the Analysis of Small Molecules. *Anal. Bioanal. Chem.* **2003**, *377*, 788–802.
- (56) Cheng, Y.; Lu, Z.; Neue, U. Ultrafast Liquid Chromatography/Ultraviolet and Liquid Chromatography/Tandem Mass Spectrometric Analysis. *Rapid Commun. Mass Spectrom.*

- 2001**, *15*, 141–151.
- (57) Xu, R. N.; Fan, L.; Rieser, M. J.; El-shourbagy, T. A. Recent Advances in High-Throughput Quantitative Bioanalysis by LC–MS/MS. *J. Pharm. Biomed. Anal.* **2007**, *44*, 342–355.
- (58) Schiavone, N. M.; Sarver, S. A.; Sun, L.; Wojcik, R.; Dovichi, N. J. High Speed Capillary Zone Electrophoresis – Mass Spectrometry via an Electrokinetically Pumped Sheath Flow Interface for Rapid Analysis of Amino Acids and a Protein Digest. *J. Chromatogr. B* **2015**, *991*, 53–58.
- (59) Jacobson, S. C.; Hergenroder, R.; Koutny, L. B.; Ramsey, J. M. High-Speed Separations on a Microchip. *Anal. Chem.* **1994**, *66*, 1114–1118.
- (60) Ouimet, C. M.; Amico, C. I. D.; Kennedy, R. T.; Kennedy, R. T. Droplet Sample Introduction to Microchip Gel and Zone Electrophoresis for Rapid Analysis of Protein-Protein Complexes and Enzymatic Reactions. *Anal. Bioanal. Chem.* **2019**, *411*, 6155–6163.
- (61) He, X.; Chen, Q.; Zhang, Y.; Lin, J. Recent Advances in Microchip-Mass Spectrometry for Biological Analysis. *Trends Anal. Chem.* **2014**, *53*, 84–97.
- (62) Razavi, M.; Frick, L. E.; Lamarr, W. A.; Pope, M. E.; Miller, C. A.; Anderson, N. L.; Pearson, T. W. High-Throughput SISCAPA Quantitation of Peptides from Human Plasma Digests by Ultrafast, Liquid Chromatography-Free Mass Spectrometry. *J. Proteome Res.* **2012**, *11*, 5642–5649.
- (63) Article, E.; Wleklinski, M.; Loren, B. P.; Ferreira, C. R.; Jaman, Z.; Avramova, L.; Sobreira, T. J. P.; Thompson, D. H.; Cooks, R. G. Chemical Science High Throughput Reaction Screening Using Desorption Electrospray Ionization Mass. *Chem. Sci.* **2018**, *9*, 1647–1653.
- (64) Sinclair, I.; Bachman, M.; Addison, D.; Rohman, M.; Murray, D. C.; Davies, G.; Mouchet, E.; Tonge, M. E.; Stearns, R. G.; Ghislain, L.; et al. Acoustic Mist Ionization Platform for Direct and Contactless Ultrahigh-Throughput Mass Spectrometry Analysis of Liquid Samples. *Anal. Chem.* **2019**, *91*, 3790–3794.
- (65) Stone, H. A.; Stroock, A. D.; Ajdari, A. Engineering Flows in Small Devices: Microfluidics Toward a Lab-on-a-Chip. *Annu. Rev. Fluid Mech.* **2004**, *36*, 381–411.
- (66) Stone, H. A.; Kim, S. Microfluidics: Basic Issues, Applications, and Challenges. *An Off. Publ. Am. Inst. Chem. Eng.* **2001**, *47* (6), 1250–1254.
- (67) Teh, S.; Lin, R.; Hung, L.; Lee, A. P. Droplet Microfluidics. *Lab Chip* **2008**, *8*, 198–220.
- (68) Zhu, P.; Wang, L. Passive and Active Droplet Generation with Microfluidics: A Review. *Lab Chip* **2017**, *17*, 34–75.
- (69) Lorenz, R. M.; Edgar, J. S.; Jeffries, G. D. M.; Chiu, D. T. Microfluidic and Optical Systems for the On-Demand Generation and Manipulation of Single Femtoliter-Volume Aqueous Droplets Generation and Manipulation of Single Femtoliter-Volume. *Anal. Chem.* **2006**, *78* (18), 6433–6439.

- (70) Zhu, Y.; Fang, Q. Analytical Detection Techniques for Droplet Microfluidics — A Review. *Anal. Chim. Acta* **2013**, *787*, 24–35.
- (71) Payne, E. M.; Holland-moritz, D. A.; Sun, S.; Kennedy, R. T.; Payne, E.; Holland-moritz, D.; Holland-moritz, D. High-Throughput Screening by Droplet Microfluidics: Perspective into Key Challenges and Future Prospects. *Lab Chip* **2020**, *20*, 2247–2262.
- (72) Shang, L.; Cheng, Y.; Zhao, Y. Emerging Droplet Microfluidics. *Chem. Rev.* **2017**, *117*, 7964–8040.
- (73) Al-hetlani, E. Continuous Magnetic Droplets and Microfluidics: Generation , Manipulation , Synthesis and Detection. *Microchim. Acta* **2019**, *186*, 1–37.
- (74) Jin, S. H.; Jeong, H.-H.; Lee, B.; Lee, S. S.; Lee, S. C. A Programmable Microfluidic Static Droplet Array for Droplet Generation, Transportation, Fusion, Storage, and Retrieval. *Lab Chip* **2015**, *15*, 3677–3686.
- (75) Donovan, B. O.; Eastburn, D. J.; Abate, A. R. Electrode-Free Picoinjection of Microfluidic Drops. *Lab Chip* **2012**, *12*, 4029–4032.
- (76) Abate, A. R.; Hung, T.; Mary, P.; Agresti, J. J.; Weitz, D. A. High-Throughput Injection with Microfluidics Using Picoinjectors. *Proc. Natl. Acad. Sci. United States Am.* **2010**, *107* (45), 19163–19166.
- (77) Mazutis, L.; Griffiths, A. D. Selective Droplet Coalescence Using Microfluidic Systems. *Lab Chip* **2012**, *12*, 1800–1806.
- (78) Ahn, K.; Agresti, J.; Chong, H.; Marquez, M.; Weitz, D. A. Electrocoalescence of Drops Synchronized by Size-Dependent Flow in Microfluidic Channels. *Am. Inst. Phys.* **2006**, *88*, 1–3.
- (79) Song, H.; Chen, D. L.; Ismagilov, R. F. Reactions in Droplets in Microfluidic Channels. *Angew. Chemie* **2006**, *45*, 7336–7356.
- (80) Link, D. R.; Anna, S. L.; Weitz, D. A.; Stone, H. A. Geometrically Mediated Breakup of Drops in Microfluidic Devices. *Phys. Rev. Lett.* **2004**, *92* (5), 1–4.
- (81) Baret, J.; Miller, O. J.; Taly, V.; El-harrak, A.; Frenz, L.; Rick, C.; Samuels, M. L.; Hutchison, J. B.; Agresti, J. J.; Link, D. R.; et al. Fluorescence-Activated Droplet Sorting (FADS): Efficient Microfluidic Cell Sorting Based on Enzymatic Activity. *Lab Chip* **2009**, *9* (13), 1849–1858.
- (82) Ahn, K.; Kerbage, C.; Hunt, T. P.; Westervelt, R. M.; Link, D. R.; Weitz, D. A. Dielectrophoretic Manipulation of Drops for High-Speed Microfluidic Sorting Devices. *Appl. Phys. Lett.* **2010**, *88* (2005), 10–13.
- (83) Gijs, M. A. M. Magnetic Bead Handling On-Chip: New Opportunities for Analytical Applications. *Microfluid Nanofluid* **2004**, *1*, 22–40.
- (84) Xu, C.; Xie, T. Review of Microfluidic Liquid–Liquid Extractors. *Ind. Eng. Chem. Res.* **2017**, *56*, 7593–7622.
- (85) Mary, P.; Studer, V.; Tabeling, P. Microfluidic Droplet-Based Liquid - Liquid Extraction.

- Anal. Chem.* **2008**, *80*, 2680–2687.
- (86) He, Y.; Pei, J.; Srinivasakannan, C.; Li, S.; Peng, J.; Guo, S. Extraction of Samarium Using a Serpentine Y-Junction Microreactor with 2-Ethylhexyl Phosphonic Acid Mono-2-Ethylhexyl. *Hydrometallurgy* **2018**, *179*, 175–180.
- (87) Lee, H.; Xu, L.; Oh, K. W. Droplet-Based Microfluidic Washing Module for Magnetic Particle-Based Assays. *Biomicrofluidics* **2014**, *8*, 1–10.
- (88) Serra, M.; Ferraro, D.; Pereiro, I.; Viovy, J.-L.; Descroix, S. The Power of Solid Supports in Multiphase and Droplet-Based Microfluidics: Towards Clinical Applications. *Lab Chip* **2017**, *17*, 3979–3999.
- (89) Doonan, S. R.; Lin, M.; Bailey, R. C. Droplet CAR-Wash: Continuous Picoliter-Scale Immunocapture and Washing. *Lab Chip* **2019**, *19*, 1589–1598.
- (90) Habib, N.; Avraham-Davidi, I.; Basu, A.; Burks, T.; Shekhar, K.; Hofree, M.; Choudhury, S. R.; Aguet, F.; Gelfand, E.; Ardlie, K.; et al. Massively-Parallel Single Nucleus RNA-Seq with Droplet-Seq. *Nat. Methods* **2018**, *14* (10), 955–958.
- (91) Obexer, R.; Godina, A.; Garrabou, X.; Mittl, P. R. E.; Baker, D.; Grif, A. D.; Hilvert, D. Emergence of a Catalytic Tetrad during Evolution of a Highly Active Artificial Aldolase. *Nat. Chem.* **2017**, *9*, 50–56.
- (92) Prakadan, S. M.; Shalek, A. K.; Weitz, D. A. Scaling by Shringing: Empowering Single-Cell “omics” with Microfluidic Devices. *Nat. Rev. Genet.* **2017**, *18* (6), 345–361.
- (93) Guo, M. T.; Rotem, A.; Heyman, A.; Weitz, D. A. Droplet Microfluidics for High-Throughput Biological Assays. *Lab Chip* **2012**, *12*, 2146–2155.
- (94) Song, H.; Li, H.-W.; Munson, M. S.; Ha, T. G. Van; Ismagilov, R. F. On-Chip Titration of an Anticoagulant Argatroban and Determination of the Clotting Time within Whole Blood or Plasma Using a Plug-Based Microfluidic System. *Anal. Chem.* **2007**, *78* (14), 4839–4849.
- (95) Pekin, D.; Skhiri, Y.; Baret, J.-C.; Corre, D. Le; Mazutis, L.; Salem, C. Ben; Millot, F.; Harrak, A. El; Hutchison, J. B.; Larson, J. W.; et al. Quantitative and Sensitive Detection of Rare Mutations Using Droplet-Based Microfluidics. *Lab Chip* **2011**, *11* (13), 2156–2166.
- (96) Pei, J.; Li, Q.; Lee, M. S.; Valaskovic, G. A.; Kennedy, R. T. Analysis of Samples Stored as Individual Plugs in a Capillary by Electrospray Ionization Mass Spectrometry. *Anal. Chem.* **2009**, *81* (15), 6558–6561.
- (97) Fidalgo, L. M.; Whyte, G.; Ruotolo, B. T.; Benesch, J. L. P.; Stengel, F.; Abell, C.; Robinson, C. V.; Huck, W. T. S. Coupling Microdroplet Microreactors with Mass Spectrometry: Reading the Contents of Single Droplets Online. *Angew. Chemie* **2009**, *48*, 3665–3668.
- (98) Ngernsutivorakul, T.; Steyer, D.; Valenta, A. C.; Kennedy, R. T. In Vivo Chemical Monitoring at High Spatiotemporal Resolution Using Microfabricated Sampling Probes and Droplet-Based Microfluidics Coupled to Mass Spectrometry. *Anal. Chem.* **2018**.

- (99) Sun, S.; Slaney, T. R.; Kennedy, R. T. Label Free Screening of Enzyme Inhibitors at Femtomole Scale Using Segmented Flow Electrospray Ionization Mass Spectrometry. *Anal. Chem.* **2012**, *84* (13), 5794–5800.
- (100) Faserl, K.; Sarg, B.; Sola, L.; Lindner, H. H. Enhancing Proteomic Throughput in Capillary Electrophoresis–Mass Spectrometry by Sequential Sample Injection. *Proteomics* **2017**, *17* (22), 1–5.
- (101) Mateos-Vivas, M.; Domínguez-Álvarez, J.; Rodríguez-Gonzalo, E.; Carabias-Martínez, R. Capillary Electrophoresis Coupled to Mass Spectrometry Employing Hexafluoro-2-Propanol for the Determination of Nucleosides and Nucleotide Mono-, Di- and Tri-Phosphates in Baby Foods. *Food Chem.* **2017**, *233*, 38–44.
- (102) Maráková, K.; Piešťanský, J.; Zelinková, Z.; Mikuš, P. Capillary Electrophoresis Hyphenated with Mass Spectrometry for Determination of Inflammatory Bowel Disease Drugs in Clinical Urine Samples. *Molecules* **2017**, *22* (11), 1973.
- (103) Faserl, K.; Sarg, B.; Gruber, P.; Lindner, H. H. Investigating Capillary Electrophoresis–Mass Spectrometry for the Analysis of Common Post-Translational Modifications. *Electrophoresis* **2018**, 1–8.
- (104) Hirayama, A.; Abe, H.; Yamaguchi, N.; Tabata, S.; Tomita, M.; Soga, T. Development of a Sheathless CE-ESI-MS Interface. *Electrophoresis* **2018**, 1–8.
- (105) Slampova, A.; Mala, Z.; Gebauer, P. Recent Progress of Sample Stacking in Capillary Electrophoresis (2016 – 2018). *Electrophoresis* **2019**, *40*, 40–54.
- (106) Kim, J.; Choi, K.; Chung, D. S. Synergistic Coupling of In-Line Single-Drop Microextraction and on-Line Large-Volume Sample Stacking for Capillary Electrophoresis / Mass Spectrometry. *Anal. Bioanal. Chem.* **2019**, No. 411, 1067–1073.
- (107) Wuethrich, A.; Haddad, P. R.; Quirino, J. P. Field-Enhanced Sample Injection Micelle-to-Solvent Stacking Capillary Zone Electrophoresis – Electrospray Ionization Mass Spectrometry of Antibiotics in Seawater after Solid-Phase Extraction. *Electrophoresis* **2016**, No. 37, 1139–1142.
- (108) Zhu, G.; Sun, L.; Yan, X.; Dovichi, N. J. Bottom-Up Proteomics of Escherichia Coli Using Dynamic PH Junction Preconcentration and Capillary Zone Electrophoresis–Electrospray Ionization–Tandem Mass Spectrometry. *Anal. Chem.* **2014**, No. 86, 6331–6336.
- (109) Pu, F.; Zhang, W.; Bateman, K. P.; Liu, Y.; Helmy, R. Using Miniature MS System with Automatic Blood Sampler for Preclinical Pharmacokinetics Study. **2017**, *9*, 1633–1641.
- (110) Lian, D. S.; Zhao, S. J.; Li, J.; Li, B. L. Progress in Stacking Techniques Based on Field Amplification of Capillary Electrophoresis. *Analytical and Bioanalytical Chemistry*. 2014, pp 6129–6150.
- (111) Dawod, M.; Chung, D. S. High-Sensitivity Capillary and Microchip Electrophoresis Using Electrokinetic Supercharging. *J. Sep. Sci.* **2011**, *34* (20), 2790–2799.
- (112) Hirokawa, T.; Okamoto, H.; Gaš, B. High-Sensitive Capillary Zone Electrophoresis

- Analysis by Electrokinetic Injection with Transient Isotachophoretic Preconcentration: Electrokinetic Supercharging. *Electrophoresis* **2003**, *24* (3), 498–504.
- (113) Xu, Z.; Kawahito, K.; Ye, X.; Timerbaev, A. R.; Hirokawa, T. Electrokinetic Supercharging with a System-Induced Terminator and an Optimized Capillary versus Electrode Configuration for Parts-per-Trillion Detection of Rare-Earth Elements in CZE. *Electrophoresis* **2011**, *32* (10), 1195–1200.
- (114) Chui, M. Q.; Thang, L. Y.; See, H. H. Integration of the Free Liquid Membrane into Electrokinetic Supercharging – Capillary Electrophoresis for the Determination of Cationic Herbicides in Environmental Water Samples. *J. Chromatogr. A* **2017**, *1481*, 145–151.
- (115) Xu, Z.; Ando, T.; Nishine, T.; Arai, A.; Hirokawa, T. Electrokinetic Supercharging Preconcentration and Microchip Gel Electrophoretic Separation of Sodium Dodecyl Sulfate-Protein Complexes. *Electrophoresis* **2003**, *24* (21), 3821–3827.
- (116) Xu, Z.; Nishine, T.; Arai, A.; Hirokawa, T. Performance of Electrokinetic Supercharging for High-Sensitivity Detection of DNA Fragments in Chip Gel Electrophoresis. *Electrophoresis* **2004**, *25* (21–22), 3875–3881.
- (117) Busnel, J. M.; Lion, N.; Girault, H. H. Electrokinetic Supercharging for Highly Efficient Peptide Preconcentration in Capillary Zone Electrophoresis. *Electrophoresis* **2008**, *29* (7), 1565–1572.
- (118) Botello, I.; Borrull, F.; Calull, M.; Aguilar, C. Electrokinetic Supercharging in CE for the Separation and Preconcentration of Barbiturate Drugs in Urine Samples. *J. Sep. Sci.* **2013**, *36* (3), 524–531.
- (119) Nyssen, L.; Fillet, M.; Cavalier, E.; Servais, A. Highly Sensitive and Selective Separation of Intact Parathyroid Hormone and Variants by Sheathless CE-ESI-MS/MS. *Electrophoresis* **2019**, *40*, 1550–1557.
- (120) Kwon, J. Y.; Chang, S. B.; Jang, Y. O.; Dawod, M.; Chung, D. S. Highly Sensitive Analysis of Catecholamines by Counter-Flow Electrokinetic Supercharging in the Constant Voltage Mode. *J. Sep. Sci.* **2013**, *36* (12), 1973–1979.
- (121) Wang, W.; Ju, F.; Ran, Y.; Zhang, H.; Chen, X. Detection of Biogenic Amines in C57BL/6 Mice Brain by Capillary Electrophoresis Electrokinetic Supercharging. *Analyst* **2016**, *141* (3), 956–962.
- (122) Simpson, S. L.; Quirino, J. P.; Terabe, S. On-Line Sample Preconcentration in Capillary Electrophoresis. *J. Chromatogr. A* **2007**, *1184* (1–2), 504–541.
- (123) Mala, Z.; Gebauer, P. Recent Progress in Analytical Capillary Isotachophoresis. *Electrophoresis* **2019**, *40*, 55–64.
- (124) Krivankova, L.; Foret, F.; Gebauer, P.; Bocek, P. Selection of Electrolyte Systems in Isotachophoresis. *J. Chromatogr.* **1987**, *390*, 3–16.
- (125) Guan, Q.; Henry, C. S. Improving MCE with Electrochemical Detection Using a Bubble Cell and Sample Stacking Techniques. *Electrophoresis* **2009**, *30* (19), 3339–3346.

- (126) Song, P.; Mabrouk, O. S.; Hershey, N. D.; Kennedy, R. T. In Vivo Neurochemical Monitoring Using Benzoyl Chloride Derivatization and Liquid Chromatography – Mass Spectrometry. *Anal. Chem.* **2011**, *84*, 412–419.
- (127) Miki, K.; Sudo, A. Effect of Urine PH, Storage Time, and Temperature on Stability of Catecholamines, Cortisol, and Creatinine. *Clin. Chem.* **1998**, *44* (8), 1759–1762.
- (128) Johnson, A. R.; Banks, M. L.; Sekkey, D. E.; Stevens Negus, S. Amphetamine Maintenance Differentially Modulates Effects of Cocaine, Methylenedioxypyrovalerone (MDPV), and Methamphetamine on Intracranial Self-Stimulation and Nucleus Accumbens Dopamine in Rats. *Neuropsychopharmacology* **2018**, *43*, 1753–1762.
- (129) Pagkalos, I.; Rogers, M. L.; Boutelle, M. G.; Drakakis, E. M. A High-Performance Application Specific Integrated Circuit for Electrical and Neurochemical Traumatic Brain Injury Monitoring. *ChemPhysChem* **2018**, *19*, 1215–1225.
- (130) Krishna, G.; Beitchman, J. A.; Bromberg, C. E.; Thomas, T. C. Approaches to Monitor Circuit Disruption after Traumatic Brain Injury : Frontiers in Preclinical Research. *Int. J. Mol. Sci.* **2020**, *21* (588), 1–27.
- (131) Lei, H.; Dirren, E.; Poitry-yamate, C.; Schneider, B. L.; Gruetter, R.; Aebischer, P. Evolution of the Neurochemical Profiles in the G93A-SOD1 Mouse Model of Amyotrophic Lateral Sclerosis. *J. Cereb. Blood Flow Metab.* **2019**, *39* (7), 1283–1298.
- (132) Mirzaei, M.; Sawan, M. Microelectronics-Based Biosensors Dedicated to the Detection of Neurotransmitters: A Review. *Sensors*. 2014, pp 17981–18008.
- (133) Christopher J. Watson, B. Jill Venton, R. T. K. In Vivo Measurements of Neurotransmitters by Microdialysis Sampling. *Anal. Chem.* **2006**, 1391–1399.
- (134) Perry, M.; Li, Q.; Kennedy, R. T. Review of Recent Advances in Analytical Techniques for the Determination of Neurotransmitters. *Analytica Chimica Acta*. 2009, pp 1–22.
- (135) Su, C.; Sun, Y.; Tzeng, S.; Yang, C.; Wang, C.-Y.; Yang, M.-H. In Vivo Monitoring of the Transfer Kinetics of Trace Elements in Animal Brains with Hyphenated Inductively Coupled Plasma Mass Spectrometry Techniques. *Mass Spectrom. Rev.* **2010**, *29*.
- (136) Xu, C.; Wu, F.; Yu, P.; Mao, L. In Vivo Electrochemical Sensors for Neurochemicals: Recent Update. *ACS Sensors* **2019**, *4*, 3102–3118.
- (137) Zestos, A. G.; Kennedy, R. T. Microdialysis Coupled with LC-MS/MS for In Vivo Neurochemical Monitoring. *AAPS J.* **2017**, *19* (5), 1284–1293.
- (138) Robinson, D. L.; Hermans, A.; Seipel, A. T.; Wightman, R. M. Monitoring Rapid Chemical Communication in the Brain. *Chem. Rev.* **2008**, *108* (7), 2554–2584.
- (139) Ngo, K. T.; Varner, E. L.; Michael, A. C.; Weber, S. G. Monitoring Dopamine Responses to Potassium Ion and Nomifensine by in Vivo Microdialysis with Online Liquid Chromatography at One-Minute Resolution. *ACS Chem. Neurosci.* **2017**, *8*, 329–338.
- (140) Lapainis, T.; Sweedler, J. V. Contributions of Capillary Electrophoresis to Neuroscience. *J Chromatogr A* **2008**, *1184*, 144–158.

- (141) Hogerton, A. L.; Bowser, M. T. Monitoring Neurochemical Release from Astrocytes Using in Vitro Microdialysis Coupled with High-Speed Capillary Electrophoresis. *Anal. Chem.* **2013**, *85*, 9070–9077.
- (142) Wang, M.; Roman, G. T.; Schultz, K.; Jennings, C.; Kennedy, R. T. Improved Temporal Resolution for in Vivo Microdialysis by Using Segmented Flow. *Anal. Chem.* **2008**, *80* (14), 5607–5615.
- (143) Petit-Pierre, G.; Colin, P.; Laurer, E.; Déglon, J.; Bertsch, A.; Thomas, A.; Schneider, B. L.; Renaud, P. In Vivo Neurochemical Measurements in Cerebral Tissues Using a Droplet-Based Monitoring System. *Nat. Commun.* **2017**, *8* (1).
- (144) Sulzer, D.; Sonders, M. S.; Poulsen, N. W.; Galli, A. Mechanisms of Neurotransmitter Release by Amphetamines : A Review. *Prog. Neurobiol.* **2005**, *75*, 406–433.
- (145) Hommerson, P.; Khan, A. M.; Jong, G. J. De; Somsen, G. W. Comparison of Atmospheric Pressure Photoionization and ESI for CZE-MS of Drugs. *Electrophoresis* **2007**, *28*, 1444–1453.
- (146) Gowers, S. A. N.; Hamaoui, K.; Cunnea, P.; Anastasova, S.; Curto, V. F.; Vadgama, P.; Yang, G.; Papalois, V.; Drakakis, E. M.; Fotopoulou, C.; et al. High Temporal Resolution Delayed Analysis of Clinical Microdialysate Steams. *Analyst* **2018**, *143*, 715–724.
- (147) Frey, O.; Holtzman, T.; McNamara, R. M.; Theobald, D. E. H.; van der Wal, P. D.; de Rooij, N. F.; Koudelka-Hep, M. Simultaneous Neurochemical Stimulation and Recording Using an Assembly of Biosensor Silicon Microprobes and SU-8 Microinjectors. *Sensors Actuators B Chem.* **2011**, *154* (2), 96–105.
- (148) Shimizu, S.; Akiyama, T.; Kawada, T.; Sata, Y.; Kamiya, A.; Shishido, T.; Sugimachi, M. Sodium Ion Transport Participates in Non-Neuronal Acetylcholine Release in the Renal Cortex of Anesthetized Rabbits. *J. Physiol. Sci.* **2017**, *67* (5), 587–593.
- (149) Yoshitake, T.; Fujino, K.; Kehr, J.; Ishida, J.; Nohta, H.; Yamaguchi, M. Simultaneous Determination of Norepinephrine, Serotonin, and 5-Hydroxyindole-3-Acetic Acid in Microdialysis Samples from Rat Brain by Microbore Column Liquid Chromatography with Fluorescence Detection Following Derivatization with Benzylamine. *Anal. Biochem.* **2003**, *312*, 125–133.
- (150) Kuczenski, R.; Segal, D. S. Concomitant Characterization of Behavioral Neurotransmitter Response to Amphetamine Microdialysis and Striatal Using in Viva. *J. Neurosci.* **1988**, *9* (6), 2051–2065.
- (151) Kuczenski, R.; Segal, D. S. Effects of Methylphenidate on Extracellular Dopamine, Serotonin, and Norepinephrine: Comparison with Amphetamine. *J. Neurochem.* **1997**, *68*, 2032–2037.
- (152) Parsons, L. H.; Justice, J. B. Serotonin and Dopamine Sensitization in the Nucleus Accumbens, Ventral Tegmental Area, and Dorsal Raphe Nucleus Following Repeated Cocaine Administration. *J. Neurochem.* **1993**, *61*, 1611–1619.
- (153) Faraji, M.; Yamini, Y.; Gholami, M. Recent Advances and Trends in Applications of Solid - Phase Extraction Techniques in Food and Environmental Analysis.

Chromatographia **2019**, 82 (8), 1207–1249.

- (154) Farajzadeh, M. A.; Khoshmaram, L.; Sheykhizadeh, S. A Review on Application of Microextraction Techniques for Analysis of Chemical Compounds and Metal Ions in Foodstuffs. *Anal. Bioanal. Chem. Res.* **2014**, 1 (1), 1–19.
- (155) Buszewski, B.; Szultka, M. Past, Present, and Future of Solid Phase Extraction: A Review. *Crit. Rev. Anal. Chem.* **2012**, 42 (3), 198–213.
- (156) Jeannot, M. A.; Cantwell, F. F. Solvent Microextraction into a Single Drop. *Anal. Chem.* **1996**, 68 (13), 2236–2240.
- (157) Belinato, R.; Dias, F. F. G.; Caliman, J. D.; Augusto, F. Opportunities for Green Microextractions in Comprehensive Two-Dimensional Gas Chromatography / Mass Spectrometry-Based Metabolomics: A Review. *J. Anal. Chim. Acta* **2018**, 1040, 1–18.
- (158) Pawliszyn, J.; Pedersen-bjergaard, S. Analytical Microextraction: Current Status. *J. Chromatogr. Sci.* **2006**, 44, 291–307.
- (159) Shen, G.; Lee, H. K. Hollow Fiber-Protected Liquid-Phase Microextraction of Triazine Herbicides. *Anal. Chem.* **2002**, 74 (3), 2650–2656.
- (160) Breisig, H.; Schmidt, M.; Wolff, H.; Jupke, A.; Wessling, M. Droplet-Based Liquid–Liquid Extraction inside a Porous Capillary. *Chem. Eng. J.* **2017**, 307, 143–149.
- (161) Ide, A. H.; Nogueira, J. M. F. Hollow Fiber Microextraction: A New Hybrid Microextraction Technique for Trace Analysis. *Anal. Bioanal. Chem.* **2018**, 410, 2911–2920.
- (162) He, Y.; Lee, H. K. Liquid-Phase Microextraction in a Single Drop of Organic Solvent by Using a Conventional Microsyringe. *Anal. Chem.* **1997**, 69 (22), 4634–4640.
- (163) Jung, M.; Shin, Y.; Oh, S.; Kim, N.; Kim, K.; Lee, D. Headspace Hanging Drop Liquid Phase Microextraction and Gas Chromatography-Mass Spectrometry for the Analysis of Flavors from Clove Buds. *Bull. Korean Chem. Soc.* **2006**, 27 (2), 231–236.
- (164) Pedersen-Bjergaard, S.; Rasmussen, K. E. Liquid - Liquid - Liquid Microextraction for Sample Preparation of Biological Fluids Prior to Capillary Electrophoresis. *Anal. Chem.* **1999**, 71 (14), 2650–2656.
- (165) Ren, Y.; Zhang, W.; Lin, Z.; Bushman, L. R.; Anderson, P. L. In-Capillary Microextraction for Direct Mass Spectrometry Analysis of Biological Samples. *Talanta* **2018**, 189, 451–457.
- (166) Ramos, M. D.; Li, B.; Jacob, N.; Jensen, H.; Honoré, S.; Pedersen-bjergaard, S. Nano-Electromembrane Extraction. *Anal. Chim. Acta* **2013**, 785, 60–66.
- (167) Liu, Y.; Guo, L.; Wang, Y.; Huang, F.; Shi, J.; Gao, G.; Wang, X.; Ye, J.; Chu, Q. Electromembrane Extraction of Diamine Plastic Restricted Substances in Soft Drinks Followed by Capillary Electrophoresis with Contactless Conductivity Detection. *Food Chem.* **2017**, 221, 871–876.
- (168) Abbasi, A.; Rahbar-kelishami, A.; Ghasemi, M. J. Development of a Microfluidic-Chip

- System Based on Parallel Flow for Intensified Gd (III) Extraction from Nitrate Media Using Cationic Extractant. *J. Rare Earths* **2018**, *36*, 1198–1204.
- (169) Priest, C.; Hashmi, S. F.; Zhou, J.; Sedev, R.; Ralston, J. Microfluidic Solvent Extraction of Metal Ions from Industrial Grade Leach Solutions : Extraction Performance and Channel Aging. *Akadémiiai Kiadó* **2013**, *3* (3), 76–80.
- (170) Karami, M.; Yamini, Y.; Abdossalami, Y. On-Chip Ion Pair-Based Dispersive Liquid-Liquid Extraction for Quantitative Determination of Histamine H2 Receptor Antagonist Drugs in Human Urine. *Talanta* **2019**, *206*, 1–8.
- (171) Lubej, M.; Novak, U.; Liu, M.; Martelanc, M.; Franko, M.; Plazl, I. Microfluidic Droplet-Based Liquid–Liquid Extraction: Online Model Validation. *Lab Chip* **2015**, *15*, 2233–2239.
- (172) Ren, Y.; Mcluckey, M. N.; Liu, J.; Ouyang, Z. Direct Mass Spectrometry Analysis of Biofluid Samples Using Slug-Flow Microextraction Nano-Electrospray Ionization. *Angew. Commun.* **2014**, *53*, 14124–14127.
- (173) Yang, Y.; Wu, J.; Deng, J.; Yuan, K.; Chen, X.; Liu, N.; Wang, X.; Luan, T. Rapid and On-Site Analysis of Amphetamine-Type Illicit Drugs in Whole Blood and Raw Urine by Slug-Flow Microextraction Coupled with Paper Spray Mass Spectrometry. *Anal. Chim. Acta* **2018**, *1032*, 75–82.
- (174) Zhang, W.; Ren, Y.; Lin, Z.; Ouyang, Z. High-Precision Quantitation of Biofluid Samples Using Direct Mass Spectrometry Analysis. *Anal. Chem.* **2019**, *91*, 6986–6990.
- (175) Poole, S. K.; Poole, C. F. Separation Methods for Estimating Octanol – Water Partition Coefficients. *J. Chromatogr. B* **2003**, *797*, 3–19.
- (176) Schmedding, D. W.; Manes, M. Improved Prediction of Octanol - Water Partition Coefficients from Liquid - Solute Water Solubilities and Molar Volumes. *Environ. Sci. Technol.* **2005**, *39* (22), 8840–8846.
- (177) Ogden, P. B.; Dorsey, J. G. Reversed Phase HPLC with High Temperature Ethanol / Water Mobile Phases as a Green Alternative Method for the Estimation of Octanol / Water Partition Coefficients. *J. Chromatogr. A* **2019**, *1601*, 243–254.
- (178) Danielsson, L.; Zhang, Y.-H. Methods for Determining N-Octanol-Water Partition Constants. *Trends Anal. Chem.* **1996**, *15* (4), 3–9.
- (179) Guo, Y.; Ma, S.; Guan, S.; Zhang, Y.; Pan, J. High-Throughput Determination of Octanol – Water Partition Coefficients by Ultrasound-Assisted Liquid-Phase Microextraction. *J. Chromatogr. Sci.* **2015**, *53*, 1400–1406.
- (180) Pei, J.; Li, Q.; Lee, M. S.; Valaskovic, G. A.; Kennedy, R. T. Analysis of Samples Stored as Individual Plugs in a Capillary by Electrospray Ionization Mass Spectrometry. *Anal. Chem.* **2009**, *81* (15), 6558–6561.
- (181) King, C.; Walsh, E.; Grimes, R. PIV Measurements of Flow within Plugs in a Microchannel. *Microfluid Nanofluid* **2007**, *3*, 463–472.

- (182) Gjelstad, A. Three-Phase Hollow Fiber Liquid-Phase Microextraction and Parallel Artificial Liquid Membrane Extraction. *Trends Anal. Chem.* **2019**, *113*, 25–31.
- (183) Pedersen-bjergaard, S.; Rasmussen, K. E. Liquid-Phase Microextraction Combined with Liquid Extraction from Small Volumes of Biological Samples. *J. Sep. Sci.* **2003**, *26*, 1520–1526.
- (184) Mousavi, L.; Tamiji, Z.; Reza, M. Applications and Opportunities of Experimental Design for the Dispersive Liquid – Liquid Microextraction Method – A Review. *Talanta* **2018**, *190*, 335–356.
- (185) Pirsahab, M.; Fattahi, N.; Shamsipur, M.; Khodadadi, T. Application of Dispersive Liquid – Liquid Microextraction Based on Solidification of Floating Organic Drop for Simultaneous Determination of Alachlor and Atrazine in Aqueous Samples. *J. Sep. Sci.* **2013**, *36*, 684–689.
- (186) Jia, Z.; Mei, L.; Lin, F.; Huang, S.; Killion, R. B. Screening of Octanol – Water Partition Coefficients for Pharmaceuticals by Pressure-Assisted Microemulsion Electrokinetic Chromatography. *J. Chromatogr. A* **2003**, *1007*, 203–208.
- (187) Hodges, G.; Eadsforth, C.; Bossuyt, B.; Bouvy, A.; Enrici, M. H.; Geurts, M.; Kotthoff, M.; Michie, E.; Miller, D.; Müller, J.; et al. A Comparison of Log K_{ow} (n - Octanol – Water Partition Coefficient) Values for Non - Ionic , Anionic , Cationic and Amphoteric Surfactants Determined Using Predictions and Experimental Methods. *Environ. Sci. Eur.* **2019**, *31* (1), 1–18.
- (188) Baena, Y.; Barbosa, H. J.; Pinzon, J. A.; Martinez, F. Estimation of the Aqueous Solubility of Some Acetanilide Derivatives from Octanol-Water Partition Coefficients and Entropies of Fusion Estimation of the Aqueous Solubility of Some Acetanilide Derivatives from Octanol-Water Partition Coefficients and Entro. *Acta Farmaceutica Bonaer.* **2004**, *23* (1).
- (189) Smith, J. T.; Vinjamoori, D. V. Rapid Determination of Logarithmic Partition Coefficients between N-Octanol and Water Using Micellar Electrokinetic Capillary Chromatography. *J. Chromatogr. B* **1995**, *669*, 59–66.
- (190) Mo, H.; Balko, K. M.; Colby, D. A. A Practical Deuterium-Free NMR Method for the Rapid Determination of 1-Octanol / Water Partition Coefficients of Pharmaceutical Agents. *Bioorg. Med. Chem. Lett.* **2010**, *20* (22), 6712–6715.
- (191) Carlsson, K.; Karlberg, B. Determination of Octanol – Water Partition Coefficients Using a Micro-Volume Liquid-Liquid Flow Extraction System. *Anal. Chim. Acta* **2000**, *423*, 137–144.
- (192) Morikawa, G.; Suzuka, C.; Shoji, A.; Shibusawa, Y.; Yanagida, A. High-Throughput Determination of Octanol / Water Partition Coefficients Using a Shake-Flask Method and Novel Two-Phase Solvent System. *J. Pharm. Biomed. Anal.* **2016**, *117*, 338–344.
- (193) Schulz, M.; Iwersen-Bergmann, S.; Andresen, H.; Schmoldt, A. Therapeutic and Toxic Blood Concentrations of Nearly 1 ,000 Drugs and Other Xenobiotics. *Crit. Care* **2012**, *16*, 2–5.

- (194) Liu, X.; Tu, M.; Kelly, R. S.; Chen, C.; Smith, B. J. Development of a Computational Approach to Predict Blood-Brain Barrier Permeability. *Drug Metab. Dispos.* **2004**, *32* (1), 132–139.
- (195) Colmenarejo, G. In Silico Prediction of Drug-Binding Strengths to Human Serum Albumin. *Med. Res. Rev.* **2003**, *23* (3), 275–301.
- (196) Hsieh, C.-M.; Wang, S.; Lin, S.-T.; Sandler, S. I. A Predictive Model for the Solubility and Octanol–Water Partition Coefficient of Pharmaceuticals. *J. Chem. Eng. Data* **2011**, *56* (4), 936–945.
- (197) Valsaraj, K. T.; Thibodeaux, L. J. Relationships between Micelle-Water and Octanol-Water Partition Constants for Hydrophobic Organics of Environmental Interest. *Water Res.* **1989**, *23* (2), 183–189.
- (198) OECD. *Test No. 107: Partition Coefficient (n-Octanol/Water): Shake Flask Method*; OECD, 1995.
- (199) Chiou, C. T.; Schmedding, D. W.; Manes, M. Partitioning of Organic Compounds in Octanol-Water Systems. *Environ. Sci. Technol.* **1982**, *16* (1), 4–10.
- (200) Tokeshi, M.; Minagawa, T.; Kitamori, T. Integration of a Microextraction System on a Glass Chip: Ion-Pair Solvent Extraction of Fe(II) with and Tri-n-Octylmethylammonium Chloride. *Anal. Chem.* **2000**, *72* (7), 1711–1714.
- (201) Reddy, V.; Zahn, J. D. Interfacial Stabilization of Organic–Aqueous Two-Phase Microflows for a Miniaturized DNA Extraction Module. *J. Colloid Interface Sci.* **2005**, *286* (1), 158–165.
- (202) Žnidaršič-Plazl, P.; Plazl, I. Steroid Extraction in a Microchannel System—Mathematical Modelling and Experiments. *Lab Chip* **2007**, *7* (7), 883–889.
- (203) Kolar, E.; Catthoor, R. P. R.; Kriel, F. H.; Sedev, R.; Middlemas, S.; Klier, E.; Hatch, G.; Priest, C. Microfluidic Solvent Extraction of Rare Earth Elements from a Mixed Oxide Concentrate Leach Solution Using Cyanex® 572. *Chem. Eng. Sci.* **2016**, *148*, 212–218.
- (204) Aota, A.; Nonaka, M.; Hibara, A.; Kitamori, T. Countercurrent Laminar Microflow for Highly Efficient Solvent Extraction. *Angew. Chemie Int. Ed.* **2007**, *46* (6), 878–880.
- (205) Minagawa, T.; Tokeshi, M.; Kitamori, T. Integration of a Wet Analysis System on a Glass Chip: Determination of Co(II) as 2-Nitroso-1-Naphthol Chelates by Solvent Extraction and Thermal Lens Microscopy. *Lab Chip* **2001**, *1* (1), 72–75.
- (206) Assmann, N.; Ladosz, A.; Rohr, P. R. von. Continuous Micro Liquid-Liquid Extraction. *Chem. Eng. Technol.* **2013**, *36* (6), 921–936.
- (207) Chiu, D. T.; Lorenz, R. M.; Jeffries, G. D. M. Droplets for Ultrasmall-Volume Analysis. *Anal. Chem.* **2009**, *81* (13), 5111–5118.
- (208) Kashid, M. N.; Harshe, Y. M.; Agar, D. W. Liquid-Liquid Slug Flow in a Capillary: An Alternative to Suspended Drop or Film Contactors. *Ind. Eng. Chem. Res.* **2007**, *46*, 8420–8430.

- (209) Mary, P.; Chen, A.; Chen, I.; R. Abate, A.; A. Weitz, D. On-Chip Background Noise Reduction for Cell-Based Assays in Droplets. *Lab Chip* **2011**, *11* (12), 2066–2070.
- (210) Chen, H.; Fang, Q.; Yin, X.; Fang, Z. Microfluidic Chip-Based Liquid–Liquid Extraction and Preconcentration Using a Subnanoliter-Droplet Trapping Technique. *Lab Chip* **2005**, 719–725.
- (211) Peroni, D.; Egmond, W. Van; Kok, W. T.; Janssen, H. Advancing Liquid / Liquid Extraction through a Novel Microfluidic Device: Theory , Instrumentation and Applications in Gas Chromatography. *J. Chromatogr. A* **2012**, *1226*, 77–86.
- (212) Sahoo, H. R.; Kralj, J. G.; Jensen, K. F. Multistep Continuous-Flow Microchemical Synthesis Involving Multiple Reactions and Separations **. *Angew. Commun.* **2007**, *46*, 5704–5708.
- (213) Wells, S. S.; Kennedy, R. T. High-Throughput Liquid–Liquid Extractions with Nanoliter Volumes. *Anal. Chem.* **2020**, *92*, 3189–3197.
- (214) Roach, L. S.; Song, H.; Ismagilov, R. F. Controlling Nonspecific Protein Adsorption in a Plug-Based Microfluidic System by Controlling Interfacial Chemistry Using Fluorous-Phase Surfactants. *Anal. Chem.* **2005**, *77* (3), 785–796.
- (215) Andrés, A.; Rosés, M.; Ràfols, C.; Bosch, E.; Espinosa, S.; Segarra, V.; Huerta, J. M. Setup and Validation of Shake-Flask Procedures for the Determination of Partition Coefficients (LogD) from Low Drug Amounts. *Eur. J. Pharm. Sci.* **2015**, *76*, 181–191.
- (216) Equitz, T. R.; Rodriguez-cruz, S. E. High-Throughput Analysis of Controlled Substances : Combining Multiple Injections in a Single Experimental Run (MISER) and Liquid Chromatography – Mass Spectrometry (LC-MS). *Forensic Chem.* **2017**, *5*, 8–15.
- (217) Zawatzky, K.; Barhate, C. L.; Regalado, E. L.; Mann, B. F.; Marshall, N.; Moore, J. C.; Welch, C. J. Overcoming “Speed Limits” in High Throughput Chromatographic Analysis. *J. Chromatogr. A* **2017**, *1499*, 211–216.
- (218) Leveridge, M.; Collier, L.; Edge, C.; Hardwicke, P.; Leavens, B.; Ratcliffe, S.; Rees, M.; Stasi, L. P.; Nadin, A.; Reith, A. D. A High-Throughput Screen to Identify LRRK2 Kinase Inhibitors for the Treatment of Parkinson’s Disease Using RapidFire Mass Spectrometry. *J. Biomol. Screen.* **2016**, *21* (2), 145–155.
- (219) Welch, C. J.; Gong, X.; Schafer, W.; Pratt, E. C.; Brkovic, T.; Pirzada, Z.; Cuff, J. F.; Kosjek, B. MISER Chromatography (Multiple Injections in a Single Experimental Run): The Chromatogram Is the Graph. *Tetrahedron: Asymmetry* **2010**, *21* (13–14), 1674–1681.
- (220) Baena, Y.; Pinzón, J. A.; Barbosa, H. J.; Martínez, F. Temperature-Dependence of the Solubility of Some Acetanilide Derivatives in Several Organic and Aqueous Solvents. *Phys. Chem. Liq.* **2004**, *42* (6), 603–613.
- (221) Yeh, M.-K. Degradation Kinetics of Neostigmine in Solution. *Drug Dev. Ind. Pharm.* **2000**, *26* (11), 1221–1226.
- (222) Ashford, M.; Fell, J. Targeting Drugs to the Colon: Delivery Systems for Oral Administration. *J. Drug Target.* **1994**, *2* (3), 241–257.

- (223) Bajpai, S. K.; Bajpai, M.; Dengre, R. Chemically Treated Hard Gelatin Capsules for Colon-Targeted Drug Delivery: A Novel Approach. *J. Appl. Polym. Sci.* **2003**, *89* (8), 2277–2282.
- (224) Chaput, J. C.; Woodbury, N. W.; Stearns, L. A.; Williams, B. A. R.; Chaput, J. C.; Woodbury, N. W.; Stearns, L. A.; Williams, B. A. R. Creating Protein Biocatalysts as Tools for Future Industrial Applications Creating Protein Biocatalysts as Tools for Future Industrial. *Expert Opin. Biol. Ther.* **2008**, *8* (8), 1086–1098.
- (225) You, L.; Arnold, F. H. Directed Evolution of Subtilisin E in *Bacillus Subtilis* to Enhance Total Activity in Aqueous Dimethylformamide. *Protein Eng.* **1994**, *9* (1), 77–83.
- (226) Kuchner, O.; Arnold, F. H. Directed Evolution of Enzyme Catalysts. *Trends Biotechnol.* **1997**, *15*, 523–530.
- (227) Yuan, L.; Kurek, I.; English, J.; Keenan, R. Laboratory-Directed Protein Evolution. *Microbiol. Mol. Biol. Rev.* **2005**, *69* (3), 373–392.
- (228) Yang, G.; Withers, S. G. Ultrahigh-Throughput FACS-Based Screening for Directed Enzyme Evolution. *ChemBioChem* **2009**, *10*, 2704–2715.
- (229) Mack, M.; Burger, M.; Pietschmann, P.; Hock, B. A High-Throughput Microtiter Plate-Based Screening Method for the Detection of Full-Length Recombinant Proteins. *Protein Expr. Purif.* **2008**, *61*, 92–98.
- (230) Behrendorff, J. B. Y. H.; Vickers, C. E.; Chrysanthopoulos, P.; Nielsen, L. K. 2,2-Diphenyl-1-Picrylhydrazyl as a Screening Tool for Recombinant Monoterpene Biosynthesis 2,2-Diphenyl-1-Picrylhydrazyl as a Screening Tool for Recombinant Monoterpene Biosynthesis. *Microb. Cell Fact.* **2013**, *12* (76), 1–11.
- (231) He, Y.; Ma, C.; Xu, J.; Zhou, L. A High-Throughput Screening Strategy for Nitrile-Hydrolyzing Enzymes Based on Ferric Hydroxamate Spectrophotometry. *Appl. Microbiol. Biotechnol.* **2011**, *89*, 817–823.
- (232) Gärtner, A.; Ruff, A. J.; Schwaneberg, U. A 96-Multiplex Capillary Electrophoresis Screening Platform for Product Based Evolution of P450. *Sci. Rep.* **2019**, *9* (15479), 1–11.
- (233) Fu, L.; Zhang, J.; Si, T. BMC Energy Recent Advances in High-Throughput Mass Spectrometry That Accelerates Enzyme Engineering for Biofuel Research. *BMC Energy* **2020**, *2* (1), 1–9.
- (234) Lowe, D. M.; Gee, M.; Haslam, C.; Leavens, B.; Christodoulou, E.; Hissey, P.; Hardwicke, P.; Argyrou, A.; Webster, S. P.; Mole, D. J.; et al. Lead Discovery for Human Kynurenine 3-Monooxygenase by High-Throughput RapidFire Mass Spectrometry. *J. Biomol. Screen.* **2014**, *19* (4), 508–515.
- (235) Soga, T.; Igarashi, K.; Ito, C.; Mizobuchi, K.; Zimmermann, H. P.; Tomita, M. Metabolomic Profiling of Anionic Metabolites by Capillary Electrophoresis Mass Spectrometry. *Anal. Chem.* **2009**, *81* (15), 6165–6174.
- (236) Diefenbach, X. W.; Farasat, I.; Guetschow, E. D.; Welch, C. J.; Kennedy, R. T.; Sun, S.; Moore, C. Enabling Biocatalysis by High-Throughput Protein Engineering Using Droplet

- Microfluidics Coupled to Mass Spectrometry. *ACS Omega* **2018**, *3*, 1498–1508.
- (237) Belov, A. M.; Kozole, J.; Bean, M. F.; Machutta, C. A.; Zhang, G.; Gao, E. N.; Ghislain, L.; Datwani, S. S.; Leveridge, M.; Annan, R. S. Acoustic Mist Ionization-Mass Spectrometry: A Comparison to Conventional High-Throughput Screening and Compound Profiling Platforms. *Anal. Chem.* **2020**, *92*, 13847–13854.
- (238) Yet, L. *Privileged Structures in Drug Discovery*; 2018.
- (239) Bringmann, G.; Gunther, C.; Ochse, M.; Schupp, O.; Tasler, S. Biaryls in Nature: A Multi-Faceted Class of Stereochemically, Biosynthetically, and Pharmacologically Intriguing Secondary Metabolites. In *Progress in the Chemistry of Organic Natural Products*; 2001; pp 1–249.
- (240) Toenjes, S. T.; Gustafson, J. L. Atropisomerism in Medicinal Chemistry: Challenges and Opportunities. *Future Med. Chem.* **2018**, *10*, 409–422.
- (241) Bringmann, G.; Gulder, T.; Gulder, T. A. M.; Breuning, M. Atroposelective Total Synthesis of Axially Chiral Biaryl Natural Products. *Chem. Rev.* **2011**, *111* (2), 563–639.
- (242) Bringmann, G.; Mortimer, A. J. P.; Keller, P. A.; Gresser, M. J.; Garner, J.; Breuning, M. Atroposelective Synthesis of Axially Chiral Biaryl Compounds. *Angew. Chemie* **2005**, *44*, 5384–5427.
- (243) Uçaktürk, E.; Başaran, A. A.; Demirel, A. H. Effect of the Mobile Phase Compositions on the Confirmation Analysis of Some Prohibited Substances in Sport by LC–ESI–MS/MS. *Chromatographia* **2020**, *83* (11), 1397–1411.
- (244) Armbruster, D. A.; Pry, T. Limit of Blank, Limit of Detection and Limit of Quantitation. *Clin Biochem Rev* **2008**, *29* (August), 49–52.
- (245) Tempels, A. F. W.; Underberg, W. J. M.; Somsen, G. W.; Jong, G. J. De. On-Line Coupling of SPE and CE-MS for Peptide Analysis. *Electrophoresis* **2007**, *28*, 1319–1326.
- (246) Sandberg, M.; Weber, S. G. Techniques for Neuropeptide Determination. *Trends Anal. Chem.* **2003**, *22* (8), 522–527.